Méthode de décomposition de domaine pour les problèmes couplés acoustique-élastique, dans le domaine temporel. Application aux explosions sous-marines.

Alice Nassor

INSTITUT POLYTECHNIQUE DE PARIS

NNT : 2023IPPAE015

Thèse de doctorat

ENSTA IP PARIS

Domain decomposition method for coupled acoustic-elastic problems in the time domain. Application to underwater explosions.

Thèse de doctorat de l'Institut Polytechnique de Paris
préparée à l'École nationale supérieure de techniques avancées

École doctorale n°626 École doctorale de l'Institut Polytechnique de Paris (ED IP Paris)
Spécialité de doctorat : Mécanique des fluides et des solides, acoustique

Thèse présentée et soutenue à Palaiseau, le 18 décembre 2023, par

ALICE NASSOR

Composition du Jury :

Olivier Doaré Professeur, ENSTA Paris (UME)	Président
Hélène Barucq Directrice de recherche, Inria Bordeaux Sud-Ouest	Rapporteuse
Pierre Gosselet Directeur de recherche, Université de Lille	Rapporteur
Régis Cottereau Chargé de recherche (HDR), CNRS (LMA)	Examinateur
Martin Gander Professeur, Université de Genève, Suisse	Examinateur
Marc Bonnet Directeur de recherche, CNRS (POEMS)	Co-Directeur de thèse
Stéphanie Chaillat Directrice de recherche, CNRS (POEMS)	Directrice de thèse
Guillaume Barras Ingénieur de recherche, Direction Générale de l'Armement	Invité
Bruno Leblé Ingénieur de recherche, Naval Group Research	Invité

Remerciements

En premier lieu, je tiens à remercier profondément mes deux rapporteurs, Hélène Barucq et Pierre Gosselet, qui m'ont fait l'honneur de relire avec beaucoup d'attention ce manuscrit. Un grand merci aux autres membres du jury, d'abord à Olivier Doaré pour avoir accepté d'en être le président, et également à Régis Cottereau et Martin Gander pour l'intérêt et l'attention qu'ils ont portés à mes travaux.

Durant cette thèse, j'ai eu la chance d'être particulièrement bien encadrée. J'aimerais exprimer mes profonds remerciements à mes directeurs de thèse. A Marc Bonnet, pour ses conseils, sa patience et sa pédagogie, ainsi que pour sa rigueur scientifique. Et à Stéphanie Chaillat, pour ses encouragements, ses idées et conseils, notamment sur les aspects numériques, ainsi que pour ses nombreuses relectures du manuscrit. Cette thèse doit également beaucoup à Bruno Leblé et je tiens sincèrement à le remercier pour avoir initié ce projet et suivi mon travail avec bienveillance et implication. Je remercie aussi chaleureusement Guillaume Barras et Océane Grosset pour les réunions de suivi régulières et motivantes.

Ces trois années de thèse ont été marquées par des difficultés inhérentes au développement informatique : incompatibilité de versions, installation de librairies exotiques, parallélisation de code... Je remercie Nicolas Kielbasiewicz pour sa disponibilité et pour son aide inestimable durant l'installation de *Code Aster*! Je remercie aussi Ladya Khoun pour nos échanges et ses morceaux de code qui m'ont bien aidée; Mickael Abbas et Nicolas Tardieu, que j'ai sollicités plusieurs fois au sujet de *Code Aster*; Et Maï Bordiec, pour m'avoir fourni de superbes maillages de sous-marin.

J'ai eu la chance de travailler pendant trois ans dans un environnement particulièrement stimulant et bienveillant. Sans les citer tous, je voudrais remercier les membres de l'UMA qui font de ce labo un espace exceptionnel. Un merci particulier à Corinne qui a résolu bien des problèmes, à Laura, pour son soutien constant dans cette aventure, et à tous les doctorants qui ont égayé mes semaines.

Je termine par remercier toutes les personnes qui n'ont pas contribué directement à cette thèse, mais qui m'accompagnent depuis tant d'années : mes amis de Rennes et mes copains des Arts, dont l'amitié est si précieuse; la famille Dubois, qui exprime souvent son soutien et sa fierté. Enfin, toute ma gratitude va à Alexis pour ses encouragements et sa confiance qui ont rendu ces trois années plus douces, à Louise, Victor et à mes parents, pour leur amour et leur soutien indéfectible.

Résumé étendu

Contexte

Décrire le comporte une onde acoustique incidente est diffusée par un corps élastique immergé dans un fluide est un problème d'une importance majeure pour la détection et l'identification d'objets immergés. Ce phénomène doit être simulé dans de nombreux domaines industriels, tels que le contrôle non destructif, l'imagerie médicale, la réduction acoustique dans l'industrie automobile, ou encore la discrétion acoustique et l'identification de cibles dans l'industrie navale [71, 109, 141]. Ce problème est dit couplé : il s'agit de deux systèmes physiques (un système acoustique et un système élastique) qui interagissent l'un avec l'autre par le biais de conditions de transmission, de sorte que la résolution indépendante de l'un des systèmes est impossible sans la résolution simultanée de l'autre. Pour résoudre un tel problème couplé, il est naturel d'exploiter le fait que les deux systèmes interagissent au moyen d'interfaces communes: les équations de chaque système peuvent être résolues séparément et alternativement, puis les conditions de continuité de l'interface relient les solutions des systèmes. L'objectif principal des algorithmes de résolution basés sur des solutions séparées dans chaque système est de mettre à jour ces solutions itérativement jusqu'à ce que les conditions de continuité soient vérifiées. De cette manière, deux méthodes numériques différentes peuvent être utilisées pour résoudre les équations dans chaque sous-domaine. Cela permet de bénéficier des avantages respectifs des deux méthodes distinctes. Cette approche de résolution d'un problème couplé en considérant deux domaines séparément est une méthode de décomposition de domaine.

Dans ce travail, nous étudions des méthodes de décomposition de domaine dites "globales en temps" pour résoudre des problèmes couplés acoustiques-élastiques transitoires. L'objectif est de développer un algorithme itératif à convergence garantie, puis de mettre en oeuvre une procédure numérique efficace basée sur cet algorithme. Cette méthode sera ensuite validée sur des cas simples, puis appliquée à des problèmes à dynamique rapide de dispersion d'ondes de choc acoustiques par des structures élastiques immergées, ce qui permettra de simuler des configurations réalistes rencontrées dans l'industrie navale.

Chapitre 1 : Décomposition de domaine pour les problèmes transitoires

Le premier chapitre de cette étude vise à introduire les méhodes de décomposition

de domaine, et spécifiquement, les méthodes permettant de traiter des problèmes transitoires acoustique-élastiques. Dans la Section 1.1, on commence par décrire le principe des méthodes de Schwarz dans le domaine fréquentiel, qui est l'origine historique des méthodes de décomposition de domaine. Pour ce faire, on s'appuie sur deux exemples : un problème elliptique et un problème de propagation d'onde. On montre alors que l'algorithme itératif de Schwarz original ne converge pas systématiquement, et on introduit les méthodes de Schwarz optimisées, basées sur l'optimisation des conditions limites définies sur les frontières des sous-domaines. Une revue de la littérature concernant ces méthode permet de mettre en évidence que les conditions limite de type Robin sont très largement employées pour construire des algorithmes itératifs convergents.

La Section 1.2 présente ensuite deux stratégies existantes permettant de prendre en compte la variable temporelle dans les méthodes de décomposition de domaine. La première méthode consiste à discrétiser le temps à l'aide d'un schéma implicite, puis d'utiliser une méthode de Schwarz afin de résoudre un problème fréquentiel à chaque pas de temps. Une autre possibilité consiste à utiliser une méthode de décomposition du domaine globales en temps, qui consistent à discrétiser à la fois l'espace et le temps pour chaque sous-domaine.

Le chapitre se termine par une brève revue de la littérature actuelle concernant les méthodes de décomposition de domaine adaptées à la résolution de problèmes d'interaction fluide-structure transitoires. On souligne qu'il existe très peu de travaux décrivant des méthodes globale en temps permettant de traiter des problèmes acoustiques-élastiques transitoires, notamment parce que ces problèmes ont été peu étudiés théoriquement. Ce manque de résultats théoriques est un obstacle à la construction d'algorithmes itératifs convergents permettant de résoudre ces problèmes.

Chapitre 2 : Un couplage acoustique-élastique global en temps convergent

L'objectif du Chapitre 2 est de définir une procédure de décomposition de domaine itérative globale en temps, permettant de résoudre des problèmes acoustique-élastiques transitoires, avec une convergence garantie. Une telle procédure a été mise en oeuvre précédement [146], en alternant des résolutions de problèmes d'évolution de Neumann sur l'ensemble de l'intervalle de temps dans chaque sous-domaines fluide et solide. Cependant, des problèmes de convergence ont été observés.Nous avons donc deux objectifs : (i) expliquer mathématiquement la non-convergence de la procédure itérative basée sur des résolutions de sous-problèmes d'évolution de Neumann, et (ii) proposer une nouvelle méthode de couplage itérative, globale en temps, avec une convergence garantie. Cette nouvelle méthode que nous proposons est adaptée des méthodes classiques de relaxation de forme d'onde de Schwarz optimisée (*optimized Schwarz waveform relaxation*) et repose sur des conditions aux limites optimisées dans chaque sous-domaine.

Dans la section 2.1, nous commençons par décrire le problème d'interaction fluide-structure transitoire continu. Nous établissons ensuite des résultats de solvabilité pour ce problème. Les résultats présentés diffèrent par la régularité des données de transmission considéres sur l'interface acoustique-élastique. Ces résul-

tats de solvabilité montrent la dépendance continue des solutions aux données et fournissent des correspondances entre les régularités des données et des solutions. Ces informations sont essentielles pour concevoir des algorithmes de couplage convergents.

En nous appuyant sur ces correspondances entre données et solutions pour le problème acoustique-élastique transitoire, nous introduisons ensuite, dans la section 2.3, une première méthode itérative, globale en temps, inspirée des méthodes de relaxation de forme d'onde de Schwarz. Cette première méthode est basée sur la résolution itérative de problèmes aux valeurs limites initiales de Neumann. Nous rappelons les résultats classiques de solvabilité des problèmes d'évolution de Neumann et mettons en évidence la perte de régularité espace-temps de la solution trace définie sur l'interface, par rapport à la régularité de la donnée. Des observations similaires sont ensuite conduites pour une procédure globale en temps ismilaire basée sur des résolutions sucessives de problèmes d'évolution de Dirichlet. Ces résultats permettent de justifier la non-convergence de la méthode itérative observée initialement [146].

Dans la Section 2.4, nous proposons une seconde méthode itérative globale en temps, basée sur l'alternance des résolutions de problèmes d'évolution de Robin dans chaque sous-domaine. Nous rappelons les résultats de solvabilité pour les problèmes aux valeurs limites initiales de Robin et mettons en évidence la conservation de la régularité espace-temps de la solution trace définie sur l'interface, par rapport à la régularité de la donnée.

Nous prouvons la convergence de cette nouvelle procédure itérative globale dans le temps dans la Section 2.5. Enfin, la Section 2.6 présente une illustration numérique sur un problème acoustique-élastique 2D simple, qui met en évidence l'effet de la régularité des données sur la solution.

Chapitre 3 : Une méthode itérative FEM/Z-BEM globale en temps

Le Chapitre 3 propose une application de l'algorithme itératif global en temps pour simuler des problèmes complexes d'interaction fluide-structure. Pour obtenir le solveur le plus efficace possible, une méthode des éléments finis (FEM) et une méthode des éléments de frontière rapide (Z-BEM) sont utilisées. La Z-BEM permet de résoudre très efficacement les problèmes de propagation d'ondes transitoires dans des domaines linéaires homogènes non bornés. Le résultat fourni par cette méthode est obtenu sur tout l'intervalle de temps. La Z-BEM est donc une méthode naturellement adaptée aux algorithmes globaux en temps, et particulièrement au couplage itératif Robin-Robin que nous proposons. D'autre part, la méthode des éléments finis est la plus appropriée pour modéliser le comportement non linéaire des structures.

La Section 3.1 rappelle brièvement la théorie des équations intégrales de frontière transitoires ainsi que celle de la BEM, puis la Section 3.2 donne quelques rappels sur le principe et les particularités de la Z-BEM. La Section 3.3 est dédiée à la validation de la méthode numérique de couplage FEM/Z-BEM sur un exemple d'interaction fluide-structure 2D simple. La convergence est évaluée et nous étudions ensuite les valeurs optimales des paramètres de couplage impliqués dans les conditions de

transmission Robin. Nous comparons également la convergence de l'algorithme Robin-Robin avec d'autres types d'itérations globales en temps (Dirichlet-Dirichlet et Neumann-Neumann). Dans la Section 3.4, on montre que la vitesse de convergence de la méthode FEM/Z-BEM itérative globale en temps peut encore être améliorée. Un problème d'interaction fluide-structure 2D plus complexe est traité, d'une part pour valider que le choix des valeurs des paramètres de couplage des conditions de Robin permet bien d'optimiser la vitesse de convergence, et d'autre part, pour évaluer l'accélération de la convergence induite. Nous appliquons également une méthode accélération de point fixe appelée Δ^2 d'Aitken, pour réduire davantage le nombre d'itérations. On propose également dans la Section 3.5, une nouvelle approximation haute fréquence adaptée à la Z-BEM avec des conditions limite de Robin, qui permet de réduire considérablement le nombre de problèmes BEM à résoudre à chaque itération.

Enfin, la Section 3.6 détaille comment cette méthode FEM/Z-BEM peut être appliquée à des problèmes d'UNDEX complexes et réalistes et en souligne les avantages pratiques, ainsi que les limitations. En effet, le couplage FEM/Z-BEM proposé repose sur la disponibilité de conditions limite de Robin non-homogènes acoustique et élastique. Or, de telles conditions limites de Robin élastiques peuvent ne pas être disponibles dans certains logiciels de simulations, ce qui pourrait limiter l'utilisation de ce couplage dans des contextes industriels.

Chapitre 4 : Un couplage acoustique/acoustique-élastique global en temps convergent

Le but du Chapitre 4 est donc de s'affranchir de la nécessité d'utiliser des condition limite de Robin non homogènes élastiques, et de proposer un couplage itératif global en temps alternatif pour résoudre des problèmes acoustiques-élastodynamiques transitoires, toujours avec une convergence garantie mais sans utiliser de conditions limites de Robin élastiques. Pour ce faire, on considère une nouvelle décomposition de domaine: déplace l'interface de couplage dans le milieu acoustique, de sorte qu'elle ne coïncide plus avec la surface fluide-structure et qu'on doit résoudre un sous-problème acoustique et un sous-problème acoustique-élastique à chaque itération.

Nous rappelons dans la Section 4.1, l'importance d'un tel couplage alternatif et ses avantages. La Section 4.3 introduit ensuite la définition du problème et les notations, puis dans la Section 4.3.2 nous présentons la définition des nouvelles itérations globales en temps. Les conditions limites de Robin sont imposées dans le domaine acoustique uniquement. La convergence garantie de ces itérations est prouvée dans la Section 4.4. Nous validons numériquement notre procédure avec une méthode FEM/Z-BEM dans la Section 4.5, en considérant des problèmes 2D simples, avant de résoudre des problèmes aux géométries 3D plus complexes dans le Chapitre 5.

Chapitre 5 : Un couplage non intrusif dans un contexte industriel. Application aux explosions sous-marines

Le dernier chapitre de ce travail vise à de démontrer que l'algorithme itératif de décomposition de domaine que nous avons développé, basé sur les résolutions suc-

cessives de problèmes d'évolution de Robin dans chaque sous-domaine, permet bien de traiter des phénomènes couplés complexes, se déroulant dans le contexte des explosions sous-marines en champ lointain. En pratique, nous visons à coupler deux solveurs de manière non-intrusive, selon la procédure itérative acoustique/acoustique-élastique décrite dans le Chapitre 4. Pour traiter la partie acoustique/élastique intérieure du problème par éléments finis, nous utilisons le logiciel FEM `Code_Aster`, développé par EDF [64], et pour traiter le domaine acoustique non borné extérieur, nous utilisons un solveur Z-BEM 3D rapide développé au laboratoire POEMS.

L'objectif de la Section 5.1 est de valider le couplage acoustique/acoustique-élastique non intrusif, lorsqu'un solveur FEM industriel est utilisé. Nous insistons sur certaines difficultés de mise en œuvre liées à l'architecture du solveur, dont le comportement ne peut être modifié. La procédure de couplage est validée sur un problème d'interaction fluide-structure 3D simple, en considérant une sphère élastique et un champ acoustique incident transitoire uniforme. Dans la Section 5.2, nous proposons une extension à notre méthode de couplage permettant de simuler le comportement de navires de surface. Pour ce faire, il faut tenir compte des conditions limites de la surface libre. L'emploi de fonctions de Green du demi-espace permet de modifier le solveur Z-BEM rapide à cet effet.

Après une brève présentation des caractéristiques d'une explosion sous-marine dans la Section 5.3, l'objectif final est de traiter un cas réaliste de sous-marin soumis à une onde de choc produite par une explosion sous-marine en champ lointain. Un cas d'étude réaliste et proche des applications industrielles visées est présenté : on considère une coque de sous-marin élastique faisant face à une onde de choc acoustique incidente et on met en place les outils nécessaires à sa résolution. Enfin, dans la Section 5.4, nous donnons quelques perspectives d'améliorations qui pourront guider les futurs études et développements numériques.

Conclusion et perspectives

Conclusion. Dans ce mémoire, un algorithme de décomposition de domaine global en temps à convergence garantie, permettant de résoudre des problèmes acoustiques-élastiques transitoires a été proposé, et une méthode numérique FEM/Z-BEM a été mise en oeuvre. Dans un premier temps, nous avons montré la solvabilité du problème acoustique-élastique transitoire pour différentes régularités espace-temps de la donnée. Nous avons également étudié la solvabilité des problèmes aux valeurs limites initiales acoustique et élastodynamique transitoires, avec des conditions limites de type Robin, Neumann et Dirichlet. Cette première partie du travail a permis, en soulignant les différentes régularités espace-temps des solutions, de montrer la conservation de la régularité de la solution trace des problèmes acoustique et élastique de Robin, par rapport à la régularité de la donnée. En nous basant sur ces observations, nous avons proposé un algorithme de décomposition de domaine global en temps, basé sur les résolutions successives de problèmes d'évolution de Robin, et nous avons prouvé sa convergence. Nous avons ainsi développé un couplage itératif, global en temps, à convergence garantie, permettant d'utiliser deux méthodes numériques distinctes, de manière non intrusive. Cette stratégie a ensuite été mise en œuvre pour coupler deux méthodes numériques efficaces: une méthode des éléments finis et une approche Z-BEM combinant (i) une méthode d'éléments de frontière (BEM)

accélérée par la méthode des matrices hiérarchiques dans le domaine de Laplace et (ii) une quadrature de convolution. Plusieurs améliorations ont été proposées pour accélérer la convergence des itérations, et la méthode a été validée sur des problèmes académiques, fournissant ainsi des résultats prometteurs pour le traitement futur de cas industriels réalistes.

Perspectives. Cette première étude sur les méthodes de décomposition de domaine globales en temps pour les problèmes acoustiques-élastiques transitoires a ouvert de nombreuses perspectives. A court terme on propose par exemple d'intégrer la méthode globale en temps permettant de traiter l'interaction entre une onde de choc acoustique et une structure élastique, au sein d'un outil numérique adapté au traitement de l'ensemble des phénomènes physiques intervenant lors de l'interaction fluide-structure entre une explosion sous-marine en champ lointain et des sous-marins ou des navires de surface. Cet outil pourrait être utilisé pour traiter de manière unifiée à la fois l'onde de choc et le mouvement des bulles.

Annexes

Le mémoire se termine avec cinq annexes qui donnent des détails sur :

- Les solutions semi-analytiques de problèmes acoustiques-élastiques 2D à symétrie radiale.
- L'évaluation semi-analytique du facteur de convergence des itérations acoustique/ acoustique-élastiques.
- Une preuve de solvabilité pour un problème de Neumann transitoire (résultat énoncé dans le corps principal du document).
- Une preuve de solvabilité pour un problème de Robin transitoire (résultat énoncé dans le corps principal du document).
- La mise en oeuvre de la Z-BEM.

Principales publications associées à ce travail

Articles. Le travail présenté dans cette thèse fait l'objet d'une publication dans une revue avec comité de lecture :

- M. Bonnet, S. Chaillat, A. Nassor. "Solvability results for the transient acoustic scattering by an elastic obstacle". In: *Journal of Mathematical Analysis and Applications* 536.1 (2024), p. 128198. ISSN: 0022-247X. DOI: https://doi.org/10.1016/j.jmaa.2024.128198.

et d'un article de conférence :

- A. Nassor, S. Chaillat, M. Bonnet, B. Leblé, G. Barras. Convergence d'un couplage élastique-acoustique FEM-BEM itératif, global en temps. CMSA 2022 - 15ème colloque national en calcul des structures, Université Polytechnique Hauts-de-France [UPHF], May 2022, Hyères-les-Palmiers, France. https://hal.science/hal-03717599/

Deux publications supplémentaires sont actuellement en préparation : (i) présentant la preuve de convergence des itérations acoustique-élastiques globales en temps, correspondant au contenu du Chapitre 2, Sections 2.4 et 2.5; et (ii) sur le couplage acoustique/acoustique-élastique, correspondant au contenu du Chapitre 4.

Conférences. Ce travail a été présenté lors d'une conférence nationale et trois conférences internationales.

Contents

Introduction **1**

1 Domain decomposition methods for transient problems **7**
1.1 Generalities on domain decomposition methods 8
1.1.1 The original Schwarz algorithm 8
1.1.2 Robin conditions 13
1.2 Specificities of domain decomposition method in the time domain . . 16
1.2.1 Step-by-step methods 17
1.2.2 Schwarz waveform relaxation methods 20
1.3 DDMs for transient fluid-structure interaction problems 24
1.4 Conclusion 25

2 A convergent global-in-time acoustic-elastic coupling **27**
2.1 Coupled fluid-structure interaction problem definition 28
2.2 Solvability results 32
2.3 Global-in-time iterative coupling procedures 35
2.3.1 Global-in-time iterative method for transient FSI problems . . 35
2.3.2 Coupling iterations using Neumann boundary conditions . . . 37
2.3.3 Coupling iterations using Dirichlet boundary conditions 41
2.3.4 Iterative loss of space-time regularity for boundary traces . . . 42
2.4 Global-in-time iterative procedure based on Robin boundary conditions 43
2.4.1 Coupling iterations using Robin boundary conditions 44
2.4.2 Robin boundary conditions definition 44
2.4.3 Solvability results for the Robin IBVPs 49
2.5 Proof of convergence for the iterative algorithm 51
2.6 Numerical illustration 56
2.7 Proofs of solvability results 59
2.8 Conclusion 73

3 A global-in-time FEM/Z-BEM iterative method **74**
3.1 Boundary element methods 75
3.1.1 BIE for transient wave propagation 77
3.1.2 Numerical solutions of time-domain BIEs 80
3.2 Z-BEM 81
3.2.1 General principle of the convolution quadrature method 82
3.2.2 Z-BEM 84

3.3 Global-in-time FEM/Z-BEM Robin-Robin iterative coupling 86
3.3.1 Model 2D FSI problem analysis 86
3.3.2 Comparison of algorithms based on Robin, Neumann and Dirichlet boundary conditions 89
3.3.3 Optimal parameters for the Robin boundary conditions 89
3.4 Convergence acceleration 99
3.4.1 Optimised Robin coupling parameters 100
3.4.2 Aitken's acceleration 100
3.5 High-frequency approximations for an efficient FSI Robin problem . . 103
3.6 Global-in-time FEM/Z-BEM coupling for UNDEX 107
3.7 Conclusion 109

4 A convergent global-in-time acoustic/acoustic-elastic coupling 111
4.1 Why another coupling algorithm? 112
4.2 Acoustic/acoustic-elastic coupling definition 113
4.3 Global-in-time iterative procedure based on acoustic/acoustic Robin boundary conditions 115
4.3.1 General acoustic/acoustic iterative method for transient FSI problems 116
4.3.2 Acoustic/acoustic iterative method with Robin boundary conditions 117
4.3.3 Robin boundary conditions definition. 117
4.3.4 Solvability of acoustic and acoustic-elastic Robin IBVPs. . . . 120
4.4 Proof of convergence of the acoustic-acoustic iterative algorithm . . . 122
4.5 Validation and optimisation of the acoustic-acoustic FEM/Z-BEM coupling 127
4.5.1 Coupling validation: 2D test case 127
4.5.2 Coupling parameter optimisation 128
4.6 Conclusion 132

5 Non-intrusive coupling in an industrial context. Application to underwater explosions. 133
5.1 Non-intrusive 3D FEM/Z-BEM coupling validation 134
5.1.1 Finite element model for a time-domain elastic-acoustic problem 134
5.1.2 `Code_Aster` for domain decomposition methods and vibroacoustic problems 136
5.1.3 Validation of the 3D FEM/Z-BEM coupling using Code Aster 141
5.2 Free surface 142
5.2.1 Fast Z-BEM with half-space Green's functions 143
5.2.2 Z-BEM for partially emerged ships 149
5.3 Modelling the interaction between a shock wave and a submarine . . 152
5.4 Conclusion 156

Conclusions and perspectives 157

Bibliography 162

Appendices **176**
A Semi-analytical solution for a radially symmetric 2D test case 177
A.1 Acoustic-elastic analytical solution 177
A.2 Acoustic/acoustic-elastic analytical solution 181
B Convergence factor evaluation for acoustic/ acoustic-elastic iterations 185
C Proof of solvability for Neumann IBVPs 189
D Proof of solvability for Robin IBVPs (Theorem 2.4.2) 196
E In-house Z-BEM solvers 204
E.1 Acoustic Robin problems in frequency-domain 204
E.2 2D Z-BEM acoustic solver 206
E.3 3D Z-BEM acoustic solver 208

List of Figures

1 Acoustic wave scattered by an elastic body immersed in a fluid. . . . 1
2 Typical bubble motion and free-field pressure history for an underwater explosion [186]. . . . 3

1.1 Example of partition into two subdomains Ω_1 and Ω_2, with and without overlap. . . . 9
1.2 2D overlapping partition of Ω into two subdomains $\Omega_1 = [-\infty, d] \times \mathbb{R}$ and $\Omega_2 = [0, \infty] \times \mathbb{R}$. . . . 10
1.3 (a) Schematic representation of the information exchange between two subdomains with a step-by-step domain decomposition method. (b) Schematic representation of the transient information exchange between two subdomains with a global-in-time domain decomposition method, over a finite time interval. . . . 21

2.1 FSI configuration: geometry and notations. . . . 29
2.2 Schematic representation of a fluid-structure interaction problem between an incident acoustic plane wave ϕ_{inc} and an elastic domain $\Omega_s(\rho_s, c_s)$. . . . 56
2.3 Scattering by a 2D cylinder: (a) comparison between the normalised fluid normal velocities obtained with three different loads regularities and (b) comparison between the normalised fluid pressures obtained with three different loads regularities. . . . 58
2.4 Scattering by a 2D cylinder: convergence of indicator $e_{v,p}$ on the transmission residuals with the iterations, for three different loads regularities ($\Delta t = 1.7\ 10^{-6}$, El=1778, $k_c = \rho_s c_f$, Aitken acceleration). 58

3.1 Impulsive point source in a bounded domain Ω. . . . 78
3.2 Geometrical notations used for the derivation of the boundary integral equation for an exterior wave propagation problem. . . . 79
3.3 Numerical representation of L=$2N_t$=200 complex frequencies s_k for different time step values, using a BDF2 scheme (N_t=100, $\epsilon = 10^{-5}$). . . . 85
3.4 Radially-symmetric pressurised elastic annulus in an acoustic fluid. . 86

3.5 (a) Fluid pressure p at a node $\in \Gamma^{\text{ext}}$ obtained with a semi-analytical method and a global-in-time FEM/Z-BEM iterative algorithm ($\Delta t = 1.7\ 10^{-6}, N_t = 1500$, El=2336). Relative error : e_p^{sol} =0.50%. (b) Normal fluid velocity at a node $\in \Gamma^{\text{ext}}$ obtained with a semi-analytical method and a global-in-time FEM/Z-BEM iterative algorithm ($\Delta t = 1.7\ 10^{-6}, N_t = 1500$, El=2336). Relative error : e_v^{res} =0.05%. 88
3.6 (a) e_v^{res} and e_p^{res} with respect to the analytic solution versus the number of iterations ($\Delta t = 1.7\ 10^{-6}, N_t = 1500$, El=2336). (b) $e_v^{\text{sol}}, e_p^{\text{sol}}$ and $e_{v,p}$ on transmission residuals versus the number of iterations ($\Delta t = 1.7\ 10^{-6}, N_t = 1500$, El=2336). 88
3.7 Relative error on pressure e_p^{sol} compared to the semi-analytical solution with the iterations for different numerical schemes, for a 2D radially-symmetric problem (Δt=7.0e-07, El=2336, $k_c = \rho_f c_f$). 90
3.8 Pressure evaluated on a point of Γ with respect to time at three iterations for the algorithm based on Neumann transmission conditions (a) and on Dirichlet transmission conditions (b) ($\Delta t = 7.0\ 10^{-7}, N_t = 2000$, El=2336). 90
3.9 (a) Spectral radius of $\left[Rg\right]^{-1}\left[Rd\right]$ depending on the coupling parameter, for several complex frequencies.(b) Spectral radius of $\left[Rg\right]^{-1}\left[Rd\right]$ taking all the complex frequencies into account. 94
3.10 Semi-analytical convergence factor depending on the coupling parameter k_c and the relaxation parameter r ($\Delta t = 1.7\ 10^{-6}, N_t = 1500$, El=2336). (b) Spectral radius of $\left[Rg\right]^{-1}\left[Rd\right]$ taking all the complex frequencies into account. 94
3.11 (a) Convergence of the indicator $e_{v,p}$ on interfacial residuals for three values of k_c ($\Delta t = 1.7\ 10^{-6}, N_t = 1500$, El=2336). (b) Convergence of the indicator $e_{v,p}$ on interfacial residuals for $k_c = \rho_f c_f$ and three values of r ($\Delta t = 1.7\ 10^{-6}, N_t = 1500$, El=2336). 96
3.12 Semi-analytical convergence factor depending on the coupling parameters k_a and k_s ($\Delta t = 1.7\ 10^{-6}, N_t = 1500$, El=2336). 97
3.13 Schematic representation of a fluid-structure interaction problem between an incident acoustic plane wave ϕ_{inc} in an acoustic domain $\Omega(\rho, c_f)$ and an elastic domain $\Omega_s(\rho_s, c_s)$. 100
3.14 (a) Normalised fluid pressure and elastic stress evaluated on point A. (b) Normalised fluid and elastic velocities evaluated on point A. . . . 101
3.15 (a) Normalised fluid pressure and elastic stress evaluated on point B. (b) Normalised fluid and elastic velocities evaluated on point B. . . . 101
3.16 (a) Normalised fluid pressure and elastic stress evaluated on point C. (b) Normalised fluid and elastic velocities evaluated on point C. . . . 101
3.17 (a) Convergence of the indicator $e_{v,p}$ on interfacial residuals with and without Aitken acceleration ($\Delta t = 1.7\ 10^{-6}, k_c = \rho_f c_f$). (b) Convergence of the indicator $e_{v,p}$ on interfacial residuals with and without Aitken acceleration ($\Delta t = 1.7\ 10^{-6}, k_c = 3\rho_f c_f$). 103
3.18 HFA validation for the radiation problem with Robin BCs. Comparison between the Z-BEM fluid pressure and the Z-BEM-HFA fluid pressure on a point of Γ_e ($\Delta t = 1.7\ 10^{-6}$, El = 1778). 108

4.1 Domain decomposition for an acoustic-acoustic coupling: FEM (solid and interior fluid), and BEM (exterior fluid) parts. . . . 113
4.2 Domain decomposition for an acoustic-acoustic coupling : notations. . 113
4.3 Radially-symmetric pressurised annulus with a finite element mesh for the interior acoustic-elastic domain and BEM elements for the exterior acoustic domain. . . . 127
4.4 (a) Dimensionless radially-symmetric scattered pressures p_e, p_i and velocities v_e, v_i on Γ_e. Numerical results obtained using the acoustic/acoustic Robin-Robin coupling method are compared to semi-analytical reference values, $e_{v,p} = 3.10^{-4}$. (b) Errors e_v^{sol}, e_p^{sol} and $e_{v,p}$ on the transmission residuals for an acoustic/acoustic-elastic radially-symmetric problem. . . . 129
4.5 Semi-analytical convergence factor depending on the coupling parameters k_e and k_i ($\Delta t = 1.7\ 10^{-6}$, a=0.9, b=1, d=1.1). . . . 130
4.6 Semi-analytical convergence factor depending on the coupling parameters for (a) d=1.1 and (b) for d=7. . . . 131
4.7 Convergence of the indicator $e_{v,p}$ on interfacial residuals for three couples of Robin parameters (k_e, k_i). . . . 132

5.1 Domain decomposition for an acoustic-acoustic coupling : notations. . 134
5.2 2D elastic annulus immersed in a circular fluid domain of radius R^a, bounded by a circular boundary Γ_e on which a Robin boundary condition is imposed. . . . 138
5.3 Fluid pressure p evaluated on a point of the coupling interface Γ_i computed with `Code_Aster` and compared with the Matlab FEM result ($e_p^{\text{num}} = 0.013$). . . . 138
5.4 Schematic radially-symmetric 3D pressurised sphere with a finite element mesh for the interior acoustic-elastic domain and BEM elements for the exterior acoustic domain. . . . 141
5.5 3D pressurised sphere: (a) error on transmission residuals e_r computed with the 3D FEM/Z-BEM coupling, with and without Aitken acceleration, as a function of the iterations. (b) pressure induced on the surface Γ_e. $e_p^{sol} = 1.2\ 10^{-4}$. . . . 142
5.6 Impulsive point source in a domain Ω, bounded by a surface (S); Notations. . . . 143
5.7 Sketch of a sphere with an interior point source, immersed in a fluid domain bounded by a free surface. . . . 146
5.8 Numerical solution $\partial_n\phi$ and analytical $\partial_n G$ evaluated on a point of Γ for an acoustic scattering problem with a free surface (a) $Z_{\text{depth}} = -2.5$m, err $=1.0\ 10^{-3}$. (b) $Z_{\text{depth}} = -10$m, err $=1.0\ 10^{-3}$. . . . 147
5.9 Sketch of an elastic sphere immersed in an acoustic half-space. . . . 148
5.10 (a) Convergence of $e_{v,p}$ on transmission residuals with the number of iterations for a 3D FSI problem with a free surface. (b) Numerical solutions $p_e - s_p$ and p_i evaluated on a point of Γ_e. $e_p^{sol} = 5\ 10^{-2}$. . . . 149
5.11 Sketch of a partially emerged ship and its image with respect to surface (S). . . . 150
5.12 Sketch of a sphere with an interior point source, partially immersed in a fluid domain bounded by a free surface. . . . 151

5.13 Numerical solution $\partial_n\phi$ and analytical $\partial_n G$ evaluated on a point of Γ for an acoustic scattering problem with an emerged sphere. 151
5.14 3D view of the finite element mesh used for the acoustic/acoustic-elastic FEM/Z-BEM coupling. 154
5.15 Cavitation region treated with finite elements in an underwater explosion event. 160
16 Radially-symmetric pressurised annulus with a finite element mesh for the interior acoustic-elastic domain and BEM elements for the exterior acoustic domain. 182
17 Numerical boundary trace Φ computed with the BEM solver for a Robin BC and analytical solution Φ^* on Γ as a functions of θ $(a = 1, k = \pi)$. $e_\Phi^{res} = 3.6\ 10^{-3}$. 206
18 Integral representation of Φ in Ω_f and analytical solution Φ^* as functions of $r(a = 1, \theta = r, k = \pi)$. $e_\Phi^{res} = 3.5\ 10^{-5}$. 207
19 Numerical boundary trace $\partial_n\phi$ and analytical solution $\partial_n G$ on an boundary element of Γ $(\Delta t = 1.7\ 10^{-6}, N_t = 1118, El = 2336)$. 208
20 Relative L^2 error on $\partial_n\phi$: $e_r = 1.2\ 10^{-2}$ $(\Delta t = 8\ 10^{-2}, N_t = 76,$ T=4.5, HFA= 36). 211

List of Tables

2.1 Fluid and solid properties used. . . . 57

3.1 Fluid and solid properties. . . . 87
3.2 Theoretical values of spectral radius ϱ and number of iterations to reach convergence ($e_{v,p} < 10^{-3}$) for couples of parameters (k_c, r). . . . 95
3.3 Theoretical values of convergence factor ϱ and number of iterations to reach convergence ($e_{v,p} < 10^{-3}$) for couples of parameters (k_a, k_s). . . . 96
3.4 ϱ variation depending on the thickness e (R_{int}=1, $\frac{\rho_f}{\rho_{\text{mat}}} = 0.128$). . . . 98
3.5 Theoretical values of convergence factor ϱ for couples of parameters (k_a, k_s) and different physical parameters values ($Z_c = \rho_f c_f$, $Z_s = \rho_{\text{mat}} c_{\text{mat}}$ and e=0.1). . . . 98
3.6 Theoretical values of convergence factor ϱ for couples of parameters (k_a, k_s) and different physical parameters values ($Z_c = \rho_f c_f$, $Z_s = \rho_{\text{mat}} c_{\text{mat}}$ and e=0.1). . . . 98
3.7 ϱ variation depending on E (0.1, $\frac{\rho_f}{\rho_{\text{mat}}} = 0.128$). . . . 98
3.8 ϱ variation depending on E ($e = 9$, $\frac{\rho_f}{\rho_{\text{mat}}} = 0.128$). . . . 99
3.9 Number of numerical iterations to converge ($e_{v,p} < 10^{-3}$) for couples of parameters (k_a, k_s), with $e = 1.5$ and $\frac{\rho_f}{\rho_{\text{mat}}} = 0.128$. . . . 100
3.10 Relative space-time L^2 error between the numerical solutions computed with and without HFA, depending on the number of computed frequency BEM problems. . . . 107

4.1 Theoretical values of the convergence factor ϱ for couples of parameters (k_e, k_i). . . . 129
4.2 Convergence factor value for various acoustic-acoustic interface radius values d and k_e and k_i values ($\Delta t = 1.7\ 10^{-6}$, $N_t = 1500$, a=0.9, b=1). . . . 131

5.1 Error e_p^{num} against the number of FEM elements. . . . 139
5.2 Physical properties of the structure and the fluid in the first study case 5.1.3. 142
5.3 Fast Z-BEM with half-space Green function: physical properties for the validation case 5.2.1. . . . 146
5.4 Relative error with the number of frequency BEM problems solved in the Z-BEM before using the HFA. . . . 147
5.5 Spherical elastic hull with a free-surface: physical properties. . . . 148
5.6 Fast Z-BEM with half-space Green function: physical properties for the validation case 5.2.1. . . . 150

7 Relative space-time L2 error on the trace of $\partial_n \phi = \partial_n G$ with the number of mesh elements, at fixed mesh density 209
8 Relative error depending on the frequency, with and without H-mat acceleration (7 points per wavelength, $\eta = 3$, $\mathrm{n_{leaf}} = 20$). 209
9 Relative error depending on the frequency, with and without H-mat acceleration (12 points per wavelength, $\eta = 3$, $\mathrm{n_{leaf}} = 20$). 209

Introduction

Context

The problem of determining how an incoming acoustic wave is scattered by an elastic body immersed in a fluid is of major importance in detecting and identifying submerged objects. This class of problem is generally called a fluid-structure interaction. This phenomena needs to be simulated in many industrial fields, such as non-destructive testing, medical imaging, noise reduction in the automobile industry, or acoustic discretion and target identification in naval industry [71, 109, 141].

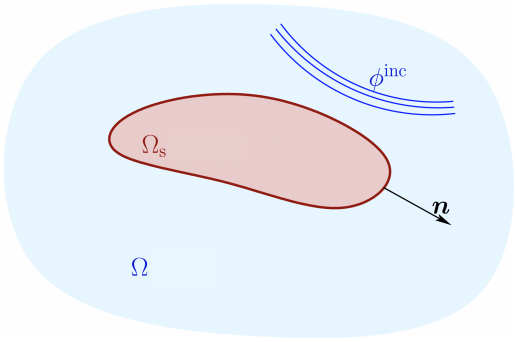

Figure 1: *Acoustic wave scattered by an elastic body immersed in a fluid.*

This problem is *coupled*: it consists in two different physical systems (an acoustic and an elastic) which interact with each other through kinematical and dynamical transmission conditions, so that the independent solution of any one system is impossible without simultaneous solution of the others. A natural way to solve a coupled problem is to exploit the fact that the two systems interact by means of common interfaces. The equations of each system are solved separately and alternatively. The interface continuity conditions relate the solutions of the systems. The main objective of solution algorithms based on separate solution in each system is to (iteratively) update them until the continuity conditions are verified. Generally, distinct domains describe different physical situations. For example, in a fluid-structure interaction problem, the fluid and the structure equations can be solved separately [74, 197]. In this way, one numerical method can be used to solve the equations of the fluid, and another method to treat the equations of the solid. It enables to profit from respective advantages of two distinct methods and to evade their drawbacks. This approach to solve a coupled problem by considering two domains separately is a *domain decomposition method*.

Domain decomposition methods are a family of methods to couple different partial differential equations (PDE) models [66, 170]. The main idea is to divide the computational domain of a PDE into smaller sub-domains and to split the problem into initial boundary value problems defined on the sub-domains. The PDE is solved separately on each sub-domain. The independent solutions do not yield the global solution of the initial problem. But the construction of a convergent sequence of local solutions can be achieved by iteratively solving local sub-problems and allowing sub-domains to exchange boundary information between the successive iterates. Generally, domain decomposition consists in ensuring that the transmission conditions between sub-domains are optimally prescribed. This domain of research is very active. We focus on time-domain decomposition methods to solve acoustic/elastic coupled evolution problems.

This work is motivated by applications in naval engineering. It is a part of the ongoing research collaboration between Naval Group Research and the POEMS teams at ENSTA Paris. It started with the PhD thesis of D. Mavaleix-Marchessoux [146]. The present PhD is funded by Naval Group and the Direction Générale de l'Armement (DGA) (through the Agence de l'Innovation de Défense (AID)). The overall goal of this collaboration is to accurately assess the potential effects of far-field underwater explosions on submarines and surface ships (UNDEX). An accurate prediction of underwater explosions effects could help improving hull designs to resist these loads and avoid weaknesses in designs leading to premature or catastrophic failures. Since the work of R. Cole [48], whose publications form the basis of most of the research on UNDEX, it has been extensively studied both at Naval Group [126, 136, 146] and at the Direction Générale de l'Armement [15, 30].

The modelling of the fluid-structure interaction taking place in this configuration is however not simple. During a far-field UNDEX, two types of solicitations are involved at two different time scales. A primary acoustic wave with a steep front (fast excitation, characteristic time of the order of a few milliseconds, fluid considered as linear acoustic) is first created by the explosion. The explosion then releases an oscillating gas bubble that creates a second, slower overall movement of heavy fluid that solicits the ship at low frequencies and over a longer time interval.

These two phenomena therefore have distinct effects and have both to be taken into account in distinct ways. It is possible to consider that during the rapid phase (shock wave) the fluid is acoustic, and that during the slow phase (oscillating bubble) the fluid is potential [146]. These approximations are reasonable in an industrial context and enable the use of linear fluid models. Nowadays the reference procedure used to evaluate these two phenomena and their effects on a submarine, is an iterative step-by-step procedure that couples two codes: one to model the structure (based on a finite element method) and one for the fluid (based on a conventional boundary element method) [74]. However, the code used for the fluid does not solve the transient wave equation, but only an approximate version. Moreover, accelerated numerical boundary element methods (BEM) have appeared and reached maturity. There is therefore a need to develop new, effective and accurate modelling tools to solve industrial underwater explosions problems.

In the previous study made in the framework of the Naval Group/ POEMS col-

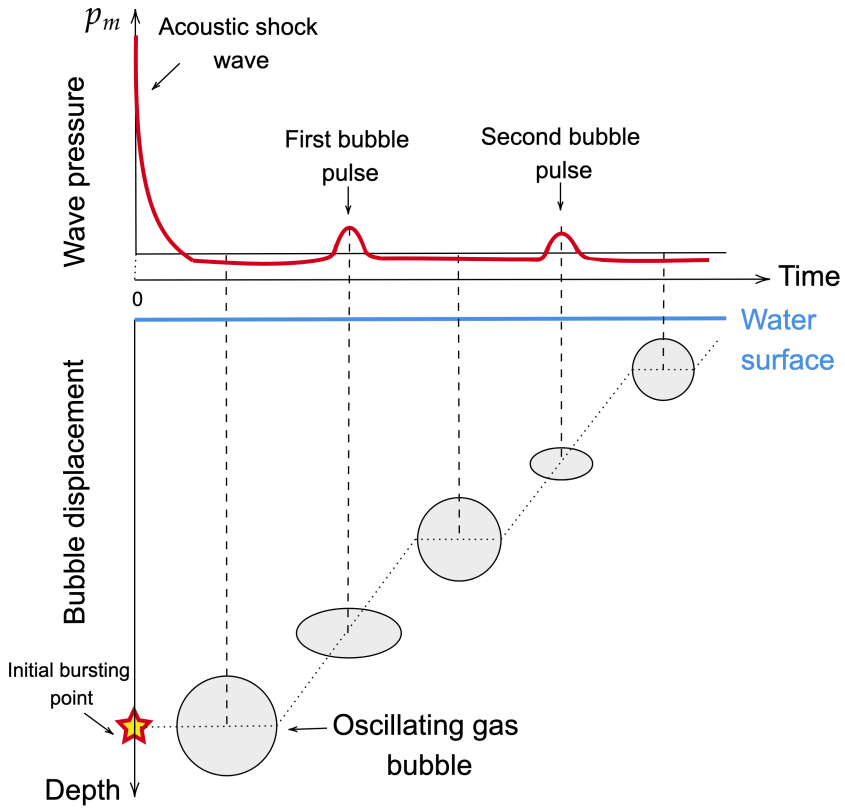

Figure 2: *Typical bubble motion and free-field pressure history for an undervwater explosion [186].*

laboration, D. Mavaleix-Marchessoux [146] worked on the primary acoustic shock wave and the movement of heavy fluid created by the far-field explosion. He associated two numerical methods: a finite element method (FEM) and a fast boundary element method (BEM). For the oscillating gas bubble, he proposed an efficient method based on an iterative FEM-BEM coupling at each time step (the fluid problem being quasi-static). For the shock wave, the acoustic fluid was treated with an improved boundary element method (Z-BEM) that implies a global treatment of the time interval. An iterative FEM/Z-BEM coupling over the whole time interval was tested, to take advantage of the *global-in-time* nature of the Z-BEM. This coupling was based on a sequence of Neumann evolution problems defined in each fluid and solid sub-domain and was found to be non-convergent. During the shock wave phase, the Z-BEM was finally used to compute the initial reflected field, and the fluid-structure interaction problem was solved using the FEM in both domains. It is however not an optimal solution because for a complex geometry, a 3D volume mesh has to be generated with a geometrically complex internal boundary. Moreover, this volume mesh must then be truncated, which may create unwanted reflections because of the approximation of the radiation condition. This complex 3D volume mesh could be avoided with a global-in-time iterative FEM/Z-BEM procedure.

The present work thus focuses on the proposition of a global-in-time iterative domain decomposition method to solve transient acoustic/elastic problems, and on its implementation as a coupled FEM/Z-BEM method. We have the three following objectives:

- We aim at coupling the FEM and the Z-BEM. It implies to use a global-in-time coupling, with iterations over the whole time interval.
- The iterative method must have a guaranteed convergence.
- We seek to explain why some procedures (e.g. solving successive Neumann evolution problems) do not lead to convergent algorithms.

Thesis contributions

To meet these requirements, we have followed three milestones, both theoretical and numerical.

We first aim at constructing domain decomposition algorithms for the fast-time fluid-structure interaction problem with guaranteed convergence. The work presented here is part of the research on non-overlapping Schwarz methods for wave propagation problems. The first developments date back to 1991 with the PhD thesis of B. Després [59], where a convergent domain decomposition algorithm was proposed, using optimised "Robin" boundary conditions in each subdomains. These Robin conditions are a combination of Dirichlet and Neumann traces and pave the way to the development of *Optimised Schwarz methods*. These methods were extended to evolution problems through global-in-time methods, also called *Schwarz Waveform Relaxation* methods [84]. They rely on the successive solutions of evolution problems, also termed initial-boundary value problems (IBVP), in each subdomains. The first contribution of this PhD work is theoretical and consists in extending the convergence analysis of non-overlapping domain decomposition methods to evolution fluid-structure interaction problems. To design convergent coupling algorithms, it turns out that the knowledge of data-to-solution mappings for the continuous transient fluid-structure interaction problem, and also for IBVPs involved in a domain decomposition approach, is essential. We thus derive new solvability results for the transient fluid-structure interaction problem (see the article [24]). We also highlight the loss of regularity of the trace solution when solving a Neumann evolution IBVP, while on the contrary, the regularity is preserved for a Robin evolution IBVP. This observation is particularly original since it differs from the classical regularity results known for elliptic problems in time. It also has a direct influence on the convergence of the algorithms considered to solve a fluid-structure interaction problem: while the convergence of the algorithm based on Neumann boundary conditions could not be proved, we show the superiority of the coupled algorithm based on Robin boundary conditions. Adapting the multi-trace formalism proposed in the recent paper [49] to evolution problems, we provide a proof of convergence for the global-in-time Robin iterations.

The second contribution is to design an efficient numerical method from the convergent algorithm we proposed. The elastic solid is modelled with the Finite Element Method, whereas the unbounded fluid medium is treated in the framework of boundary integral equations, using the Boundary Element Method, with an efficient Z-BEM method. Following the work of [146], the Z-BEM method is accelerated by H-matrices and a high-frequency approximation is used to reduce the number of frequency BEM problems solved. We also propose a high-frequency approximation

well-suited for acoustic evolution problems with Robin conditions. We validate the method with academic numerical examples.
An important question is to choose the coupling parameters appearing in the Robin boundary conditions definition. They are not easy to choose and require a crucial tuning to get efficiency. Based on the physical interpretation of the problem and on the thickness of the elastic structure, we propose to choose these parameters with respect to the elastic and acoustic impedances. The efficiency gain is then highlighted. Imposing non-homogeneous Robin boundary conditions might not be possible in industrial FEM solvers, and it might be impossible to use this global-in-time iterative algorithm. To overcome this problem, we present an alternative global-in-time iterative method, based on the resolutions of an acoustic and an acoustic/elastic Robin IBVPs in each subdomain. Its convergence is proved and the influence of the coupling parameter value are investigated. It might then be the most efficient solution for the targeted industrial applications.

Finally, the third contribution is to show the capabilities of the approach in the industrial context. To this aim, we investigate the possibility to use the algorithm in a non-intrusive way, with distinct commercial or open source solvers. We also extend our global-in-time iterative method to surface ships or to submarines in shallow waters. Using the method of images, we adapt the Z-BEM by modifying the fundamental solution to take the free-surface or the sea bed into account. The efficiency of the the global-in-time iterative method is illustrated with 3D fluid-structure interaction problems.

Outline of the work

This dissertation is decomposed into five chapters. In Chapter 1, we give an overview on the literature of domain decomposition methods. We emphasise on the methods adapted for evolution problems and on the optimised conditions developed to improve the algorithms convergence.

In Chapter 2, we theoretically study the well-posedness of the target coupled fluid-structure interaction problem, but also for the IBVPs defined on each subdomain and formulated with different boundary conditions. These solvability results have a direct impact on the convergence of the iterative algorithms and allow to justify the iterations convergence or non-convergence. The study of the solutions regularities leads to the definition and the comparison of two global-in-time iterative couplings, based on Neumann and Robin transmission conditions respectively. In particular, we prove the convergence of the iterative global-in-time algorithm formulated with Robin boundary conditions.

We propose in Chapter 3 a global-in-time iterative FEM/Z-BEM coupling algorithm with guaranteed convergence. Numerical experiments allow to verify the effective convergence of the algorithm based on Robin IBVPs. This chapter is then devoted to the numerical analysis of a particular choice of the coupling parameter value introduced in the Robin condition. We investigate its influence on the convergence speed, and propose an optimal choice. We also use relaxation and Aitken acceleration to speed up the convergence.

In Chapter 4, a second acoustic/acoustic-elastic convergent algorithm is theoret-

ically studied. It is based on a new domain decomposition and an acoustic-acoustic coupling interface with Robin transmission conditions. We prove the convergence of the iterations and expose which advantages derive from its use. We implement the algorithm with a FEM/Z-BEM iterative coupling and show its convergence on 2D examples.

This work concludes with the treatment of more complex underwater explosion problems in Chapter 5. We first extend the procedure to emmerged elastic obstacles by adapting the Z-BEM method to take a free-surface into account. We then consider a 3D submarine stiffened hull subjected to a remote underwater explosion. The purpose of this chapter is to show the efficiency of the computational method when used with an industrial code (`Code_Aster`).

The document ends with conclusions and research perspectives that could follow on from this thesis.

CHAPTER 1

Domain decomposition methods for transient problems

Domain decomposition methods (DDM) are not new and date back to the 1870s. Since then, many variations and improvements have been developed. Domain decomposition (DD) is nowadays a large field of research and the literature is vast. For general references, the reader may refer to [66, 93, 170]. [78] provides an extensive historical review. The objective in this chapter is not to provide an exhaustive review of these methods, but rather to show the references that inspired our work. Our final goal in this work is to solve fluid-structure interaction problems in the time domain with domain decomposition methods. Therefore, the present chapter first gives some reminders about DD methods for elliptic and time-harmonic wave propagation problems, and it is then mainly focused on time-domain DDMs. In Section 1.1, we study some time-harmonic DDMs on particular cases. We aim at illustrating the influence of the choice of boundary conditions in each subdomain, on the convergence of the iterative domain decomposition methods. Section 1.2 is then devoted to DDMs for evolution problems, and more precisely on global-in-time iterative methods. We also focus on the optimisation of the boundary conditions in each subdomain when the domain decomposition iterations do converge. Finally, we focus in Section 1.3 on DDMs for transient fluid-structure interaction problems.

Contents

1.1 Generalities on domain decomposition methods 8
1.1.1 The original Schwarz algorithm 8
1.1.2 Robin conditions 13
1.2 Specificities of domain decomposition method in the time domain 16
1.2.1 Step-by-step methods 17
1.2.2 Schwarz waveform relaxation methods 20
1.3 DDMs for transient fluid-structure interaction problems 24
1.4 Conclusion 25

1.1 Generalities on domain decomposition methods

Our final goal in this work is to solve fluid-structure interaction problems in the time domain using domain decomposition methods. The purpose of this first Section is thus to explain the concept of domain decomposition methods. We first expose the original Schwarz method in the frequency domain: we show on a Poisson problem that this original iterative algorithm does not converge when the geometry is decomposed into non-overlapping subdomains, and also illustrate how the convergence of the iterations depends on the size of the overlap. We then describe the interest of the optimised Schwarz methods and review some well-known optimised transmission conditions. Some ideas will later be transposed in the time domain, to address evolution problems.

1.1.1 The original Schwarz algorithm

Schwarz methods were initially introduced by H. Schwarz [180] to establish the existence and uniqueness of solutions for the Poisson equation with prescribed boundary values on regions with non-smooth boundaries. The idea is to split the irregular domain into sub-domains with more regular boundaries and to set up an adapted iterative method to exchange information between the subproblems. A basic example consists in considering the Poisson equation on a region Ω with a zero Dirichlet data given on the domain boundary $\partial\Omega$.

$$\begin{cases} -\Delta u = f & \text{in } \Omega, \\ u = 0 & \text{on } \partial\Omega. \end{cases} \tag{1.1}$$

Let suppose that Ω is partitioned into two *overlapping* subdomains Ω_i (with i=1,2) as illustrated on Figure 1.1. The original *Schwarz alternating algorithm* is an iterative method based on solving alternatively sub-problems in domains Ω_1 and Ω_2. Under some regularity assumptions on f and the boundaries of the subdomains (usually f is square-summable and the boundaries are Lipschitz), the solution is proved to exist as the limit of a sequence of local solutions (u_1^n, u_2^n) constructed with an initial guess (u_1^0, u_2^0). The algorithm updates $(u_1^n, u_2^n) \to (u_1^{n+1}, u_2^{n+1})$ by

$$\begin{aligned} -\Delta u_1^{n+1} &= f && \text{in } \Omega_1 && && -\Delta u_2^{n+1} = f && \text{in } \Omega_2 && (1.2) \\ u_1^{n+1} &= 0 && \text{on } \Sigma_1, && \text{then,} && u_2^{n+1} = 0 && \text{on } \Sigma_2, && (1.3) \\ u_1^{n+1} &= u_2^n && \text{on } \sigma_1 && && u_2^{n+1} = u_1^{n+1} && \text{on } \sigma_2. && (1.4) \end{aligned}$$

H. Schwarz proved the convergence of the alternating algorithm using the maximum principle and thus the well-posedness of the Poisson problem in complex geometries. The Schwarz method thus requires at each iteration the solution of two subproblems of the same kind than the original problem. In this case, Dirichlet-type boundary conditions are imposed across the interfaces for each subproblem. The method can be extended to more than two subdomains. In this case the formulation must ensure that the newest available information at the interfaces is always taken, if several choices are possible. The convergence of the method for many subdomains can be proved with similar arguments to those for the original Schwarz

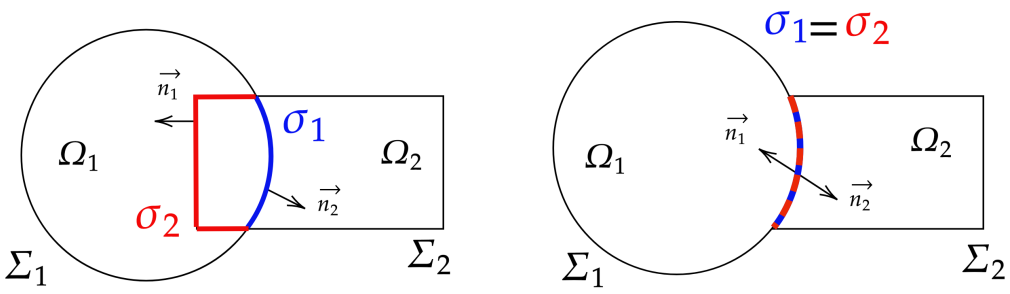

Figure 1.1: *Example of partition into two subdomains Ω_1 and Ω_2, with and without overlap.*

method with two subdomains. This original algorithm is however not parallel as the local problem in the sub-domain Ω_1 must be solved before the local problem in the sub-domain Ω_2. Later P.-L. Lions modified the original Schwarz algorithm (1.4) that is sequential, to enable its parallelisation and proved its convergence using the maximum principle [132]. The *parallel Schwarz algorithm* is an iterative method which updates $(u_i^n) \to (u_i^{n+1})$, at the same time in all subdomains i ($i = 1$ and 2 for example) by

$$-\Delta\left(u_i^{n+1}\right) = f \qquad \text{in } \Omega_i, \tag{1.5}$$

$$u_i^{n+1} = 0 \qquad \text{on } \Sigma_i, \tag{1.6}$$

$$u_i^{n+1} = u_{3-i}^n \qquad \text{on } \sigma_i. \tag{1.7}$$

The only modification is the iteration index in the second transmission condition, which makes this method parallel: given an initial guess (u_1^0, u_2^0), we simultaneously compute both subdomain solutions in parallel at each iteration n.

It easy to show that the classical Schwarz algorithms (both alternating and parallel) do not always converge with Dirichlet transmission conditions. We now consider two 2D model problems to illustrate this non-convergence: first, an elliptic problem in the non-overlapping case, and then a propagative (non-elliptic) problem.

Elliptic problem. We first consider a classical 2D elliptic example. The objective is to prove the convergence in an overlapping case and to show the dependence of the convergence factor to the overlap size d. The problem is defined on $\Omega = \mathbb{R}^2$ for a positive and real parameter α:

$$(-\Delta + \alpha)\, u = f \quad \text{on } \Omega$$

where Ω is unbounded, f is a source term and u is bounded at infinity. The unbounded 2D domain Ω is decomposed into $\Omega = \Omega_1 \cup \Omega_2$, with $\Omega_1 :=]-\infty, d[\times\mathbb{R}$ and $\Omega_2 :=]0, \infty[\times\mathbb{R}$ (Figure 1.2). The positive parameter d defines the overlap size and

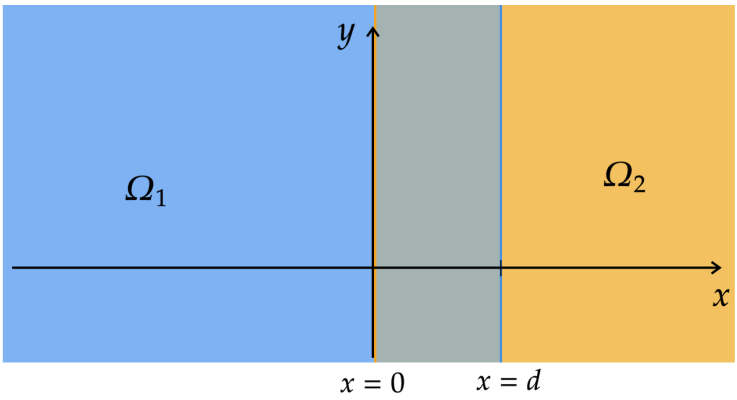

Figure 1.2: *2D overlapping partition of* Ω *into two subdomains* $\Omega_1 = [-\infty, d] \times \mathbb{R}$ *and* $\Omega_2 = [0, \infty] \times \mathbb{R}$.

d=0 defines the non-overlapping case. Given initial guesses u_1^0 and u_2^0, the parallel Schwarz algorithm consists in computing at each iteration n:

$$\begin{cases} (-\Delta + \alpha)\, u_1^{n+1}(x,.) = f(x,.) & \text{in } \Omega_1 \\ u_1^{n+1}(d,.) = u_2^n(d,.) \end{cases}$$

$$\begin{cases} (-\Delta + \alpha)\, u_2^{n+1}(x,.) = f(x,.) & \text{in } \Omega_2 \\ u_2^{n+1}(0,.) = u_1^n(0,.) \end{cases}$$

where the local solutions u_1 and u_2 are bounded at infinity. We define the error to the exact solution u:

$$e_i^n := u - u_i^n \quad (i = 1, 2). \tag{1.8}$$

By linearity the error verifies

$$\begin{cases} (-\Delta + \alpha)\, e_1^{n+1}(x,.) = 0 & \text{on } \Omega_1 \\ e_1^{n+1}(d,.) = e_2^n(d,.) \end{cases} \tag{1.9}$$

$$\begin{cases} (-\Delta + \alpha)\, e_2^{n+1}(x,.) = 0 & \text{on } \Omega_2 \\ e_2^{n+1}(0,.) = e_1^n(0,.) \end{cases} \tag{1.10}$$

For a given Fourier variable k, let the Fourier transform in the y direction be denoted by

$$\widehat{u}(x,k) := (\mathcal{F}u)(x,k) = \int_{\mathbb{R}} u(x,y) e^{-iky} dy.$$

By taking the partial Fourier transform of the first line of (1.9) in the vertical direction y:

$$\left(\alpha - \frac{\partial^2}{\partial x^2} + k^2\right) \hat{e}_1^{n+1}(x,k) = 0 \quad \text{in } \Omega_1.$$

This is an ordinary differential equation (ODE) whose solution has the form

$$\hat{e}_1^{n+1}(x,k) = \sum_j \gamma_j(k) \exp\left(\lambda_j(k) x\right)$$

We then compute

$$\lambda_1(k) = \lambda^+(k) = \sqrt{\alpha + k^2} \quad \text{and} \quad \lambda_2(k) = \lambda^-(k) = -\sqrt{\alpha + k^2}$$

Therefore

$$\hat{e}_1^{n+1}(x,k) = \gamma_+^{n+1}(k)\exp\left(\lambda^+(k)x\right)$$

There is no second term as the solution must be bounded at $x = -\infty$ which implies $\gamma_-^{n+1} = 0 \quad \forall n, k$. We then reformulate this expression to introduce the overlap value d, by changing the value of the coefficient γ_+ at each iteration

$$\hat{e}_1^{n+1}(x,k) = \gamma_1^{n+1}(k)\exp\left(\lambda^+(k)(x-d)\right)$$

We follow the same procedure for the subdomain Ω_2 and equation (1.10). An expression for the error $\hat{e}_2$ is obtained as

$$\hat{e}_2^{n+1}(x,k) = \gamma_2^{n+1}(k)\exp\left(\lambda^-(k)x\right)$$

To obtain the convergence factor, γ_1^{n+1} and γ_2^{n+1} have to be determined. We use the interface condition (at $x = d$ and $x = 0$) and we obtain

$$\gamma_1^{n+1}(k) = \gamma_2^{n+1}(k)\exp(\lambda^-(k)d) \quad \text{and} \quad \gamma_2^{n+1}(k) = \gamma_1^{n+1}(k)\exp(-\lambda^+(k)d)$$

The relation linking the successive iterations $n+1$ and $n-1$ is then given by

$$\gamma_j^{n+1}(k) = \varrho(k,\alpha,d)^2\gamma_j^{n-1}(k) \tag{1.11}$$

with the convergence factor ϱ

$$\varrho(k,\alpha,d) = e^{-\sqrt{\alpha+k^2}d}. \tag{1.12}$$

The convergence factor ϱ and the convergence rate of the algorithm depends on the overlap size d. The algorithm convergence rate is reduced when the overlap size becomes smaller. Moreover, in the non-overlapping case (d$=0$), the convergence factorϱ is identically equal to 1 and the algorithm does not converge. But when d>0, $\varrho < 1$ and the convergence is guaranteed. This dependence of the convergence rate on the size of the overlap is valid for operators verifying the maximum principle (for which the solution decays with respect to the boundary values) [170].

The original Schwarz algorithm only converges for elliptic problems with a non-zero overlap region. If the initial Schwarz algorithm [180] is indeed based on an overlapping partition and the first convergence proof of Lions [133] actually rests on the existence of the overlap, overlapping strategies however present many drawbacks for practical implementations. First of all, the size of the local sub-problems is increased by the size of the overlap, making the local solves somehow unnecessarily more expensive. In addition, the generation of overlapping mesh partitions and the implementation of overlapping domain decomposition methods are more involved than non-overlapping strategies. These limitations are not prohibitive and many successful methods are built on overlapping partitions, however, we only consider non-overlapping methods in this work.

Propagation problem. We now consider another non-elliptic example for wave propagation to determine the expression of its theoretical convergence factor and show its non-convergence. The Helmholtz problem is defined on $\Omega = \mathbb{R}^2$ by

$$\left(-\Delta - \frac{\omega^2}{c^2}\right) u = f, \quad \text{in } \Omega \tag{1.13}$$

where c is the acoustic velocity and f is a source term of frequency ω. u satisfies the Sommerfeld radiation condition at infinity. We then denote the wave number $\kappa = \frac{\omega}{c}$. Ω is decomposed with the same spacial decomposition $\Omega = \Omega_1 \cup \Omega_2$ as for the elliptic problem (Figure 1.2). For an initial guess (u_1^0, u_2^0) the classical parallel Schwarz algorithm consists in computing at each iteration $n > 0$

$$\begin{cases} (-\Delta - \kappa^2)\, u_1^{n+1}(x,.) = f(x,.) & \text{in } \Omega_1 \\ u_1^{n+1}(d,.) = u_2^n(d,.) \end{cases} \tag{1.14}$$

$$\begin{cases} (-\Delta - \kappa^2)\, u_2^{n+1}(x,.) = f(x,.) & \text{in } \Omega_2 \\ u_2^{n+1}(0,.) = u_1^n(0,.) \end{cases} \tag{1.15}$$

where u_1^n and u_2^n both verify the Sommerfeld radiation condition at infinity. Due to the negative sign of the order zero term, the Helmholtz operator is not positive. (1.14) and (1.15) are not necessarily well-posed. Moreover, even when the local problems are well-posed, a bad convergence rate is expected. Following a procedure similar to the one for the elliptic problem, we consider the error to the analytical solution $e_i^n := u - u_i^n$ (i=1,2) and thus by linearity, the case $f(x,.) = 0$. By using the partial Fourier transform in y direction, we solve two ODEs:

$$\begin{cases} \left(-\frac{\partial^2}{\partial x^2} - \kappa^2 + k^2\right) \widehat{e}_1^{n+1} = 0 \\ \widehat{e}_1^{n+1}(d,k) = \widehat{e}_2^{n+1}(d,k) \end{cases}$$

and

$$\begin{cases} \left(-\frac{\partial^2}{\partial x^2} - \kappa^2 + k^2\right) \widehat{e}_2^{n+1} = 0 \\ \widehat{e}_2^{n+1}(0,k) = \widehat{e}_1^{n+1}(0,k). \end{cases}$$

The solutions $\widehat{e}_1^n$ and $\widehat{e}_2^n$ verify the relations

$$\widehat{e}_j^{n+1} = A_j e^{\lambda(k)x} + B_j e^{-\lambda(k)x}, \quad j = 1, 2,$$

where $\lambda(k)$ is the root of the characteristic equation $\lambda^2 + (\kappa^2 - k^2) = 0$. We have

$$\lambda(k) = \begin{cases} \sqrt{k^2 - \kappa^2} & \text{for } |k| \geq \kappa \\ i\sqrt{\kappa^2 - k^2} & \text{for } |k| < \kappa. \end{cases} \tag{1.16}$$

$\lambda(k)$ is a complex valued function, which is real for the vanishing modes ($|k| \geq \kappa$) and imaginary otherwise ($|k| < \kappa$). We then use the interface condition (at $x = d$ and $x = 0$). Since the Sommerfeld radiation condition excludes the incoming modes at infinity, we obtain the solutions

$$\widehat{e}_1^{n+1}(x,k) = \widehat{e}_1^{n+1}(d,k) e^{\lambda(k)(x-d)}$$
$$\widehat{e}_2^{n+1}(x,k) = \widehat{e}_2^{n+1}(0,k) e^{-\lambda(k)x}.$$

We use the interface condition (at $x = d$ and $x = 0$) and we obtain

$$\widehat{e}_1^{n+1}(d,k) = \widehat{e}_1^{n-1}(d,k)e^{-2\lambda(k)d} \quad \text{and} \quad \widehat{e}_2^{n+1}(d,k) = \widehat{e}_2^{n-1}(d,k)e^{-2\lambda(k)d}$$

We finally have the relation

$$\widehat{e}_j^{n+1}(d,k) = \varrho(k,d)^2\widehat{e}_j^{n-1}(d,k)$$

where the convergence factor ϱ is

$$\varrho(k,d) = e^{-\lambda(k)d}$$

with $\lambda(k)$ given by (1.16). In the non-overlapping case $d = 0$, the convergence factor $\varrho(k,d)$ is equal to 1 and the classical Schwarz algorithm does not converge. But even in the overlapping case, as $\lambda(k)$ is imaginary, this convergence factor is complex and equal to 1 in modulus. For this reason the classical Schwarz algorithm does not converge for the Helmholtz equation, even in the overlapping case. This conclusion and the result about the elliptic problems witout overlap, led P.-L. Lions to propose optimised Schwarz methods.

1.1.2 Robin conditions

In the original Schwarz algorithm, the information coming from an adjacent subdomain is communicated to the local sub-problem through a non-homogeneous Dirichlet (as proposed by Schwarz [180]) or Neumann boundary condition. However, such an algorithm does not converge for non-overlapping partition. There are cases such as Helmholtz problems, where they do not converge even with a non-zero overlap. These drawbacks have all historically been avoided by introducing different boundary conditions at the interfaces between subdomains in the local sub-problems. This motivated the development of *optimised Schwarz methods*. The idea proposed by Lions [133] for the Laplace equation is to combine Dirichlet and Neumann traces using a real coupling parameter, to form Robin transmission conditions. Després then proposed in [59] to use Robin conditions to solve the Helmholtz equation with a domain decomposition algorithm. These Robin conditions allow the convergence, whereas classical Dirichlet or Neumann conditions lead to a non-convergent algorithm. As an illustration we show in this section how Robin boundary conditions improve the convergence of the Schwarz algorithm. We focus on the the same model problems as in Section 1.1.1.

Elliptic problem. The algorithm introduced by P.L. Lions [132] for the elliptic problem is based on improving Schwarz methods by replacing the Dirichlet interface conditions by Robin interface conditions, parameterised by a parameter k_c to be specified later. Given initial guesses u_1^0 and u_2^0, the parallel Schwarz algorithm consists in computing at each iteration $n > 0$:

$$\begin{cases} (-\Delta + \alpha)\, u_1^{n+1}(x,.) = f(x,.) \quad \text{in } \Omega_1 \\ \left(\frac{\partial}{\partial \mathbf{n}_1} + k_c\right) u_1^{n+1}(d,.) = \left(\frac{\partial}{\partial \mathbf{n}_1} + k_c\right) u_2^n(d,.) \end{cases}$$

$$\begin{cases} (-\Delta + \alpha)\, u_2^{n+1}(x,.) = f(x,.) \quad \text{in } \Omega_2 \\ \left(\frac{\partial}{\partial \mathbf{n_2}} + k_c\right) u_2^{n+1}(0,.) = \left(\frac{\partial}{\partial \mathbf{n_2}} + k_c\right) u_1^{n}(0,.) \end{cases}$$

where u_1^n and u_2^n both verify the Sommerfeld radiation condition at infinity. Following a similar convergence analysis to the one for the Dirichlet Helmholtz problem [66], we show a relation similar to (1.11) with a convergence factor

$$\varrho(k,\alpha,d) = \left|\frac{\lambda(k) - k_c}{\lambda(k) + k_c}\right| e^{-\lambda(k)d} \tag{1.17}$$

where $\lambda(k) = \sqrt{\alpha + k^2}$. For any Robin parameter k_c with a positive real part, the convergence factor ϱ is strictly lower than 1 in modulus and the algorithm does converge independently of the overlap size d. Compared to the convergence factor (1.12) for the classical Schwarz method, the convergence factor (1.17) for the optimised Schwarz method with Robin condition improves the convergence by a factor

$$\varrho(k,\alpha,0) = \left|\frac{\lambda(k) - k_c}{\lambda(k) + k_c}\right| < 1.$$

We also observe that by taking the limit $k_c \to \infty$, the previous case with the Dirichlet transmission condition is restored (and ϱ tends to 1 when there is no overlap). By setting $k_c = 0$, the Neumann transmission condition is obtained, which has the same non convergent behaviour as the Dirichlet case.

P.L. Lions also developed in [132] a proof of convergence for this algorithm with impedance-type conditions. This proof is based on the decay of an energy estimate defined on the interface. It consists in summing the energy identities verified by the error (defined by (1.8)) over the iterations, and showing that the energy, verified by the error, tends to zero with the number of iterations. The idea for this proof was then used, for example for the Helmholz equation in [61] and for the Maxwell equations in [62]. An optimal choice for the parameters k_c is also proposed to minimise the convergence factor. In the elliptic case, due to the form of the convergence factor (1.17), it is clear that ϱ is optimal ($\varrho = 0$) for the optimal value $k_c = \lambda(k) = \sqrt{\alpha + k^2}$.

Propagation problem. In [60], Després introduces Robin conditions in the Helmholtz problem, with the same decomposition illustrated in Figure 1.2. The idea is to rewrite the usual transmission conditions, which correspond to the continuity of the solution and its normal derivative, by recombining them in Robin-type conditions, using a special coefficient $i\kappa$. Given initial guesses u_1^0 and u_2^0, the Després algorithm consists in computing at each iteration $n > 0$:

$$\begin{cases} (-\Delta - \kappa^2)\, u_1^{n+1}(x,.) = f(x,.) \quad \text{in } \Omega_1 \\ \left(\frac{\partial}{\partial \mathbf{n_1}} + k_c\right) u_1^{n+1}(d,.) = \left(\frac{\partial}{\partial \mathbf{n_1}} + k_c\right) u_2^{n}(d,.) \end{cases} \tag{1.18}$$

$$\begin{cases} (-\Delta - \kappa^2)\, u_2^{n+1}(x,.) = f(x,.) \quad \text{in } \Omega_2 \\ \left(\frac{\partial}{\partial \mathbf{n_2}} + k_c\right) u_2^{n+1}(0,.) = \left(\frac{\partial}{\partial \mathbf{n_2}} + k_c\right) u_1^{n}(0,.) \end{cases} \tag{1.19}$$

with $k_c = i\kappa$ and where u_1^n and u_2^n both verify the Sommerfeld radiation condition at infinity.

In [61], Després proves that the local boundary value problems (1.18) and (1.19) are always well-posed, i.e. that they all admit a unique solution, for any value of κ. This also means that in the discrete setting the local matrices are always invertible. This is a necessary condition for guaranteed convergence which is not satisfied with Dirichlet or Neumann boundary conditions. Following a similar convergence analysis to the one for the Dirichlet Helmholtz problem [66], the convergence factor is

$$\varrho(k,d) = \left| \frac{\lambda(k) - k_c}{\lambda(k) + k_c} \right| e^{-\lambda(k)d} \tag{1.20}$$

where $\lambda(k)$ is still given by (1.16) and $k_c = i\kappa$. For vanishing modes ($|k| \geq \kappa$) $\lambda(k)$ is still real and negative such that the Schwarz algorithm converges and is converging faster for larger overlap sizes. But now, for the propagative modes ($|k| < \kappa$), the overlapping size d does not play any role in the convergence and as $i\kappa$ has a positive imaginary part, the convergence factor ϱ is strictly lower than 1 in modulus. In [59], Després proves the guaranteed convergence of the relaxed iterative method to the solution, using a proof based on the decay of energy estimate defined on the interface. Although the optimised Schwarz method without relaxation may converge in some particular configurations, in the general case the relaxation is necessary.

An improved version of the Després conditions was also suggested in [79]. "Two-sided Robin transmission conditions" are derived with two different coefficients α_i (i=1,2) instead of a unique k_c. They are termed by opposition to the "one-sided" version defined by (1.18) and (1.19). At each iteration $n > 0$, the conditions are

$$\left(\frac{\partial}{\partial \mathbf{n}_1} + \alpha_1 \right) u_1^{n+1}(d,.) = \left(\frac{\partial}{\partial \mathbf{n}_1} + \alpha_2 \right) u_2^{n}(d,.) \tag{1.21}$$

and

$$\left(\frac{\partial}{\partial \mathbf{n}_2} + \alpha_2 \right) u_2^{n+1}(0,.) = \left(\frac{\partial}{\partial \mathbf{n}_2} + \alpha_1 \right) u_1^{n}(0,.) \tag{1.22}$$

where α_1 and α_2 are complex. They must be chosen with a strictly positive imaginary part to ensure the well-posedness of the local sub-problems [79]. As the convergence factor is defined by (1.20), we also show that ϱ is optimal ($\varrho = 0$) for the *optimal* value $\alpha_1 = \alpha_2 = \lambda(k)$, with $\lambda(k)$ defined by (1.16). This value annihilates the convergence factor and ensures the optimal convergence of the schema (in two iterations for a two domain decomposition) [79].

More generally, these Robin coupling parameters are used as optimisation parameters to improve the convergence and their choice is crucial to guarantee good convergence properties. The classical approach to find an optimised value for α_i consists in following the optimisation strategy proposed in the optimised Schwarz methods literature [78]. In these classical works, a convergence analysis of coupled problems with Robin transmission conditions have been derived, based on the application of a Fourier transform. The Fourier transform is applied in one direction and the theoretical convergence factor is defined. This theoretical expression is then minimised. This optimisation strategy has been applied to a great variety of problems: Helmholtz equation [142], maxwell equation [65] or scattering problem [189] for example. These studies all show a large improvement on the convergence properties. It is efficient for problems with a straight interface, but the Fourier approach

fails for curved interfaces. As a result, the first optimisation analyses were only performed for simple 2D problems. In [65] a 3D optimisation procedure is derived for a Maxwell equation and in [87] a 3D convergence analysis is performed on a diffusion-reaction problem. A similar but more general optimisation procedure is adapted in [88] for spherical interfaces.

Other conditions. Thereafter, many variations of this original idea have been proposed, by using more sophisticated local and non-local impedance operators to construct the conditions. A review of the transmission operator used in transmission conditions for time-harmonic propagative problems is given for example in [167]. These boundary conditions must satisfy the following three requirements:

- They must link the trace solutions of each sub-domain at iteration n, to the trace solutions of the neighbouring sub-domain at iteration n-1, in order to couple the sub-problems.
- They must be consistent, at convergence, with the exact transmission conditions.
- They must ensure that the local subproblems are well-posed and that the method is convergent.

Remark. The term impedance is justified by the fact that such an operator has the homogeneity of an impedance. From a more physical point of view, this type of condition can be seen as a way to ensure a coupling that provides consistency with certain limiting cases. For FSI for example, when the fluid or solid density goes to zero, then the other medium has to get a free surface boundary condition. Otherwise, when the density goes to infinity, the other medium has to get a wall boundary condition. Neither Dirichlet nor Neumann coupling condition would work in both limits, but the impedance coupling condition does.

These optimised algorithms for time-harmonic problems show how crucial the choice of the conditions is to construct convergent iterative algorithms. It also shows that: it is often necessary to use impedance-like boundary conditions to obtain a convergent non-overlapping domain decomposition method, and that optimising these impedance conditions has a direct impact on the convergence. While similar observations can be derived for evolution problems (the ones we study in this work), additional difficulties arise.

1.2 Specificities of domain decomposition method in the time domain

For parabolic equations two approaches can be adopted. One possibility is to discretise in time first using an implicit scheme and then to employ the Schwarz method in order to solve the steady problems at each time step. Another possibility is to use the space-time domain decomposition method. This method consists in discretising the space and the time interval, differently for each subdomain according to its physical properties. In this Section, we compare the two approaches in the context of transient fluid-structure interaction (FSI).

1.2.1 Step-by-step methods

Classical domain decomposition methods to treat evolution problems consists in uniformly discretising the time on the whole domain by an implicit schema. At a fixed time step, the resulting equation is equivalent to an elliptic problem in each subdomain, which can be solved in parallel. At each time step, information is shared through the interface Γ. There are a lot of applications of this iterative domain decomposition method, for parabolic problems for example [36] or for hyperbolic problems [9].
For step-by-step DDMs, we can consider explicit algorithms, also called *weakly* or *loosely coupled* strategies. In each subdomain, the steady subproblems are solved only once per time step and do not satisfy the exact equilibrium conditions on the interface. This can induce instabilities in these explicit coupling schemes.
The other way is to treat implicitly the coupling conditions at each time step with implicit algorithms, leading to a *strongly* or *fully coupled* system. The coupled problem is then solved via subiterations between subdomains and the exact equilibrium conditions are verified. In this case, the numerical schema is stable. But the drawback is a relatively large number of subiterations to solve and the increasing computational cost.
For FSI, it has been shown in the literature that the stability of explicit coupling schemes is dictated by the amount of added-mass effect in the system. These explicit algorithms are especially not recommended for problems with comparable fluid and structure densities (which means a high added mass effect), as they lead to unconditional numerical instability, the so-called added-mass instability [6, 40]. These explicit scheme are thus more used for FSI problems with compressible flows [117, 151, 199]. Implicit and semi-implicit couplings have been developed for incompressible fluids and problems with high added-mass effect. Despite their additional computational cost due to the iterations within each time step, they prevent a lot of stability issues [6, 75, 119, 160]. There are then two difficulties. The first one is to reduce the number of iterations required. Either relaxation techniques can be used [119], or quasi-Newton techniques, which update the interface data communicated between the subproblems with a Newton-Raphson approach [58]. Both can be combined as in [187]. The second one consists in making each iteration fast. There are for example different types of preconditioners [198] or different ways to discretise the unknowns to speed up the numerical solution [144].

Different strategies rely on the choice of transmission conditions to solve the steady sub-problems at each iteration. Like for time-harmonic problems, Dirichlet conditions were first used, then Robin and more complex conditions [132, 170]. In particular, transmission conditions are designed to minimise the convergence rate in [112]. For FSI problems, the transmission conditions are usually the kinematic and dynamic interface conditions between the solid and the fluid: the velocity of the fluid is prescribed at the fluid-structure interface to be the velocity of the structure, and the traction on the surface of the structure is computed using the fluid pressure and viscous stress. In other words, the kinematic and dynamic interface conditions are enforced by applying a Dirichlet boundary condition in the fluid subdomain and a Neumann boundary condition in the solid subdomain, resulting in a Dirichlet–Neumann schema. As it is based on the physical transmission conditions

this scheme is often the simplest to use within an explicit scheme, but it is however very sensitive to the fluid density and to the added-mass effect especially for incompressible fluids. The Dirichlet–Neumann coupling is sometimes unconditionally unstable [40]. For this reason and as there is no proof of guaranteed convergence, the Dirichlet-Neumann coupling iterations sometimes diverge. Other boundary conditions have been explored to improve the algorithms stability. It is proposed in [6] to replace the Dirichlet boundary condition for the fluid solver by a Robin boundary condition. The new Robin-Neumann conditions are shown to be mathematically equivalent with the conventional Dirichlet-Neumann conditions [56]. Rather than transferring Dirichlet or Neumann interface data, the two contributions are linearly combined through Robin conditions. In some cases this scheme can highly reduce the added-mass instability and improve the convergence rate compared to a Dirichlet-Neumann scheme, when the linear Robin combination parameter is carefully selected [6, 37]. It opened the way to a whole family of coupling strategies: Robin-Neumann, Robin-Dirichlet, Robin-Robin [7, 37, 160, 188]. In particular the Robin-Robin schema is also often used [7, 86, 88, 89]. These Robin-based methods are now very popular as they allow a loosely-coupled and yet added-mass-free FSI coupling. However, many studies still investigate the optimisation of these boundary conditions through the choice of the coupling parameter value for both subproblems.

Coupling parameter optimisation for step-by-step procedures. The coupling parameter in the Robin boundary conditions is the term which balances the Neumann and Dirichlet contributions. It is denoted α_i in (1.21) and (1.22). The value of this coupling parameter does not have any impact on the mathematical model (as long as it is nonzero). However, it impacts the numerical convergence of the procedure. Some studies have shown through numerical experiments, that different values of α_i can strongly improve or deteriorate the numerical stability. Nonetheless, the determination of an appropriate value for a specific problem is still an open question [37, 160]. Generally speaking, for FSI problems, decreasing α_i tends to improve the numerical stability of the coupling by weighting the Neumann contribution. However it slows down the convergence and reduces the solution accuracy, in the sense that for a given convergence bound the remaining artificial flux increases. On the other hand when α_i increases, the Dirichlet part increases the added-mass instability [37].

The classical approach to define an optimised Robin coupling parameter in the context of step-by-step procedures consists in analysing simplified problems on particular geometries and deriving suggestions for the choice of α_i. These simplified problems are simple enough to be analysed theoretically but feature a behaviour similar to the more complex systems so that the theoretical optimised values might be reused. There are different strategies, as illustrated in [86] for an haemodynamics application:

- In [159], an heuristic method to design α_i based on simplified model equations is proposed. The structure model is reduced to a 1D model, by using a membrane model that approximates a thin structure behaviour. The membrane equation is inserted into the fluid equation as a boundary term and the FSI problem becomes a fluid problem with a suitable Robin boundary condition. This formulation leads to a plausible approximation of the fluid coefficient α_i,

depending on the physical densities, the geometry and the time step. With this optimised Robin condition, it is shown that a speed-up of up to one order of magnitude can be achieved. Another heuristic approximation is proposed for the structure coefficient in [6]. The same strategy is used for many other FSI problems with a high added-mass effect and the convergence is systematically improved [7, 159, 160].

- Some other studies use a modal analysis as described for time-harmonic problems in Section 1.1.2. The modal analysis might be adapted from the optimised Schwarz methods literature for elliptic problems [78]. A rigorous convergence analysis is for example proposed in [86] to define a theoretical optimised Robin coupling parameter value, for three different reduced FSI problems (Laplace, Helmoltz and Maxwell equations). A Fourier transform in one direction, and the convergence factor is explicitly defined in the frequency space. Minimising this factor for all the relevant frequencies of the problem allows to find an optimised expression for α_i, which is then used for all the time steps. This optimisation strategy is more general and confirmed by 2D numerical experiments. The proposed optimised parameter significantly improves the convergence rate of the Robin-Robin schemes. Another analytical study about a Robin-Neumann step-by-step schema is also investigated in [37], with a simplified FSI model featuring an Euler-Bernoulli beam and a 2D incompressible, inviscid flow. For this problem, a semi-analytical solution can be found, using the method of separation of variables and Fourier series. It enables to find an explicit form for the convergence factor, depending on α_i, which can be minimised. Similar methods are reused in a lot of works [63, 89, 158]. The optimised expression for α_i obtained on a simplified problem can then be used for more complex problems with comparable behaviours and still provide meaningful stability results [89].

A recent work also investigates the use of a spatially varying Robin interface conditions [38]. In the case of a non-uniform structure, the Robin parameter value in the boundary condition for the structure subproblem varies with the local material and geometric properties. Two numerical tests show that a spatially varying Robin interface condition can clearly improve the solution accuracy for the same computational cost. In [34], the authors propose an adaptive time step strategy, to adapt the value α_i at each time step. This strategy is also efficient in the case of large added mass effect. The numerical experiments show that this method is accurate with respect to the case of fixed small time steps and saves significant computational effort.

Some studies propose other approaches to reduce the impact of the Robin parameter on the number of iterations, and thus the importance of finding a good choice. It is shown in [7] that a Robin-Robin schema can be reformulated as preconditioned Richardson iterations over an adapted interface equation. This allows to introduce more efficient Krylov methods for the solution of the FSI problem, which are less sensitive to the Robin parameter value [7]. Another recent work [188] has derived an acceleration method for Robin-Neumann iterations, which also reduces the performance dependence to α_i. The interface Robin-Neumann/quasi-Newton accelerated schema is proposed to "relax" the Robin fluid traction by means of an

Aitken's relaxation method (firstly introduced in the context of FSI in [57]). The numerical tests show a large reduction of the dependency on the Robin parameter. With that, finding a good choice for the parameter α_i may still be beneficial, but is no longer of primary importance.

In conclusion, for most of the FSI problems solved with a step-by-step partitioned procedure, the optimal coupling parameter value α_i depends on a lot of parameters (material properties, geometry, time step size), rests upon simplified or approximated equations, and is highly problem-dependent. The proposed optimisation methods however enable an important first estimation of optimised coupling parameters. In particular, the acceleration techniques that also reduces the algorithm dependence on α_i are promising. But finding the best Robin parameter is still an ongoing research topic.

Drawbacks of step-by-step procedures. Step-by-step algorithms have some drawbacks. First, it is necessary to impose a uniform time discretisation for all subdomains. They loose one of the main features of domain decomposition algorithms, namely to adapt the solution process to the physical properties of the subdomain. It is still possible to refine in space. But for evolution problems this is not sufficient, since the space and time discretisation are linked in general by stability constraints and conditions on the dispersion of the numerical scheme. Secondly, the algorithm needs to communicate small amounts of information at each time step. In the context of parallel computing, each communication involves in addition to the cost for the data transmitted a startup cost independent of the amount of data transmitted. The interest of this strategy can thus be reduced due to the communication time. An algorithm with a reduced number of communications would be more interesting. Finally, this step-by-step strategy is sometimes not adapted to efficient numerical methods. For example, a global-in-time method as Z-BEM, which is a very efficient way to solve transient BIEs (see Section 3.1), is not adapted to step-by-step coupling strategies. In this case, global-in-time strategies are required.

1.2.2 Schwarz waveform relaxation methods

The Optimised Schwarz Methods were originally developed for stationary problems and have also been adapted to time-domain problems with step-by-step solutions, or with *global-in-time* strategies. The most used global-in-time approaches are based on Waveform Relaxation (WR) methods. In the work of Picard, an iterative method of successive approximations is proposed to prove the existence of solutions of a specific class of ordinary differential equations of the form $du/dt = f(u)$ [168]. This method distributes the computation on parallel computers by partitioning the system into subsystems and then use a Picard iteration to compute the global solution. The author showed that the convergence of the iterations was sufficient to prove the solution existence. This method was then parallelised by [128] to numerically solve a system of ODEs for problems related to integrated circuits. The waveform relaxation is a sort of domain decomposition method and has then been used to extend the classical Schwarz methods to time dependent problems [84, 90]. It led to the creation of *Schwarz waveform relaxation* (SWR) algorithms. These methods are based on a spatial decomposition of the domain similarly to classical DDMs for

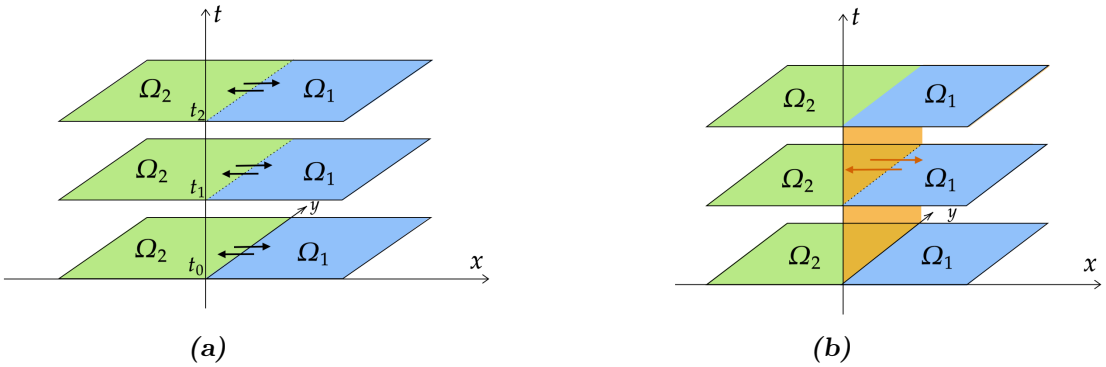

Figure 1.3: *(a) Schematic representation of the information exchange between two subdomains with a step-by-step domain decomposition method. (b) Schematic representation of the transient information exchange between two subdomains with a global-in-time domain decomposition method, over a finite time interval.*

stationary problems, but preserve the time dimension. Time dependent subproblems are solved on each subdomain over the whole time interval $[0, T]$ and transient boundary information are communicated through the interface. The subproblems solutions are then iterated, by means of global-in-time iterations [22]. Figure 1.3 illustrates the information transmission between subdomains for a step-by-step DDM and a Schwarz waveform relaxation method (global-in-time DDM). These global-in-time strategies have been adapted for various transient problems: parabolic PDEs [5, 90], wave equation [81] or advection diffusion equation [19]. Relying on a DDM approach, the spatial decomposition still enable the subdomains to have different physics, discretisations or numerical treatments. Moreover, one main computational advantage of WR methods over step-by-step approaches is that different time discretisations can be used for different components of the system according to the physical properties [99, 104].

Robin conditions for global-in-time procedures. The first Schwarz waveform relaxation (SWR) algorithm used Dirichlet conditions on the interfaces. For example in [82], a Dirichlet-Neumann and a Neumann-Neumann Waveform Relaxation method are proposed, as a natural generalisation of optimised Schwarz methods (OSM) for transient problems. But Schwarz waveform relaxation algorithms converge relatively slowly (except sometimes when the time interval is bounded and very short). Moreover it was shown in [81] that the Dirichlet transmission conditions used for the transmission of the information do not allow to construct non-overlaping SWR algorithm (see [19] for example).

To improve this convergence rate, optimised transmission conditions have been proposed. The corresponding algorithms are called optimised Schwarz waveform relaxation. Among other possibilities, Robin SWR uses Robin transmission conditions, Optimal SWR is related to transparent transmission conditions, and quasi-optimal SWR is based on accurate absorbing conditions. Generally speaking, optimised Schwarz waveform relaxation usually refers to Robin SWR, where the Robin parameters are optimised to ensure the fastest convergence possible of the algo-

rithm. Robin SWR was first introduced in [81] for one-dimensional wave and heat equations. The authors use Robin conditions and show that it leads to convergent non-overlapping Schwarz waveform relaxation algorithms. This optimised algorithm converges in a finite number of steps, equal to the number of subdomains. Since these first studies, the optimised Robin conditions have been used to solve a large number of problems: diffusion problems [104], parabolic problems [5], or advection reaction diffusion equations [19, 145].

Coupling parameter optimisation for optimised Schwarz waveform relaxation methods. Using optimised Schwarz waveform relaxation algorithms, the fundamental question is the selection of the Robin coupling parameter to optimise the convergence of the algorithm. A lot of research has been devoted to the determination of the optimal choice, for example for the wave equation [80] or the shallow water equation [145].

Two main strategies exist to find the optimal coupling parameter. The most common one consists in performing a convergence analysis to obtain an explicit estimate of the convergence factor and then to optimise it [19, 100]. It is usual to use a Fourier transform with respect to time to express the convergence factor in the frequency domain. Then the convergence factor is used to calculate an efficient Robin parameter in a defined range of frequencies [5, 51]. However, this strategy is problem dependent and the optimisation must be solved for each problem. The study in [5] also shows that there is not always a single Robin coefficient value, that would optimise the convergence independently of the number of iterations performed. The optimal value might change depending on the targeted iteration count and solution accuracy.

Some other studies use the theory of absorbing boundary conditions first introduced by [68] for the wave equation. These conditions allow to treat equations on an unbounded Ω domain. The problem is solved on a bounded sub-domain Ω_b. To ensure that the solution on Ω_b corresponds to the solution on Ω, a boundary conditions on $\partial\Omega_b$ is imposed such that no wave reflects on this boundary. These conditions have been applied to domain decomposition to make the interface between two subdomains "transparent" [153]. This leads to the so-called "Optimal SWR" methods, which have the optimal convergence of Schwarz algorithms in the sense that the algorithm converges in as many iterations as there are sub-domains [80]. These optimal transparent transmission operators are however non-local Dirichlet-to-Neumann operators. They can not be easily used in an algorithm and are inefficient due to their large computational cost [3]. They have to be locally approximated, usually with a Taylor development [145]. In [145] both methods (optimisation of the convergence rate and approximation of transparent conditions with a Taylor development) are compared for a convection-diffusion problem. The algorithm convergence rate is shown to be smaller when obtained with a Taylor's expansion for the high frequencies but the situation is reversed for low frequencies. Alternatively, some studies search for more specific approximations of the transparent operators. In [4], a particular asymptotic expansion is used instead of a Taylor development to derive an *a priori* approximation.

In the field of optimised Schwarz waveform relaxation it is nowadays clear that

using Robin boundary conditions in each subdomain rather than Neumann or Dirichlet can improve the convergence rate. However there are still a lot of ongoing studies on how to choose the coupling parameters values.

Convergence. There are two classical approaches to analyse the convergence of optimised Schwarz waveform relaxation algorithms. First, analyses were based on energy estimates [51, 80, 99, 104, 145]. Energy estimates are useful tools for proving well-posedness of initial boundary value problems. They have been used to analyse the convergence of Schwarz algorithms for steady problems before [59, 132]. Most of the convergence analysis proposed in the literature are based on this kind of approach. These convergence analyses are mostly performed using the continuous model, but we can mention for example [99] which proposes convergence proofs by energy estimates at the discrete (or semi-discrete) time level. This approach is quite general but does not provide an explicit expression of the convergence rate. For this reason, there are few studies that concretely estimate the convergence factor of Schwarz waveform relaxation methods (SWR). As a result, it is difficult to derive an explicit optimised value for the Robin parameter.

More detailed information on the convergence can be obtained using Fourier analysis, as first introduced in [90]. This second approach was essential for the optimisation of transmission conditions, see for example [19, 51] for parabolic problems, and [80] for the wave equation. Fourier transforms are used, then the classical domain decomposition methods developed for steady problems (as described in Section 1.1.1) are used, allowing to obtain convergence rates for each Fourier mode. When used for optimised Schwarz waveform relaxation methods, this approach thus helps choosing an optimised value for the Robin coupling parameter, that optimises the convergence factor over the bounded range of frequencies relevant to the analysis. We can also mention an alternative approach, based on discrete-time analysis: for simple schemes, it is based on the Z-transform (a discrete equivalent to the Laplace transform) rather than on Fourier transform [47, 102]. However, for both of these methods, numerical results obtained with this choice of Robin parameters do not always perform as efficiently as expected [193]. It is due to the fact that the Fourier- or Z-transform supposes an infinite time interval, while the actual simulation is necessarily performed on a finite one. The recent article [83] illustrates that the classical Fourier analysis result for Schwarz waveform relaxation does not predict the convergence rate for evolution problems. The authors propose a new Fourier analysis combined with kernel estimates that can explain more precisely the convergence phases of Schwarz waveform relaxation methods and that is also a new way to optimise the convergence factor in Robin boundary conditions. It has however only been applied for the heat equation and for the advection-reaction-diffusion equation.

The convergence of waveform relaxation methods depends on the type of equations that are solved, on the boundary conditions and also on the considered time interval. In [84] and [90], two classical bounds for the convergence of the original non-optimised SWR algorithms were derived when applied to the heat equation, both in one and higher spatial dimensions. An overlapping SWR method is studied in [84] and its linear convergence on unbounded time intervals (or long time windows) is shown for the heat equation by maximum principle arguments. At the same

time, [90] proves the superlinear convergence of the SWR method with overlap on bounded time intervals (for the convection-diffusion equation). More generally, SWR algorithms are known to have different convergence regimes: for linear dissipative systems of ODEs on long time windows, convergence is in general linear [35] whereas over short time windows, superlinear convergence is often observed [22]. The same conclusion is derived for the heat equation for example [84]. The convergence dependence on the considered time interval is a major difference to the step-by-step DDMs. Moreover [83] shows that SWR methods have different convergence phases when applied to the heat equation, which contrast to the linear convergence of the Schwarz methods for steady problems. For a time dependent heat equation the SWR method is shown to have first a rapid convergence phase, followed by a slow down, and finally convergence increases again to become superlinear. These different convergence phases were recently illustrated and justified with a Fourier mode analysis, but only with Dirichlet boundary conditions in the subdomains and with an overlap. Moreover the convergence analysis is justified in this article for large time intervals, but not for short time intervals. There are thus still a lot of ongoing works aiming at precisely estimating the convergence of SWR methods.

Remark. In this section we presented two approaches to treat transient problems with DDMs, the step-by-step methods based on domain decomposition and SWR methods. There are however other time parallel approaches developed to parallelised the solution of transient ODEs. We can mention multiple shooting [175], space-time multigrid methods [156] or direct time parallel methods [96]. A recent review on this topic is given in [164]. Comparisons between these strategies to time parallelise the computations might be found in [195] and in [106] for example.

1.3 DDMs for transient fluid-structure interaction problems

In this work, we focus on a transient fluid-structure interaction problem that we want to solve with a DDM, to iteratively use two distinct solvers in a non-intrusive manner. Our goal is to develop a global-in-time iterative domain decomposition method inspired from the SWR methods and adapted for a transient FSI problem. As illustrated in Section 1.2.1, most of the DDM used to solve fluid-structure interaction problems rely on step-by-step procedures, because of a mathematical obstacle preventing the development of this kind of global-in-time DDMs for fluid-structure interaction. As mentioned in Section 1.2.2, in domain decomposition approaches, the knowledge of the well-posedness for the continuous transient fluid-structure interaction problem, and also for initial-boundary value problems (IBVPs) involved, is essential in designing coupling algorithms. For the analysis of these transient IBVPs, mathematical methods and results are available and well documented since over a half-century (see for example [131]).

The acoustic scattering by a linear elastic obstacle has been extensively treated for the time-harmonic regime [107, 108, 141]. The study of the existence and uniqueness of its solution goes back at least to 1986 [101]. Usually in these studies, the

acoustic domain is unbounded and modeled with a boundary integral equation or by adding artificial absorbing conditions to truncate the domain. A more general case with a Lipschitz incident scattering wave is considered in [16]. In this article, the well-posedness of the frequency-domain counterpart of the acoustic-elastic FSIP (2.7) is established, with the variational approach and an artificial boundary.

However, there are very few results regarding the well-posedness of transient acoustic/elastic scattering problems. For the problem in the time domain, [13] uses a Laplace transform to show the well-posedness in the Laplace domain and then to deduce the well-posedness of the weak problem in time domain. This implies to introduce an artificial truncature to the fluid domain and an absorbing boundary condition based on a Dirichlet-to-Neumann operator. Another solvability result for the 3D problem is given in [129]. The authors extend the framework of [69, Ch. 7], based on the convergence of Galerkin approximations for IBVPs. The authors consider the variational form of a fluid-structure interaction problem and search for weak solutions that converge in the weak sense to a limit which solves the original strong formulation of the problem. Since our main objective in this work is to extend the principle of global-in-time domain decomposition methods to transient acoustic/elastic scattering problems, the first step will be to study and extend the current solvency results concerning these transient problems.

1.4 Conclusion

In this work, we will focus on an evolution fluid-structure interaction problem and solve it with a domain decomposition method. Two classical ways of treating transient problems with DDM approaches are step-by-step and SWR approaches. We have seen that step-by-step procedures have three disadvantages: they require as many resolutions in each sub-domain as there are time steps during the simulation time, and are efficient only if each stationary resolution has a low computational cost. And they need to impose a uniform time step for all subdomains, which means loosing one of the main features of DDMs, namely to adapt the numerical method to the physical properties of the subdomain. Lastly, the algorithm needs to communicate at each time step, which implies an additional computational cost due to the transmitted data, but also to an overhead cost independent of the amount of data transmitted. In parallel programming it is particularly recommended not to often communicate small amounts of information, and it can be very interesting to communicate larger packages of data at once over larger time interval.

To avoid these disadvantages, global-in-time domain decomposition methods were introduced [80]. They consist in solving time-dependent problems in the subdomains, in parallel, and exchange information through the space-time interface $\Gamma \times [0, T]$, instead of exchanging information at each time step. Procedures of this type are interesting when we want to use a costly or global-in-time numerical method in one subdomain and it is impossible to perform it for each time step for the whole simulation time. It also enables to use different time steps in each subdomain according to its physical properties [99, 104]. It is becoming a popular computational method for solving evolution partial differential equations in parallel. In the optimised Schwarz waveform relaxation literature, the fundamental question is the

selection of the Robin parameter to optimise the convergence of the algorithm.

Unlike step-by-step methods, SWR approaches have rarely been used to solve FSI problems. In this work we thus propose a DDM inspired from optimised Schwarz waveform relaxation for rapid transient fluid-structure interaction problems and provide a mathematical analysis of its convergence.

CHAPTER 2

A convergent global-in-time acoustic-elastic coupling

The objective of this chapter is to define a global-in-time iterative procedure based on a domain decomposition strategy to solve transient fluid-structure interaction problems, with a guaranteed convergence. Such an algorithm has been carried out before [146], by alternating resolutions of Neumann evolution problems over the whole time interval in the fluid and solid subdomains, but convergence issues have been observed. We therefore have two goals: (i) to mathematically explain these Neumann non-convergence and (ii) to propose an alternative global-in-time iterative coupling method, with a guaranteed convergence. This method is adapted from the classical optimised Schwarz waveform relaxation methods and relies on optimised boundary conditions in each subdomain.
To reach these goals, we first state the continuous transient FSI problem in Section 2.1. We then establish solvability results for this problem. The results differ by the assumed regularity on the transmission data on the acoustic-elastic interface. These solvability results provide mappings between the data and solution regularities, which are essential in designing convergent coupling algorithms. Knowing these data-to-solution mappings for the transient FSI problem, we then introduce in Section 2.3 a global-in-time iterative procedure, inspired from Schwarz Waveform Relaxation methods. This method is based on the iterative resolution of Neumann initial-boundary value problems (IBVPs). We then recall classical solvability results for the Neumann evolution problem and highlight the loss of the space-time regularity of the solution on the interface of the Neumann and Dirichlet problem with respect to the regularity of the data. These results allow to justify the non-convergence of the iterative method and prompt us in Section 2.4, to propose a second iterative method based on alternating Robin evolution problems solutions in each subdomain. We recall solvability results for the Robin IBVPs and highlight the conservation of the space-time regularity of the solution on the interface of the Robin problem with respect to the regularity of the data. In Section 2.5, we prove the convergence of this global-in-time iterative procedure. Finally, Section 2.6 presents a numerical illustration on a 2D test case which highlights the effect of data regularity on the solution.

Contents

2.1 Coupled fluid-structure interaction problem definition . 28
2.2 Solvability results 32
2.3 Global-in-time iterative coupling procedures 35
2.3.1 Global-in-time iterative method for transient FSI problems 35
2.3.2 Coupling iterations using Neumann boundary conditions . 37
2.3.3 Coupling iterations using Dirichlet boundary conditions . 41
2.3.4 Iterative loss of space-time regularity for boundary traces 42
2.4 Global-in-time iterative procedure based on Robin boundary conditions 43
2.4.1 Coupling iterations using Robin boundary conditions . . . 44
2.4.2 Robin boundary conditions definition 44
2.4.3 Solvability results for the Robin IBVPs 49
2.5 Proof of convergence for the iterative algorithm 51
2.6 Numerical illustration 56
2.7 Proofs of solvability results 59
2.8 Conclusion 73

2.1 Coupled fluid-structure interaction problem definition

In this section, we introduce the linear evolution problem governing the transient scattering of acoustic waves by an elastic obstacle. We consider a bounded linear elastic solid Ω_s submerged in a linear acoustic fluid (mass density ρ_f, acoustic wave velocity c_f) occupying the unbounded fluid region $\Omega_f := \mathbb{R}^d \setminus \overline{\Omega_s}$ (where d = 2 or d = 3 is the spatial dimension). We denote by $\Gamma := \partial\Omega_f = \partial\Omega_s$ the Lipschitz continuous boundary separating the solid and fluid domains, and by $\mathbf{n}$ the unit outward normal to Γ with respect to the solid domain. The elasticity tensor C is elliptic, the other coefficients c_f, ρ_f, ρ_s being positive and bounded away from 0. The fluid variables are the velocity potential ϕ, the velocity $\mathbf{v} = \nabla\phi$ and the pressure $p = -\rho_f \partial_t \phi$. The solid variables are the displacement $\mathbf{u}$ and the stress vector $\mathbf{t} := \sigma[\mathbf{u}].\mathbf{n}$.

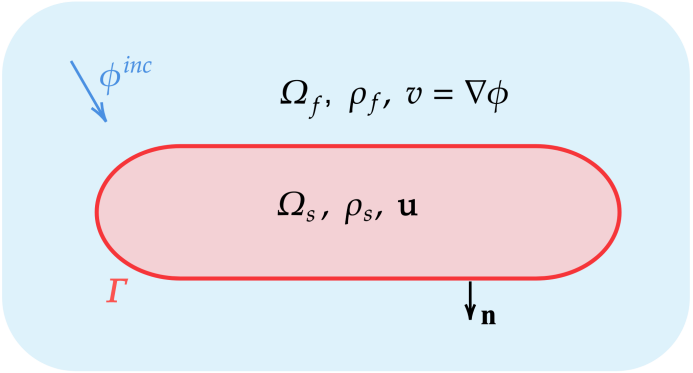

Figure 2.1: *FSI configuration: geometry and notations.*

We consider a velocity potential field ϕ, assumed to satisfy the wave equation

$$-\Delta\phi + \frac{1}{c_f^2}\partial_t^2\phi = 0 \quad \text{in } \Omega_f \times \mathbb{R}. \tag{2.1}$$

as the main variable describing the fluid motion. The primary excitation is a linear incident velocity potential field ϕ^{inc}, that solves at all times the homogeneous wave equation in $\mathbb{R}^d$, i.e.,

$$-\Delta\phi^{\text{inc}} + \frac{1}{c_f^2}\partial_t^2\phi^{\text{inc}} = 0 \quad \text{in } \mathbb{R}^d \times \mathbb{R}.$$

We assume that no disturbance caused by the presence of the elastic solid occurs before t = 0 ($\phi^{inc}(.,t) = 0$ in a neighbourhood of Ω_s for any t < 0). The main variable describing the solid motion is taken as the displacement $\mathbf{u}$, verifying the elastic wave equation

$$-\mathbf{\Delta_s}\mathbf{u} + \rho_s\partial_t^2\mathbf{u} = \mathbf{0} \quad \text{in } \Omega_s \times [0,T],$$

where $\mathbf{\Delta_s}$ is the Navier differential operator such that $\mathbf{\Delta_s} = \text{div}\,(\mathcal{C} : \nabla^{\mathbf{s}}\mathbf{u})$. The FSI then occurs due to the kinematical and dynamical transmission conditions (TCs):

$$\text{(a) } \partial_n\phi = \partial_t\mathbf{u}.\mathbf{n} \qquad \text{(b) } \mathbf{t}[\mathbf{u}] = \rho_f\partial_t\phi\mathbf{n} \qquad \text{in } \Gamma \times [0,T] \tag{2.2}$$

which express the continuity across Γ of the normal velocity and the traction vector. Moreover it is convenient to additively decompose the fluid variable ϕ in the FSIP definition. This decomposition can be done in several ways and influences the definition of the TCs (2.2):

1. The simplest additive decomposition consists in introducing a scattered field and to decompose ϕ according to

   $$\phi = \phi^{\text{inc}} + \phi^{\text{sc}}.$$

   The transmission conditions (2.2) can then be expressed in terms of ϕ^{sc} as

   $$\partial_n\phi^{\text{sc}} = \partial_t\mathbf{u}.\mathbf{n} - \partial_n\phi^{\text{inc}}, \qquad \mathbf{t}[\mathbf{u}] = \rho_f\partial_t\phi^{\text{sc}}\mathbf{n} + \rho_f\partial_t\phi^{\text{inc}}\mathbf{n} \qquad \text{in } \Gamma\times[0,T].$$

2. Introducing a Neumann-reflected and a radiated fields:

$$\phi = \phi^{\text{inc}} + \phi_N^{\text{ref}} + \phi^{\text{rad}}$$

The radiated field is the additive correction to the fluid motion induced by the interfacial motion. The reflected field ϕ^{ref} is defined so that the fluid motion for a rigid and motionless solid is given by $\phi^{\text{Ref}} := \phi^{\text{inc}} + \phi_N^{\text{ref}}$ and obtained by the resolution of an initial-boundary value problem:

$$\begin{cases} \Delta\phi_N^{\text{ref}} - \dfrac{1}{c^2}\partial_t^2\phi_N^{\text{ref}} = 0 & \text{on } \Omega_f \times [0,T], \\ \partial_n\phi_N^{\text{ref}} = -\partial_n\phi^{\text{inc}} & \text{on } \Gamma \times [0,T], \\ \phi_N^{\text{ref}}(0) = \partial_t\phi_N^{\text{ref}}(0) = 0 & \text{in } \Omega_f. \end{cases}$$

3. Introducing a Robin-reflected and a radiated fields

$$\phi = \phi^{\text{inc}} + \phi_R^{\text{ref}} + \phi^{\text{rad}}$$

where ϕ_R^{ref} is defined on the basis of the acoustic Robin IBVP, with a positive factor k_a:

$$\begin{cases} \Delta\phi_R^{\text{ref}} - \dfrac{1}{c^2}\partial_t^2\phi_R^{\text{ref}} = 0 & \text{on } \Omega_f \times [0,T], \\ (k_a\partial_n - \rho_f\partial_t)\phi^{\text{ref}} = -(k_a\partial_n - \rho_f\partial_t)\phi^{\text{inc}} & \text{on } \Gamma \times [0,T], \\ \phi_R^{\text{ref}}(0) = \partial_t\phi_R^{\text{ref}}(0) = 0 & \text{on } \Omega_f. \end{cases} \tag{2.3}$$

Using either of the foregoing additive decompositions, the coupled FSIP is thereafter formulated in terms of ϕ, as the main unknown for the fluid response. The main unknown ϕ is either referring to the scattered ϕ^{sc} or to the radiated variable ϕ^{rad}, depending on the chosen decomposition. In this chapter, we focus on an equivalent non-dimensional version of the FSI problem, obtained by expressing the coordinates $\mathbf{x}, t$, field variables, $\phi, \mathbf{u}, \mathbf{t}$ and material parameters $\mathcal{C}, \rho_s$ as

$$\mathbf{x} = b\widehat{\mathbf{x}}, \quad t = \frac{b\widehat{t}}{c_f}, \quad \phi = bc_f\widehat{\phi}, \quad \mathbf{u} = b\widehat{\mathbf{u}}, \quad \mathbf{t} = \rho_f c_f^2\widehat{\mathbf{t}}, \quad \mathcal{C} = \rho_f c_f^2\widehat{\mathcal{C}}, \quad \rho_s = \rho_f\widehat{\rho_s}$$

where b is a characteristic length. We hence consider the dimensionless IBVP (2.4). It consists of the standard exterior acoustic problem (2.4)(a) coupled with the elastodynamic equation (2.4)(b) governing the equilibrium of an elastic scatterer via the TCs (2.4)(c). The first transmission condition is a dynamic interface condition and the second is a kinematic interface condition, imposed to ensure the continuity of the normal component of the velocity.

$$\begin{cases} \Delta\phi - \partial_t^2\phi = 0 \text{ in } \Omega_f \times [0,T], & \phi(0) = \partial_t\phi(0) = 0 \quad \text{in} \quad \Omega_f & \text{(a)} \\ -\boldsymbol{\Delta}_{\mathbf{s}}\mathbf{u} + \rho_s\partial_t^2\mathbf{u} = \mathbf{0} \text{ in } \Omega_s \times [0,T], & \mathbf{u}(0) = \partial_t\mathbf{u}(0) = \mathbf{0} \quad \text{in} \quad \Omega_s & \text{(b)} \\ \mathbf{t} = \partial_t\phi\mathbf{n} + h\mathbf{n}, & \partial_n\phi = \partial_t\mathbf{u}.\mathbf{n} + \nu \quad \text{in } \Gamma \times [0,T] & \text{(c)} \end{cases} \tag{2.4}$$

where h and ν are prescribed time-dependent normal velocity and traction jumps across Γ, whose values depend on the chosen decomposition of ϕ:

$$\begin{array}{lllll} 1. & \nu = -\partial_n \phi^{\text{inc}} & h = \partial_t \phi^{\text{inc}} & \left(\phi = \phi^{\text{inc}} + \phi^{\text{sc}}\right) \\ 2. & \nu = 0 & h = \partial_t \left(\phi^{\text{inc}} + \phi_N^{\text{ref}}\right) & \left(\phi = \phi^{\text{inc}} + \phi_N^{\text{ref}} + \phi^{\text{rad}}\right) \\ 3. & \nu = -\dfrac{1}{k_a}\partial_t \left(\phi^{\text{inc}} + \phi_R^{\text{ref}}\right) & h = \partial_t \left(\phi^{\text{inc}} + \phi_R^{\text{ref}}\right) & \left(\phi = \phi^{\text{inc}} + \phi_R^{\text{ref}} + \phi^{\text{rad}}\right) \end{array} \tag{2.5}$$

All field variables of the system (2.4) are assumed to be at initial rest, so that homogeneous initial conditions are prescribed. The decomposition in a scattering and a radiation problem allows to deal with compactly supported variables in the coupled problem (2.4). As the radiated variable are at initial rest, all fluid variables are supported in a bounded fluid domain at any finite time t: $\Omega_{f(t)} = \{\mathbf{x} \in \Omega_f \mid \|\mathbf{x} - \Gamma\| < c_f t\}$. A consequence is that there is no need to artificially truncate the fluid domain and to add an absorbing boundary condition like in [16] and [13]. To simplify the notation, we omit thereafter the superscript "rad", with all fluid variables, which are understood to pertain to the radiated motion.

Variational formulation. In $\mathbb{R}^d$, we use the spaces

$$L^2(\Omega) := \left\{ f \mid \int_\Omega f^2 < \infty \right\}, \quad \text{and} \quad H^1(\Omega) := \left\{ f \mid f \in L^2(\Omega), \nabla f \in \left(L^2(\Omega)\right)^d \right\}.$$

In addition to the standard Sobolev spaces $L^2(\Omega_f), \mathbf{L^2}(\Omega_s) := L^2\left(\Omega_s, \mathbb{R}^d\right), H^1(\Omega_f)$ and $\mathbf{H^1}(\Omega_s) := H^1\left(\Omega_s, \mathbb{R}^d\right)$, we will use the spaces $H^1_\Delta(\Omega_f)$ and $\mathbf{H^1}_\Delta(\Omega_s)$ defined by

$$H^1_\Delta(\Omega_f) = \left\{ \phi \in H^1(\Omega_f), \Delta\phi \in L^2(\Omega_f) \right\}$$

and

$$\mathbf{H}^1_\Delta(\Omega_s) = \left\{ \mathbf{u} \in \mathbf{H^1}(\Omega_s), \mathbf{\Delta_s u} \in L^2(\Omega_s) \right\}.$$

We use the abbreviation for all the spaces as $C^m_T(X)$ for the space $C^m([0,T];X)$ of m times continuously differentiable functions $f : [0,T] \to X$ with values in a Hilbert space X.

To write this FSIP (2.4) in weak form, we use the standard approach. We multiply by time-independent test functions $\widetilde{\phi} \in H^1(\Omega_f)$ and $\widetilde{\mathbf{u}} \in \mathbf{H^1}(\Omega_s)$ for the wave equation and the elastodynamic equation respectively and perform an integration by parts. We denote $(v,w)_\Gamma$ or $(\mathbf{v},\mathbf{w})_\Gamma$ the $L^2(\Gamma)$ scalar products. The variational formulation involves the bilinear forms a, b (for the fluid domain) and A, B (for the solid domain) defined by

$$\begin{array}{ll} a(\phi,\widetilde{\phi}) = \int_{\Omega_f} \nabla\phi.\nabla\widetilde{\phi} d\Omega, & b(\phi,\widetilde{\phi}) = \int_{\Omega_f} \phi\widetilde{\phi} d\Omega, \\ A(\mathbf{u},\widetilde{\mathbf{u}}) = \int_{\Omega_s} \nabla^{\mathbf{s}}\mathbf{u} : \mathcal{C} : \nabla^{\mathbf{s}}\widetilde{\mathbf{u}} d\Omega, & B(\mathbf{u},\widetilde{\mathbf{u}}) = \int_{\Omega_s} \rho_s \mathbf{u}.\widetilde{\mathbf{u}} d\Omega. \end{array} \tag{2.6}$$

where $\nabla^{\mathbf{s}}\mathbf{u} := \frac{1}{2}\left(\nabla\mathbf{u} + (\nabla^{\mathbf{s}}\mathbf{u})^T\right)$ is the linearised strain tensor associated with a displacement $\mathbf{u}$ in Ω_s and $\mathcal{C}$ and ρ_s are the material parameters of the solid.

We then use the classical Green identities [148, Thm 4.4] for both the fluid and the solid media for Lipschitz domains Ω_f and Ω_s. Using the TCs in the resulting

interfacial integrals, the FSI problem (2.4) can be recast in variational form: find $(\phi, \mathbf{u}) \in C_T^0(\mathbf{H^1}) \cap C_T^1(\mathbf{L^2})$ such that, for all $\left(\widetilde{\phi}, \widetilde{\mathbf{u}}\right) \in \mathbf{H^1}$,

$$\begin{cases} a(\phi(t), \widetilde{\phi}) + b(\partial_t^2\phi(t), \widetilde{\phi}) + A(\mathbf{u}(t), \widetilde{\mathbf{u}}) + B(\partial_t^2\mathbf{u}(t), \widetilde{\mathbf{u}}) + I(\partial_t\mathbf{u}(t), \partial_t\phi(t), \widetilde{\mathbf{u}}, \widetilde{\phi}) = F_t(\widetilde{\mathbf{u}}, \widetilde{\phi}) \\ \mathbf{u}(0) = \partial_t\mathbf{u}(0) = 0 \text{ in } \Omega_s \qquad \phi(0) = \partial_t\phi(0) = 0 \text{ in } \Omega_f, \end{cases} \tag{2.7}$$

where F_t is the linear functional associated with the time-dependent interface data (h, ν), given by

$$F_t(\widetilde{\mathbf{u}}, \widetilde{\phi}) := (h(t)\mathbf{n}, \widetilde{\mathbf{u}})_\Gamma - \left(\nu(t), \widetilde{\phi}\right)_\Gamma \tag{2.8}$$

and I is the coupling bilinear form, given by

$$I\left(\mathbf{u}, \phi, \widetilde{\mathbf{u}}, \widetilde{\phi}\right) := -(\partial_t\phi, \mathbf{n}.\widetilde{\mathbf{u}})_\Gamma + \left(\partial_t\mathbf{u}.\mathbf{n}, \widetilde{\phi}\right)_\Gamma. \tag{2.9}$$

The FSI problem (2.4) and the variational problem (2.7) are equivalent in the following sense [24, Sec. 8]:

Proposition 1. $(\phi, \mathbf{u}) \in C_T^0(\mathbf{H}^1) \cap C_T^1(\mathbf{L}^2)$ *solves the FSIP* (2.4) *if and only if* $(\phi, \mathbf{u})$ *solves the variational problem* (2.7).

2.2 Solvability results

In this section, we analyse the well-posedness of the continuous transient acoustic-elastic scattering problem (2.4) and provide existence and uniqueness results, as well as continuous data-to-solution maps. Several results are given for different spatial regularity of the data. The proofs of well-posedness are given in Section 2.7.

Generally speaking, a mathematical problem is well-posed if its solution (a) exists, (b) is unique and (c) depends continuously on the problem data. For the linear FSIP (2.4), requirement (c) leads to a data g in a space D and a solution ϕ in a solution space X, verifying $\|\phi\|_X \leq C\|g\|_D$ for some constant C. Depending on D and X, multiple data-to solution mappings may be established. These mappings will be used later to design a convergent domain decomposition coupling algorithm.

The acoustic scattering by a linear elastic obstacle has been previously treated for the time-harmonic regime [107, 108, 141]. A more general case with a Lipschitz incident scattering wave is considered in [16]. In this article, the well-posedness of the frequency-domain counterpart of the acoustic-elastic FSIP (2.4) is established, with the standard variational approach and an artificial boundary. For the transient case, solvability results for the 2D transient FSIP in variational form are given in [13], but a 2D Dirichlet-to-Neumann map is used to artificially truncate the domain. Another solvability result for the 3D problem is given in [129] by extending the framework of [69, Ch. 7], based on the convergence of Galerkin approximations for IBVPs. While useful in abstract, those results are not well suited for studying the convergence of acoustic-elastic coupling iterations.

This motivated us to formulate and prove new solvability results for the transient acoustic-elastic scattering problem that can be later used to prove the convergence of

domain decomposition method based on global-in-time coupling iterations (see Section 2.5). We want these iterations to converge in $L^2([0,T],L^2(\Gamma))$ norm of iteration residuals, written in terms of velocities and conormal derivative of fluid and solid quantities on the shared interface Γ. In this context, the specificity of our work is that we establish solvability results for the FSIP, such that the relevant parts of the solution have a $L^2([0,T],L^2(\Gamma))$ regularity on Γ, while keeping regularity requirements on the data as low as possible to allow severe loadings potentially undergone in practice by submerged structures. To allow the least restrictive possible assumptions on the data, we focus on the weak forms of the FSIP (2.7). Three solvability results are derived, for different space regularity for the data. Theorem 2.2.1 is established for an interfacial data with a $H^{-1/2}(\Gamma)$ space regularity. Theorem 2.2.2 assumes an improved space regularity, $H^{1/2}(\Gamma)$ for that data. Finally Theorem 2.2.3 is established by mean of a Sobolev interpolation using the theorems 2.2.1 and 2.2.2. The transmission data has $L^2(\Gamma)$ regularity in space in that case. It is the main result for the justification of the iterative coupling procedure. These results and their proofs, detailed in Section 2.7, are an important contribution provided by this work.

To derive the first two results, we use a classical methodology based on the semigroup theory [28, 54, 114]. This method yields well-posedness results for strong (in time) solutions which are then used as a basis to obtain well-posedness results in the weak form for variational formulations. It consists in two main ideas:

1. We first assume a sufficient regularity in the data with respect to time to allow the existence of classical time derivatives wherever needed. We reformulate the evolution problem as a first-order system in time, and prove the existence and uniqueness of the strong solution using the Hille-Yosida theorem.

2. We then use energy identities and density arguments to extend the solvability results to a problem in weak form, assuming lower data regularity.

In the literature, the classical variational analysis framework for evolutions partial differential equations was primarily developed for homogeneous boundary conditions and body sources, not for transmission problems with interfacial data. It can however be adapted to cases involving non-homogeneous boundary data, which do not correspond to the classical theory, by reformulating the transmission problem to the classical format [110].

Spaces and norms definition.

We consider the FSI transmission problem (2.4) and its variational formulation (2.7). We denote Ω_s the elastic solid bounded by $\Gamma = \partial\Omega_s$, submerged in an acoustic fluid domain $\Omega_f := \mathbb{R}^3 \setminus \overline{\Omega_s}$. T is a chosen finite duration. We use shorthand notations for product spaces of potential-displacement pairs (or their velocities) equipped with the relevant graph norm, denoted

$$\mathbf{L}^2 := L^2(\Omega_f) \times \mathbf{L}^2(\Omega_s), \quad \mathbf{H}^s := H^s(\Omega_f) \times \mathbf{H}^s(\Omega_s), \quad \mathbf{H}^1_\Delta := H^1_\Delta(\Omega_f) \times \mathbf{H}^1_\Delta(\Omega_s)$$

and product spaces of pairs of interfacial traces or transmission data, denoted as

$$\mathbf{H}^s(\Gamma) := H^s(\Gamma) \times \mathbf{H}^s(\Gamma), \qquad \mathbf{L}^2(\Gamma) := \mathbf{H}^0(\Gamma).$$

Those results are formulated in terms of spaces of functions $f : [0,T] \to X$ with values in a Hilbert space X, which are taken as either $C_T^m(X)$ or $L^2([0,T];X)$, $H^m([0,T];X)$ (often abbreviated as $L_T^2(X)$, $H_T^m(X)$, respectively), equipped with the respective norms

$$\|\phi\|^2_{L^2([0,T];H)} = \int_0^T \|\phi(t)\|_H^2 \, dt, \quad \|\phi\|^2_{H^m([0,T];H)} = \sum_{k=0}^m \int_0^T \left\|\partial_t^k \phi(t)\right\|_H^2 dt.$$

For the $L^2(\Gamma)$ and $\mathbf{L}^2(\Gamma)$ norms, we retain the standard definitions $\|\phi\|_\Gamma^2 := \int_\Gamma \phi^2 dS$ and $\|\mathbf{u}\|_\Gamma^2 := \int_\Gamma |\mathbf{u}|^2 \, dS$.

Solvability results.

For the first result we consider transmission data with the "standard" space regularity for the variational problem (2.7).

Theorem 2.2.1 (Primary solvability result, data in $H^{-1/2}(\Gamma)$)**.** *Let Γ be a Lipschitz closed surface. Let $(\nu, h\mathbf{n}) \in H_T^1(\mathbf{H}^{-1/2}(\Gamma))$ with $(\nu, h\mathbf{n})(0) = (\nu', h'\mathbf{n})(0) = (0, \mathbf{0})$. Then, the transmission problem admits a unique solution $(\phi, \mathbf{u})$ with*

$$(\phi, \mathbf{u}) \in C_T^0(\mathbf{H}^1), \quad (\phi', \mathbf{u}') \in C_T^0(\mathbf{L}^2)$$

If $(\nu, h\mathbf{n}) \in H_T^2(\mathbf{H}^{-1/2}(\Gamma))$ with $(\nu, h\mathbf{n}) = (0, \mathbf{0})$, we have

$$(\phi, \mathbf{u}) \in C_T^0(\mathbf{H}^1_\Delta), \quad (\phi', \mathbf{u}') \in C_T^0(\mathbf{H}^1), \quad (\phi'', \mathbf{u}'') \in C_T^0(\mathbf{L}^2).$$

The proof for this Theorem 2.2.1 is given in Section 2.7. Then, still motivated by the objective of proving the convergence of global-in-time coupling iterations, we want to establish a solvability result for the FSIP with a transmission data that has $\mathbf{L}^2(\Gamma)$ regularity in space. We therefore aim at applying Sobolev interpolation and we thus first consider cases where the data has identical regularity in time but improved regularity in space relative to Theorem 2.2.1.

Theorem 2.2.2 (Primary solvability result, data in $H^{1/2}(\Gamma)$)**.** *Let Γ be a $C^{1,1}$ closed surface. Let $(\nu, h\mathbf{n}) \in L_T^2(\mathbf{H}^{1/2}(\Gamma))$. Then, the transmission problem admits a unique solution $(\phi, \mathbf{u})$ with*

$$(\phi, \mathbf{u}) \in C_T^0(\mathbf{H}^1), \quad (\phi', \mathbf{u}') \in C_T^0(\mathbf{L}^2).$$

If $(\nu, h\mathbf{n}) \in H_T^1(\mathbf{H}^{1/2}(\Gamma))$ with $(\nu, h\mathbf{n}) = (0, \mathbf{0})$, we have

$$(\phi, \mathbf{u}) \in C_T^0(\mathbf{H}^2), \quad (\phi', \mathbf{u}') \in C_T^0(\mathbf{H}^1), \quad (\phi'', \mathbf{u}'') \in C_T^0(\mathbf{L}^2).$$

Taking advantage of this to obtain corresponding improvement on the solution space regularity is not straightforward. For instance, elliptic regularity arguments cannot be readily invoked due to insufficient regularity of the accelerations. The energy estimates used to prove Theorem 2.2.2 also do not directly adapt to data with extra spatial smoothness. The main steps of the proof thus have to be modified, allowing to obtain by the same general approach the following additional set

of primary solvability results, proved in Section 2.7. Finally, to design a convergent coupling method based on global-in-time iterations, it convenient to consider transmission data whose space regularity is $\mathbf{L}^2(\Gamma)$ rather than $\mathbf{H}^{1/2}(\Gamma)$ or $\mathbf{H}^{-1/2}(\Gamma)$. Interpolation space arguments (see [131, Ch 1, 4]) are applicable to Theorems 2.2.1 and 2.2.2, yielding additional solvability mappings.

Theorem 2.2.3 (Interpolation solvability result)**.** *Let Γ be a $C^{1,1}$ closed surface. Let $(\nu, h\mathbf{n}) \in H^1_T(\mathbf{L}^2(\Gamma))$ with $(\nu, h\mathbf{n})(0) = (0, \mathbf{0})$. Then, the transmission problem admits a unique solution $(\phi, \mathbf{u})$ with*

$$(\phi, \mathbf{u}) \in C^0_T(\mathbf{H}^{3/2}), \quad (\phi', \mathbf{u}') \in C^0_T(\mathbf{H}^{1/2}).$$

In addition, the velocities have boundary traces, with $\phi' \,|_\Gamma \in L^2_T(\Gamma)$ and $\mathbf{u}' \,|_\Gamma \in \mathbf{L}^2_T(\Gamma)$ and we also have $\partial_n\phi \,|_\Gamma \in L^2_T(\Gamma)$ and $\mathbf{t}[\mathbf{u}] \,|_\Gamma \in \mathbf{L}^2_T(\Gamma)$.

This solvability result 2.2.3 is proved in Section 2.7. Here, the mapping derived has a data with $\mathbf{L}^2(\Gamma)$ space regularity while the solution has Neumann traces $\partial_n\phi, \mathbf{t}[\mathbf{u}]$ and boundary traces of velocities $\phi', \mathbf{u}'$ in $L^2_T(\Gamma)$, which is very useful for the analysis and justification of domain decomposition methods based on iteratively solving IBVPs in each domain. This result in particular will be used in Section 2.5 to prove the convergence of a domain decomposition algorithm to solve the FSIP (2.4). This also implies that both the acoustic and elastodynamic components of the transient FSIP (2.4) are Robin solutions whose respective Robin data is in $L^2_T(\Gamma)$.

These three solvability results provide mappings between the data and solution regularities. They are reported in the article [24]. The third Theorem 2.2.3 in particular, is an original result. It assumes transmission data with a space regularity $\mathbf{L}^2(\Gamma)$ and is useful to justify the convergence of iterations based on alternative solutions of IBVPs in each sub-domains.

2.3 Global-in-time iterative coupling procedures

In this section we introduce an iterative global-in-time method to solve a FSI problem. Many non-overlapping domain decomposition methods, including the Schwarz waveform relaxation methods (see Section 1.2.2) consist, for the present context of transient problems, in the construction of sequences $(\phi^n, \mathbf{u}^n)_{n\geq 0}$ which converge to the solution $(\phi, \mathbf{u})$ of problem (2.4) as $n \to \infty$, each iterate $(\phi^n, \mathbf{u}^n)$ solving a pair of decoupled initial-boundary value problems (IBVPs) in $\Omega_f \times [0, T]$ and $\Omega_s \times [0, T]$. We then justify with mathematical arguments how the choice of the IBVPs boundary conditions influence the iterations convergence.

2.3.1 Global-in-time iterative method for transient FSI problems

The resolution of a coupled problem like the radiation problem (2.4) with a partitioned approach inspired from SWR, leads to study two boundary value problems

defined in each subdomain. We consider one acoustic initial boundary value problem in the Ω_f fluid domain, and one elastodynamic IBVP in the Ω_s solid domain. Recalling that we omit the mention "rad" of all the radiated variables in (2.4), the elastodynamic IBVP at each iteration $n \geq 1$ is assumed to have the form:

$$\begin{cases} -\boldsymbol{\Delta}_{\mathbf{s}}\mathbf{u}^n + \rho_s \partial_t^2 \mathbf{u}^n = \mathbf{0} & \text{in } \Omega_s \times [0,T], \\ \boldsymbol{\Pi}_{\mathbf{s}}\left[\mathbf{u}^n\right] = \mathbf{G}_{\mathbf{s}}\left[\mathbf{u}^{n-1}, \phi^{n-1}\right] & \text{on } \Gamma \times [0,T], \\ \mathbf{u}^n(0) = \partial_t \mathbf{u}^n(0) = 0 & \text{in } \Omega_s. \end{cases} \tag{2.10}$$

Similarly, the acoustic IBVP at each iteration $n \geq 1$ is assumed to have the form:

$$\begin{cases} \Delta \phi^n - \partial_t^2 \phi^n = 0 & \text{in } \Omega_f \times [0,T], \\ \Pi_f\left[\phi^n\right] = G_f\left[\mathbf{u}^{n-1}, \phi^{n-1}\right] & \text{on } \Gamma \times [0,T], \\ \phi^n(0) = \partial_t \phi^n(0) = 0 & \text{in } \Omega_f. \end{cases} \tag{2.11}$$

$\boldsymbol{\Pi}_{\mathbf{s}}$ and Π_f are boundary operators such that $\mathbf{u}^n \to \boldsymbol{\Pi}_{\mathbf{s}}[\mathbf{u}^n]$ and $\phi^n \to \Pi_f[\phi^n]$, to be specified. At iteration n, $\mathbf{G}_{\mathbf{s}}\left[\phi^{n-1}, \mathbf{u}^{n-1}\right]$ and $G_f\left[\phi^{n-1}, \mathbf{u}^{n-1}\right]$ are boundary data that depend on the interfacial quantities for the previous iterate $n-1$, and on their first derivatives. We will note ${\mathbf{g}_{\mathbf{s}}}^n = \mathbf{G}_{\mathbf{s}}\left[\mathbf{u}^{n-1}, \phi^{n-1}\right]$ and $g_f^n = G_f\left[\mathbf{u}^{n-1}, \phi^{n-1}\right]$. With the notations $\phi = \phi[g_f]$ and $\mathbf{u} = \mathbf{u}[\mathbf{g}_{\mathbf{s}}]$ emphasising the dependence of these solutions on the respective boundary data, the iterative DDM consists in an algorithm defining a data sequence $(g_f^n, {\mathbf{g}_{\mathbf{s}}}^n)_{n\geq 0}$ such that the solution iterates verify the transmission conditions of the coupled FSIP (2.4c) in $\Gamma \times [0,T]$, in the limit $n \to \infty$, i.e.:

$$\text{(a)}\ \left(\mathbf{t}[{\mathbf{g}_{\mathbf{s}}}^n] - \partial_t \phi[g_f^n]\mathbf{n} - h\mathbf{n}\right) \to \mathbf{0}, \quad \text{(b)}\ \left(\partial_n \phi[g_f^n] - \partial_t \mathbf{u}[{\mathbf{g}_{\mathbf{s}}}^n]\mathbf{n} - \nu\right) \to 0 \tag{2.12}$$

with h and ν defined by (2.5). To satisfy these TCs in the limit, the sequence $\left(g_f^n, {\mathbf{g}_{\mathbf{s}}}^n\right)$ of data must have a definition that depends on the choice of the boundary operators $\boldsymbol{\Pi}_{\mathbf{s}}$ and Π_f. Indeed, the boundary operators and data must be such that if the iterative process converges, the limiting equalities

$$\boldsymbol{\Pi}_{\mathbf{s}}\left[\mathbf{u}\right] = \mathbf{G}_{\mathbf{s}}\left[\mathbf{u}, \phi\right], \quad \text{and} \quad \Pi_f\left[\phi\right] = G_f\left[\mathbf{u}, \phi\right] \tag{2.13}$$

are equivalent to the transmission conditions (2.4c) of the original FSIP. Natural choices for $\boldsymbol{\Pi}_{\mathbf{s}}$ and Π_f include

- boundary operators based on Neumann boundary conditions:

  $$\boldsymbol{\Pi}_{\mathbf{s}}[\mathbf{u}] := \mathbf{t}[\mathbf{u}] \qquad \text{and} \qquad \Pi_f[\phi] := \partial_n \phi.$$

  They specify the value of the (co)normal derivatives of the primary variables on Γ.

- boundary operators based on Dirichlet boundary conditions:

  $$\boldsymbol{\Pi}_{\mathbf{s}}[\mathbf{u}] := \partial_t \mathbf{u} \qquad \text{and} \qquad \Pi_f[\phi] := \partial_t \phi.$$

  They specify the value of the velocities on the boundary Γ.

- boundary operators based on Robin boundary conditions:

$$\mathbf{\Pi_s}[\mathbf{u}] := \mathbf{t}[\mathbf{u}] + \mathbf{K}\partial_t\mathbf{u} \quad \text{and} \quad \Pi_f[\phi] := -\partial_t\phi + K\partial_n\phi.$$

  where $K : L^2(\Gamma) \to L^2(\Gamma)$ and $\mathbf{K} : \mathbf{L}^2(\Gamma) \to \mathbf{L}^2(\Gamma)$ are time-independent symmetric, positive and boundedly invertible operators.

There exist other type of conditions ([66], [99], [113]).

Assume for the sake of argument that the iterative procedure is convergent, IBVPs (2.10) and (2.11) are solved until the difference between two successive iterates is small enough (stagnation criterion). For a given tolerance ϵ, the satisfaction of the criterion

$$\frac{\|(\partial_t\mathbf{u}^n - \partial_t\mathbf{u}^{n-1}).\mathbf{n}\|^2_{L^2_T(\Gamma)} + \|(\partial_n\phi^n - \partial_n\phi^{n-1})\|^2_{L^2_T(\Gamma)}}{\|\partial_t\mathbf{u}^{n-1}.\mathbf{n}\|^2_{L^2_T(\Gamma)} + \|\partial_n\phi^{n-1}\|^2_{L^2_T(\Gamma)}} \leq \epsilon \tag{2.14}$$

indicates that the solution has converged. In case of convergence, the transmission residual quantities associated with given boundary trace solutions also have to converge towards zero:

$$e_v^{\text{sol}} := \frac{\|\partial_n\phi^n - (\partial_t\mathbf{u^n}.\mathbf{n} + \nu)\|^2_{L^2_T(\Gamma)}}{\|\partial_n\phi^n\|^2_{L^2_T(\Gamma)}} \underset{n\to\infty}{\to} 0, \tag{2.15}$$

and

$$e_p^{\text{sol}} := \frac{\|\mathbf{t}[\mathbf{u^n}].\mathbf{n} - (h + \partial_t\phi^n)\|^2_{L^2_T(\Gamma)}}{\|\mathbf{t}[\mathbf{u^n}].\mathbf{n}\|^2_{L^2_T(\Gamma)}} \underset{n\to\infty}{\to} 0. \tag{2.16}$$

A third indicator $e_{v,p}$ combining the two interfacial transmission residuals is defined on the interface Γ by:

$$e_{v,p} := \frac{\|\partial_n\phi^n - (\partial_t\mathbf{u^n}.\mathbf{n} + \nu)\|^2_{L^2_T(\Gamma)} + \|\mathbf{t}[\mathbf{u^n}].\mathbf{n} - (h + \partial_t\phi^n)\|^2_{L^2_T(\Gamma)}}{\|\partial_n\phi^n\|^2_{L^2_T(\Gamma)} + \|\mathbf{t}[\mathbf{u^n}].\mathbf{n}\|^2_{L^2_T(\Gamma)}}. \tag{2.17}$$

2.3.2 Coupling iterations using Neumann boundary conditions

It could be found natural to adapt the IBVPs (2.10) and (2.11) by choosing

$$\mathbf{\Pi_s}[\mathbf{u}] := \mathbf{t}[\mathbf{u}] \qquad \text{and} \qquad \Pi_f[\phi] := \partial_n\phi$$

as boundary operators, based on the TCs (2.4c) of the coupled FSIP (2.4). In this case, it is straightforward to see that a sequence $(g_f, \mathbf{g_s})$ of Neumann data defined on $\Gamma \times [0, T]$ by

$$\mathbf{G_s}\left[\phi^{n-1}\right] := \left(\partial_t\phi^{n-1} + h\right)\mathbf{n}, \quad \text{and} \quad G_f\left[\mathbf{u}^{n-1}\right] := \partial_t\mathbf{u}^{n-1}.\mathbf{n} + \nu \tag{2.18}$$

will satisfy the TCs (2.4c) in the limit $n \to \infty$ if the iterations are convergent. We thus may define at each iteration, two Neumann IBVPs. In Ω_s the Neumann elastodynamic IBVP is:

$$\begin{cases} -\boldsymbol{\Delta}_{\mathbf{s}}\mathbf{u}^n + \rho_s \partial_t^2 \mathbf{u}^n = \mathbf{0} & \text{in } \Omega_s \times [0,T], \\ \mathbf{t}[\mathbf{u}]^n = \mathbf{G}_{\mathbf{s}}\left[\phi^{n-1}\right] & \text{on } \Gamma \times [0,T], \\ \mathbf{u}^n(0) = \partial_t \mathbf{u}^n(0) = \mathbf{0} & \text{in } \Omega_s, \end{cases} \tag{2.19}$$

and in Ω_f the acoustic Neumann IBVP is:

$$\begin{cases} \Delta \phi^n - \partial_t^2 \phi^n = 0 & \text{in } \Omega_f \times [0,T], \\ \partial_n \phi^n = G_f\left[\mathbf{u}^{n-1}\right] & \text{on } \Gamma \times [0,T], \\ \phi^n(0) = \partial_t \phi^n(0) = 0 & \text{in } \Omega_f. \end{cases} \tag{2.20}$$

However, Neumann conditions are known, in the domain decomposition theory, to often lead to convergence issues [39, 127] (see Section 1.1.1). Indeed, coupling iterations based on the Neumann IBVPs (2.19) and (2.20) were implemented in [146] and numerically found to diverge. To explain this non-convergence, we investigate the behaviour of this iterative procedure from a mathematical point of view.

Solvability results for the Neumann IBVPs

We now look at the well-posedness of the two Neumann IBVPs (2.19) and (2.20) and study the regularity of their trace solutions. The solvability of Neumann evolution problems is well-documented [110, 124, 125, 194]. In our case we are especially interested to recall some mappings between data and solution spaces, as they play an essential to explain the observed non-convergence of the global-in-time iterative algorithm based on problems (2.19) and (2.20).

We mention that the well-posedness proof for an evolution Neumann IBVP is given for example in [110, Sec 8.3]. The solvability mappings obtained are not quite optimal (see [125] for optimal results regarding the regularity requirements) but the proof is clear and concise. For completeness we provide a proof in Appendix C which follows the same methodology as for the FSIP (2.4) in Section 2.7, and yields the same solvability results as in [110]. As with the FSIP (2.4), the well-posedness result are first derived for the strong solution, using the semigroup theory and the Hille-Yosida theorem. Functional-analysis arguments are then used to additionally obtain well-posedness in the weak framework of variational formulations.

The generic elastodynamic Neumann IBVP in Ω_s is given by:

$$\begin{cases} -\boldsymbol{\Delta}_{\mathbf{s}}\mathbf{u} + \rho_s \partial_t^2 \mathbf{u} = \mathbf{0} & \text{in } \Omega_s \times [0,T], \\ \mathbf{t}[\mathbf{u}] = \mathbf{g}_{\mathbf{s}} & \text{on } \Gamma \times [0,T], \\ \mathbf{u}(0) = \partial_t \mathbf{u}(0) = \mathbf{0} & \text{in } \Omega_s. \end{cases} \tag{2.21}$$

and the generic acoustic Neumann IBVP in Ω_f by:

$$\begin{cases} \Delta \phi - \partial_t^2 \phi = 0 & \text{in } \Omega_f \times [0,T], \\ \partial_n \phi = g_f & \text{on } \Gamma \times [0,T], \\ \phi(0) = \partial_t \phi(0) = 0 & \text{in } \Omega_f. \end{cases} \tag{2.22}$$

The well-posedness proof is based on the application of the Hille-Yosida theorem (see Appendix C) and enables to prove the following solvability result:

Proposition 2 (Strong solvability for the Neumann IBVP)**.** *For the acoustic and the elastodynamic Neumann IBVP, we have:*
1. For $\mathbf{g_s} \in C^2_T(\mathbf{H}^{-1/2}(\Gamma))$*, such that* $\mathbf{g_s}(0) = 0$*, the system* (2.21) *has a unique solution* $\mathbf{u}$ *which verifies*

$$\mathbf{u} \in C^1_T(\mathbf{H}^1(\Omega_s)) \cap C^0_T(\mathbf{H}^1_\Delta(\Omega_s)).$$

2. For $g_f \in C^2_T(H^{-1/2}(\Gamma))$*, such that* $g_f(0) = 0$*, the system* (2.22) *has a unique solution* ϕ *which verifies*

$$\phi \in C^1_T(H^1(\Omega_f)) \cap C^0_T(H^1_\Delta(\Omega_f)).$$

This well-posedness proof also allows to derive useful energy estimates. For the Neumann IBVP (2.22), we derive the following estimate:

Lemma 2.3.1. *For any datum* $g_f \in C^2_T(H^{-1/2}(\Gamma))$ *defined on* $[0,T]$*, with* $g_f(0) = 0$*, the strong solution* $\mathbb{U} = (\phi, \partial_t\phi)$ *of the Neumann IBVP* (2.22) *verifies the estimate*

$$\sup_{t\in[0,T]} \|\mathbb{U}(t)\|^2_{H^1(\Omega_f)} \leq C\|g_f\|^2_{H^1_T(H^{-1/2}(\Gamma))}.$$

The constant $C > 0$ *depends on* T *and* Γ *but not on the datum* g_f*.*

These estimates indicate that the norm of the solution in the energy space is controlled by the norm of the datum. The solution ϕ and its time derivative $\partial_t\phi$ thus continuously depend the data. We follow the same method and derive similar energy estimates for the elastic IBVP (2.21). These estimates verified by the problems strong solutions then allow to obtain the following solvability theorem for the Neumann IBVPs in variational form, under weaker regularity assumptions on the data.

We consider the variational forms of problems (2.21) and (2.22). They are defined with the bilinear forms a, b, A, B (2.6). The elastic displacement $\mathbf{u}$ verifies the weak identity:

$$\text{Find } \mathbf{u}(t) \in \mathbf{H}^1(\Omega_s) \text{ such that}$$
$$\begin{cases} A(\mathbf{u}(t), \widetilde{\mathbf{u}}) + B(\partial_t^2\mathbf{u}(t), \widetilde{\mathbf{u}}) = (\mathbf{g_s}(t), \widetilde{\mathbf{u}})_\Gamma \quad \forall \widetilde{\mathbf{u}} \in \mathbf{H^1}(\Omega_s), t \in [0,T] \\ \mathbf{u}(0) = \partial_t\mathbf{u}(0) = 0 \quad \text{in } \Omega_s \end{cases} \tag{2.23}$$

and the velocity potential in Ω_f verifies the weak identity:

$$\text{Find } \phi(t) \in H^1(\Omega_f) \text{ such that}$$
$$\begin{cases} a(\phi(t), \widetilde{\phi}) + b(\partial_t^2\phi(t), \widetilde{\phi}) = -(g_f(t), \widetilde{\phi})_\Gamma \quad \forall \widetilde{\phi} \in H^1(\Omega_f), t \in [0,T] \\ \phi(0) = \partial_t\phi(0) = 0 \quad \text{in } \Omega_f \end{cases} \tag{2.24}$$

where g_f and $\mathbf{g_s}$ are the boundary data. The energy identity 2.3.1 allows to prove the following solvability result:

Theorem 2.3.2 (solvability of Neumann IBVPs)**.** *Let Γ be a Lipschitz closed surface. Let $g_f \in H^1_T(H^{-1/2}(\Gamma))$ and $\mathbf{g_s} \in \mathbf{H}^1_T(H^{-1/2}(\Gamma))$, with $g_f(0) = 0$ and $\mathbf{g_s}(0) = \mathbf{0}$. Then:*

1. The elastodynamic Neumann IBVP (2.23) has a unique solution $\mathbf{u}$ verifying (continuously in $\mathbf{g_s}$)

$$\mathbf{u} \in C^0_T(\mathbf{H}^1(\Omega_s)), \qquad \partial_t \mathbf{u} \in \mathbf{C}^0_T(L^2(\Omega_s)).$$

2. The acoustic Neumann IBVP (2.24) has a unique solution ϕ verifying (continuously in g_f)

$$\phi \in C^0_T(H^1(\Omega_f)), \qquad \partial_t \phi \in C^0_T(L^2(\Omega_f)).$$

Deterioration of Neumann data iterates

These solvability results (proved in Appendix C, and also presented in [110, Sec 8.3]) highlight that transient Neumann IBVPs do not preserve the space-time regularity of the solutions. Theorem 2.3.2 shows that for a Neumann datum $g \in H^1_T(H^{-1/2}(\Gamma))$, the IBVP (2.24) has a solution ϕ in $C^0_T(H^1(\Omega_f))$. By comparison with elliptic or frequency domain Neumann BVPs with $H^{-1/2}(\Gamma)$ Neumann data, the solution therefore loses about one order of regularity in time with respect to g. Equivalently, the solution ϕ can be in $C^1_T(L^2(\Omega_f))$, preserving the time regularity, but the spatial regularity then decreases, and defining a trace solution in velocity is not possible. The paper [125] contains many results on the well-posedness of the Neumann IBVP in terms of data-to-solution mappings. For example [125, Theorem 3.1.(iii)] states that:

$$\begin{aligned} \text{If } g \in H^1_T(L^2(\Gamma)), \text{ then:} \qquad \phi &\in C^0_T(H^{3/2}(\Omega)) \\ \partial_t \phi &\in C^0_T(H^{\alpha}(\Omega)) \\ \partial_t \phi\,|_\Gamma &\in C^0_T(H^{\alpha-1/2}(\Gamma)), \end{aligned}$$

where α is a known constant slightly larger than $1/2$. In this case, the boundary trace of the velocity solution is well-defined. But the time regularity of $\partial_t \phi\,|_\Gamma$ (and $\partial_t \mathbf{u}\,|_\Gamma$ similarly) is insufficient for (2.18) to generate $H^1_T(L^2(\Gamma))$ Neumann data for the next iteration. As a result, Neumann-Neumann iterations based on (2.18), (2.19) and (2.20) are such that the regularity of the successive Neumann data g_s^n and g_f^n deteriorates as iterations progress, making it impossible for them to converge in any space chosen a priori.

This contrasts with the well-known results for second-order elliptic Neumann BVPs, for which the above deterioration does not occur. As an example, the latter kind of problem typically has the form

$$\text{Find } \phi \in H^1(\Omega), \quad a(\phi, \widetilde{\phi}) = g(\widetilde{\phi}) \quad \text{for all } \widetilde{\phi} \in H^1(\Omega),$$

with a bilinear form a that is coercive on $H^1(\Omega)$. For an interfacial Neumann data g with $H^{-1/2}(\Gamma)$ space regularity, this elliptic problem has, by the Lax-Milgram theorem, a unique solution $\phi \in H^1(\Omega)$ [124]. A gain of $3/2$ in Sobolev regularity is thus achieved from the data g to the solution ϕ in Ω. Consequently, for classical

second order elliptic cases, the Neumann data yields the same time regularity for the trace solution in velocity $\partial_t\phi\,|_\Gamma$. By contrast Theorem 2.3.2 shows the same gain in spatial Sobolev regularity for the Neumann IBVP solution, but at the cost of one unit of Sobolev regularity in time. All the available results on the solvability of transient Neumann IBVPs confirm this observation and show that the Sobolev interior regularity of the solution ϕ is about $1/2$ above that of the Neumann data g, with same regularity in time for both, instead of $3/2$ for time-harmonic Neumann BVPs [124, 125, 194].

2.3.3 Coupling iterations using Dirichlet boundary conditions

Alternatively, an iterative method based on Dirichlet boundary conditions can be proposed. We adapt the IBVPs (2.10) and (2.11) by choosing

$$\mathbf{\Pi_s}[\mathbf{u}] := \mathbf{u} \qquad \text{and} \qquad \Pi_f[\phi] := \phi$$

as boundary operators. In this case, it is straightforward to see that to satisfy the TCs (2.4c) at convergence, a sequence $(\mathbf{G_s}, G_f)$ of Dirichlet data has to be defined on $\Gamma \times [0,T]$ by

$$\mathbf{G_s}\left[\phi^{n-1}\right] := \int_0^t \left(\partial_n\phi^{n-1} - \nu\right)\mathbf{n}(\tau)d\tau, \quad \text{and} \quad G_f\left[\mathbf{u}^{n-1}\right] := \int_0^t (\mathbf{t}[\mathbf{u}]^{n-1}.\mathbf{n} - h)(\tau)d\tau \tag{2.25}$$

We thus define at each iteration, two Dirichlet IBVPs. In Ω_s the Dirichlet elastodynamic IBVP is:

$$\begin{cases} -\mathbf{\Delta_s}\mathbf{u}^n + \rho_s\partial_t^2\mathbf{u}^n = \mathbf{0} & \text{in } \Omega_s \times [0,T], \\ \mathbf{u}^n = \mathbf{G_s}\left[\phi^{n-1}\right] & \text{on } \Gamma \times [0,T], \\ \mathbf{u}^n(0) = \partial_t\mathbf{u}^n(0) = \mathbf{0} & \text{in } \Omega_s, \end{cases} \tag{2.26}$$

and in Ω_f the acoustic Dirichlet IBVP is:

$$\begin{cases} \Delta\phi^n - \partial_t^2\phi^n = 0 & \text{in } \Omega_f \times [0,T], \\ \phi^n = G_f\left[\mathbf{u}^{n-1}\right] & \text{on } \Gamma \times [0,T], \\ \phi^n(0) = \partial_t\phi^n(0) = 0 & \text{in } \Omega_f. \end{cases} \tag{2.27}$$

These conditions are used to specify the value of the velocities on Γ (instead of the pressure and elastic stress which were imposed through Neumann conditions).

Solvability results for the Dirichlet IBVPs

The well-posedness for the Dirichlet IBVPs (2.27) and (2.26) has been proved and the associated data-to-solution mappings has been studied. A well-posedness proof for a second order hyperbolic Dirichlet BVP is given in [123] using a classical methodology based on energy estimates and functional analysis arguments, and different data-to-solution mappings are derived. We consider the generic elastodynamic Dirichlet IBVP in Ω_s given by:

$$\begin{cases} -\mathbf{\Delta_s}\mathbf{u} + \rho_s\partial_t^2\mathbf{u} = \mathbf{0} & \text{in } \Omega_s \times [0,T], \\ \mathbf{u} = \mathbf{g_s} & \text{on } \Gamma \times [0,T], \\ \mathbf{u}(0) = \partial_t\mathbf{u}(0) = \mathbf{0} & \text{in } \Omega_s. \end{cases} \tag{2.28}$$

and the generic acoustic Dirichlet IBVP in Ω_f given by:

$$\begin{cases} \Delta\phi - \partial_t^2\phi = 0 & \text{in } \Omega_f \times [0,T], \\ \phi = g_f & \text{on } \Gamma \times [0,T], \\ \phi(0) = \partial_t\phi(0) = 0 & \text{in } \Omega_f. \end{cases} \tag{2.29}$$

According to [123, Theorem 2.1], the following solvability result holds:

Proposition 3 (Strong solvability for the acoustic Dirichlet IBVP)**.** *For $g_f \in H_T^1(\Gamma)$, the system (2.29) has a unique solution ϕ which verifies*

$$\phi \in C_T^0(H^1(\Omega_f)), \quad \partial_t\phi \in C_T^0(L^2(\Omega_f)), \quad \partial_n\phi\,|_\Gamma \in L_T^2(\Gamma).$$

This result provides a continuous data-to-solution mapping. Stronger solvability results are also given there under stronger hypotheses on the data regularity. The solvability results in [123] holds for a generic Dirichlet evolution problem of the form

$$A(x,t)\phi + \partial_t^2\phi = f \quad \text{in } \Omega \times [0,T]$$

with a Dirichlet boundary condition on Γ and initial conditions at $t = 0$. The operator A is a second order elliptic operator. This regularity result thus also applies for the elastodynamic IBVP (2.28) and hold a similar data-to-solution mapping. In particular, $\mathbf{g_s} \in H_T^1(\Gamma)$ results in $\mathbf{t}[\mathbf{u}]\,|_\Gamma \in L_T^2(\Gamma)$.

With reference to (2.25), solving (2.26) with $\mathbf{G_s}[\phi^{n-1}] \in H_T^1(\Gamma)$ and (2.27) with $G_f[\mathbf{u}^{n-1}] \in H_T^1(L^2(\Gamma))$ yields data for the next iterate that verify $\mathbf{G_s}[\phi^n] \in H_T^1(L^2(\Gamma))$ and $G_f[\mathbf{u}^n] \in H_T^1(L^2(\Gamma))$. This indicates that, like their Neumann-Neumann counterpart, Dirichlet-Dirichlet iterations suffer from progressive deterioration of regularity and are thus unsuitable for the present global-in-time iterative treatment. It is moreover easy to verify, using classical regularity results, that the time-harmonic version of Dirichlet-Dirichlet iterations does not undergo progressive regularity degradation, and thus is a valid candidate for such iterations (whose convergence then remains to be established).

2.3.4 Iterative loss of space-time regularity for boundary traces

We illustrated how Neumann and Dirichlet IBVPs admit trace solutions whose regularity is insufficient for maintaining the regularity of the successive Dirichlet or Neumann data as iterations progress. Theorem 2.3.2 for example shows that transient Neumann IBVPs have solutions whose spatial regularity is lower (by about one unit) than that of the solutions of second-order elliptic Neumann BVPs. Consequently, for transient Neumann IBVPs, the boundary trace solution in velocity is not always well-defined and when it is defined, it has a lower regularity compared to the boundary data. Theorem 3 shows a similar behaviour for Dirichlet IBVPs. These observations are well-known [110, 123, 125] but are especially important for iterative domain decomposition methods that proceed by generating convergent sequences of IBVP solutions in each domain.

In fact, global-in-time iterations involving Neumann (or Dirichlet) boundary conditions in each subdomain, as defined in Section 2.3.2, are likely to be badly convergent or non convergent, since they resort to recursively defined Neumann (or Dirichlet) IBVPs, whose data deteriorates in regularity as iterations progress. As an example, consider an elliptic acoustic iterative example defined in Ω, with the following Neumann boundary conditions in Γ, for any $n > 0$:

$$\begin{cases} \partial_n \phi^n = i\omega \mathbf{u}^{n-1}.\mathbf{n} \\ \mathbf{t}[\mathbf{u}]^n = i\omega \phi^{n-1}\mathbf{n} \end{cases}$$

where ω is the frequency and $\mathbf{u}^{n-1}$, an elastic displacement value defined on Γ. The boundary data being $\mathbf{u}^{n-1}.\mathbf{n} \in L^2(\Gamma)$, classical elliptic regularity results implies that the problem has a solution $\phi^n \in H^1(\Omega)$ at least, and therefore, a boundary trace solution $\mathbf{n}\phi^n \ |_\Gamma \in L^2(\Gamma)$. In this case, the $L^2(\Gamma)$ regularity of the trace solution is preserved and iterating the elliptic problem solutions allows to stay in a fixed regularity space. A well-posedness proof for a time-harmonic acoustic-elastic problem presented in [16], shows similar regularity results. On the contrary, consider an equivalent time-domain Neumann problem as described in Section 2.3.2, with the following transient Neumann boundary conditions on Γ:

$$\begin{cases} \partial_n \phi^n = \partial_t \mathbf{u}^{n-1}.\mathbf{n} \\ \mathbf{t}[\mathbf{u}]^n = \partial_t \phi^{n-1}\mathbf{n} \end{cases}$$

If the boundary data $\partial_t \mathbf{u}^{n-1}$ is in $H^1_T(L^2_T(\Gamma))$, the solvability results [125] imply that the problem has a solution $\phi^n \in C^0_T(H^{3/2}(\Omega))$ and therefore, a boundary trace solution in velocity $\partial_t \phi^n \mathbf{n} \in C^0_T(H^{\alpha-1/2}(\Gamma))$. It is thus impossible to keep control variable iterates in a fixed regularity space (in $H^1_T(L^2_T(\Gamma))$ for example), which is a prerequisite to build convergent iterations. This explain the non-convergence of global-in-time iterations based on Neumann IBVPs observed in [146]. Dirichlet IBVPs solutions have the same behaviour and a similar procedure based on alternating Dirichlet IBVPs resolutions should present the same convergence problems (see Section 3.3.2).

Alternatively, in the context of global-in-time domain decomposition, it is known that using Robin boundary conditions in each subdomain instead of Neumann or Dirichlet can improve the convergence rate (see Chapter 1). This thus lead us to consider an alternative global-in-time iterative procedure based on Robin IBVPs.

2.4 Global-in-time iterative procedure based on Robin boundary conditions

The previous observations prompt us to consider another iterative procedure. In [146], the author suggests to modify the boundary conditions of each elastodynamic and acoustic evolution problem, at each iteration, and to choose impedance type conditions (Robin conditions) to improve the iterations convergence.

2.4.1 Coupling iterations using Robin boundary conditions

We now choose a linear combination of interfacial variables for the boundary operators in the IBVPs (2.10) and (2.11):

$$\mathbf{\Pi_s}[\mathbf{u}] := \mathbf{t}[\mathbf{u}] + \mathbf{K}\partial_t\mathbf{u}, \qquad \text{and} \qquad \Pi_f[\phi] := -\partial_t\phi + K\partial_n\phi \tag{2.30}$$

where $K : L^2(\Gamma) \to L^2(\Gamma)$ and $\mathbf{K} : \mathbf{L}^2(\Gamma) \to \mathbf{L}^2(\Gamma)$ are two linear time-independent symmetric, positive and boundedly invertible operators. In Ω_s, the elastodynamic Robin IBVP is given for $n \geq 1$ by:

$$\begin{cases} -\mathbf{\Delta_s}\mathbf{u}^n + \rho_s\partial_t^2\mathbf{u}^n = \mathbf{0} & \text{in } \Omega_s \times [0,T], \\ \mathbf{t}[\mathbf{u}^n] + \mathbf{K}\partial_t\mathbf{u}^n = \mathbf{G_s}\left[\mathbf{u}^{n-1}, \phi^{n-1}\right] & \text{on } \Gamma \times [0,T], \\ \mathbf{u}^n(0) = \partial_t\mathbf{u}^n(0) = \mathbf{0} & \text{in } \Omega_s. \end{cases} \tag{2.31}$$

In Ω_f, the acoustic Robin IBVP is:

$$\begin{cases} \Delta\phi^n - \partial_t^2\phi^n = 0 & \text{in } \Omega_f \times [0,T], \\ -\partial_t\phi^n + K\partial_n\phi^n = G_f\left[\mathbf{u}^{n-1}, \phi^{n-1}\right] & \text{on } \Gamma \times [0,T], \\ \phi^n(0) = \partial_t\phi^n(0) = 0 & \text{in } \Omega_f. \end{cases} \tag{2.32}$$

In the elastic condition $\mathbf{t}[\mathbf{u}] = \mathbf{G_s} - \mathbf{K}\partial_t\mathbf{u}$ the stress vector applied on the surface is modified with a quantity of opposite direction to the velocity. Similarly in the acoustic condition $p = G_f - Kv$ the pressure $p = -\partial_t\phi$ applied on the surface is modified by a quantity of opposite direction to the velocity ($\mathbf{K}$ and K being positive). If the iterations are convergent, the solution iterates $(\mathbf{u}^n, \phi^n)$ must verify the TCs (2.4c) of the coupled FSIP (2.4) in $\Gamma \times [0,T]$, in the limit $n \to \infty$. While the forms of the Neumann data for the Neumann IBVPs in Section 2.3.2 and the Dirichlet data for the Dirichlet IBVPs in Section 2.3.3 were straightforward and directly derived from the TCs, choosing the form of the Robin boundary data for the Robin IBVPs (2.31) and (2.32) is less evident.

2.4.2 Robin boundary conditions definition

The form of the Robin boundary conditions must be chosen to allow the convergence to the TCs with the iterations. We now aim at defining the exact form of the Robin boundary data $\mathbf{G_s}$ and G_f. Inspired by [49] where iterations with Robin boundary conditions are proved to be convergent and used to solve Helmholtz equations, we first introduce incoming and outgoing trace operators to reformulate the Robin iterations.

Incoming and outcoming trace operators.

The incoming trace operators are defined by

$$\mathbf{B}(\mathbf{u}) = \mathbf{t}[\mathbf{u}] + \mathbf{K}\partial_t\mathbf{u} \quad \text{and} \quad B(\phi) = -\partial_t\phi + K\partial_n\phi. \tag{2.33}$$

These trace operators can be understood as incoming operators on Γ in the sense that traces satisfying $B(\phi) = 0$ or $\mathbf{B}(\mathbf{u}) = 0$ are incoming relative to Ω_f and

Ω_s. We recall that $\mathbf{K}$ and K are two linear operators. They are assumed to be symmetric, positive and coercive $L^2_T(\Gamma) \to L^2_T(\Gamma)$ operators (they are thus invertible with bounded inverse). The elastic transmission operator $\mathbf{K}$ is additionally chosen to be of the form

$$\mathbf{K}\mathbf{w} = K_s(\mathbf{n}.\mathbf{w})\mathbf{n} + \mathbf{K}_T(P\mathbf{w}), \tag{2.34}$$

where $P := \mathbf{I} - \mathbf{n} \otimes \mathbf{n}$ is the projection on the tangent plane at a point of Γ. The linear operator $\mathbf{K}_T$ assumed to be symmetric and positive, is a mapping between tangential vector fields (i.e. vector fields $\mathbf{w}$ such that $\mathbf{w}.\mathbf{n} = 0$ on Γ). In particular $\mathbf{n}.\mathbf{K}_T(P\mathbf{w}) = 0$ for any vector field $\mathbf{w}$.

Still following [49], we also add two outgoing trace operators

$$\overline{B}(\phi) = \partial_t\phi + K\partial_n\phi \quad \text{and} \quad \overline{\mathbf{B}}(\mathbf{u}) = -\mathbf{t}[\mathbf{u}] + \mathbf{K}\partial_t u, \tag{2.35}$$

as it will prove very convenient to express all boundary traces as combinations of incoming and outgoing traces. They are termed "outgoing" traces in the sense that traces satisfying $\overline{B}(\phi) = 0$ or $\overline{\mathbf{B}}(\mathbf{u}) = 0$ are outgoing relative to Ω_f or Ω_s, respectively. B and $\overline{B}$ act on functions defined in Ω_f, while $\mathbf{B}$ and $\overline{\mathbf{B}}$ act on functions in Ω_s. All relevant boundary traces can be formulated as combinations of incoming and outgoing traces. Relations (2.33) and (2.35) can readily be inverted and any set of Dirichlet and Neumann traces on Γ are given in terms of the incoming and outgoing traces by

$$\begin{aligned} \partial_n\phi_i = \tfrac{1}{2}K^{-1}\left(\overline{B}(\phi) + B(\phi)\right); \quad \partial_t\phi = \tfrac{1}{2}\left(\overline{B}(\phi) - B(\phi)\right) \\ \mathbf{t} = \tfrac{1}{2}\left(\mathbf{B}(\mathbf{u}) - \overline{\mathbf{B}}(\mathbf{u})\right); \quad \partial_t\mathbf{u} = \tfrac{1}{2}\mathbf{K}^{-1}\left(\mathbf{B}(\mathbf{u}) + \overline{\mathbf{B}}(\mathbf{u})\right) \end{aligned} \tag{2.36}$$

With these notations and choosing

$$\mathbf{\Pi_s}[\mathbf{u}] = \mathbf{B}(\mathbf{u}), \qquad \text{and} \qquad \Pi_f[\phi] = B(\phi)$$

the Robin conditions (2.30) at iteration n are written

$$\mathbf{B}(\mathbf{u}^n) = \mathbf{G_s}[\mathbf{u}^{n-1}, \phi^{n-1}] \quad \text{and} \quad B(\phi^n) = G_f[\mathbf{u}^{n-1}, \phi^{n-1}], \tag{2.37}$$

The left hand side quantities are the incoming traces of ϕ^{n-1} and $\mathbf{u}^{n-1}$ through Γ, while the right hand side quantities are the Robin boundary data depending on the traces ϕ^{n-1} and $\mathbf{u}^{n-1}$ of the previous iterate. Moreover at convergence, the transmission conditions (2.4c) have to be verified and take the form

$$\begin{aligned} \mathbf{n}\left(B(\phi) - \overline{B}(\phi)\right) + \left(\mathbf{B}(\mathbf{u}) - \overline{\mathbf{B}}(\mathbf{u})\right) = 2h\mathbf{n}, \qquad \text{(a)} \\ K^{-1}\left(B(\phi) + \overline{B}(\phi)\right) - K_s^{-1}\left(\mathbf{n}.\mathbf{B}(\mathbf{u}) + \mathbf{n}.\overline{\mathbf{B}}(\mathbf{u})\right) = 2\nu. \qquad \text{(b)} \end{aligned} \tag{2.38}$$

These equations will help defining the appropriate form for $\mathbf{G_s}$ and G_f.

Derivation of RR iterations.

The Robin global-in-time iterations for the FSIP (2.4) can be formulated by means of the following heuristic. It can be thought of as an example of the "LArge Time

INcrement" (LATIN) framework, as it follows the general approach of this method of computational mechanics [122, 155]. It consists in alternating the verification of two sets of equations, namely

$$\begin{cases} (\varepsilon) : \text{uncoupled evolution equations for each medium } \Omega_s, \Omega_f \\ (\tau) : \text{transmission equations linking the two media at their shared interface } \Gamma. \end{cases}$$

In our case, (ε) are the uncoupled evolution problems (2.10) and (2.11) with arbitrary Robin datum, while (τ) refer to the TCs (2.4c).

Let then $({\mathbf{g_s}}^{n-1}, g_f^{n-1})$ be some Robin datum. Let $\mathbf{u}[{\mathbf{g_s}}^{n-1}], \phi[g_f^{n-1}]$ solve the Robin IBVPs (2.10) and (2.11), and have well-defined velocity and Neumann traces (or, equivalently, incoming and outgoing traces) on Γ. We then define the next datum iterate $({\mathbf{g_s}}^{n}, g_f^{n})$, and resulting solution iterate $(\mathbf{u}^n, \phi^n) = (\mathbf{u}[{\mathbf{g_s}}^{n}], \phi[g_f^{n}])$, by requiring that the transmission conditions (2.4c) be verified by the final incoming traces and the initial outgoing traces. We accordingly set

$$(B(\phi), \mathbf{B}(\mathbf{u})) = (B(\phi^n), \mathbf{B}(\mathbf{u}^n)) \quad \text{and} \quad (\overline{B}(\phi), \overline{\mathbf{B}}(\mathbf{u})) = (\overline{B}(\phi^{n-1}), \overline{\mathbf{B}}(\mathbf{u}^{n-1}))$$

in (2.38) and solve the resulting equations for $(B(\phi^n), \mathbf{B}(\mathbf{u}^n))$. This results in the final incoming traces being given by

$$\mathbf{B}(\mathbf{u^n}) = \mathbf{G_s}[\mathbf{u}^{n-1}, \phi^{n-1}], \quad \text{and} \quad B(\phi^n) = G_f[\mathbf{u}^{n-1}, \phi^{n-1}] \tag{2.39}$$

with

$$\begin{aligned} G_f[\mathbf{u}, \phi] &= \left(I - 2K_s H^{-1}\right) \overline{B}(\phi) + 2KH^{-1}\mathbf{n}.\overline{\mathbf{B}}(\mathbf{u}) + 2KH^{-1}\left(h + K_s \nu\right), \\ \mathbf{G_s}[\mathbf{u}, \phi] &= 2\mathbf{n}K_s H^{-1}\overline{B}(\phi) + \left(\mathbf{I} - 2\mathbf{n}KH^{-1}\mathbf{n}\right)\overline{\mathbf{B}}(\mathbf{u}) - 2\mathbf{n}KH^{-1}\left(h + K_s\nu\right) + 2h\mathbf{n}, \end{aligned} \tag{2.40}$$

in terms of the initial outgoing traces (with $H := K + K_s$ and I the identity operator in $L^2_T(\Gamma)$). Equations (2.39), (2.40) constitute the proposed iterations based on Robin conditions. These iterations thus consist in (i) evaluating the datum $({\mathbf{g_s}}^{n}, g_f^{n})$ and (ii) solving the Robin IBVPs (2.10) and (2.11) with that datum. Choosing adapted values for the positive parameters K and $\mathbf{K}_s$ can improve the convergence rate, as we will study later (see Section 3.3.3). Iterations can be started by solving problems (2.10) and (2.11) with arbitrarily chosen $({\mathbf{g_s}}^{0}, g_f^{0})$. The simplest choice is to set $({\mathbf{g_s}}^{0}, g_f^{0}) = (\mathbf{0}, 0)$, yielding $\overline{\mathbf{B}}(\mathbf{u}^0) = \mathbf{0}$ and $\overline{B}(\phi^0) = 0$ in formulas (2.40).

In this work, we will implement these iterations in a simpler form, by using the particular values $K = k_a I$, $K_s = k_s I$ and $\mathbf{K}_T = k_s(\mathbf{I} - \mathbf{n}\otimes\mathbf{n})$ (with $k_a, k_s > 0$) in the transmission operators. In this case, the incoming and outgoing traces are given by

$$\begin{aligned} B(\phi) &= -\partial_t\phi + k_a\partial_n\phi, & \mathbf{B}(\mathbf{u}) &= \mathbf{t}[\mathbf{u}] + k_s\partial_t\mathbf{u} \\ \overline{B}(\phi) &= \partial_t\phi + k_a\partial_n\phi, & \overline{\mathbf{B}}(\mathbf{u}) &= -\mathbf{t}[\mathbf{u}] + k_s\partial_t\mathbf{u}. \end{aligned}$$

We have $KH^{-1} = k_a/(k_a+k_s)I$ and $K_sH^{-1} = k_s/(k_a+k_s)I$, and the iterations (2.39) can be given a more-explicit form with

$$\begin{aligned} G_f[\mathbf{u}, \phi] &= \frac{k_a - k_s}{k_a + k_s}\overline{B}(\phi) + \frac{2k_a}{k_a + k_s}\mathbf{n}.\overline{\mathbf{B}}(\mathbf{u}) + \frac{2k_a}{k_a + k_s}(h + k_s\nu) \\ \mathbf{G_s}[\mathbf{u}, \phi] &= \frac{2k_s}{k_a + k_s}\overline{B}(\phi)\mathbf{n} + \left(\mathbf{I} - \frac{2k_a}{k_a + k_s}\mathbf{n}\otimes\mathbf{n}\right).\overline{\mathbf{B}}(\mathbf{u}) - \frac{2k_a}{k_a + k_s}(h - k_s\nu)\mathbf{n} + 2h\mathbf{n}. \end{aligned}$$

Matrix notation.

Still following [49], we now introduce matrix notations, in order to express $\mathbf{G_s}$ and G_f in a compact form. These notations will also be very helpful for studying the convergence of Robin-Robin coupling iterations thereafter. We set

$$\mathbb{B} = \begin{Bmatrix} B(\phi) \\ \mathbf{B}(\mathbf{u}) \end{Bmatrix}, \quad \overline{\mathbb{B}} := \begin{Bmatrix} \overline{B}(\phi) \\ \overline{\mathbf{B}}(\mathbf{u}) \end{Bmatrix}, \quad \mathbb{H} := \begin{Bmatrix} \nu \\ h\mathbf{n} \end{Bmatrix}. \tag{2.41}$$

The corresponding standard L^2 scalar product and norm on $\Gamma \times [0,T]$ are then

$$(\mathbb{B}, \mathbb{B}')_{\Gamma,T} := (B, B')_{\Gamma,T} + (\mathbf{B}, \mathbf{B}')_{\Gamma,T}\,; \quad \|\mathbb{B}\|^2_{\Gamma,T} := (\mathbb{B}, \mathbb{B})_{\Gamma,T}\,.$$

With the weighting operator matrix

$$\mathbb{K} := \begin{bmatrix} K^{-1} & 0 \\ 0 & \mathbf{K}^{-1} \end{bmatrix},$$

we define the weighted $L^2_T(\mathbf{L}^2(\Gamma))$ space-time scalar product and norm by

$$(\mathbb{B}, \mathbb{B}')_{\Gamma,T,\mathbb{K}} := (\mathbb{B}, \mathbb{K}\mathbb{B}')_{\Gamma,T}\,; \qquad \|\mathbb{B}\|^2_{\Gamma,T,\mathbb{K}} := (\mathbb{B}, \mathbb{K}\mathbb{B})_{\Gamma,T}\,.$$

By virtue of the assumptions made on K and $\mathbf{K}$, the norms $\|.\|^2_{\Gamma,T}$ and $\|.\|^2_{\Gamma,T,\mathbb{K}}$ are equivalent. We will denote by $\mathbb{L}^2_T(\Gamma)$ the space of sets of boundary traces $\mathbb{B}$ with finite norm $\|\mathbb{B}\|^2_{\Gamma,T}$ or $\|\mathbb{B}\|^2_{\Gamma,T,\mathbb{K}}$. Using these notations, the transmission conditions (2.38) take the form

$$\mathbb{B} = \mathbb{X}\mathbb{B} + \mathbb{L}\mathbb{H},$$

while the iterative procedure based on Robin iteration equations (2.37) becomes

$$\mathbb{B}_n = \mathbb{X}\overline{\mathbb{B}}_{n-1} + \mathbb{L}\mathbb{H} \tag{2.42}$$

where the vector $\mathbb{H}$ holds the transmission data and the operator matrices $\mathbb{X}$ and $\mathbb{L}$ are given by

$$\mathbb{X} = \mathbb{I} + 2\begin{bmatrix} -K_s H^{-1} & KH^{-1}\mathbf{n} \\ \mathbf{n}K_s H^{-1} & -\mathbf{n}KH^{-1}\mathbf{n} \end{bmatrix}, \qquad \mathbb{L} = \begin{bmatrix} 2KH^{-1}K_s & 2KH^{-1}\mathbf{n} \\ -2\mathbf{n}KH^{-1}K_s & 2\mathbf{I} - 2\mathbf{n}KH^{-1}\mathbf{n} \end{bmatrix}.$$

We note that the left hand side quantity is the incoming trace operator defined on Γ, while the right hand side quantity depends on the outgoing trace operator. In other words, this equation (2.42) expresses that on Γ, the incoming traces for the current iterate n are formulated in terms of the outgoing traces of the previous iterate $n-1$.

The matrix operator $\mathbb{X}$ (which plays the role of the *exchange operator* in [49]) has two properties, both easily checked by inspection, that will prove crucial for proving the convergence of Robin global-in-time iterations (see Section 2.5). Firstly, it is its own inverse:

$$\mathbb{X}\mathbb{X} = \mathbb{I} = \begin{bmatrix} I & 0 \\ 0 & \mathbf{I} \end{bmatrix}. \tag{2.43}$$

Secondly, we have

$$\mathbb{X}'\mathbb{K}\mathbb{X} = \mathbb{K}$$

so that $\mathbb{X}$ defines an isometry for the $\|.\|^2_{\Gamma,T,\mathbb{K}}$ norm:

$$\|\mathbb{X}\mathbb{B}\|^2_{\Gamma,T,\mathbb{K}} = \|\mathbb{B}\|^2_{\Gamma,T,\mathbb{K}} \quad \forall \mathbb{B} \in \mathbb{L}^2_T(\Gamma)$$

In particular, the iteration equation (2.42) can be inverted using the property (2.43), giving the identity

$$\overline{\mathbb{B}}_{n-1} = \mathbb{X}\left(\mathbb{B}_n - \mathbb{L}\mathbb{H}\right)$$

which plays a key role in the convergence proof for the iterative process. Upon convergence, (2.42) becomes

$$\mathbb{B} = \mathbb{X}\overline{\mathbb{B}} + \mathbb{L}\mathbb{H},$$

which is equivalent to the TCs (2.4c).

Likewise, considering a simpler form for these iterations, by using the particular values $K = k_a I$, $K_s = k_s I$ and $\mathbf{K}_T = k_s(\mathbf{I} - \mathbf{n}\otimes\mathbf{n})$ (with $k_a, k_s > 0$) in the transmission operators, the operator matrix $\mathbb{X}$ and $\mathbb{L}$ become

$$\mathbb{X} = \begin{bmatrix} \frac{k_a - k_s}{k_a + k_s} & \frac{2k_a}{k_a+k_s}\mathbf{n} \\ \frac{2k_a}{k_a+k_s}\mathbf{n} & \mathbf{I} - \frac{2k_a}{k_a+k_s}\mathbf{n}\otimes\mathbf{n} \end{bmatrix}, \qquad \mathbb{L} = \begin{bmatrix} \frac{2k_a k_s}{k_a+k_s} & \frac{2k_a}{k_a+k_s} \\ \frac{2k_a k_s}{k_a+k_s}\mathbf{n} & 2\mathbf{I} - \frac{2k_a}{k_a+k_s}\mathbf{n} \end{bmatrix}.$$

Relaxed iterations. An alternative scheme can be defined with "relaxed" Robin transmission conditions. This relaxation, used for example by [80] or recently in [49] for Robin iterative algorithms, introduces a tunable relaxation parameter $0 < r < 1$ that expands the scope of convergence rate optimisation. The iterations (2.39) become

$$B(\phi^n) = (1-r)B(\phi^{n-1}) + rG_f[\mathbf{u}^{n-1}, \phi^{n-1}] \tag{2.44}$$

and

$$\mathbf{B}(\mathbf{u}^n) = (1-r)\mathbf{B}(\mathbf{u}^{n-1}) + r\mathbf{G}_\mathbf{s}[\mathbf{u}^{n-1}, \phi^{n-1}] \tag{2.45}$$

with $\mathbf{G}_\mathbf{s}[\mathbf{u}^{n-1}, \phi^{n-1}]$ and $G_f[\mathbf{u}^{n-1}, \phi^{n-1}]$ still given by (2.40), and where $0 < r \leq 1$ is the relaxation parameter. Iterations (2.39) then correspond to (2.44) and (2.45) with $r = 1$. Using the matrix notations, the relaxed Robin iteration equation (2.42) becomes

$$\mathbb{B}_n = (1-r)\mathbb{B}_{n-1} + r\mathbb{X}\overline{\mathbb{B}}_{n-1} + r\mathbb{L}\mathbb{H}.$$

This iteration equation can be inverted as well, yielding

$$\overline{\mathbb{B}}_{n-1} = \mathbb{X}\left[\frac{1}{r}\overline{\mathbb{B}}_n + \left(1 - \frac{1}{r}\right)\mathbb{B}_{n-1} - \mathbb{L}\mathbb{H}\right] \tag{2.46}$$

This reformulation of the transmission conditions and the Robin-Robin iterations in terms of incoming and outgoing traces is crucial for proving the convergence of the proposed Robin iterations (see Section 2.5).

2.4.3 Solvability results for the Robin IBVPs

The convergence of the proposed Robin-Robin iterations relies in part in solvability results for Robin acoustic and elastodynamic IBVPs. We thus address now this issue, and focus on how the solvability depends on the Robin boundary datum. These solvability results will play a key role in the justification of the forthcoming domain decomposition iterative algorithm (see Section 2.5). The proof of well-posedness follows the same method as for the FSIP (2.4) in Section 2.2 and for the Neumann evolution problems in Section 2.3.2. This proof is detailed in Appendix D. The well-posedness result are first derived for the strong solution, using the semigroup theory and the Hille-Yosida theorem. Functional-analysis arguments are then used to additionally obtain well-posedness in the weak framework of variational formulations.
The generic elastodynamic Robin IBVP has the form:

$$\begin{cases} -\boldsymbol{\Delta}_{\mathbf{s}}\mathbf{u} + \rho_s \partial_t^2 \mathbf{u} = \mathbf{0} & \text{in } \Omega_s \times [0,T], \\ \mathbf{t}[\mathbf{u}] + k_s \partial_t \mathbf{u} = \mathbf{g_s} & \text{on } \Gamma \times [0,T], \\ \mathbf{u}(0) = \partial_t \mathbf{u}(0) = \mathbf{0} & \text{in } \Omega_s. \end{cases} \tag{2.47}$$

Likewise, the generic acoustic Robin IBVP is of the form:

$$\begin{cases} \Delta\phi - \partial_t^2 \phi = 0 & \text{in } \Omega_f \times [0,T], \\ -\partial_t \phi + k_a \partial_n \phi = g_f & \text{on } \Gamma \times [0,T], \\ \phi(0) = \partial_t \phi(0) = 0 & \text{in } \Omega_f. \end{cases} \tag{2.48}$$

Their variational formulations are defined with the bilinear forms a, b, A, B (2.6). The elastic displacement $\mathbf{u}$ verifies the weak identity:

$$\text{Find } \mathbf{u}(t) \in \mathbf{H}^1(\Omega_s) \text{ such that}$$
$$\begin{cases} A(\mathbf{u}(t), \widetilde{\mathbf{u}}) + C(\partial_t \mathbf{u}(t), \widetilde{\mathbf{u}}) + B(\partial_t^2 \mathbf{u}(t), \widetilde{\mathbf{u}}) = (\mathbf{g_s}(t), \widetilde{\mathbf{u}})_\Gamma \quad \forall \widetilde{\mathbf{u}} \in \mathbf{H^1}(\Omega_s), t \in [0,T] \\ \mathbf{u}(0) = \partial_t \mathbf{u}(0) = 0 \quad \text{in } \Omega_s \end{cases} \tag{2.49}$$

and the velocity potential in Ω_f verifies the weak identity:

$$\text{Find } \phi(t) \in H^1(\Omega_f) \text{ such that}$$
$$\begin{cases} a(\phi(t), \widetilde{\phi}) + c(\partial_t \phi(t), \widetilde{\phi}) + b(\partial_t^2 \phi(t), \widetilde{\phi}) = -\frac{1}{k_a}(g_f(t), \widetilde{\phi})_\Gamma \quad \forall \widetilde{\phi} \in H^1(\Omega_f), t \in [0,T] \\ \phi(0) = \partial_t \phi(0) = 0 \quad \text{in } \Omega_f \end{cases} \tag{2.50}$$

where g_f and $\mathbf{g_s}$ are Robin boundary data and where the bilinear forms c and C are:

$$c\left(\phi, \widetilde{\phi}\right) := \frac{\rho_f}{k_a} \int_\Gamma \phi \widetilde{\phi} d\Gamma \quad \text{and} \quad C(\partial_t \mathbf{u}, \widetilde{\mathbf{u}}) := k_s \int_\Gamma \partial_t \mathbf{u} \widetilde{\mathbf{u}} d\Gamma \tag{2.51}$$

The bilinear forms c and C are involved in the Robin problems (2.49) and (2.50), but neither appear in Neumann or Dirichlet IBVPs nor in the target FSI transmission problem (2.7). This feature results in different properties of the solutions in terms of

their regularity and those differences in turn affect the convergence of iterative FSI solution algorithms. The well-posedness proof is based, again, on the application of the Hille-Yosida theorem (see Appendix D) and enables to prove the following solvability result:

Proposition 4 (Strong solvability for the Robin IBVP)**.** *For the acoustic and the elastodynamic Robin IBVP, we have:*
1. For $\mathbf{g_s} \in C^2_T(\mathbf{L}^2(\Gamma))$*, with* $\mathbf{g_s}(0) = \mathbf{0}$*, the system* (2.47) *has a unique solution* $\mathbf{u}$ *which verifies*

$$\mathbf{u} \in C^1_T(\mathbf{H}^1(\Omega_s)).$$

2. For $g_f \in C^2_T(L^2(\Gamma))$*, with* $g_f(0) = 0$*, the system* (2.48) *has a unique solution* ϕ *which verifies*

$$\phi \in C^1_T(H^1(\Omega_f)).$$

This well-posedness proof also allows to derive useful energy estimates. For the Robin IBVP (2.48) these estimates are given by:

Lemma 2.4.1. *For any datum* $g_f \in C^2_T(L^2(\Gamma))$ *defined on* $[0,T]$*, with* $g_f(0) = 0$*, the strong solution* $\mathbb{U} = (\phi, \partial_t\phi)$ *of the Robin IBVP* (2.48) *verifies the estimate*

$$\sup_{t\in[0,T]} \|\mathbb{U}(t)\|^2_{H^1(\Omega_f)} \leq C\|g_f\|^2_{L^2_T(\Gamma)}.$$

The velocity trace on Γ *also verifies the estimate*

$$\|\partial_t\phi\|^2_{L^2_T(\Gamma)} \leq C\|g_f\|^2_{L^2_T(\Gamma)}.$$

The constants $C > 0$ *in each estimate depend on* T *and* Γ *but not on the datum* g_f*.*

These estimates indicate that the norm of the solution in the energy space is controlled by the norm of the datum. The solution ϕ and its time derivative $\partial_t\phi$ thus continuously depend the data. We follow the same method and derive similar energy estimates for the elastic IBVP (2.47). These estimates verified by the problems strong solutions then allow to obtain the following solvability theorem for the Robin IBVPs in variational form, under weaker regularity assumptions on the data:

Theorem 2.4.2 (Solvability of Robin IBVPs)**.** *Let* Γ *be a Lipschitz closed surface. Let* $\mathbf{g_s} \in \mathbf{L}^2_T(\Gamma)$ *and* $g_f \in L^2_T(\Gamma)$*. Then:*

1. The elastodynamic Robin IBVP (2.49) *has a unique solution* $\mathbf{u}$ *verifying (continuously in* $\mathbf{g_s}$*)*

$$\mathbf{u} \in L^2_T(\mathbf{H}^1(\Omega_s)), \qquad \partial_t\mathbf{u} \in \mathbf{L}^2_T(\Omega_s), \qquad \partial_t\mathbf{u}|_\Gamma \in \mathbf{L}^2_T(\Gamma).$$

2. The acoustic Robin IBVP (2.50) *has a unique solution* ϕ *verifying (continuously in* g_f*)*

$$\phi \in L^2_T(H^1(\Omega_f)), \qquad \partial_t\phi \in L^2_T(\Omega_f), \qquad \partial_t\phi|_\Gamma \in L^2_T(\Gamma).$$

Moreover, the above results on velocity traces imply that we also have

$$\partial_n\phi|_\Gamma \in L^2_T(\Gamma), \qquad \mathbf{t}[\mathbf{u}]|_\Gamma \in \mathbf{L}^2_T(\Gamma).$$

Unlike the Neumann and Dirichlet IBVPs, this solvability result highlights that transient Robin IBVPs produce boundary velocities and (co)normal derivatives whose regularity is the same as that of the Robin data. As an illustration, consider a time-domain Robin-Robin iteration as described in Section 2.3.4, with the following transient Robin boundary conditions on Γ:

$$\begin{cases} -\partial_t \phi^n + k_a \partial_n \phi^n = G_f\left[\mathbf{u}^{n-1},\ \phi^{n-1}\right] \\ \mathbf{t}[\mathbf{u}]^n + k_s \partial_t \mathbf{u}^n = \mathbf{G_s}\left[\mathbf{u}^{n-1},\ \phi^{n-1}\right] \end{cases}$$

If the boundary datum $G_f\left[\mathbf{u}^{n-1},\ \phi^{n-1}\right]$ is in $L^2_T(\Gamma)$, according to the Theorem 2.4.2, the Robin IBVP admits a velocity solution with $L^2_T(\Omega)$ interior regularity. In this case, the boundary trace solution in velocity is well-defined in $L^2_T(\Gamma)$. Transient Robin IBVPs thus have solutions whose regularity is similar to that of solutions of second-order elliptic Robin BVPs. Most importantly, the next Robin data generated by (2.39) will have the same regularity. In other words, unlike their Neumann-Neumann and Dirichlet-Dirichlet counterpart, Robin-Robin iterations do not experience regularity degradation.

Conclusion. The Robin acoustic and elastodynamic IBVPs are shown to be well-posed. Moreover, the recursive iterations with Robin boundary conditions can be shown to preserve the $L^2_T(\Gamma)$ regularity of all interfacial variables: each Robin datum $(\mathbf{G_s}, G_f)$ given by (2.40) is a $L^2_T(\Gamma)$ function, which in turn ensures that the next global-in-time Robin iterate has a $L^2_T(\Gamma)$ regularity and so on. This observation is very important for iterative domain decomposition methods that proceed by generating convergent sequences of IBVP solutions in each domain. In fact, global-in-time iterations involving Robin IBVPs will be shown in the next section not to suffer from the regularity-preservation issue observed with the global-in-time Neumann iterations and to produce a convergent iterative method.

2.5 Proof of convergence for the iterative algorithm

A sequence of Robin IBVPs solutions preserves the regularity of the velocity trace solution from one iteration to another. For a transmission data $(\nu, h\mathbf{n}) \in L^2_T(\mathbf{L}^2_T(\Gamma))$, the procedure preserves the regularity of all the velocity interface variables. We now develop a proof of convergence for the iterations in time-domain based on Robin IBVPs, under the solvability assumptions of Theorem 2.4.2. The case of a time-harmonic acoustic-acoustic problem is considered in [49]. The proof is based on establishing that the error between an iterate and the converged solution vanishes in the limit of infinitely many iterations. We follow a similar methodology.

Having reformulated the Robin TCs in terms of incoming and outgoing traces, the proof of convergence is based on establishing that the error between an iterate and the converged solution vanishes in the limit of infinitely many iterations. $\phi, v, \mathbf{u}, \mathbf{t}$ are the converged interfacial traces on Γ (which solve the FSIP (2.4)). We introduce error fields $\phi^q - \phi, v^q - v, \mathbf{u}^q - \mathbf{u}$ and $\mathbf{t}^q - \mathbf{t}$ at the q-th iteration. To limit notation repetitions the notations ϕ^q etc. refer to error fields, rather than absolute fields, for the remainder of this section. The errors ϕ^q verify the homogeneous wave equation

in Ω_f, while $\mathbf{u}^q$ solve the homogeneous elastodynamic equation in Ω_s. In particular we assume that $\mathbb{H} = 0$ in (2.41), which means that the velocity and pressure jumps h and ν are equal to zero. We introduce the energy $E^q(s)$ of the q-th iterate error at time s given by

$$E^q(s) := \frac{1}{2}\mathcal{E}\left(\phi^q(s), \mathbf{u}^q(s)\right) \tag{2.52}$$

where the energy functional $\mathcal{E}$ is defined, for any pair $(\phi, \mathbf{u}) \in C_T^0\left(H^1(\Omega_f) \times \mathbf{H}^1(\Omega_s)\right)$ satisfying (2.4a,b), by

$$\mathcal{E}\left(\phi(s), \mathbf{u}(s)\right) := a\left(\phi(t), \phi(s)\right) + b\left(\phi'(s), \phi'(s)\right) + A\left(\mathbf{u}(s), \mathbf{u}(s)\right) + B\left(\mathbf{u}'(s), \mathbf{u}'(s)\right), \tag{2.53}$$

with the bilinear forms a, b for the fluid domain and A, B for the solid defined by (2.6). $\mathcal{E}\left(\phi(s), \mathbf{u}(s)\right)$ is thus the sum of the potential and kinetic energies reached in the fluid and solid from a state of initial rest; in particular $\mathcal{E}\left(\phi(s), \mathbf{u}(s)\right) \geq 0$. The convergence proof will entail showing that $E^q(s) \to 0$ as $q \to \infty$. We start the discussion with an important identity for (2.52) and its summation over iterates.

Lemma 2.5.1. *For any set of fluid and solid variables solving the field equations, the energy $E^q(s)$ at any finite time $s \leq T$ is related to the incoming and outgoing traces by*

$$E^q(s) = \frac{1}{4}\left\|\mathbb{B}^q\right\|^2_{\Gamma,s,\mathbb{K}} - \frac{1}{4}\left\|\overline{\mathbb{B}^q}\right\|^2_{\Gamma,s,\mathbb{K}}$$

Moreover, let N be any integer, and assume $\mathbb{H} = 0$. The energies, incoming and outgoing traces of the first N relaxed iterate verify the identity

$$\sum_{q=0}^{N-1}\left\{E^q(s) + \frac{1}{r}\left(\frac{1}{r} - 1\right)\left\|\mathbb{X}\overline{\mathbb{B}}_q - \mathbb{B}_q\right\|^2_{\Gamma,s,\mathbb{K}}\right\} + \frac{1}{r}\left\|\mathbb{B}^N\right\|^2_{\Gamma,s,\mathbb{K}} = \frac{1}{r}\left\|\mathbb{B}^0\right\|^2_{\Gamma,s,\mathbb{K}} \tag{2.54}$$

Since the right-hand side in (2.54) does not depend on N while all terms are positive, the sum has a finite limit as $N \to \infty$, implying that

$$\lim_{q\to\infty}\left\{E^q(T) + \frac{1}{r}\left(\frac{1}{r} - 1\right)\left\|\mathbb{X}\overline{\mathbb{B}}^q - \mathbb{B}^q\right\|^2_{\Gamma,s,\mathbb{K}}\right\} = 0 \tag{2.55}$$

The fact that the error fields vanish in the limit $q \to \infty$ cannot be inferred solely from $\lim_{q\to\infty} E^q(\mathrm{T}) = 0$. It requires additional arguments. Here, the fact that $E^q(\mathrm{s})$ vanishes at any time $s \leq T$ together with the boundedness of the right-hand side of (2.54) for any value $s \leq T$ of the final time allows to establish convergence for any $0 < r \leq 1$.

Proof of lemma 2.5.1. Observing that equations (2.35) can be inverted and that (2.36) gives the trace variables in terms of the incoming and outgoing traces, it allows to express the right-hand side of (2.54) in terms of the incoming and outgoing traces

$$\begin{aligned}-\rho_f(v^q, \partial_t\phi^q)_{\Gamma,s} + (\mathbf{t}^q, \partial_t\mathbf{u}^q)_{\Gamma,s} &= \frac{1}{4}\left((B+\overline{B}), k^{-1}(B-\overline{B})\right)_{\Gamma,s,\mathbb{K}} + \frac{1}{4}\left((\mathbf{B}+\overline{\mathbf{B}}), (k_s)^{-1}(\mathbf{B}-\overline{\mathbf{B}})\right)_{\Gamma,s,\mathbb{K}} \\ &= \frac{1}{4}\left\|\mathbb{B}^q\right\|^2_{\Gamma,s,\mathbb{K}} - \frac{1}{4}\left\|\overline{\mathbb{B}}^q\right\|^2_{\Gamma,s,\mathbb{K}}\end{aligned} \tag{2.56}$$

Using the above equality in (2.52) yields the first identity of the lemma.
Then, since the traces of successive iterates of the error fields satisfy (2.46) with $\mathbb{H} = 0$, we rewrite $\overline{\mathbb{B}}^q$ in terms of $\mathbb{B}^q$ and $\mathbb{B}^{q+1}$, to obtain

$$\begin{aligned} -\rho_f(v^q, \partial_t\phi^q)_{\Gamma,s} + (\mathbf{t}^q, \partial_t\mathbf{u}^q)_{\Gamma,s} &= \frac{1}{4}\left\|\mathbb{B}^q\right\|^2_{\Gamma,s,\mathbb{K}} - \frac{1}{4}\left\|\mathbb{X}\left[\frac{1}{r}\mathbb{B}^{q+1} + \left(1-\frac{1}{r}\right)\mathbb{B}^q\right]\right\|^2_{\Gamma,s,\mathbb{K}} \\ &= \frac{1}{4}\left\|\mathbb{B}^q\right\|^2_{\Gamma,s,\mathbb{K}} - \frac{1}{4}\left\|\frac{1}{r}\mathbb{B}^{q+1} + \left(1-\frac{1}{r}\right)\mathbb{B}^q\right\|^2_{\Gamma,s,\mathbb{K}}. \end{aligned} \tag{2.57}$$

The the second equality is stemming from the isometry property of $\mathbb{X}$. The Hilbert space identity

$$\left\|\frac{1}{r}a + \left(1-\frac{1}{r}\right)b\right\|^2 = \frac{1}{r}\|a\|^2 + \left(1-\frac{1}{r}\right)\|b\|^2 - \frac{1}{r}\left(1-\frac{1}{r}\right)\|a-b\|^2$$

can then be applied in the above right-hand side. We have

$$\left\|\frac{1}{r}\mathbb{B}^{q+1} + (1-\frac{1}{r})\mathbb{B}^q\right\|^2_{\Gamma,s,\mathbb{K}} = \frac{1}{r}\left\|\mathbb{B}^{q+1}\right\|^2_{\Gamma,s,\mathbb{K}} + (1-\frac{1}{r})\left\|\mathbb{B}^q\right\|^2_{\Gamma,s,\mathbb{K}} - \frac{1}{r}(1-\frac{1}{r})\left\|\mathbb{B}^{q+1}-\mathbb{B}^q\right\|^2_{\Gamma,s,\mathbb{K}}$$

After noticing that the transition equation (2.46) with $\mathbb{H} = 0$ gives $\mathbb{B}^{q+1} - \mathbb{B}^q = r(\mathbb{X} - \overline{\mathbb{B}^q}\mathbb{B}^q)$, the identity (2.57) becomes

$$-\rho_f(v^q, \partial_t\phi^q)_{\Gamma,s} + (v_i^q, \partial_t\phi_i^q)_{\Gamma,s} = \frac{1}{4r}\left\|\mathbb{B}^q\right\|^2_{\Gamma,s,\mathbb{K}} - \frac{1}{4r}\left\|\mathbb{B}^{q+1}\right\|^2_{\Gamma,s,\mathbb{K}} + \frac{1}{4}(1-\frac{1}{r})\left\|\mathbb{X}\overline{\mathbb{B}}^q - \mathbb{B}^q\right\|^2_{\Gamma,s,\mathbb{K}}$$

Using the above equality in the right-hand side of (2.52) and rearranging so that the left and right-hand sides of the resulting identity feature only positive terms, we obtain

$$E^q(s) + \frac{1}{4r}\left\|\mathbb{B}^{q+1}\right\|^2_{\Gamma,s,\mathbb{K}} + \frac{1}{4}\left(\frac{1}{r}-1\right)\left\|\mathbb{X}\overline{\mathbb{B}}^q - \mathbb{B}^q\right\|^2_{\Gamma,s,\mathbb{K}} = \frac{1}{4r}\left\|\mathbb{B}^q\right\|^2_{\Gamma,s,\mathbb{K}} \tag{2.58}$$

(noticing that $\frac{1}{r}\left(\frac{1}{r}-1\right) > 0$ for any $0 < r \leq 1$). We finally perform N successive iterations (with $0 < q \leq N-1$), sum the energy equalities (2.58) for each iteration and notice a telescopic sum effect (the same terms $\frac{1}{4r}\left\|\mathbb{B}^q\right\|^2_{\Gamma,s,\mathbb{K}}$ appearing in the left- and right-hand sides of the sum for $1 < q \leq N-1$ and cancelling each other). This results in the second identity claimed in the lemma. □

Considering the energy defined at each iteration q as a function of the error fields, lemma 2.5.1 reformulates it as a function of the incoming and outgoing trace operators. The summation of the energies at each iteration shows that the error fields, and then the energy, tend towards 0 in the limit of the number of iterations.

Theorem 2.5.2. *The two-operator global-in-time iterations are convergent:* $\|\phi^q(s)\|_{H^1(\Omega_f)}$, $\|\partial_t\phi^q(s)\|_{L^2(\Omega_f)}$, $\|\mathbf{u}^q(s)\|_{\mathbf{H}^1(\Omega_s)}$ $\|\partial_t\mathbf{u}^q(s)\|_{\mathbf{L}^2(\Omega_s)}$ *all vanish in the limit* $q \to \infty$ *for the error fields, uniformly in time.*

Proof of theorem 2.5.2. The identity (2.54) holds for any choice of final time $s \leq T$. In particular, we have

$$\sum_{q=0}^{N-1} E^q(s) \leq \frac{1}{4r} \left\| \mathbb{B}^0 \right\|^2_{\Gamma,s,\mathbb{K}} = B(s)$$

We notice that $s \to B(s)$ is continuous, positive and non-decreasing, it is hence bounded above by $B(T)$. By definition of $2E^q(s)$

$$2E^q(s) = \underbrace{a\left(\phi^q(s), \phi^q(s)\right)}_{\|\nabla\phi^q(s)\|^2_{\rho_f}} + \underbrace{b\left(\partial_t\phi^q(s), \partial_t\phi^q(s)\right)}_{\|\partial_t\phi^q(s)\|^2_{\rho_f}} + \underbrace{A\left(\mathbf{u}^q(s), \mathbf{u}^q(s)\right)}_{\|\nabla\mathbf{u}^q(s)\|^2_{\rho_s}} + \underbrace{B\left(\partial_t\mathbf{u}^q(s), \partial_t\mathbf{u}^q(s)\right)}_{\|\partial_t\mathbf{u}^q(s)\|^2_{\rho_s}} \tag{2.59}$$

where $\|\cdot\|_{\rho_f}, \|\cdot\|_{\rho_s}$ denote weighted versions (by ρ_f and ρ_s, respectively) of the $L^2(\Omega_f)$ and $L^2(\Omega_s)$ norms. Therefore we have

$$\sum_{q=0}^{N-1} \|\partial_t\phi^q(s)\|^2_{\rho_f} \leq B(s), \quad \sum_{q=0}^{N-1} \|\partial_t\mathbf{u}^q(s)\|^2_{\rho_s} \leq B(s)$$

implying that $\|\partial_t\phi^q(s)\|^2_{\rho_f}$ and $\|\partial_t\mathbf{u}^q(s)\|^2_{\rho_s}$ vanish in the limit $q \to \infty$. Moreover $\phi^q(t) = \int_0^t \partial_t\phi^q(s)ds$, so

$$\sum_{q=0}^{N-1} \|\phi^q(t)\|^2_{\rho_f} \leq \int_0^t \sum_{q=0}^{N-1} \|\partial_t\phi^q(s)\|^2_{\rho_f} ds \leq \int_0^t B(s)ds$$

and by definition of (2.59), which gives a majoration of

$$\sum_{q=0}^{N-1} \|\nabla\phi^q(s)\|^2_{\rho_f} \leq 2\sum_{q=0}^{N-1} E^q(s) \leq 2B(s)$$

we obtain:

$$\sum_{q=0}^{N-1} \|\nabla\phi^q(t)\|^2_{\rho_f} + \|\phi_q(t)\|^2_{\rho_f} = \sum_{q=0}^{N-1} \|\phi^q(t)\|^2_{H^1(\Omega_f)} \leq \int_0^t B(s)ds + 2B(t) \quad \forall s \leq T$$

as the right hand side doesn't depend on q, in the limit of $q \to \infty$.

$$\lim_{q\to\infty} \|\phi^q(t)\|_{H^1(\Omega_f)} = 0 \quad \forall t \in [0,T]$$

Likewise $\mathbf{u}^q(t) = \int_0^t \partial_t\mathbf{u}^q(s)ds$, so

$$\sum_{q=0}^{N-1} \|\mathbf{u}^q(t)\|^2_{\rho_s} \leq \int_0^t \sum_{q=0}^{N-1} \|\partial_t\mathbf{u}^q(s)\|^2_{\rho_s} ds \leq \int_0^t B(s)ds.$$

By definition of (2.59), we have a majoration of

$$\sum_{q=0}^{N-1} \|\nabla\mathbf{u}^q(s)\|^2_{\rho_s} \leq 2\sum_{q=0}^{N-1} E^q(s) \leq 2B(s),$$

and we then apply the Korn's inequality (see e.g. [46, Thm. 6.15-1]), which gives a majoration of $\|\mathbf{u}^q(s)\|^2_{H^1(\Omega_s)}$ using the jacobian matrix symmetric part $\varepsilon(\mathbf{u}^q(s))$:

$$\|\mathbf{u}^q(t)\|^2_{H^1(\Omega_s)} \leq C_K \left(\|\mathbf{u}^q(t)\|^2_{L^2(\Omega_s)} + \|\varepsilon(\mathbf{u}^q(t))\|^2_{L^2(\Omega_s)} \right) \quad \text{with } C_K > 0$$

This majoration implies

$$\begin{aligned} \sum_{q=0}^{N-1} \|\mathbf{u}^q(t)\|^2_{H^1(\Omega_s)} &\leq C_K \left(\sum_{q=0}^{N-1} \|\mathbf{u}^q(t)\|^2_{\rho_s} + \frac{1}{2} \sum_{q=0}^{N-1} \|\nabla \mathbf{u}^q(t)\|^2_{\rho_s} \right) \\ &\leq C_K \left(\int_0^t B(s)ds + B(t) \right) \end{aligned}$$

as the right hand-side of (2.60) doesn't depend on q, in the limit of $q \to \infty$

$$\Rightarrow \lim_{q\to\infty} \|\mathbf{u}^q(t)\|_{H^1(\Omega_s)} = 0 \quad \forall t \in [0,T] \tag{2.60}$$

This convergence result shows that the error fields vanish in energy norm in the respective domains in the limit $q \to \infty$ for the error fields, uniformly in time. □

For the relaxed iterations (with a relaxation parameter r: $0 < r < 1$), we can prove a stronger convergence result. As for Helmholtz, [49] shows a stronger result, namely the geometric convergence, we would like to prove the geometric convergence of the Robin-Robin global-in-time iterations. But in the case of relaxed iterations in the time-domain, we only show the following result

Theorem 2.5.3. *Let $0 < r < 1$. The two-operator relaxed iterations based on Robin boundary conditions are convergent: $\|\phi^q(t)\|_{H^1(\Omega_f)}$, $\|\partial_t \phi^q(t)\|_{L^2(\Omega_f)}$, $\|\mathbf{u}^q(t)\|_{\mathbf{H}^1(\Omega_s)}$ and $\|\partial_t \mathbf{u}^q(t)\|_{\mathbf{L}^2(\Omega_s)}$ all vanish in the limit $q \to \infty$ for the error fields, uniformly in time. In addition, the Robin error trace iterates $\mathbb{B}^q$ vanish in the limit $q \to \infty$. If in addition the target FSI solution has its incoming and outgoing traces in $\mathbb{L}^2_T(\Gamma)$, the incoming trace iterates also converge in $\mathbb{L}^2_T(\Gamma)$ to the FSI traces:*

$$\mathbb{B}^q \to \mathbb{B} \quad \textit{in } \mathbf{L}^2_T(\Gamma) \quad (q \to \infty).$$

Proof of theorem 2.5.3. For 0<r<1, (2.55) implies that the sequence of partial

$$\sum_{q=0}^{N-1} \left\| \mathbb{X}\overline{\mathbb{B}}^q - \mathbb{B}^q \right\|^2_{\Gamma,T,\mathbb{K}} = \sum_{q=0}^{N-1} \left\| \mathbb{B}^{q+1} - \mathbb{B}^q \right\|^2_{\Gamma,T,\mathbb{K}}$$

is convergent with N $\to \infty$ from which we deduce that $\mathbb{B}^q$ is a Cauchy sequence of elements of $\mathbb{L}^2_T(\Gamma)$, and hence has a limit $\mathbb{B} \in \mathbb{L}^2_T(\Gamma)$ since $\mathbb{L}^2_T(\Gamma)$ is complete. Moreover, we must have $\mathbb{B} = 0$ since otherwise the Robin problem with data $\mathbb{B}$ that defines the converged error fields would have a solution of nonzero energy.

Now, we assume the target FSI solution has its boundary traces $\mathbb{B}^\star$, $\overline{\mathbb{B}}^\star$ in $\mathbb{B} \in \mathbb{L}^2_T(\Gamma)$. The absolute trace iterates $\mathbb{B}^q + \mathbb{B}^\star$ generated by the iterations verify

$$\left(\mathbb{B}^{q+1} + \mathbb{B}^\star\right) - \left(\mathbb{B}^q + \mathbb{B}^\star\right) = \mathbb{B}^{q+1} - \mathbb{B}^q$$

and hence also define a Cauchy sequence in $\mathbb{B} \in \mathbb{L}^2_T(\Gamma)$. Therefore the absolute trace iterates converge to $\mathbb{B}^\star$. □

Conclusion. We have shown that the error fields vanish in energy norm in the respective domains with the number of iterations, for any choice of positive coupling parameters k_a, k_s and of relaxation parameter r. This proves the convergence of the global-in-time coupling iterations based on Robin IBVPs, to the solution of the FSIP (2.4). We highlight that the proof is based on the particular form of the Robin datum at each iteration. Provided that these Robin data are well chosen at each iteration, convergence of the iterations is then guaranteed and they allow to solve the coupled FSIP. The availability of tunable parameters (impedances k_a, k_s and relaxation parameter r) expands the scope of convergence rate optimisation.

The two-operator variant was introduced reflexively by analogy with [49] (for time-harmonic acoustic-acoustic coupling) where it is necessary to obtain a geometric convergence for the relaxed iterations. It is however unclear in the present transient case whether the iterations convergence is geometric, and it has not been shown for the moment.

2.6 Numerical illustration

To illustrate the consequences of the above theorems on solutions space-time regularity, we consider a 2D configuration representative of the interaction between an acoustic wave and an immersed elastic solid. This 2D problem permits to illustrate how the solution of FSI transmission problem (2.4) depends on the data's space-time regularity. We consider the scattering of a wave by a bounded 2D elastic cylinder Ω_s, immersed in an acoustic fluid occupying the unbounded fluid region (Figure 2.2). We assume 2D conditions and plane strain deformations for the solid. Both media are at initial rest. The coupled FSI problem is defined on the exterior surface Γ.

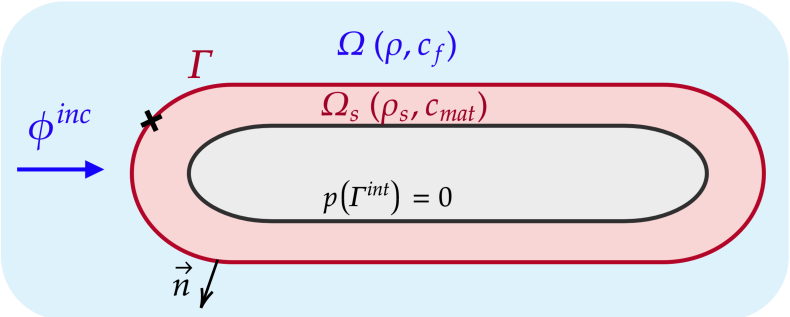

Figure 2.2: *Schematic representation of a fluid-structure interaction problem between an incident acoustic plane wave ϕ_{inc} and an elastic domain $\Omega_s(\rho_s, c_s)$.*

The potential fluid has a time dependent velocity potential $\phi(t)$, a velocity $\mathbf{v} = \nabla\phi$ and a pressure $p = -\rho_f \partial_t \phi \ \forall t \in [0, T]$. The solid variables are the displacement $\mathbf{u}$ and the stress vector $\mathbf{t} := \sigma[\mathbf{u}].\mathbf{n}$, where $\mathbf{n}$ is the outward unit normal to Ω_s. We numerically solve problem with an incident acoustic wave field ϕ_{inc} of the form of

$$\phi_{\text{inc}}(t, \mathbf{x}) = f(t - \frac{1}{c}\widehat{\mathbf{p}}.\mathbf{x})$$

where the function $t \to f(t)$ defines the time modulation of the propagating pulse and is assumed to have a compact support T. The unit vector $\widehat{\mathbf{p}}$ defines the direction of propagation. f is defined by

$$f(t) = \begin{cases} a(2\frac{t}{T_p})^\gamma \times (2 - 2\frac{t}{T_p})^\gamma & \text{if } t \in [0, T_p], \\ 0 & \text{if } t > T_p, \end{cases} \tag{2.61}$$

The exponent γ allows to impose the space-time regularity of the problem's data. In the numerical results, we use $a = 10^8$, a time parameter $T_p = 4.675\ 10^{-4}$. The obstacle has a characteristic length L and its height is l. The fluid and structure physical parameters are listed in Table 2.1. The time interval $[0, T]$ has a final time $T = 2.3\ 10^{-3}$ s and is discretised with $M = 1118$ time steps ($\Delta t = 1.7\ 10^{-6}$s).

We used a global-in-time iterative FEM/Z-BEM method based on Robin boundary conditions (see Section 3.3). The GMRES tolerance for the BEM frequency-domain solver is set to 10^{-6} and the accuracy ϵ of the discrete inverse Z transform is set to 10^{-5}. 1778 boundary elements are used on the exterior boundary and the 2D spatial elastic discretisation has $1.54\ 10^4$ DOF (mesh size h= 0.005 m). We solve the fluid-structure interaction problem with an iterative global-in-time FEM/Z-BEM coupling. We use an in-house FEM solver Matlab, based on the programmation material provided in [25]. We also developed a in-house fast Z-BEM solver Matlab based on the CQM method as described in [147]. We use an H-matrix method [43, 97] and a high frequency approximation (HFA) [146] to accelerate the resolution. For each transient BEM problem, 70 harmonic BEM problems corresponding to the lowest frequencies are computed and the other frequency solutions are approximated with an HFA. These 70 resolutions allow to solve the transient BEM problem with an error lower than 1% compared to the transient BEM solution obtained without HFA (see Section 3.5). We consider three values of γ and solve the FSI problem with

c_f	ρ_f	E	c_{mat}	ρ_s	ν	L	l
1500	1000	$210\ 10^9$	$6.0202\ 10^3$	7800	0.3	1.5	0.8
m.s^{-1}	kg.m^{-3}	$\text{kg.m}^{-1}\text{.s}^{-2}$	m.s^{-1}	kg.m^{-3}	/	m	m

Table 2.1: *Fluid and solid properties used.*

the three corresponding load. We use the same spatial and time discretisations for the three problems. Importantly, the load defined by $\gamma = 3$ is the only one to have a sufficient space-time regularity to meet the requirement of Theorem 2.2.3 and to allow the definition of a solution in $C^0([0, T])$. In Figure 2.3, we show for a given point on fluid-structure boundary (depicted on Figure 2.2): (a) the normalised elastic normal velocity with respect to time and (b) the normalised total fluid pressure also with respect to time, obtained after convergence of the global-in-time coupling. The convergence is reached when the relative error on the transmission residuals (2.17) becomes smaller than 10^{-3}, which is obtained after 49 iterations for the most regular case ($\gamma = 3$). As expected, with the discontinuous incident load $\gamma = 1$, the solution is discontinuous and strongly affected by instability phenomena. The load with a discontinuous derivative $\gamma = 2$ also shows instabilities and discontinuities but

to a lesser extent. Finally, the load $\gamma = 3$ is the only one that provides a regular solution in time. The space-time regularity of the data also affects the convergence

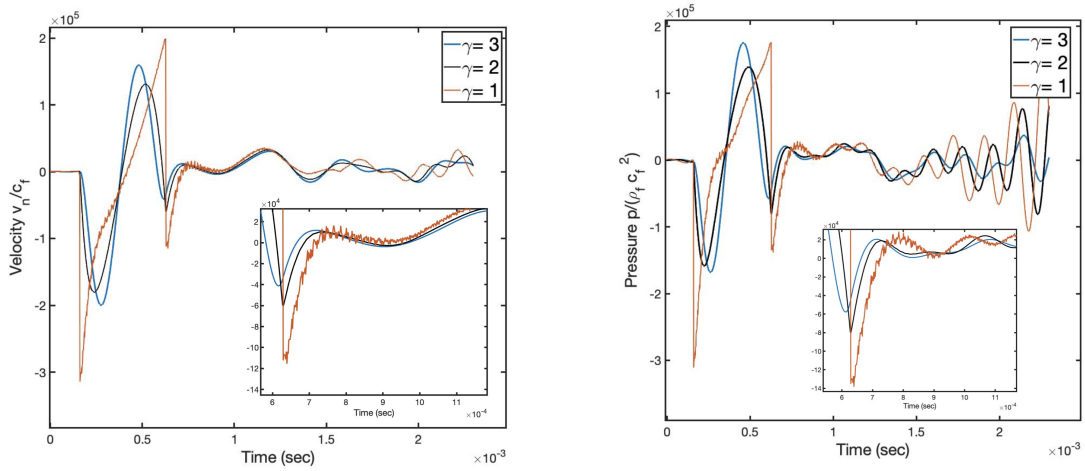

Figure 2.3: *Scattering by a 2D cylinder: (a) comparison between the normalised fluid normal velocities obtained with three different loads regularities and (b) comparison between the normalised fluid pressures obtained with three different loads regularities.*

of the iterative algorithm. To observe the algorithm convergence, we use the error indicator (2.17) defined on the transmission residuals in velocity and stress on the interface Γ. On Figure 2.4 the convergence of the transmission residuals with respect to the number of iterations is depicted, for three loads with different regularities. We observe that the convergence rate improves with the regularity of the imposed load: 49 iterations are necessary to reach the convergence for the most regular case ($\gamma = 3$) while 62 iterations are needed for the less regular one ($\gamma = 1$).

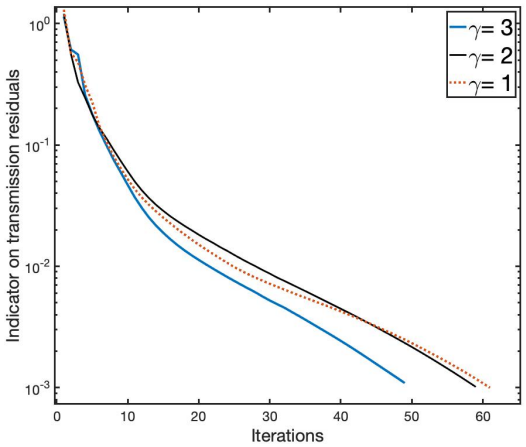

Figure 2.4: *Scattering by a 2D cylinder: convergence of indicator $e_{v,p}$ on the transmission residuals with the iterations, for three different loads regularities (Δt = 1.7 10^{-6}, El=1778, $k_c = \rho_s c_f$, Aitken acceleration).*

2.7 Proofs of solvability results

This section is now devoted to the proof of the three solvability theorems of Section 2.2. We first recall some results we will use. We begin by recalling the weak form of the first Green identity for both the fluid and the solid media, as they will be repeatedly invoked in this work. The following theorem rephrases Theorem 4.4 of [148].

Theorem 2.7.1 (first Green identities.)**.** *Let Ω_s be a bounded Lipschitz domain; its complement $\Omega = \mathbb{R}^d \setminus \overline{\Omega_s}$ then being an unbounded Lipschitz domain. The outward unit normal $\mathbf{n}$ to Ω_s is used on the common boundary $\Gamma = \partial\Omega = \partial\Omega_s$ for both domains. We denote by γ and γ_s the trace operators Ω and Ω_s, respectively.*
Let $u, v \in H^1(\Omega)$. If in addition $\Delta u \in L^2(\Omega)$, we have

$$(\nabla u, \nabla v)_\Omega = (-\Delta u, v)_\Omega - (\partial_n u, \gamma v)_\Gamma \tag{2.62}$$

Likewise, let $\mathbf{u}, \mathbf{v} \in \mathbf{H}^1(\Omega_s)$. If in addition $\boldsymbol{\Delta}_\mathbf{s}\mathbf{u} \in \mathbf{L}^2(\Omega)$, we have

$$(\mathcal{C} : \nabla^\mathbf{s}\mathbf{u}, \nabla^\mathbf{s}\mathbf{v})_{\Omega_s} = (-\boldsymbol{\Delta}_\mathbf{s}\mathbf{u}, \mathbf{v})_{\Omega_s} + (\mathbf{t}[\mathbf{u}], \gamma\mathbf{v})_\Gamma \tag{2.63}$$

The signs in front of the last terms of both identities stem from the orientation convention chosen for Γ.

2.2.1. Proof of Theorem 2.2.1

Theorem 2.2.1 is proven by means of the Hille-Yosida theorem. Its main steps are as follows: (i) recast the FSIP (2.4) in a first-order form; (ii) define a boundary data lifting; (iii) apply the Hille-Yosida theorem for the complementary part of the FSI solution, which obeys a non-homogeneous first-order system with homogeneous interface conditions; (iv) show that a weaker norm of the strong solution is controlled by a weaker norm of the data; and finally (v) define by density a weak solution satisfying the variational formulation (2.7).

Existence and uniqueness of a strong solution.

(i) First-order form of the FSIP.

In preparation to applying the Hille-Yosida theorem, we begin by recasting the FSIP into a first-order differential problem. Setting $\psi := \phi'$ and $\mathbf{v} := \mathbf{u}'$ to treat the velocities as separate unknowns, the system (2.4) yields the following first-order system for $\mathbb{U}(t) := (\phi, \psi, \mathbf{u}, \mathbf{v})^T(t)$:

$$\mathbb{U}' + A\mathbb{U} = 0, \quad \mathbb{U}(0) = 0, \quad B\mathbb{U} = \mathbb{H} \tag{2.64}$$

where $\mathbb{H} := (\nu, h\mathbf{n})^T$ is the boundary data. The unbounded differential operator A in $\Omega_f \times \Omega_s \times \Omega_f \times \Omega_s$ is defined by

$$A = \begin{bmatrix} 0 & -I & 0 & 0 \\ -\Delta & 0 & 0 & 0 \\ \mathbf{0} & \mathbf{0} & \mathbf{0} & -\mathbf{I} \\ \mathbf{0} & \mathbf{0} & -\boldsymbol{\Delta}_\mathbf{s} & \mathbf{0} \end{bmatrix}.$$

Applying A and the boundary operator B defined in $\Gamma \times \Gamma$ to $\mathbb{U}$, gives

$$A\mathbb{U} = \begin{Bmatrix} -\psi \\ -\Delta\phi \\ -\mathbf{v} \\ -\rho_s^{-1}\boldsymbol{\Delta}_\mathbf{s}\mathbf{u} \end{Bmatrix}, \quad B\mathbb{U} = \begin{Bmatrix} \partial_n\phi - \mathbf{v}.\mathbf{n} \\ \mathbf{t} - \rho_f\psi\mathbf{n} \end{Bmatrix}. \tag{2.65}$$

Due to the form of $\mathbb{U}$, we define the Hilbert space $\mathcal{H}$ by

$$\mathcal{H} := \mathbf{H}^1 \times \mathbf{L}^2 = H^1(\Omega_f) \times \mathbf{H}^1(\Omega_s) \times L^2(\Omega_f) \times \mathbf{L}^2(\Omega_s)$$

and the scalar product given, for any $\mathbb{U}, \widetilde{\mathbb{U}}$ in $\mathcal{H}$, by

$$(\mathbb{U}, \widetilde{\mathbb{U}})_\mathcal{H} := a(\phi, \widetilde{\phi}) + b(\phi, \widetilde{\phi}) + A(\mathbf{u}, \widetilde{\mathbf{u}}) + B(\mathbf{u}, \widetilde{\mathbf{u}}) + b(\psi, \widetilde{\psi}) + B(\mathbf{v}, \widetilde{\mathbf{v}}), \tag{2.66}$$

using the bilinear forms (2.6). Let also the space $\mathcal{H}_A$ and its scalar product $(\cdot,\cdot)_{\mathcal{H}_A}$ be defined by

$$\mathcal{H}_A := \{\mathbb{U} \in \mathcal{H}, A\mathbb{U} \in \mathcal{H}\} = \mathbf{H}^1_\Delta \times \mathbf{H}^1, \quad \left(\mathbb{U}, \widetilde{\mathbb{U}}\right)_{\mathcal{H}_A} = \left(\mathbb{U}, \widetilde{\mathbb{U}}\right)_\mathcal{H} + \left(A\mathbb{U}, A\widetilde{\mathbb{U}}\right)_\mathcal{H}. \tag{2.67}$$

We set the domain $\mathcal{D}(A)$ of operator A defined by (2.65) as

$$\mathcal{D}(A) = \{\mathbb{U} \in \mathcal{H}_A, B\mathbb{U} = 0\}.$$

This domain embeds the interfacial constraints $B\mathbb{U} = 0$ as essential conditions. Finally, the following density property, proved in [24, Sec. 8], is crucial for applying the Hille-Yosida theorem:

Lemma 2.7.2. *The space $\mathcal{D}(A)$ is a dense subspace of $(\mathcal{H}, \|\cdot\|_\mathcal{H})$.*

We note that the norm $\|.\|_\mathcal{H}$ arising from (2.67) is equivalent to the standard Sobolev product norm of $H^1(\Omega_f) \times \mathbf{H}^1(\Omega_s) \times L^2(\Omega_f) \times \mathbf{L}^2(\Omega_s) = \mathcal{H}$. This follows from the fact that relevant Sobolev norms in Ω_f or Ω_s can be expressed in terms of the bilinear forms (2.6), the $L^2(\Omega_f)$ and $H^1(\Omega_f)$ norms being then given by

$$\|\phi\|^2_{\Omega_f} = b(\phi, \phi), \qquad \|\phi\|^2_{1,\Omega_f} = a(\phi, \phi) + b(\phi, \phi). \tag{2.68}$$

and the $\mathbf{L}^2(\Omega_s)$ and $\mathbf{H}^1(\Omega_s)$ norms by

$$\|\mathbf{u}\|^2_{\Omega_s} = B(\mathbf{u}, \mathbf{u}), \qquad \|\mathbf{u}\|^2_{1,\Omega_s} = A(\mathbf{u}, \mathbf{u}) + B(\mathbf{u}, \mathbf{u}). \tag{2.69}$$

The norms given by (2.69) are equivalent to the usual L^2 and H^1 norms, for the solid thanks to Korn's inequality [46, Thm 6.15] and the assumed properties of the material parameters.

(ii) Interface data lifting.

To apply the Hille-Yosida theorem to the IBVP problem in first-order form, we need change the unknowns in order to obtain a system similar to (2.64) but with homogeneous boundary conditions. This is achieved by lifting the boundary data ν and h. This operation consists in finding a vector of functions $\mathbb{U}_L = (\phi_L, \psi_L, \mathbf{u}_L, \mathbf{v}_L)$ that verify the boundary conditions $B\mathbb{U}_L = \mathbb{H}$. Moreover, it is convenient to have $\mathbb{U}_L$ also verify the initial-rest conditions. To this end, let $\mu \in \mathbb{R}$, $\mu \neq 0$. The system

$$(\mu I + A)\,\mathbb{U}_L = 0, \quad B\mathbb{U}_L = \mathbb{H}, \tag{2.70}$$

has a unique solution $\mathbb{U}_L$. More precisely, we have the solvability result:

Lemma 2.7.3. *Let the data $\mathbb{H} \in X_T\left(\mathbf{H}^{-1/2}(\Gamma)\right)$ for some Banach space X, with $\mathbb{H} := (0, \mathbf{0})^T$. Then, the system (2.70) has a unique solution $\mathbb{U}_L$, defined by $\mathbb{U}_L = \{\phi_L, \psi_L, \mathbf{u}_L, \mathbf{v}_L\}^T \in X_T(\mathcal{H})$, verifying $\|\mathbb{U}_L\|_{X_T(\mathcal{H})} \leq C\|\mathbb{H}\|_{X_T(\mathbf{H}^{-1/2}(\Gamma))}$.*

Proof of Lemma 2.7.3. Eliminating ψ_L and $\mathbf{v}_L$, the remaining equations of system (2.70) are

$$\begin{aligned} -\Delta\phi_L + \mu^2\phi_L = 0 \ \text{ in } \Omega_f \times [0,T], \qquad & -\boldsymbol{\Delta}_{\mathbf{s}}\mathbf{u}_L + \rho_s\mu^2\mathbf{u}_L = \mathbf{0} \ \text{ in } \Omega_s \times [0,T], \\ \partial_n\phi_L - \mu\mathbf{u}_L.\mathbf{n} = \nu \ \text{ on } \Gamma \times [0,T], \qquad & \mathbf{t}[\mathbf{u}_L] - \mu\phi_L\mathbf{n} = h\mathbf{n} \ \text{ on } \Gamma \times [0,T]. \end{aligned}$$

They define for each $t \in [0,T]$ a transmission problem, which is set in weak form as

$$\text{Find } (\phi, \mathbf{u})(t) \in \mathbf{H}^1, \quad \mathcal{A}\left(\phi(t), \mathbf{u}(t); \widetilde{\phi}, \widetilde{\mathbf{u}}\right) = \mathcal{F}_t(\widetilde{\phi}, \widetilde{\mathbf{u}}) \quad \text{for all } (\widetilde{\phi}, \widetilde{\mathbf{u}}) \in \mathbf{H}^1 \tag{2.71}$$

with

$$\mathcal{A}\left(\phi(t), \mathbf{u}(t); \widetilde{\phi}, \widetilde{\mathbf{u}}\right) = a(\phi, \widetilde{\phi}) + \mu^2 b(\phi, \widetilde{\phi}) + A(\mathbf{u}, \widetilde{\mathbf{u}}) + \mu^2 B(\mathbf{u}, \widetilde{\mathbf{u}}) + \mu\left(\mathbf{u}.\mathbf{n}, \widetilde{\phi}\right)_\Gamma - \mu\left(\phi\mathbf{n}, \widetilde{\mathbf{u}}\right)_\Gamma$$

and $\mathcal{F}_t$ defined by (2.8). The bilinear forms are defined by (2.6). To apply the Lax-Milgram theorem, the bilinear form $\mathcal{A}$ has to be continuous and coercive. For the coercivity, we note that, if we choose $\left(\widetilde{\phi}, \widetilde{\mathbf{u}}\right) = (\phi, \mathbf{u})$, then

$$\left(\mathbf{u}.\mathbf{n}, \widetilde{\phi}\right)_\Gamma - \left(\phi\mathbf{n}, \widetilde{\mathbf{u}}\right)_\Gamma = 0.$$

This implies that for any $(\phi, \mathbf{u}) \in \mathbf{H}^1$, we have,

$$\mathcal{A}\left(\phi, \mathbf{u}; \widetilde{\phi}, \widetilde{\mathbf{u}}\right) \geq C\|(\phi, \mathbf{u})\|^2_{\mathbf{H}^1},$$

for some $C > 0$, i.e., that the bilinear form $\mathcal{A}$ is coercive on $\mathbf{H}^1$. Moreover, the linear functional $\mathcal{F}_t$ is continuous on $\mathbf{H}^1$ by assumption on $(\nu, h\mathbf{n})$. Problem (2.71) is therefore uniquely solvable in $\mathbf{H}^1$ by Lax-Milgram's theorem. The remaining equations of (2.70) then give $(\psi_L, \mathbf{v}_L) = \mu\,(\phi_L, \mathbf{u}_L) \in \mathbf{H}^1$, which gives the problem solvability. Finally, we have for each $t \in [0,T]$, $\|\mathbb{U}_L(t)\|_{\mathcal{H}} \leq C\|\mathbb{H}(t)\|_{\mathbf{H}^{-1/2}(\Gamma)}$, hence the claimed space-time estimate. □

Remark. For each $t \in [0,T]$, the system (2.70) is elliptic, hence the solvability result (Lemma 2.7.3) by invoking the standard Lax-Milgram argument. Moreover, the interior and boundary spatial regularity of ϕ_L and ψ_L results from usual elliptic regularity theory.

The interface data lifting now consists in reformulating the FSI system (2.64) using the new unknown $\mathbb{U}_c = \{\phi_C, \psi_C, \mathbf{u}_C, \mathbf{v}_C\}^T$ defined by $\mathbb{U}_c := \mathbb{U} - \mathbb{U}_L$. Since $\mathbb{U}$ and $\mathbb{U}_L$ respectively verify (2.64) and (2.70) and introducing the generic system

$$\mathbb{Z}' + A\mathbb{Z} = \mathbb{F}, \quad B\mathbb{Z} = 0, \quad \mathbb{Z}(0) = 0 \quad t \in [0,T] \tag{2.72}$$

where $\mathbb{Z}$ is the unknown and $\mathbb{F}$ is the datum. It follows that $\mathbb{U}_c$ solves system (2.72) with the particular data $\mathbb{F} := \mu\mathbb{U}_L - \mathbb{U}_L'$. This reformulation of the initial IVTP as a non-homogeneous first-order system with homogeneous interface conditions allows now to apply the Hille-Yosida theorem.

(iii) Application of the Hille-Yosida theorem.

The format of (2.72), together with the density property of Lemma 2.7.2, allows its solvability to be decided for any right-hand side $\mathbb{F}$ having appropriate regularity, if it satisfies the conditions of the Hille-Yosida theorem [91, Chap. II, Theorem 1.3]. The application of this theorem yields the desired strong solvability result:

Proposition 5 (Strong solvability for the FSIP)**.** *Assume that either* $\mathbb{F} \in C^1_T(\mathcal{H})$ *or* $\mathbb{F} \in C^0_T(\mathcal{D}(A))$*. Then, the system* (2.72) *has a unique solution* $\mathbb{Z} \in C^1_T(\mathcal{H}) \cap C^0_T(\mathcal{D}(A))$*.*

Proof of Proposition 5. To prove the solvability of problem (2.72) using the Hille-Yosida theorem, we need to verify that there exists $\lambda \in \mathbb{R}$ such that $A_\lambda = A + \lambda I : \mathcal{D}(A) \to \mathcal{H}$ is *maximal monotone*. A_λ is said to be maximal monotone if it satisfies

1. $(A_\lambda U, U)_H \geq 0$ for any $U \in D(A)$ (A_λ monotone),
2. For any $F \in H, \exists U \in D(A)$ such that $(A_\lambda + I)U = F$ ($A_\lambda + I$ surjective).

Proving that the above conditions are indeed met will be facilitated by the following lemma:

Lemma 2.7.4. *For any* $\mathbb{U} \in \mathcal{D}(A)$*, we have*

$$(a)\ \ (A\mathbb{U}, \mathbb{U})_{\mathcal{H}} = -b(\psi,\phi) - B(\mathbf{v},\mathbf{u}), \qquad (b)\ \ 2|(A\mathbb{U}, \mathbb{U})_{\mathcal{H}}| \leq \|\mathbb{U}\|^2_{\mathcal{H}}.$$

Proof of Lemma 2.7.4. We obtain the first identity by using the definitions (2.65) of A and (2.66) of the scalar product $(.,.)_{\mathcal{H}}$. Applying the first Green identity (2.62):

$$\begin{aligned}(A\mathbb{U}, \mathbb{U})_{\mathcal{H}} &= b\left(\Delta\phi, \psi\right) + \left(\partial_n\phi, \psi\right)_\Gamma + b\left(-\psi, \phi\right) + b\left(-\Delta\phi, \psi\right) + B\left(\rho_s^{-1}\boldsymbol{\Delta}_{\mathbf{s}}\mathbf{u}, \mathbf{v}\right) \\ &\quad + \left(\mathbf{t}[\mathbf{u}], \mathbf{v}\right)_\Gamma + B(-\mathbf{v}, \mathbf{u}) + B\left(-\rho_s^{-1}\boldsymbol{\Delta}_{\mathbf{s}}\mathbf{u}, \mathbf{v}\right) \\ &= \left(\partial_n\phi, \psi\right)_\Gamma + b\left(-\psi, \phi\right) + \left(\mathbf{t}[\mathbf{u}], \mathbf{v}\right)_\Gamma + B(-\mathbf{v}, \mathbf{u})\end{aligned}$$

Using the essential conditions $B\mathbb{U} = 0$ yields (a). Then, (b) results from applying Young's inequality to the right-hand side of (a) and recalling the definition (2.66) of $\|\mathbb{U}\|^2_{\mathcal{H}}$. □

To apply the Hille-Yosida theorem, we then prove of the monotonicity of A_λ and the surjectivity of $A_\lambda + I$.

1. Monotonicity. Using definitions (2.65) of A and (2.66) of the scalar product in $\mathcal{H}$ and applying Lemma 2.7.4a, we obtain after rearrangement

$$\begin{aligned}(A\mathbb{U},\mathbb{U})_{\mathcal{H}} + \lambda(\mathbb{U},\mathbb{U})_{\mathcal{H}} &= \lambda a(\phi,\phi) + \lambda A(\mathbf{u},\mathbf{u}) + \lambda b(\phi,\phi)\\ &\quad + \lambda b(\psi,\psi) - b(\psi,\phi) + \lambda B(\mathbf{u},\mathbf{u}) + \lambda B(\mathbf{v},\mathbf{v}) - \lambda B(\mathbf{v},\mathbf{u})\\ &= \lambda a(\phi,\phi) + \lambda A(\mathbf{u},\mathbf{u}) + \frac{1}{2}b(\phi-\psi,\phi-\psi) + \frac{1}{2}B(\mathbf{u}-\mathbf{v},\mathbf{u}-\mathbf{v})\\ &\quad + \left(\lambda-\frac{1}{2}\right)[b(\phi,\phi)+b(\psi,\psi)] + \left(\lambda-\frac{1}{2}\right)[B(\mathbf{u},\mathbf{u})+B(\mathbf{v},\mathbf{v})],\end{aligned} \tag{2.73}$$

implying that $(A\mathbb{U},\mathbb{U})_{\mathcal{H}} + \lambda(\mathbb{U},\mathbb{U})_{\mathcal{H}} \geq 0$, i.e. monotonicity holds, for any $\lambda \geq \frac{1}{2}$.

2. Surjectivity. Now, for $\mu = \lambda+1$, we investigate whether the equation $(A+\mu I)\mathbb{U} = \mathbb{F}$ is solvable for $\mathbb{U} = (\phi,\psi,\mathbf{u},\mathbf{v})^T \in \mathcal{D}(A)$ given $\mathbb{F} = (f,\mathbf{f},g,\mathbf{g})^T \in \mathcal{H}$, i.e. that of the system

$$\begin{array}{llll}
\text{(a)} & \mu\phi - \psi = f & \text{in } \Omega_f, & \\
\text{(b)} & \mu\psi - \Delta\phi = g & \text{in } \Omega_f, & \text{(e)} \quad \partial_n\phi - \mathbf{v}.\mathbf{n} = 0 \quad \text{on } \Gamma,\\
\text{(c)} & \mu\mathbf{u} - \mathbf{v} = \mathbf{f} & \text{in } \Omega_s & \text{(f)} \quad \mathbf{t} - \psi\mathbf{n} = \mathbf{0} \quad \text{on } \Gamma.\\
\text{(d)} & \mu^2\mathbf{v} - \boldsymbol{\Delta}_{\mathbf{s}}\mathbf{u} = \mathbf{g} & \text{in } \Omega_s, &
\end{array} \tag{2.74}$$

Using (a) and (c) to eliminate ψ and $\mathbf{v}$ with the first two equations, the problem on $(\phi,\mathbf{u})$ defined by the remaining equations (b), (d), (e) and (f) reads

$$\begin{array}{llll}
\text{(b)} & \mu^2\phi - \Delta\phi = g + \mu f & \text{in } \Omega_f, & \text{(e)} \quad \partial_n\phi - \mu\mathbf{u}.\mathbf{n} = -\mathbf{f}.\mathbf{n} \quad \text{on } \Gamma,\\
\text{(d)} & \mu^2\mathbf{u} - \rho_{\mathbf{s}}^{-1}\boldsymbol{\Delta}_{\mathbf{s}}\mathbf{u} = \mathbf{g} + \mu\mathbf{f} & \text{in } \Omega_s, & \text{(f)} \quad \mathbf{t} - \mu\phi\mathbf{n} = -f\mathbf{n} \quad \text{on } \Gamma,
\end{array}$$

and is set in variational form as

$$\text{Find } (\phi,\mathbf{u}) \in \mathbf{H}^1, \quad \mathcal{A}\left(\phi(t),\mathbf{u}(t);\widetilde{\phi},\widetilde{\mathbf{u}}\right) = \mathcal{F}_t(\widetilde{\phi},\widetilde{\mathbf{u}}) \quad \text{for all } (\widetilde{\phi},\widetilde{\mathbf{u}}) \in \mathbf{H}^1 \tag{2.75}$$

where $\mathcal{A}$ is the bilinear form in problem (2.71) and

$$\mathcal{F}_t(\widetilde{\phi},\widetilde{\mathbf{u}}) = \left(g+\mu f,\widetilde{\phi}\right) + \left(\mathbf{f}.\mathbf{n},\widetilde{\phi}\right)_\Gamma + (\mathbf{g}+\mu\mathbf{f},\widetilde{\mathbf{u}}) - (f\mathbf{n},\widetilde{\mathbf{u}})_\Gamma.$$

The bilinear form $\mathcal{A}$ is already known to be coercive on $\mathbf{H}^1$, and the linear functional $\mathcal{F}$ is continuous on $\mathbf{H}^1$ for any $\mathbb{F} \in \mathcal{H}$. Problem (2.75) is hence uniquely solvable by the Lax-Milgram theorem. On reconstructing $(\psi,\mathbf{v})$ from (2.74a,c) this implies the unique solvability of (2.74) in $\mathcal{D}(A)$, and hence of the system $(A+\mu I)\mathbb{U} = \mathbb{F}$ in $\mathcal{D}(A)$ for any $\mathbb{F} \in \mathcal{H}$.

3. Conclusion. Choosing $\mu = \lambda + 1$, the monotonicity *(1)* and the surjectivity *(2)* show that $A+\lambda I : \mathcal{D}(A) \to \mathcal{H}$ is maximal monotone for any $\lambda \geq \frac{1}{2}$. The Hille-Yosida theorem [91, Chap. II, Theorem 1.3] hence applies to the generic system (2.72), and gives Proposition 5. □

At this point, we have shown that the system (2.72) has a unique strong solution $\mathbb{U}_c$ for any $\mathbb{F} = \mu\mathbb{U}_L - \mathbb{U}_L'$ with sufficient regularity. According to Lemma 2.7.3, we also know that if $\mathbb{H} \in C_T^2(\mathbf{H}^{-1/2})$ with $\mathbb{H}(0) = 0$, we have $\mathbb{U}_L \in C_T^2(\mathcal{H})$ with $\mathbb{U}_L(0) = 0$. Moreover, by definition, the FSI strong solution is given by $\mathbb{U} = \mathbb{U}_L + \mathbb{U}_c$ and

$$\mathbb{U} \in C_T^1(\mathcal{H}) \cap C_T^0(D(A)).$$

Existence and uniqueness of a weak solution We now aim at finding a weak solution of the variational problem (2.7). It will be defined and shown to exist on the basis of energy estimates verified by the strong solution $\mathbb{U}$.

(iv) Energy estimates.

To show the energy estimates and then define the weak solution for problem (2.7), we need to show that $\mathbb{U}$ admits another representation. We will need the following Lemma:

Lemma 2.7.5. *Let $\mathbb{Z}$ solve (2.72) for given $\mathbb{F}$. If $\mathbb{F}(0) = 0$ and either $\mathbb{F} \in C_T^2(\mathcal{H})$ or $\mathbb{F} \in C_T^1(\mathcal{D}(A))$, we have $\mathbb{Z} \in C_T^1(\mathcal{D}(A))$, and its time derivative $\mathbb{Z}' \in C_T^1(\mathcal{H}) \cap C_T^0(\mathcal{D}(A))$ solves*

(i) $(\mathbb{Z}')' + A\mathbb{Z}' = \mathbb{F}'$ and $\mathbb{B}\mathbb{Z}' = 0$ in $[0, T]$,

(ii) $\mathbb{Z}'(0) = 0$.

Proof of Lemma 2.7.5. The system (2.72) may be differentiated in time (since all quantities are C^1 in time with values in the requisite spaces); moreover, $\mathbb{Z}'(0) = \mathbb{F}(0) - A\mathbb{Z}(0) = 0$. □

Using the Lemma 2.7.5 and introducing $\mathbb{Z}$ that solves (2.72) with $\mathbb{F} = \mathbb{U}_L$, we have that

$$\mathbb{U} = \mathbb{U}_L + \mu\mathbb{Z} - \mathbb{Z}'. \tag{2.76}$$

We now establish estimates for the strong solution given by (2.76) to show that a weaker norm of the strong solution is controlled by a weaker norm of the data.

Lemma 2.7.6. *For any $\mathbb{H} \in C_T^2(\mathbf{H}^{-1/2}(\Gamma))$ with $\mathbb{H}(0) = 0$, the strong solution $\mathbb{U}$ of the FSI system (2.64) verifies the estimate*

$$\sup_{t\in[0,T]} \|\mathbb{U}(t)\|_{\mathcal{H}}^2 \leq C\|\mathbb{H}\|_{H_T^1(\mathbf{H}^{-1/2}(\Gamma))}^2. \tag{2.77}$$

If $\mathbb{H} \in C_T^3(\mathbf{H}^{-1/2}(\Gamma))$ with $\mathbb{H}(0) = \mathbb{H}'(0) = 0$, we have the higher-regularity estimate

$$\sup_{t\in[0,T]} \|\mathbb{U}(t)\|_{\mathcal{H}_A}^2 \leq C\|\mathbb{H}\|_{H_T^2(\mathbf{H}^{-1/2}(\Gamma))}^2. \tag{2.78}$$

The constant $C > 0$ in each estimate depends on T and Γ but not on $\mathbb{H}$.

Proof of Lemma 2.7.6. We recall the representation (2.76) of $\mathbb{U}$. Testing the system $\mathbb{Z}' + A\mathbb{Z} = \mathbb{U}_L$ against $\mathbb{Z}$, we have $(\mathbb{Z}', \mathbb{Z})_{\mathcal{H}} = (\mathbb{U}_L, \mathbb{Z})_{\mathcal{H}} - (A\mathbb{Z}, \mathbb{Z})_{\mathcal{H}}$ which, using Lemma 2.7.4 for $\mathbb{U} = \mathbb{Z} \in C^1_T(\mathcal{D}(A))$, gives

$$2\left(\mathbb{Z}'(\tau), \mathbb{Z}(\tau)\right)_{\mathcal{H}} \leq 2\left(\mathbb{U}_L(\tau), \mathbb{Z}(\tau)\right)_{\mathcal{H}} + \|\mathbb{Z}(\tau)\|^2_{\mathcal{H}}$$

Integrating over $\tau \in [0, t]$, we thus obtain

$$\|\mathbb{Z}(t)\|^2_{\mathcal{H}} \leq 2\int_0^t \|\mathbb{Z}(\tau)\|^2_{\mathcal{H}} d\tau + \|\mathbb{U}_L\|^2_{L^2_T(\mathcal{H})} \quad t \in [0, T]. \tag{a}$$

The same derivation applies to $\mathbb{Z}'$ (by testing against $\mathbb{Z}'$ the system $(\mathbb{Z}')' + A\mathbb{Z}' = \mathbb{U}'_L$ obeyed by $\mathbb{Z}'$, see Lemma 2.7.5), to obtain

$$\|\mathbb{Z}'(t)\|^2_{\mathcal{H}} \leq 2\int_0^t \|\mathbb{Z}'(\tau)\|^2_{\mathcal{H}} d\tau + \|\mathbb{U}'_L\|^2_{L^2_T(\mathcal{H})}, \quad t \in [0, T]. \tag{b}$$

As usual, Grönwall's lemma plays a key role in the derivation of such estimates. The following version [54, Chap. 18] is used:

Lemma 2.7.7 (Grönwall's lemma)**.** *Let the univariate function $\Phi \in L^\infty([0, T])$ verify $\Phi(t) \geq 0$ almost everywhere in $[0, T]$. Assume in addition that the inequality*

$$\Phi(t) \leq C_1 \int_0^t \Phi(s) ds + C_2$$

holds almost everywhere in $[0, T]$ for some constants $C_1, C_2 \geq 0$. Then:

$$\Phi(t) \leq C_2 \exp(C_1 t).$$

In particular, if C_2 =0, $\Phi(t)$=0 almost everywhere in $[0, T]$.

Grönwall's lemma is applicable to inequalities (a) and (b) with, respectively, $\Phi(t) = \|\mathbb{Z}(t)\|^2_{\mathcal{H}}$ and $\Phi(t) = \|\mathbb{Z}'(t)\|^2_{\mathcal{H}}$. Consequently there exists $C > 0$ such that

$$\|\mathbb{Z}(t)\|^2_{\mathcal{H}} \leq C\|\mathbb{U}_L\|^2_{L^2_T(\mathcal{H})}, \qquad \|\mathbb{Z}'(t)\|^2_{\mathcal{H}} \leq C\|\mathbb{U}'_L\|^2_{L^2_T(\mathcal{H})} \qquad t \in [0, T]. \tag{c}$$

Since $\mathbb{U}_L \in C^2_T(\mathcal{H})$, estimate (2.77) follows by using (c) in the solution representation (2.76) and Lemma 2.7.3. If $\mathbb{H}$ in fact verifies the given higher-regularity assumptions and initial conditions, the estimates (2.77) apply to both $\mathbb{U}$ and $\mathbb{U}'$ with datum $\mathbb{H}$ and $\mathbb{H}'$ respectively. Since $\mathbb{U}'(t) = A\mathbb{U}(t)$ holds in $\mathcal{H}$, we have for all $t \in [0, T]$:

$$\|\mathbb{U}(t)\|^2_{\mathcal{H}_A} = \|\mathbb{U}(t)\|^2_{\mathcal{H}} + \|A\mathbb{U}(t)\|^2_{\mathcal{H}} = \|\mathbb{U}(t)\|^2_{\mathcal{H}} + \|\mathbb{U}'(t)\|^2_{\mathcal{H}} \leq C\|\mathbb{H}\|^2_{H^2_T(\mathbf{H}^{-1/2}(\Gamma))}. \qquad \square$$

and we similarly obtain estimate (2.78).

We have shown that the FSI system (2.64) is well-posed. The energy estimates of Lemma 2.7.6 now show that the solution $\mathbb{U}$ with a data $\mathbb{H} \in C^2_T(\mathbf{H}^{-1/2})$ is in fact controlled in the weaker $C^0_T(\mathcal{H})$ norm, by the weaker $H^1_T(\mathbf{H}^{-1/2}(\Gamma))$ norm of the data $\mathbb{H}$. Moreover, for any data with extra regularity in time such as $\mathbb{H} \in C^3_T(\mathbf{H}^{-1/2}(\Gamma))$, the solution $\mathbb{U}$ is controlled in the $C^0_T(\mathcal{H}_A)$ norm and by the weaker $H^2_T(\mathbf{H}^{-1/2}(\Gamma))$ norm of the data, with higher regularity. We are now going to use these energy estimates to obtain a well-posedness result for the FSIP in weak form, under weaker regularity assumptions on the data $\mathbb{H}$.

(v) Existence and uniqueness of a weak solution.

We now aim at reaching the main goal of this contribution and proving a solvability result for the FSIP in variational form, under weaker regularity assumptions on $\mathbb{H}$, using the estimate (2.77). To this aim, let consider some transmission data $\mathbb{H} = (\nu, h\mathbf{n}) \in H^1_T(\mathbf{H}^{-1/2}(\Gamma))$ with $\mathbb{H}(0) = 0$. Since $C^2_T\left(\mathbf{H}^{-1/2}(\Gamma)\right)$ is dense in $H^1_T\left(\mathbf{H}^{-1/2}(\Gamma)\right)$, there exists a sequence $\mathbb{H}_n = (\nu_n, h_n\mathbf{n}) \in C^2_T\left(\mathbf{H}^{-1/2}(\Gamma)\right)$ such that $(\nu_n, h_n\mathbf{n}) \to (\nu, h\mathbf{n}) \in H^1_T(\mathbf{H}^{-1/2}(\Gamma))$ [29, Sec. 8.3]. As, according to Theorem 5, the FSI system (2.64) is well-posed, it has for each data $\mathbb{H}_n$ a unique solution $\mathbb{U}_n$. This solution is given by (2.76) with $\mathbb{Z}$ solving (2.72) for $\mathbb{F} = \mathbb{U}^n_L$. Applying by linear superposition the energy estimate (2.77) to the data $\mathbb{H}_n - \mathbb{H}_m$ and corresponding solution $\mathbb{U}_n - \mathbb{U}_m$, we readily find that $(\mathbb{U}_n)$ is a Cauchy sequence in $C^0_T(\mathcal{H})$. Upon taking the limit $n \to \infty$ in that estimate, the limit $\mathbb{U} \in C^0_T(\mathcal{H})$ of $\mathbb{U}^n$ satisfies

$$\sup_{t\in[0,T]} \|\mathbb{U}(t)\|^2_{\mathcal{H}} \leq C\|\mathbb{H}\|^2_{H^1_T(\mathbf{H}^{-1/2}(\Gamma))},$$

This limit $\mathbb{U}$ defines the expected weak solution of the variational FSI problem (2.7). We now need to prove that this is actually the case, and that $\mathbb{U}$ is the only such solution.

1. $\mathbb{U}$ defines a weak solution of the variational problem (2.7). Let $(\widetilde{\phi}, \widetilde{\mathbf{u}}) \in \mathbf{H}^1$ be a pair of time-independent functions, and let $\varphi \in C^\infty_0([0,T])$. We write the wave equations verified (by virtue of (2.64)) by each ϕ_n in $L^2(\Omega_f \times [0,T])$ and $\mathbf{u}_n$ in $L^2(\Omega_s \times [0,T])$ in the weak form, for the test functions $\widetilde{\phi}\varphi$ and $\widetilde{\mathbf{u}}\varphi$. Integrating in time, we have

$$\int_0^T \left(-\Delta\phi_n + \phi_n'', \widetilde{\phi}\right)_{\Omega_f} \varphi(t)dt + \int_0^T (-\boldsymbol{\Delta}_{\mathbf{s}}\mathbf{u}_n + \rho_s\mathbf{u}_n'', \widetilde{\mathbf{u}})_{\Omega_s} \varphi(t)dt = 0.$$

We first perform integrations by parts in space using the first Green identity which is valid since each $(\phi_n, \mathbf{u}_n)$ belongs to $C^0_T(\mathbf{H}^1_\Delta)$. We then express $\partial_n\phi_n$ and $\mathbf{t}[\mathbf{u}_n]$ by means of the transmission conditions (which they verify in the $L^2_T(H^{-1/2}(\Gamma))$ sense), to obtain

$$\int_0^T \left[a\left(\phi_n, \widetilde{\phi}\right) + b\left(\phi_n'', \widetilde{\phi}\right) + A\left(\mathbf{u}_n'', \widetilde{\mathbf{u}}\right) + B\left(\mathbf{u}_n'', \widetilde{\mathbf{u}}\right) + I\left(\phi', \mathbf{u}'; \widetilde{\phi}, \widetilde{\mathbf{u}}\right)\right] \varphi(t)dt$$
$$= \int_0^T \left[(h_n\mathbf{n}(t), \widetilde{\mathbf{u}})_\Gamma - \left(\nu_n(t), \widetilde{\phi}\right)_\Gamma\right] \varphi(t)dt.$$

The bilinear forms a, b, A, B defined by (2.6) and I by (2.9). Then, all time derivatives are transferred to the test function φ with integrations by parts, since $\varphi \in C^\infty_0([0,T])$. It yields

$$\int_0^T \left[a(\phi_n, \widetilde{\phi}) + A\left(\mathbf{u}_n, \widetilde{\mathbf{u}}\right)\right] \varphi(t)dt + \int_0^T \left[b(\phi_n, \widetilde{\phi}) + B\left(\mathbf{u}_n, \widetilde{\mathbf{u}}\right)\right] \varphi''(t)dt$$
$$- \int_0^T \left[I(\phi_n, \mathbf{u}_n, \widetilde{\phi}, \widetilde{\mathbf{u}})\right] \varphi'(t)dt = \int_0^T \left[(h_n\mathbf{n}(t), \widetilde{\mathbf{u}})_\Gamma - \left(\nu_n(t), \widetilde{\phi}\right)_\Gamma\right] \varphi(t)dt.$$

By assumption $\mathbb{H}_n \to \mathbb{H}$ in $L^2_T(\mathbf{H}^{-1/2}(\Gamma))$, which implies the convergence $\mathbb{U}_n \to \mathbb{U}$ in $L^2_T(\mathcal{H})$. Moreover, using the continuity properties of the bilinear forms a, b, A, B, I, the limiting form of the above identity as $n \to \infty$ is

$$\int_0^T \left[a(\phi, \widetilde{\phi}) + A\left(\mathbf{u}, \widetilde{\mathbf{u}}\right)\right] \varphi(t)dt + \int_0^T \left[b(\phi, \widetilde{\phi}) + B\left(\mathbf{u}, \widetilde{\mathbf{u}}\right)\right] \varphi''(t)dt$$
$$- \int_0^T \left[I(\phi, \mathbf{u}, \widetilde{\phi}, \widetilde{\mathbf{u}})\right] \varphi'(t)dt = \int_0^T \left[(h\mathbf{n}, \widetilde{\mathbf{u}})_\Gamma - \left(\nu, \widetilde{\phi}\right)_\Gamma\right] \varphi(t)dt.$$

for any $\varphi \in C_0^\infty([0,T])$. The components of $\mathbb{U}$ therefore satisfy the variational formulation (2.7) as an equality in $\mathcal{D}'([0,T])$, in the sense of distributions in the time variable.

2. Uniqueness. Assume that the variational formulation (2.7) has two distinct nonzero solutions $\mathbb{U}_1$ and $\mathbb{U}_2$ for the same datum $\mathbb{H}$, both satisfying initial-rest conditions. By linearity, the components of $\mathbb{W} := \mathbb{U}_1 - \mathbb{U}_2$ must then solve the homogeneous form of the variational problem (2.7) with $\mathbb{H} = 0$. The function $\mathbb{Z}(t) := \int_0^t \mathbb{W}(s)ds$ is also at initial-rest and (by integration over the time interval $[0,t]$) solves the same homogeneous variational problem. Moreover, due to the integration in time, $\mathbb{Z} \in C^0_T(\mathcal{D}(A)) \cap C^1_T(\mathcal{H})$, i.e., is a strong solution of the homogeneous evolution problem. By Proposition 5, we must hence have $\mathbb{Z} = 0$, implying $\mathbb{W} = 0$. This proves the uniqueness of the weak solution and the proof of the first part of Theorem 2.2.1 is complete.

3. Data with higher time regularity. If in fact $\mathbb{H} \in H^2_T(\mathbf{H}^{-1/2}(\Gamma))$ with $\mathbb{H}(0) = \mathbb{H}'(0) = 0$, the previous analysis applies to both $\mathbb{H}$ and $\mathbb{H}'$, so that $(\phi, \mathbf{u}) \in C^1_T(\mathbf{H}^1)$ and $(\phi', \mathbf{u}') \in C^1_T(\mathbf{L}^2)$. In particular, $(\phi'', \mathbf{u}'') \in C^0_T(\mathbf{L}^2)$. Since, in addition, each $(\phi_n, \mathbf{u}_n)$ in the limiting process verifies the homogeneous wave equation, the limit $(\phi, \mathbf{u})$ satisfies $(\Delta\phi, \Delta_s\mathbf{u}) \in C^0_T(\mathbf{L}^2)$. Hence $(\phi, \mathbf{u}) \in C^0_T(\mathbf{H}^1_\Delta)$, and the claimed regularity for the second part of Theorem 2.2.1 follows.

2.2.2. Proof of Theorem 2.2.2.

The proof method for Theorem 2.2.2 relies on the general steps previously used for Theorem 2.2.1.

(i) First-order form of the FSIP.

The FSIP reads the same first-order form as (2.64)

$$\mathbb{U}' + A\mathbb{U} = 0, \qquad \mathbb{U}(0) = 0, \qquad B\mathbb{U} = \mathbb{H} \tag{2.79}$$

To account for the assumed additional regularity in space of the data $\mathbb{H}$, A is now considered as an operator on $\mathcal{D}(A)$ with domain $\mathcal{D}(A^2)$, where

$$\mathcal{D}(A^2) := \{\mathbb{U} \in \mathcal{D}(A) \text{ such that } A\mathbb{U} \in \mathcal{D}(A) \subset \mathcal{H}_A\}, \qquad \|\mathbb{U}\|^2_{\mathcal{D}(A^2)} := \|\mathbb{U}\|^2_{\mathcal{H}_A} + \|A\mathbb{U}\|^2_{\mathcal{H}_A}. \tag{2.80}$$

The main modifications in the proof steps, relative to the first proof of theorem 2.2.1 in Section 2.7, then result from replacing the spaces $\mathcal{H}$ and $\mathcal{D}(A)$ with $\mathcal{D}(A)$ and $\mathcal{D}(A^2)$, respectively, in the application of the Hille-Yosida theorem to the system (2.79). We note that the space $\mathcal{D}(A^2)$ embeds not only the interfacial constraints $\mathbb{U} = 0$ given by the equation $B\mathbb{U} = 0$, but also the additional higher-order constraints $\mathbb{B}(\mathbb{A}\mathbb{U}) = 0$, i.e.

$$\text{(a)}\quad \partial_n\psi - \rho_s^{-1}\mathbf{n}.\mathbf{\Delta_s u} = 0, \qquad \text{(b)}\quad \mathbf{t} - \Delta\phi\mathbf{n} = \mathbf{0} \tag{2.81}$$

as essential conditions. The following counterpart of the density property of Lemma 2.7.2, proved in [24, Sec. 8], is verified by $\mathcal{D}(A^2)$:

Lemma 2.7.8. *The space $\mathcal{D}(A^2)$ is a dense subspace of both $(\mathcal{H}_A, \|\cdot\|_{\mathcal{H}_A})$ and $(\mathcal{D}(A), \|\cdot\|_{\mathcal{H}_A})$.*

(ii) Interface data lifting.

Towards applying the Hille-Yosida theorem, problem (2.79) needs as before to be recast as a first-order system with homogeneous TCs. We define again the lifting $\mathbb{U}_L$ of $\mathbb{H}$ by the system (2.70). The extra regularity in space of $\mathbb{H}$ directly translates into corresponding extra regularity for $\mathbb{U}_L$: adapting Lemma 2.7.3 and using elliptic regularity at each t, if $\mathbb{H} \in X_T\left(\mathbf{H}^{1/2}(\Gamma)\right)$ for some Banach space X, the system (2.70) has a unique solution $\mathbb{U}_L \in X_T(\mathcal{H}_A)$, verifying $\|\mathbb{U}_L\|_{X_T(\mathcal{H}_A)} \leq C\|\mathbb{H}\|_{X_T(\mathbf{H}^{1/2}(\Gamma))}$.

(iii) Application of the Hille-Yosida theorem.

We apply again the Hille-Yosida theorem to the generic problem (2.72) using the unknown $\mathbb{U}_c := \mathbb{U} - \mathbb{U}_L$ and the data $\mathbb{F} := \mu\mathbb{U}_L - \mathbb{U}_L'$. The definition (2.80) of $\mathcal{D}(A)$ is such that the Hille-Yosida theorem still applies to $A : \mathcal{D}(A^2) \to \mathcal{D}(A)$, via a direct transposition of the arguments of the proof of Theorem 2.2.1 in Section 2.7 and with the help of the following adaptation of Lemma 2.7.4:

Lemma 2.7.9. *For any $\mathbb{U} \in \mathcal{D}(A^2)$, we have*

$$\begin{aligned} &(a) \quad (A\mathbb{U}, \mathbb{U})_{\mathcal{H}_A} = -b(\psi,\phi) - B(\mathbf{v},\mathbf{u}) - b(\Delta\phi,\psi) - B(\Delta_s\mathbf{u},\mathbf{v}) \\ &(b) \quad 2|(A\mathbb{U}, \mathbb{U})_{\mathcal{H}_A}| \leq \|\mathbb{U}\|^2_{\mathcal{H}_A}. \end{aligned} \tag{2.82}$$

Proof. Lemma (2.7.9) is obtained by using identity (a) of Lemma 2.7.4 with $\mathbb{U}$ replaced by $A\mathbb{U}$. □

Then we can verify that all conditions of the Hille-Yosida theorem are satisfied:

1. Monotonicity. Thanks to Lemma 2.7.9, identity (2.73) also holds for $A\mathbb{U}$ instead of $\mathbb{U}$, replacing all components of $\mathbb{U}$ by those of $A\mathbb{U}$ in the right-hand side. The monotonicity of $A_\lambda := A + \lambda I : \mathcal{D}(A^2) \to \mathcal{D}(A)$ follows in the same way, still subject to $\lambda \geq \frac{1}{2}$.

2. Surjectivity. The solvability in $\mathcal{D}(A^2)$ of $(A + \mu I)\mathbb{U} = \mathbb{F}$ for given $\mathbb{F} \in \mathcal{D}(A)$ is still decided by the variational problem (2.75). The regularity assumption $\mathbb{F} \in \mathcal{D}(A)$

implies the desired smoothness of its unique solution $\mathbb{U}$, namely $\mathbb{U}, A\mathbb{U}, A^2\mathbb{U}$ being in $\mathcal{H}$, by elliptic regularity. This regularity in turn allows each component of the equality $A\mathbb{U}+\eta\mathbb{U}=\mathbb{F}$ to hold in $H^{1/2}(\Gamma)$, and we use those relations to compute

$$\mathbf{t}[\mathbf{v}_L]-(\Delta\phi_L)\mathbf{n}=g\mathbf{n}-\mathbf{t}[\mathbf{f}]=\mathbf{0},\qquad \partial_n\psi_L-(\rho_s^{-1}\boldsymbol{\Delta}_\mathbf{s}\mathbf{u}_\mathbf{L}).\mathbf{n}=\mathbf{g}.\mathbf{n}-\partial_n f=0\qquad \text{on }\Gamma, \tag{2.83}$$

since the constraints $B\mathbb{U}=0$ are satisfied by both $\mathbb{U}$ (by the definition of problem (2.75)) and $\mathbb{F}\in\mathcal{D}(A)$. Concluding, $(A+\mu I)\mathbb{U}=\mathbb{F}$ has a unique solution $\mathbb{U}\in\mathcal{D}(A^2)$ for any $\mathbb{F}\in\mathcal{D}(A)$.

3. Conclusion. Choosing $\mu=\lambda+I$, $A+\lambda I:\mathcal{D}(A^2)\to\mathcal{D}(A)$ is maximal monotone for any $\lambda\geq\frac{1}{2}$. The Hille-Yosida theorem hence applies to the generic system (2.72). The Hille-Yosida theorem on its strong solvability now holds with $\mathcal{H},\mathcal{D}(A)$ replaced by $\mathcal{D}(A),\mathcal{D}(A^2)$.

Following the same arguments as in Section 2.7, the FSI solution $\mathbb{U}=\mathbb{U}_L+\mathbb{U}_c$ is unique and the FSI system (2.64) then admits a unique solution $\mathbb{U}\in C^1_T(\mathcal{D}(A))\cap C^0_T(\mathcal{D}(A^2))$.

(iv) Energy estimates.

To derive energy estimates, we start by observing that for any $\mathbb{F}\in C^1_T(\mathcal{D}(A))$, the solution $\mathbb{Z}\in C^0_T(\mathcal{D}(A^2))$ of the generic system (2.72) verifies

$$\text{(a)}\quad \sup_{t\in[0,T]}\|\mathbb{Z}(t)\|^2_{\mathcal{H}_A}\leq C\|\mathbb{F}\|^2_{L^2_T(\mathcal{H}_A)},\qquad \text{(b)}\quad \sup_{t\in[0,T]}\|\mathbb{Z}'(t)\|^2_{\mathcal{H}_A}\leq C\|\mathbb{F}'\|^2_{L^2_T(\mathcal{H}_A)}. \tag{2.84}$$

Both inequalities stem from repeating the proof of Lemma 2.7.6 leading to inequalities (c) there, with $\mathcal{H},\mathcal{D}(A)$ replaced by $\mathcal{H}_A$, $\mathcal{D}(A^2)$ and invoking the improved Green identity of Lemma 2.7.9.

Let now $\mathbb{H}\in C^2_T(\mathbf{H}^{1/2}(\Gamma))$ with $\mathbb{H}(0)=0$, so that $\mathbb{U}_L\in C^2_T(\mathcal{H}_A)$ and $\mathbb{U}_L(0)=0$. Invoking Lemma 2.7.8, there exists a sequence $\mathbb{U}^m_L\in C^2_T(\mathcal{D}(A^2))$ with $\mathbb{U}^m_L(0)=0$ such that $\|\mathbb{U}_L-\mathbb{U}^m_L\|_{C^2_T(\mathcal{H}_A)}\to 0$. Let then $\mathbb{Z}_m\in C^1_T(\mathcal{D}(A))\cap C^0_T(\mathcal{D}(A^2))$ solve (2.72) with $\mathbb{F}=\mathbb{U}^m_L$. The representation (2.76) of $\mathbb{U}$ solving the FSI system (2.64) suggests to define the approximating sequence $\mathbb{U}^m$ given by either

$$\text{(a) }\mathbb{U}^m=\eta\mathbb{Z}_m-\mathbb{Z}'_m+\mathbb{U}_L,\qquad \text{(b) }\mathbb{U}^m=(\eta I+A)\mathbb{Z}_m+(\mathbb{U}_L-\mathbb{U}^m_L) \tag{2.85}$$

(with case (b) obtained by using in (a) the equality $\mathbb{Z}'_m=\mathbb{U}^m_L-A\mathbb{Z}_m$ in $\mathcal{H}_A$). Applying estimate (2.84a) with $\mathbb{F}=\mathbb{U}^m_L$ to (2.85b), we have

$$\sup_{t\in[0,T]}\|\mathbb{U}^m(t)\|^2_{\mathcal{H}}\leq\sup_{t\in[0,T]}C\|\mathbb{Z}_m(t)\|^2_{\mathcal{H}_A}\leq C\|\mathbb{U}^m_L\|^2_{L^2_T(\mathcal{H}_A)}. \tag{2.86}$$

Alternatively, estimates (2.84a,b) with $\mathbb{F}=\mathbb{U}^m_L$ applied to (2.85a) give

$$\sup_{t\in[0,T]}\|\mathbb{U}^m(t)\|^2_{\mathcal{H}_A}\leq C\|\mathbb{U}^m_L\|^2_{H^1_T(\mathcal{H}_A)}. \tag{2.87}$$

Remark. By contrast with the proof of Theorem 2.2.1, estimates (2.86) and (2.87) cannot be directly obtained for the FSI solution $\mathbb{U}$ from its representation (2.76), as $\mathbb{Z}$ in the latter does not verify $\mathbb{B}(A\mathbb{Z})=0$ and thus is not in $\mathcal{D}(A^2)$, preventing the

use of Lemma 2.7.9b. Identity (a) in Lemma 2.7.9 could of course be augmented with interfacial terms (so as to remove the requirement $\mathbb{B}(A\mathbb{U}) = 0$ there) but the resulting appearance of higher-order derivatives in interfacial terms would prove equally problematic. Hence our recourse, permitted by the density result of Lemma 2.7.8, to approximations (2.85) of $\mathbb{U}$ that have the correct interfacial traces while allowing to invoke Lemma 2.7.9.

(v) Variational problem.

We note that $\mathbb{U}^m \in C^1_T(\mathcal{D}(A)) \cap C^0_T(\mathcal{D}(A^2))$ defined by (2.85) solves the system

(i) $\mathbb{U}'_m + A\mathbb{U}_m = \mathbb{F}_m$,

(ii) $\mathbb{U}_m(0) = 0$,

(iii) $B\mathbb{U} = \mathbb{H}$,

with the components $(f_m, \mathbf{f}_m, g_m, \mathbf{g}_m)$ of $\mathbb{F}_m$ given by

$$f_m = \mu(\phi^m_L - \phi_L) - (\phi^{m\prime}_L - \phi'_L), \qquad \mathbf{f}_m = \mu(\mathbf{u}^m_L - \mathbf{u}_L) - (\mathbf{u}^{m\prime}_L - \mathbf{u}'_L), \tag{2.88}$$

$$g_m = \mu(\psi^m_L - \psi_L) - (\psi^{m\prime}_L - \psi'_L), \qquad \mathbf{g}_m = \mu(\mathbf{v}^m_L - \mathbf{v}L) - (\mathbf{v}L^{m\prime} - \mathbf{v}L'). \tag{2.89}$$

Consequently, after eliminating $\psi_m, \mathbf{v}_m$, the remaining unknowns $\phi_m, \mathbf{u}_m$ of $\mathbb{U}_m$ are found to satisfy the inhomogeneous wave equations

$$-\Delta\phi_m + \phi''_m = f'_m + g_m \ \text{ in } \Omega_f, \qquad -\boldsymbol{\Delta}_{\mathbf{s}}\mathbf{u}_m + \rho_s\mathbf{u}''_m = \rho_s(\mathbf{f}'_m + \mathbf{g}_m) \ \text{ in } \Omega_s. \tag{2.90}$$

Proceeding as in Section 2.1, we take weighted residuals of the above equations using the same test functions $\widetilde{\phi}\varphi$ and $\widetilde{\mathbf{u}}\varphi$, apply the Green identities, use the TCs and transfer all time derivatives to φ via integration by parts. This results in the identity

$$\begin{aligned}&\int_0^T \left\{ \left[a\left(\phi_m, \widetilde{\phi}\right) + A\left(\mathbf{u}_m, \widetilde{\mathbf{u}}\right) \right] \varphi(t) + \left[b\left(\phi_m, \widetilde{\phi}\right) + B\left(\mathbf{u}_m, \widetilde{\mathbf{u}}\right) \right] \varphi''(t) - \left[I\left(\phi_m, \mathbf{u}_m; \widetilde{\phi}, \widetilde{\mathbf{u}}\right) \right] \varphi'(t) \right\} dt \\ &= \int_0^T \left[(h\mathbf{n}(t), \widetilde{\mathbf{u}})_\Gamma - \left(\nu(t), \widetilde{\phi}\right)_\Gamma \right] \varphi(t) dt + \int_0^T \left[b\left(f'_m + g_m, \widetilde{\phi}\right) + B\left(\mathbf{f}'_m + \mathbf{g}_m, \widetilde{\mathbf{u}}\right) \right] \varphi(t) dt.\end{aligned} \tag{2.91}$$

Either estimate (2.86) or (2.87) implies that $\mathbb{U}^m$ is a Cauchy sequence in $C^0_T(\mathcal{H})$, while the last integral in (2.91) vanishes as $m \to \infty$ by the definition of $\mathbb{U}^m_L$. Taking the limit $m \to \infty$ in (2.91), the limit $(\phi, \mathbf{u}) \in \mathbf{H}^1$ of $(\phi_m, \mathbf{u}_m)_m$ is as a result found to verify the variational formulation (2.7) for any datum $\mathbb{H} \in C^2_T(\mathbf{H}^{1/2}(\Gamma))$. Moreover, taking the limit $m \to \infty$ in estimates (2.86) and (2.87), the limit $\mathbb{U}$ verifies the estimates

$$\text{(a)} \ \sup_{t\in[0,T]} \|\mathbb{U}(t)\|^2_{\mathcal{H}} \le C\|\mathbb{U}_L\|^2_{L^2_T(\mathcal{H}_A)}, \ \text{(b)} \ \sup_{t\in[0,T]} \|\mathbb{U}(t)\|^2_{\mathcal{H}_A} \le C\|\mathbb{U}_L\|^2_{H^1_T(\mathcal{H}_A)}. \tag{2.92}$$

Then, considering some transmission data $\mathbb{H} \in L^2_T(\mathbf{H}^{1/2}(\Gamma))$, there exists a sequence $\mathbb{H}_n \in C^2_T(\mathbf{H}^{1/2}(\Gamma))$ with $\mathbb{H}_n(0) = 0$ such that $\|\mathbb{H}_n - \mathbb{H}\|_{L^2_T(\mathbf{H}^{1/2}(\Gamma))} \to 0$. A

lifting $\mathbb{U}_L^n \in C_T^2(\mathcal{H}_A)$ can be associated to each $\mathbb{H}_n$, leading to $\mathbb{U}_n$ solving the variational problem (2.7) for that data. The estimate (2.92a) shows that $\mathbb{U}_n$ defines a Cauchy sequence in $C_T^0(\mathcal{H})$, whose limit $\mathbb{U} \in C_T^0(\mathcal{H})$ also satisfies the variational formulation (2.7) and depends continuously on $\|\mathbb{H}\|_{L_T^2(\mathbf{H}^{1/2}(\Gamma)}$.

Similarly, approximating $\mathbb{H} \in H_T^1(\mathbf{H}^{1/2}(\Gamma))$ with $\mathbb{H}(0) = 0$ by a sequence $\mathbb{H}_n \in C_T^2(\mathbf{H}^{1/2}(\Gamma))$ with $\mathbb{H}_n(0) = 0$, $\mathbb{U}_n$ is, by the estimate (2.92b) applied to $(\mathbb{U}_n, \mathbb{U}_L^n)$, a Cauchy sequence in $C_T^0(\mathcal{H}_A)$. Its limit $\mathbb{U}$ satisfies the variational formulation (2.7) and, by taking the limit $n \to \infty$ in (2.92b), depends continuously on $\|\mathbb{H}\|_{H_T^1(\mathbf{H}^{1/2}(\Gamma)}$. Moreover, we have $(\phi'', \mathbf{u}'') = (\Delta\phi, \rho_s^{-1}\boldsymbol{\Delta}_\mathbf{s}\mathbf{u}) \in C_T^0(\mathbf{L}^2)$. Thanks to the latter and the assumed regularity of Γ, elliptic regularity provides $(\phi, \mathbf{u}) \in C_T^0(\mathbf{H}^2)$.

Conclusion. The FSIP (2.4) and the variational problem (2.7) being equivalent (by Prop. 1), the proof of Theorem 2.2.2 is complete for the two considered cases.

2.2.3. Proof of Theorem 2.2.3.

Once multiple primary solvability mappings such as those of Theorem 2.2.1 and Theorem 2.2.2 are available, other mappings results follow by interpolation arguments. In particular, we can now find mappings for which the data has $\mathbf{L}^2(\Gamma)$ space regularity and solution has boundary traces in velocity in $L_T^2(\Gamma)$ and $\mathbf{L}_T^2(\Gamma)$.

(i) Proof of regularity from interpolation.

Interpolating the data and solution spaces given by Theorem 2.2.1 and Theorem 2.2.2, and invoking the interpolation property for spaces of continuous functions with Hilbert range (see e.g. [131, Chap. 1, Sec. 14.2]), we deduce the continuity of the following data-to-solution mappings:

$$\begin{aligned}(\nu, \mathbf{h}) \in \Big[H_T^1(\mathbf{H}^{1/2}(\Gamma)),\, H_T^1(\mathbf{H}^{-1/2}(\Gamma))\Big]_{1/2} &\to (\phi, \mathbf{u}) \in \big[C_T^0(\mathbf{H}^2),\, C_T^0(\mathbf{H}^1)\big]_{1/2} \\ &\to (\phi', \mathbf{u}') \in \big[C_T^0(\mathbf{H}^1),\, C_T^0(\mathbf{L}^2)\big]_{1/2}\end{aligned} \tag{2.93}$$

where $[X, Y]_\theta$ denotes the interpolation space with weight $\theta \in [0, 1]$ (in particular $[X, Y]_0 = X$ and $[X, Y]_1 = Y$). Moreover, we have

$$\begin{aligned}\Big[H_T^1(\mathbf{H}^{1/2}(\Gamma)),\, H_T^1(\mathbf{H}^{-1/2}(\Gamma))\Big]_{1/2} = H_T^1\left(\Big[\mathbf{H}^{1/2}(\Gamma),\, \mathbf{H}^{-1/2}(\Gamma)\Big]_{1/2}\right) &= H_T^1(\mathbf{L}^2(\Gamma)), \\ \big[C_T^0(\mathbf{H}^2),\, C_T^0(\mathbf{H}^1)\big]_{1/2} = C_T^0\left([\mathbf{H}^2,\, \mathbf{H}^1]_{1/2}\right) &= C_T^0(\mathbf{H}^{3/2}), \\ \big[C_T^0(\mathbf{H}^1),\, H_T^1(\mathbf{L}^2)\big]_{1/2} = C_T^0\left([\mathbf{H}^1,\, \mathbf{L}^2]_{1/2}\right) &= C_T^0(\mathbf{H}^{1/2}).\end{aligned} \tag{2.94}$$

Using these equalities in the above mappings yields the claimed continuous mappings:

$$\begin{aligned}(\nu, \mathbf{h}) \in H_T^1(\mathbf{L}^2(\Gamma)) \to (\phi, \mathbf{u}) \in C_T^0(\mathbf{H}^{3/2}), \\ (\nu, \mathbf{h}) \in H_T^1(\mathbf{L}^2(\Gamma)) \to (\phi', \mathbf{u}') \in C_T^0(\mathbf{H}^{1/2}).\end{aligned} \tag{2.95}$$

(ii) Proof of boundary trace of velocity.

The above data-to-velocity mapping falls just short of the applicability of the trace theorem. Useful estimates for boundary traces may however be obtained using the following lemma (proved in [24, Sec 8]):

Lemma 2.7.10 (Integral identities on boundary traces)**.** *Let the interface Γ be a $C^{1,1}$ closed surface. Let $\boldsymbol{\Theta} \in C^1_c(\overline{D};\mathbb{R}^d)$ be an extension in a neighbourhood D of Ω_s of the unit normal on Γ (such an extension exists, see [130, Chap. I, Lemma 3.1]). Any pair $(\phi,\mathbf{u})$ solving $-\Delta\phi+\phi''=0$ in $\Omega_f\times[0,T]$ and $-\rho_s^{-1}\boldsymbol{\Delta}_{\mathbf{s}}\mathbf{u}+\mathbf{u}''=0$ in $\Omega_s\times[0,T]$ verifies the integral identity*

$$\|\phi'\|^2_{\Gamma,T}+\|\mathbf{u}'\|^2_{\Gamma,T}+\|\partial_n\phi\|^2_{\Gamma,T}+\|\partial_n\mathbf{u}\|^2_{\Gamma,T,\mathbf{Q}^{-1}}=\|\nabla_{\mathbf{s}}\phi\|^2_{\Gamma,T}+\|\nabla_{\mathbf{s}}\mathbf{u}\|^2_{\Gamma,T,\mathcal{C}}+\mathcal{C}(\phi,\mathbf{u};\boldsymbol{\Theta}), \tag{2.96}$$

where $\nabla_{\mathbf{s}}\phi:=\nabla\phi-\partial_n\phi\mathbf{n}$ is the tangential gradient of ϕ ($\nabla_{\mathbf{s}}\phi$ is entirely determined by the boundary trace $\phi|_\Gamma$ of ϕ, see e.g. [154, Sec. 2.5.6]), $\mathbf{Q}$ is the symmetric positive definite Christoffel matrix (defined by $Q_{ik}=\mathcal{C}_{ijk\ell}n_kn_\ell$), $\|\mathbf{f}\|^2_{\Gamma,T,A}:=(A.\mathbf{f},\mathbf{f})_{\Gamma,T}$ for A symmetric positive definite, and we have

$$\begin{aligned}\mathcal{C}(\phi,\mathbf{u};\boldsymbol{\Theta})=&\left(|\phi'|^2-|\nabla\phi|^2,\ Div\boldsymbol{\Theta}\right)_{\Omega_f,T}+2\left((\nabla\phi\otimes\nabla\phi),\nabla\boldsymbol{\Theta}\right)_{\Omega_f,T}\\&+2\left(\phi',\nabla\phi.\boldsymbol{\Theta}\right)_{\Omega_f}\Big|_0^T+\left(|\mathbf{u}'|^2-\nabla\mathbf{u}:\mathcal{C}:\nabla\mathbf{u},\ Div\boldsymbol{\Theta}\right)_{\Omega_s,T}\\&+2\left(\nabla\mathbf{u}:\mathcal{C}:\nabla\mathbf{u},\nabla\boldsymbol{\Theta}\right)_{\Omega_s,T}+2\left(\mathbf{u}',\nabla\mathbf{u}.\boldsymbol{\Theta}\right)_{\Omega_s}\Big|_0^T.\end{aligned} \tag{2.97}$$

We then temporarily assume that the data is in $H^1_T(\mathbf{H}^{1/2}(\Gamma))$, i.e., sufficiently smooth to lead to a solution smooth enough to justify all integrations by parts producing (2.96). We first note that

$$|\mathcal{C}(\phi,\mathbf{u};\boldsymbol{\Theta})|\le C\|(\nu,h\mathbf{n})\|^2_{H^1_T(\mathbf{L}^2(\Gamma))}. \tag{a}$$

This follows directly from the interior regularity result of (i) for the space-time norms, and from Theorem 2.2.1 for the space norms at $t=T$. We also have

$$\|\nabla_{\mathbf{S}}\phi\|^2_{\Gamma,T}+\|\nabla_{\mathbf{S}}\mathbf{u}\|^2_{\Gamma,T,\mathcal{C}}\le C\|(\nu,h\mathbf{n})\|^2_{H^1_T(\mathbf{L}^2(\Gamma))} \tag{b}$$

by similar arguments together with:

- available estimates for surface gradients, see e.g. [148, Lemma 4.23]
- the (uniform on Γ) inequality $|\partial_n\mathbf{u}|^2\le C|\partial_n\mathbf{u}.\mathbf{Q}^{-1}.\partial_n\mathbf{u}|\le C|\partial_n\mathbf{u}|^2$ exploiting classical ellipticity properties of the elasticity tensor $\mathcal{C}$.

Since in addition $\mathbf{t}[\mathbf{u}]=\mathbf{n}.\mathcal{C}:\nabla_{\mathbf{S}}\mathbf{u}+\mathbf{Q}+\partial_n\mathbf{u}$, we have

$$\|\mathbf{t}[\mathbf{u}]\|^2_{\Gamma,T}\le C\left(\|\partial_n\mathbf{u}\|^2_{\Gamma,T}+\|\nabla_{\mathbf{s}}\mathbf{u}\|^2_{\Gamma,T}\right)\le C\left(\|\partial_n\mathbf{u}\|^2_{\Gamma,T}+\|(\nu,h\mathbf{n})\|^2_{H^1_T(\mathbf{L}^2(\Gamma))}\right) \tag{c}$$

We finally use (a), (b) and (c) in (2.97) and obtain

$$\|\phi'\|^2_{\Gamma,T}+\|\partial_n\phi\|^2_{\Gamma,T}+\|\mathbf{u}'\|^2_{\Gamma,T}+\|\mathbf{u}[\mathbf{u}]\|^2_{\Gamma,T}\le C\|(\nu,h\mathbf{n})\|^2_{H^1_T(\mathbf{L}^2(\Gamma))}. \tag{2.98}$$

All claims of (ii) finally follow by the density of $H^1_T(\mathbf{H}^{1/2}(\Gamma))$ in $H^1_T(\mathbf{L}^2(\Gamma))$.

2.8 Conclusion

This chapter had two purposes: (i) to mathematically study the well-posedness of all the continuous evolution problems involved in the construction of a convergent iterative global-in-time algorithm to solve fluid-structure interaction problems and (ii) to use these solvability results to prove the convergence of the global-in-time iterations based on the successive solutions of Robin IBVPs.
The solvability results for the transient acoustic-elastic scattering problem, the Neumann IBVPs and the Robin IBVPs show that

- The data-to-solution mappings we recall for the acoustic-elastic coupled problem provide important information regarding the transmission data regularity needed to obtain a $L^2_T(\mathbf{H}^1)$ trace solution regularity. We highlight in particular the difference with classical time-harmonic results for FSIPs, where a data $(\nu, h\mathbf{n}) \in L^2_T(\mathbf{H}^{-1/2}(\Gamma))$ is sufficient to imply a solution with $L^2_T(\mathbf{H}^1)$ space-time regularity. For the transient FSI problem (2.4) one extra unit of data regularity either in space or in time is needed to reach such a solution.

- Transient Neumann IBVPs have solutions whose regularity is lower than that of the transmission data. This is characteristic of the Neumann evolution problem and contrasts with classical second-order elliptic cases for which the Neumann data yields the same time regularity for the trace solution in velocity. For example in the elliptic case, an interfacial Neumann data with $H^{-1/2}(\Gamma)$ space regularity entails a solution with the same regularity. Consequently an iterative procedure based on the successive resolutions of Neumann IBVPs in each subdomain cannot be proved convergent.

- Transient Robin IBVPs present different regularity properties. We highlight that their velocity trace solutions remain in the same space of regularity as the transmission data. Consequently, we show that an iterative procedure based on successive resolutions of such Robin IBVPs remain in a fixed regularity space and might be convergent.

We used these original data-to-solution mappings to prove that an algorithm based on successive resolutions of Robin IBVPs for a data $\mathbb{H} \in \mathbb{H}^1_T(\Gamma)$ is convergent in $\mathbf{L}^2_T(\Gamma)$, as well as iterations based on relaxed Robin boundary conditions (2.44) and (2.45). The algorithm proposed in this chapter has thus a guaranteed convergence and allows to solve a transient FSI problem. A first numerical illustration shows that a minimal space-time regularity in needed for the data $\mathbb{H}$ to reach a continuous solution in time with the Robin global-in-time iterations, which meet the requirement of the solvability results we proved.

In the next chapter, these procedures are numerically applied and compared in order to confirm the theoretical conclusions obtained in this chapter.

CHAPTER 3

A global-in-time FEM/Z-BEM iterative method

In this chapter, we propose to apply the global-in-time iterative method to simulate complex fluid-structure interaction problems. To obtain the most efficient solver we couple the FEM and the Z-BEM methods. The Z-BEM allows to solve transient wave propagation problems in unbounded linear homogeneous domains very efficiently. Its definition makes it a natural candidate for global-in-time algorithms. Its use is therefore perfectly suitable for the iterative Robin-Robin coupling that we propose. On the other hand, finite elements are the most appropriate method for modelling the potentially complex and non-linear behaviour of structures. In Section 3.1, we recall the theory of transient boundary integral equations as well as of BEMs. Then Section 3.2 gives some reminders about the principle and the particularities of the Z-BEM. In Section 3.3, the coupling method is validated numerically on a simple 2D FSI example. The convergence is evaluated and we then study the optimal values of the coupling parameters involved in the Robin transmission conditions. We also compare the Robin-Robin algorithm convergence with other types of global-in-time iterations (Dirichlet-Dirichlet, Neumann-Neumann). In Section 3.4, we further improve the convergence of our global-in-time iterative FEM/Z-BEM coupling. The optimised coupling parameters are applied to a more complex 2D problem, with the aim of validating our estimate for the optimised Robin coupling parameter value and evaluating the convergence acceleration. We also apply a Aitken's fixed-point acceleration to further reduce the number of iterations. In Section 3.5 we propose a new high-frequency approximation adapted for the Z-BEM procedure with Robin boundary conditions, that drastically reduces the number of time-harmonic BEM problems to solve. Finally we detail how this FEM/Z-BEM method can be applied to realistic complex UNDEX problems without major adjustment (Section 3.6).

Contents

3.1 Boundary element methods 75

3.1.1 BIE for transient wave propagation 77

3.1.2 Numerical solutions of time-domain BIEs 80

3.2 Z-BEM 81

3.2.1 General principle of the convolution quadrature method . 82

3.2.2 Z-BEM 84
3.3 Global-in-time FEM/Z-BEM Robin-Robin iterative coupling 86
3.3.1 Model 2D FSI problem analysis 86
3.3.2 Comparison of algorithms based on Robin, Neumann and Dirichlet boundary conditions 89
3.3.3 Optimal parameters for the Robin boundary conditions . 89
3.4 Convergence acceleration 99
3.4.1 Optimised Robin coupling parameters 100
3.4.2 Aitken's acceleration 100
3.5 High-frequency approximations for an efficient FSI Robin problem 103
3.6 Global-in-time FEM/Z-BEM coupling for UNDEX . . . 107
3.7 Conclusion 109

3.1 Boundary element methods

Boundary element methods (BEM) correspond to the discretisation of boundary integral equations (BIE). It was historically introduced for time-harmonic elastostatics by [172] and [52]. The BEM was then extended to evolution problems with the addition of some techniques initially developed for finite element methods (mesh techniques, shape functions, Gauss quadrature...) [17, 121]. This method is based on the reformulation of the PDE as a boundary integral equation and on the knowledge of a fundamental solution characteristic of the domain. The boundary integral representation is usually obtained with a reciprocity theorem and a Green's identity [178]. The derivation for acoustic problems in unbounded domains is described in Section 3.1.1. To solve an exterior problem, only the evaluation of the fields on the boundary of the domain is needed. This drastic reduction of the problem size is one of the BEM main advantages. The BEM is therefore well-suited for unbounded media or problems where the surface versus volume ratio is small. Moreover the BEM can easily handle unbounded domains as it intrinsically accurately takes into account the radiation condition at infinity [154]. It does not require to approximate absorbing or transparent boundary conditions to truncate the computational domain, which thus avoid undesirable reflections [94, 152].

The BEM have been shown to be competitive to volume discretisation methods in the context of scattering problems [12]. But one main difficulty remains: the necessary knowledge of problem-specific Green's functions. This leads to significant restrictions on the range of the problems to which BEMs can be applied.

For linear and homogeneous media, fundamental solutions and their derivatives are generally available. Some of them, particularly in the case of acoustics are detailed in [26]. On the other hand, non-linearities and inhomogeneous media are rarely included in the formulation, as Green's functions are hardly explicitly known. They would generally introduce volume integrals and require the volume to be discretised, removing the main advantages of the BEM.

Another numerical difficulty is related to the fundamental solutions. By definition, they are singular at some points and, the singularity increases with the order of derivation. In fact, these fundamental solutions have a strong singularity when it is evaluated on a field point $\mathbf{y}$ equal to the source (or collocation) point $\mathbf{x}$. For example, the classical fundamental solution for free space generated by a unit point source located at $\mathbf{x}$ is given by

$$G(\mathbf{y}, \mathbf{x}) = \frac{1}{4\pi r}, \quad r := |\mathbf{r}| = |\mathbf{y} - \mathbf{x}| \,.$$

For transient acoustic wave propagation problems in an unbounded domain, with a point source applied at $\mathbf{y}$ with a time modulated intensity $f(t)$, the *free space fundamental solution* is given by

$$G(\mathbf{y} - \mathbf{x}, t \mid f) = \frac{f(t - \frac{r}{c})}{4\pi r}, \quad r := |\mathbf{x} - \mathbf{y}| \,.$$

As a consequence, to solve boundary integral equations with the BEM, the accurate evaluation of singular (and hypersingular) integrals is therefore necessary. And if this singularity is not integrable, one has to regularise the integral which is then defined in a distributional sense. This is nowadays well known and very well addressed [190].

One can finally mention the progress that has made it possible to overcome one of the initial drawbacks of the BEM: the extension to problems involving unbounded material interfaces. Recent advances for time-harmonic problems of scattering from unbounded material interfaces have led to the development of highly efficient solvers, using in particular the windowed Green's function (WGF) method (see for example [120]).

The BEM is mainly used for time-harmonic problems, for which only a spatial discretisation is necessary. Two main discretisation approaches exist: the collocation method, which consists of enforcing a BIE at a finite number of points [26], and the Galerkin method, a variational approach based on a weak form of the BIE. In contrast to the collocation method, the Galerkin approach may entail a symmetric system of equations (at the cost of evaluating double surface integrals) which is very useful for its mathematical analysis [26]. Independently of the discretisation method chosen, a fully-populated matrix system is obtained due to the use of Green's functions. It can be written in the general form

$$\Big[K\Big] \{\phi\} = \{f\}$$

where $\{\phi\}$ represents the N unknown degrees of freedom (DOF), while the N $\times$ N matrix of influence coefficients $\Big[K\Big]$ contains evaluations of the boundary integrals. This fully-populated matrix is a major drawback of the BEM. The storage of such

a system has a quadratic cost and its solution with a direct solver (a LU factorisation for example) has a cubic complexity. With an iterative solver (GMRES for example [173]), each iteration requires one evaluation of the matrix-vector product $\left[K\right]\{\phi\}$, a task requiring a computing time of order $O(N^2)$. With n_{it} iterations to achieve convergence, the system resolution thus requires $O(n_{it}N^2)$ operations. Standard BEMs are therefore hardly applicable for problems larger than N=$O(10^4)$ on personal desktop. For time-harmonic problems this also limits the frequency range possibly studied, as the boundary mesh size is related to the problem frequency.

This complexity can however be improved by applying fast boundary element methods to reduce the memory requirement and speed-up a matrix-vector product. We mention two fast boundary element methods: the fast multipole method (FMM) and hierarchical matrices (H-matrix). The FMM reformulates the fundamental solution with a series expansion in order to factorise some operations [41, 53, 95]. The computational complexity of each matrix-vector product using the FMM for oscillatory kernels is reduced to O(Nlog(N)) instead of $O(N^2)$ for classical BEMs. The second fast boundary element method is purely algebraic and consists in partitioning the system matrix into several block matrices of various sizes and then approximating these matrices by low rank submatrices. The matrices are hierarchically partitioned into blocks using the H-matrix concept proposed in [97] and the blocks are approximated using a compression algorithm, such as the adaptative cross approximation [135] or the hybrid cross approximation for example [27]. Both FMM and H-matrix methods have been compared for example in [33].

Most of previous works on fast BEMs have been done for time-harmonic problems but this work concerns boundary element methods for transient acoustic problems. In Section 3.1.1 the transient differential acoustic problem is defined and reformulated as a boundary integral equation.

3.1.1 BIE for transient wave propagation

We first consider an acoustic domain Ω without any obstacle, bounded by a boundary $\Gamma = \partial\Omega$. The scalar velocity potential ϕ verifies the wave equation and for example a Neumann BC

$$\begin{cases} \Delta\phi - \frac{1}{c_f^2}\frac{\partial^2\phi}{\partial t^2} = 0 & \forall(t,\mathbf{x}) \in [0,T]\times\Omega, \\ \nabla\phi.\mathbf{n} = g & \forall(t,\mathbf{x}) \in [0,T]\times\Gamma, \\ \phi(0,\mathbf{x}) = \frac{\partial\phi}{\partial t}(0,\mathbf{x}) = 0 & \forall\mathbf{x}\in\Omega \end{cases} \tag{3.1}$$

where $T \in]0,+\infty[$ is the finite duration, and c_f is the fluid sound velocity. In the time domain for a finite T, there is no need to specify radiation conditions, because the propagation takes place in a finite domain, due to the finite speed c_f, and so the support of $\phi(t,.)$ is a bounded region of Ω for all t $\in [0,T]$. The Neumann BC involves $\mathbf{n}$, the outward normal to Ω and a function g defined on Γ. The problem is at initial rest. In general, initial conditions are not zero and there are body sources [26].

To establish the boundary integral equation of (3.1), we consider a fixed point $\mathbf{y}\in\Omega$ and an impulsive point source is applied at $\mathbf{y}$, with a time modulated amplitude

$\delta(t)$ (Figure 3.1). The acoustic wave propagation problem is

$$\begin{cases} \Delta G - \frac{1}{c_f^2}\frac{\partial^2 G}{\partial t^2} + \delta(\mathbf{y}-\mathbf{x})\delta(t) = 0 & \forall (t,\mathbf{x}) \in [0,T]\times\Omega, \\ \nabla G.\mathbf{n} = g & \forall (t,\mathbf{x}) \in [0,T]\times\Gamma, \\ G(0,\mathbf{x}) = \frac{\partial G}{\partial t}(0,\mathbf{x}) = 0 & \forall \mathbf{x} \in \Omega. \end{cases} \tag{3.2}$$

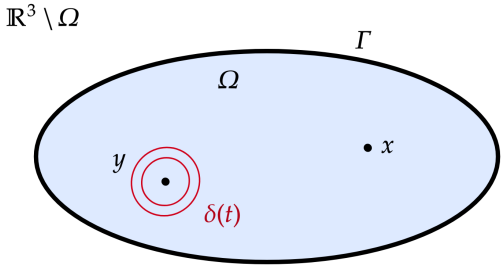

Figure 3.1: *Impulsive point source in a bounded domain* Ω.

The solution G of the problem is the free space fundamental solution and for 3D acoustic problems, it is given by:

$$G = (t,\mathbf{x},\mathbf{y}|\delta) = \frac{\delta(t - r/c_f)}{4\pi r}, \qquad r = \|\mathbf{y}-\mathbf{x}\|.$$

The idea is to apply the time convolution between (3.2) satisfied by the impulsive fundamental solution G and the solution $\phi(t,\mathbf{x})$. The time convolution product $\star$ is defined for causal functions by

$$(u \star v) = \int_0^t u(t-\tau)v(\tau)d\tau = \int_0^t v(t-\tau)u(\tau)d\tau = (v \star u), \quad \forall t \geq 0.$$

The convolution product has two important properties:

$$\frac{\partial (u \star v)}{\partial t} = \frac{\partial u}{\partial t} \star v = \frac{\partial v}{\partial t} \star u \tag{3.3}$$

and for a Dirac distribution δ the convolution product with a function f holds

$$f(t) = \int_0^t f(t-\tau)\delta(\tau)d\tau = (f \star \delta)(t).$$

Equation (3.2) becomes

$$\begin{gathered} \int_0^t \left[\Delta G(t-\tau) - \frac{1}{c_f^2}\partial_t^2 G(t-\tau)\right]\phi(\tau)d\tau + \int_0^t \delta(\mathbf{y}-\mathbf{x})\phi(t-\tau)\delta(\tau)d\tau = 0, \\ \Rightarrow (\Delta G \star \phi)(t,\mathbf{x}) - \frac{1}{c_f^2}\left(\partial_t^2 G \star \phi\right)(t,\mathbf{x}) + \delta(\mathbf{y}-\mathbf{x})\phi(t,\mathbf{x}) = 0. \end{gathered} \tag{3.4}$$

As the solution ϕ verifies the wave equation, using the property (3.3), the second term is reformulated as

$$\frac{1}{c_f^2}\left(\partial_t^2 G \star \phi\right)(t,\mathbf{x}) = \frac{1}{c_f^2}\left(G \star \partial_t^2 \phi\right)(t,\mathbf{x}) = \left(G \star \Delta\phi\right)(t,\mathbf{x}). \tag{3.5}$$

Recalling the second Green's identity

$$\forall u, v \in H^1_\Delta(\Omega) \quad \int_\Omega \left[\Delta u.v - u.\Delta v\right] dV = \int_{\partial\Omega} \left[\frac{\partial u}{\partial n} v - u.\frac{\partial v}{\partial n}\right] d\Gamma.$$

we integrate (3.5) over the domain Ω to write the variational formulation of (3.4). Since G is a distribution and is not integrable, the integral representation has to be obtained by a limiting process. As described in [148], we consider a truncated domain $\Omega_\epsilon \subset \Omega$ obtained by removing a ball of radius ϵ and centre $\mathbf{y}$, and when $\epsilon \to 0$, the boundary integral representation writes

$$\int_\Gamma \left[\partial_n G \star \phi - G \star \partial_n \phi\right](t,\mathbf{x}) d\Gamma + \phi(t,\mathbf{y}) = 0 \quad \forall (t,\mathbf{x}) \in [0,T] \times \Omega.$$

Due to the singularity of fundamental solution G, this boundary integral representation is not valid when $\mathbf{y} = \mathbf{x}$. Obtaining the boundary integral equation defined on the boundary Γ is therefore the most difficult part, because a passage to the limit when $\mathbf{y} \to \mathbf{x}$ is necessary. The interested reader may refer to [23] in order to read the complete derivation of the boundary integral equation. As an illustration, we consider the exterior problem depicted on Figure 3.2: the boundary is $\Gamma_s = \partial\Omega_s$ surrounded by a spherical bounded domain Ω_f. The sphere of radius R is bounded by a boundary Γ_f and its centre is a point within Ω_s.

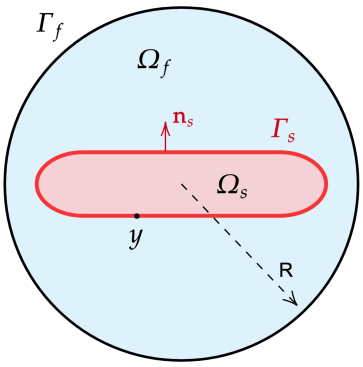

Figure 3.2: *Geometrical notations used for the derivation of the boundary integral equation for an exterior wave propagation problem.*

Let $\mathbf{y}$ be a fixed point of the domain. For the domain Ω_f, the boundary integral equation is defined on the boundary $\partial\Omega_f = \Gamma_f \cap \Gamma_s$. However, R being large enough so that all the variables vanish on Γ_f due to causality. The boundary integral representation equations is written in a uniform way with a parameter κ, depending on the position of $\mathbf{y}$ in the domain:

$$\kappa\phi(t,\mathbf{y}) = \int_{\Gamma_s} \left(\partial_n \phi(t,\mathbf{x}) \star G(t,\mathbf{x},\mathbf{y}) - \partial_n G(t,\mathbf{x},\mathbf{y}) \star \phi(t,\mathbf{x})\right) d\Gamma_s$$

with $\kappa = 1$ if $\mathbf{y} \in \Omega$, $\kappa = 0$ if $\mathbf{y} \in \mathbb{R}^3 \setminus \Omega$ and $\kappa = 1/2$ if $\mathbf{y} \in \Gamma$. Let now $\mathbf{y}$ be a point on Γ_s and $\mathbf{n}$ the outward normal to Ω_f. According to the usual convention the equation is written as a function of the outward normal $\mathbf{n_s} = -\mathbf{n}$ to Ω_s:

$$\boxed{\frac{1}{2}\phi(t,\mathbf{y}) = -\int_{\Gamma_s} \left(\partial_{n_s}\phi(t,\mathbf{x}) \star G(t,\mathbf{x},\mathbf{y}) - \partial_{n_s} G(t,\mathbf{x},\mathbf{y}) \star \phi(t,\mathbf{x})\right) d\Gamma_s} \tag{3.6}$$

It is classical to introduce the single-layer and double-layer retarded potentials defined with densities f, g by:

$$\mathcal{G}\{f\}(t,\mathbf{y}) = \int_{\Gamma_x} G(t,\mathbf{y}-\mathbf{x}) \star f(t,\mathbf{x}) d\Gamma_x, \quad \mathcal{H}\{g\}(t,\mathbf{y}) = \int_{\Gamma_x} \frac{\partial G}{\partial n}(t,\mathbf{y}-\mathbf{x}) \star g(t,\mathbf{x}) d\Gamma_x$$

for $\mathbf{y} \in \mathbb{R}^3 \setminus \Gamma$. The boundary integral equation (3.6) reads as:

$$\boxed{\frac{1}{2}\phi(t,\mathbf{y}) = \mathcal{H}\{\phi\}(t,\mathbf{y}) - \mathcal{G}\left\{\frac{\partial \phi}{\partial n}\right\}(t,\mathbf{y}) \quad (t,\mathbf{y}) \in [0,T] \times \Gamma_s} \tag{3.7}$$

3.1.2 Numerical solutions of time-domain BIEs

Efficient solvers for ime domain boundary integral equations are still not as developed as for elliptic problems. A review of the available methods is given in [50]. The transient BEM problem (3.7) can be solved either directly in the time domain, using time-domain Galerkin methods or time-stepping collocation methods, or through a transfer in the complex frequency domain with Laplace-transform based approaches. All these approaches have different advantages and drawbacks.

1. **Space-time Galerkin boundary element methods.** One option is to use a Galerkin method to discretise the retarded boundary integral equation [10, 67]. This leads to a space–time weak formulation of the BIE. The integral problem can then be discretised by a stable scheme and a discrete space- and time-dependent system can thus be built. The main advantage of these approaches is the possibility to use variable time steps. But these methods are also very expensive in terms of computational and storage costs since they require double integrations both in space. Moreover, such formulations require an adequate choice of the time step size. If improved and more stable versions have been published [1, 10], an improperly chosen time step size still leads to instabilities or numerical damping. The spatial integration domains are generally delimited by wave fronts and are very complicated to handle numerically, especially in the case of curved boundary elements. These issues can be overcome with the help of specially designed time basis functions [177], of adapted quadrature schemes [154] or by analytically performing some of the involved integrations [2]. Finally fast boundary element methods for space-time formulations are hard to formulate [191] and these methods are thus not widely used for large industrial problems. The method is for example implemented in a parallelised BEM software for general engineering problems [149].

2. **Retarded potential methods.** These approaches are based on the time discretisation of the boundary integral equation with an implicit scheme. The

most frequently adopted discretisation scheme is the collocation technique with a direct step-by-step evaluation of the time convolution: an elliptic boundary integral equation is solved at each time step [143]. These so called marching-on-time (MOT) solvers present two major drawbacks that have been partly overcome. First, at each time step, the elliptic problem has a non-zero initial data, which is unconvenient for boundary integral method, usually used with vanishing initial conditions and volume forces, and non-homogeneous boundary data. Various strategies have been developed to overcome this problem [50]. Secondly these methods are often unstable and require a very precise choice of time step. A too large or too small time step leads to important instabilities, high computational costs (especially for rapid problems) or undesirable numerical damping. The field of fast solvers that are based on MOT is relatively well-developed and many improvements to overcome this drawback have been proposed, for example with a proper choice of temporal basis functions, implicit time-stepping schemes, or carefully designed spatial integration schemes [176]. Finally, the mathematical analysis of such methods remain incomplete as in more than two dimensions stability and convergence of collocation schemes can only be shown for special geometries [55].

3. **Methods based on a Laplace (or Fourier) transform.** A third way to evaluate the time convolution in the time-domain BIE is to apply a convolution quadrature method (CQM), as developed by C. Lubich [139]. The convolution quadrature method combines Laplace (or Fourier) transform of the fundamental solution and a usual time-stepping approach [11, 98, 179]. This results in a stable and efficient time-stepping algorithm. CQM-based solution algorithms are becoming a popular approach to solve time domain BIEs, since they rely on the relative simplicity of frequency-domain BEMs. These methods allow to apply many robust techniques developed for frequency domain problems (including fast solvers based on fast multipole method). The main drawback is the time step for the time discretisation whose size must be constant. A generalisation to non-uniform time schemes is therefore not straightforward [137].

In this work we focus on the third category and especially on the so called "Z-BEM" procedure.

3.2 Z-BEM

In this section we describe the Z-BEM. This method is not new but it is important to understand the constraints we have to deal with to define an iterative framework. We first introduce the main principles of the convolution quadrature method (CQM) where a convolution product is evaluated with a tailored quadrature. We then explain how the CQM is used to solve transient BIEs in the context of Z-BEM. We finally introduce some high-frequency approximation to improve the method efficiency.

3.2.1 General principle of the convolution quadrature method

The CQM was historically proposed in [139] and [140] by C. Lubich. It provides a stable time-stepping scheme using the Laplace transform of the fundamental solution. The CQM enables to reformulate time-domain BIEs in the frequency domain. In this work we consider time-domain boundary integral equations which include two convolution products, such as

$$\frac{1}{2}\phi(t,\mathbf{y}) = \int_\Gamma \frac{\partial G}{\partial n}(t,r) \star \phi(t,\mathbf{x}) d\Gamma_x - \int_\Gamma G(t,r) \star \frac{\partial \phi}{\partial n}(t,\mathbf{x}) d\Gamma_x. \tag{3.8}$$

We introduce the unknown $f = \frac{\partial \phi}{\partial n}$. $\forall t \geq 0$, we want to evaluate $q(t)$ given by

$$q(t) = (G \star f)(t) = \int_0^t G(t-\tau) f(\tau) d\tau = \int_0^t f(t-\tau) G(\tau) d\tau = (f \star G)(t). \tag{3.9}$$

G can be expressed in terms of its Laplace transform $\overline{G}$ using the Bromwich integral (or inverse Mellin formula), applying then Fubini's theorem. It follows:

$$q(t) = \frac{1}{2i\pi} \int_{\gamma - i\infty}^{\gamma + i\infty} \overline{G}(s) \int_0^t e^{s(t-\tau)} f(\tau) d\tau ds.$$

The starting point of the CQM is to introduce a time continuous function h, parameterised by s:

$$h(t;s) = \int_0^t e^{s(t-\tau)} f(\tau) d\tau.$$

We observe that h is solution of the ODE

$$\begin{cases} \frac{dh}{dt}(h;s) = sh(t;s) + f(t) \\ h(t \leq 0; s) = 0 \end{cases} \tag{3.10}$$

If we split the time interval $[0,T]$ into $N+1$ time steps of equal length $\Delta t = T/N$ and introduce the discrete time levels $t_n = n\Delta t$. Our goal is now to determine the discrete values $q_n = q(t_n)$ of the convolution product q at the discrete times t_n. The ODE (3.10) is then solved numerically with $h_n(s) = h(t_n; s)$. Various integration scheme can be used, e.g. an Euler integration scheme or a multistep scheme. With a general linear k-step scheme, it follows:

$$\begin{cases} \frac{dh_n(s)}{dt_n} = \frac{1}{\Delta t} \sum_{j=0}^{k} \alpha_j h_{n+j-k}(s) = \sum \beta_j (s h_{n+j-k}(s) + f_{n+j-k}) \\ h_{-p}(s) = f_{-p} = 0 \qquad \forall p \in [1,k] \end{cases} \tag{3.11}$$

The coefficients α_j and β_j depend on the multistep scheme we choose. We then introduce the *$\mathcal{Z}$-transform*. It converts a discrete transient signal into a complex frequency-domain representation. It might be considered as a discrete equivalent of the Laplace transform. The $\mathcal{Z}$-transform $\mathcal{Z}[(x_n)](\xi)$ of a discrete-time signal (x_n) is defined by

$$\mathcal{Z} : (x_n) = \{x_0, x_1, ...\} \mapsto \mathcal{Z}[(x_n)](\xi) = \sum_{n=0}^{\infty} x_n \xi^n \equiv X(\xi), \quad \xi \in \mathbb{C}. \tag{3.12}$$

Using this definition, we multiply (3.11) by $\Delta t \xi^n$ for some $\xi \in \mathbb{C}$, and take its $\mathcal{Z}$-transform. By summing over n from 0 to ∞, we obtain

$$\begin{aligned}
&\sum_{j=0}^{k} \alpha_j \xi^n h_{n+j-k}(s) = \Delta t \sum_{j=0}^{k} \beta_j \xi^n (s h_{n+j-k}(s) + f_{n+j-k}) \\
\Rightarrow &\sum_{j=0}^{k} \alpha_j \xi^{k-j} (h_{n+j-k}(s) \xi^{n+j-k}) = \Delta t \sum_{j=0}^{k} \beta_j \xi^{k-j} (s h_{n+j-k} \xi^{n+j-k} + f_{n+j-k} \xi^{n+j-k}) \\
\Rightarrow &\sum_{j=0}^{k} \alpha_j \xi^{k-j} H(\xi; s) = \Delta t \sum_{j=0}^{k} \beta_j \xi^{k-j} (s H(\xi; s) + F(\xi))
\end{aligned}$$

Introducing the ratio $p(\xi) = \frac{\sum_{j=0}^{k} \alpha_j \xi^{k-j}}{\sum_{j=0}^{k} \beta_j \xi^{k-j}}$, H and F are then related through

$$H(\xi, s) = \frac{1}{\frac{p(\xi)}{\Delta t} - s} F(\xi)$$

Finally the $\mathcal{Z}$-transform $Q(\xi) = \mathcal{Z}[q_n]\{\xi\}$ of the convolution product $q_n = q(t_n)$ is given by:

$$Q(\xi) = \frac{1}{2i\pi} \int_{\gamma - i\infty}^{\gamma + i\infty} \overline{G}(s) H(\xi; s) ds = \frac{1}{2i\pi} \int_{\gamma - i\infty}^{\gamma + i\infty} \overline{G}(s) \frac{1}{\frac{p(\xi)}{\Delta t} - s} F(\xi) ds$$

where $\overline{G}$ is a complex-valued function, defined and derivable at any point, with values in $\mathbb{C}$. γ is a closed path belonging to the domain of definition of $\overline{G}$ and $s = \frac{p(\xi)}{\Delta t}$ is a point that does not belong to γ. Assuming the applicability of the residue theorem, we evaluate this integral's residual in the complex plan at $s = \frac{p(\xi)}{\Delta t}$. The convolution product is finally given by

$$\boxed{Q(\xi) = \overline{G}\left(\frac{p(\xi)}{\Delta t}\right) F(\xi)}. \tag{3.13}$$

From this relation, there are several ways of using the CQM to solve time-domain boundary integral equations. Historically, the CQM proposed by C. Lubich consists in decomposing the $\mathcal{Z}$-transforms $\overline{G}$ and F into series

$$\overline{G}(s) = \sum_{m=0}^{\infty} \omega_m(\Delta t, \overline{G}) \xi^m, \quad \text{and} \quad F(\xi) = \sum_{j=0}^{\infty} f_j \xi^j$$

and in expressing the convolution product as a product.

$$Q(\xi) = \overline{G}(s) F(\xi) = \sum_{m=0}^{\infty} \sum_{j=0}^{\infty} \omega_m(\Delta t, \overline{G}) f_j \xi^{m+j}$$

In this way, the convolution product is a series, whose coefficients $\omega_m(\Delta t, \overline{G})$ are calculated in the frequency domain. There exists different strategies to efficiently compute these weights [12, 139]. As $F(\xi)$ is known (it is the $\mathcal{Z}$ transform of the

discretised data $\frac{\partial \phi}{\partial n}(t_n)$), and as $\overline{G}(s) = \sum_{m=0}^{\infty} \omega_m(\Delta t, \overline{G})\xi^m$, the convolution product $Q(\xi)$, and thus the BEM operators are numerically evaluated if we know the weights ω_m. It is then easy to obtain the discrete-time convolution product q_n, expressed by taking the term of rank n in the series, divided by $\xi^n = \xi^{m+j}$. Using this discretised convolution product in the boundary integral equation and taking the $\mathcal{Z}$-transform of the obtained equation leads to a full-populated matrix system where the coefficient are the quadrature weights. This approach is detailed in [98] and [12]. It is also applied with different integration schemes for example in [45]. This procedure however requires the quadrature weights to be calculated before solving the BIE, and their explicit formulation can be expensive to compute.

Another possibility is to use the CQM to discretise in time the whole transient wave propagation problem. The resulting equation can be reformulated as a BIE in the frequency domain [179] and then be solved with a classical frequency-domain BEM. This method is used for example in [21] and [120]. We follow this approach in the next Section.

3.2.2 Z-BEM

The Z-BEM consists in reformulating the time-domain BIE in the complex frequency domain. Based on (3.13), with $r = \|\mathbf{y} - \mathbf{x}\|$ and $s = \frac{p(\xi)}{\Delta t}$:

$$\frac{1}{2}\Phi(\xi, \mathbf{y}) - \int_\Gamma \frac{\partial \overline{G}}{\partial n}(s, r)\Phi(\xi, \mathbf{x})d\Gamma + \int_\Gamma \overline{G}(s, r)\frac{\partial \Phi}{\partial n}(\xi, \mathbf{x})d\Gamma = 0 \tag{3.14}$$

where $\Phi(\xi, .)$ is the $\mathcal{Z}$ transform of the series $\phi_n = \psi(t_n, .)$. To solve a Neumann problem, $\partial_n\Phi$ is the data and Φ is the unknown in (3.14). After spatial discretisation of Γ in N boundary elements, this BIE is written as a matrix system of the form:

$$[H](s)\{\Phi\} = [G](s)\{\partial_n\Phi\}, \qquad s = \frac{p(\xi)}{\Delta t}, \tag{3.15}$$

where $\{\Phi\}$ represents the N unknown degrees of freedom, $\{\partial_n\Phi\}$ is a vector of N evaluations of the data on Γ and $[H]$ and $[G]$ are $N \times N$ matrix discretisations of the double-layer and single-layer operators respectively, as used in (3.7). It can easily be solved with the BEM in the complex frequency domain. The solution $\Psi(., \xi)$ is evaluated in the Laplace domain. The time domain solution $\phi_n(t_n, .)$ is then obtained by taking the term of rank n in the series Φ and applying the Cauchy's residue theorem on a closed contour C of radius ρ:

$$\psi(t_n, .) = \frac{1}{2i\pi}\int_C \Phi(\xi, .)\xi^{-(n+1)}d\xi \qquad \forall n \in \mathbb{N}$$

In practice, we use a trapezoidal quadrature rule to evaluate the integral. The contour C of integration is discretised with L complex frequencies

$$\phi(t_n, .) \simeq \frac{1}{L}\sum_{k=0}^{L-1} \Phi(\xi_k, .)\xi_k^{-n} \quad \forall n \in [0, M]$$

These L complex values are defined by $\xi_k = \rho e^{2i\pi k/L}$. Each coefficient $\phi(t_n, .)$ is then obtained from $L = 2N_t$ complex evaluations. It has been shown that ρ must

be chosen such as $\rho^L = \epsilon$, in order to reach a $O(\epsilon)$ accuracy. This computation has a O(L log L) complexity. The L values of the complex frequencies $s = \frac{p(\xi)}{\Delta t}$ at which a frequency BEM problem must be solved, only depend on the desired accuracy ϵ required for the evaluation of the integral and on the time discretisation (on the time step size Δt and on the number M of time steps) [139]. There are thus $L-1 = 2N_t - 1$ $\mathcal{Z}$-transforms Φ to calculate, which requires the resolution of $2N_t$-1 frequency BIEs of the form (3.14). However as $\Phi = \overline{\Phi}$, half of the complex values are conjugate of the first ones ($\xi_{2N_t-k} = \overline{\xi_k}$), which allows to solve only M+1 BIEs. The problem can finally be solved with a computational cost with respect to time of O(Mlog(M)). Figure 3.3 illustrates the dependence of the CQM complex frequencies

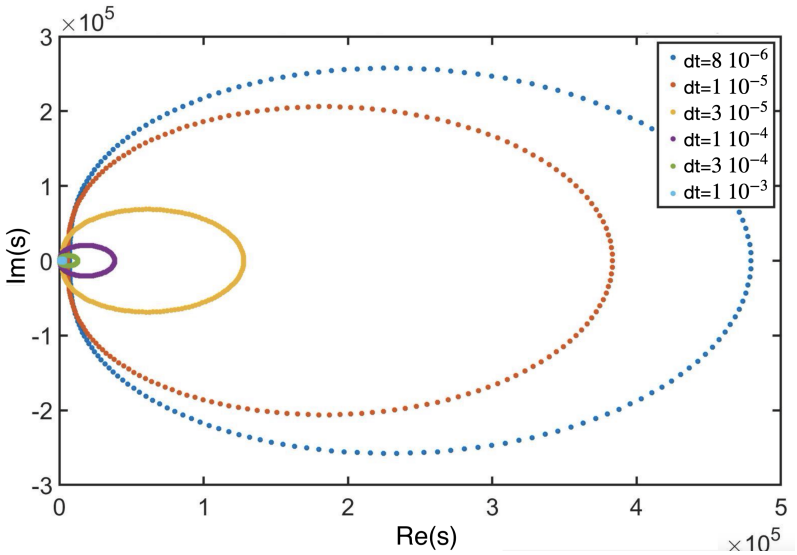

Figure 3.3: *Numerical representation of L=$2N_t$=200 complex frequencies s_k for different time step values, using a BDF2 scheme (N_t=100, $\epsilon = 10^{-5}$).*

to the time discretisation. Six different time steps Δt are considered. For each Δt, the interval $[0, T]$ with $T = M\Delta t$ is used to define L=$2N_t$ ξ_k and L complex frequencies $s_k = \frac{p(\xi_k)}{\Delta t}$, with a BDF2 scheme and N_t=100. This Figure 3.3 illustrates that the Z-BEM complex frequencies s_k only depend on the time discretisation: on the time step Δt and on the total number M of time steps. The choice of Δt impacts the radius of curvature of the ellipse in the complex plane and thus the maximum amplitude taken by the complex frequencies: the smaller the time step is, the larger the corresponding complex frequencies are. The total number of time steps M discretising the time interval determines the density of points on this ellipse.

After recalling the principles of the Z-BEM, we now use it to define an iterative global-in-time FEM/Z-BEM coupling, following the algorithm described in Chapter 2. The next section aims at verifying the numerical behaviour of the coupling.

3.3 Global-in-time FEM/Z-BEM Robin-Robin iterative coupling

In this Section, we analyse the convergence of a global-in-time FEM/Z-BEM iterative procedure based on Robin boundary conditions, applied to a 2D FSI problem. This problem has the advantage of admitting a semi-analytical solution. Its convergence can thus be analysed theoretically.

3.3.1 Model 2D FSI problem analysis

A bounded elastic ring Ω_s of interior and exterior radius R_{int} and R_{ext} is immersed in a acoustic fluid (mass density ρ_f, acoustic wave velocity c_f) occupying the unbounded fluid region $\Omega_f := \mathbb{R}^2 \setminus \overline{\Omega_s}$ (see Figure 3.4). A uniform normal pressure p^{int} is prescribed on the interior surface Γ^{int} of this radially symmetric geometry, which creates a deformation in the elastic solid and a radiated FSI problem on the exterior interface. We assume 2D conditions and plane strain deformations for the solid. Both media are at initial rest. The potential fluid has a time dependent velocity potential $\phi(t)$, a velocity $\mathbf{v}(t) = \nabla\phi(t)$ and a pressure $p(t) = -\rho_f \partial_t \phi(t)$ $\forall t \in [0, T]$. The solid variables are the displacement $\mathbf{u}$ and the stress vector $\mathbf{t} := \sigma[\mathbf{u}].\mathbf{n}$. We use a global-in-time iterative FEM/Z-BEM method based on Robin BCs.

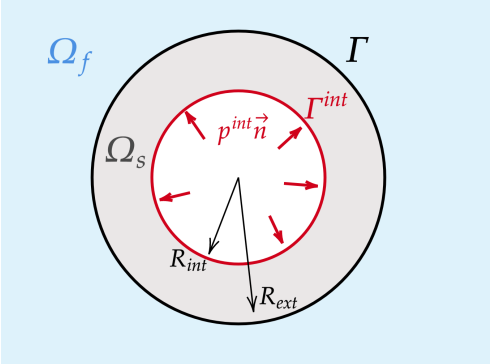

Figure 3.4: *Radially-symmetric pressurised elastic annulus in an acoustic fluid.*

Knowing the semi-analytical solution of the 2D radially symmetric problem (see Appendix A), we first validate the convergence of the iterative Robin-Robin coupling procedure. The relative L^2 error between the known semi-analytical solution and the computed result is evaluated. All numerical results of this section have been obtained with an in-house global-in-time FEM/Z-BEM code (the Z-BEM code is described and validated in Appendix E.2) and under the following conditions: the incident pressure is a spherical wave that propagates in an acoustic medium at speed c_f, before interacting with the interior surface (r=R^{int}) of the annulus. The fluid and structure physical parameters are listed in Table 3.1. The time interval $[0, T]$ is discretised with N_t= 1500 time steps (Δt = 1.7 10^{-6}s). The number L of complex frequencies is set to twice the number of time steps: L = 2 N_t= 3000. The accuracy ϵ of the discrete inverse $\mathcal{Z}$-transform is set to 10^{-5} and the value of ρ_{BEM} is set according to ϵ, such that $\rho_{BEM} L = \epsilon$ [146]. The backward differentiation

formula of order 2 (BDF2) is used and the GMRES tolerance for the frequency-domain fast BEM solver is 10^{-6}. The 45 first BIEs are solved and a high frequency approximation is used to approximate the other frequency solutions (the method is detailed in Section 3.5), which enables to approximate the transient BEM solution with an error smaller than 10^{-2}. We consider a very smooth incident pressure p^{int} applied on the intern boundary:

$$\begin{cases} p^{int}(t) = a(2t/T_p)^\gamma \times (2 - 2t/T_p)^\gamma & \text{if } t \in [0, T_p], \\ p^{int}(t) = 0 & \text{if } t > T_p. \end{cases} \tag{3.16}$$

This causal signal is five time derivable, with an amplitude a=10^8 and a time parameter $T_p = 3\ 10^{-4}$s. To evaluate the algorithm's convergence speed we consider

Name	c_f	ρ_f	E	c_{mat}	ρ_s	ν	R_{int}	R_{ext}
Value	1500	1000	210 10^9	6.0202 10^3	7800	0.3	0.9	1
Unity	m.s^{-1}	kg.m^{-3}	kg.m^{-1}.s^{-2}	m.s^{-1}	kg.m^{-3}	/	m	m

Table 3.1: *Fluid and solid properties.*

the relative error in L_2-norm between a variable (computed on the whole interface and on the whole time interval) and the semi-analytical solution:

$$e_v^{\text{res}} := \frac{\|v^i - v_{\text{analytic}}\|_{L^2([0,T],\Gamma^{\text{ext}})}}{\|v_{\text{analytic}}\|_{L^2([0,T],\Gamma^{\text{ext}})}} \quad \text{and} \quad e_p^{\text{res}} := \frac{\|p^i - p_{\text{analytic}}\|_{L^2([0,T],\Gamma^{\text{ext}})}}{\|p_{\text{analytic}}\|_{L^2([0,T],\Gamma^{\text{ext}})}} \tag{3.17}$$

where v^i and p^i are the fluid velocity and the fluid pressure at iteration i evaluated on the interface. They correspond to the relative errors in pressure and velocity at iteration i. When the convergence is reached, the transmission conditions are verified at the interface

$$\partial_n \phi = \partial_t \mathbf{u}.\mathbf{n} \quad \text{and} \quad \mathbf{t}[\mathbf{u}] = h.\mathbf{n} - p.\mathbf{n}$$

To estimate the number of iterations required to reach the convergence when no reference solution is available, indicators on transmission residuals in velocity and pressure we use e_v^{sol} and e_p^{sol} defined by (2.15). A third indicator $e_{v,p}$ combining the two interfacial variables is defined in Section 2.3.2 by (2.17). As a first validation both fluid pressure and normal velocity solutions on the acoustic-elastic interface are obtained numerically with a coupling parameter $k_c = \rho_f c_f$. After 10 global-in-time iterations with Robin boundary conditions, the iterative algorithm and the semi-analytical method are seen in Figure 3.5a and Figure 3.5b to be in good agreement. As illustrated in Figure 3.6a, the relative errors e_v^{res} and e_p^{res} compared to the semi-analytical solution are lower than 10^{-3} after 6 and 9 iterations respectively. Figure 3.6b shows the convergence of the relative errors $e_p^{\text{sol}}, e_v^{\text{sol}}$ and $e_{v,p}$, with respect to the number of iterations. In this case, 9 FEM/Z-BEM global-in-time iterations are needed to reach $e_{v,p} < 10^{-3}$. Both Figures 3.6a and 3.6b show a stepwise decrease: there is a successive decrease in the velocity error e_v^{sol} at one iteration, and then in the pressure error e_p^{sol} at the next iteration. As a result, the overall error on residual $e_{v,p}$ (in red in the Figure) taking into account the two transmission residuals decreases in a smooth way.

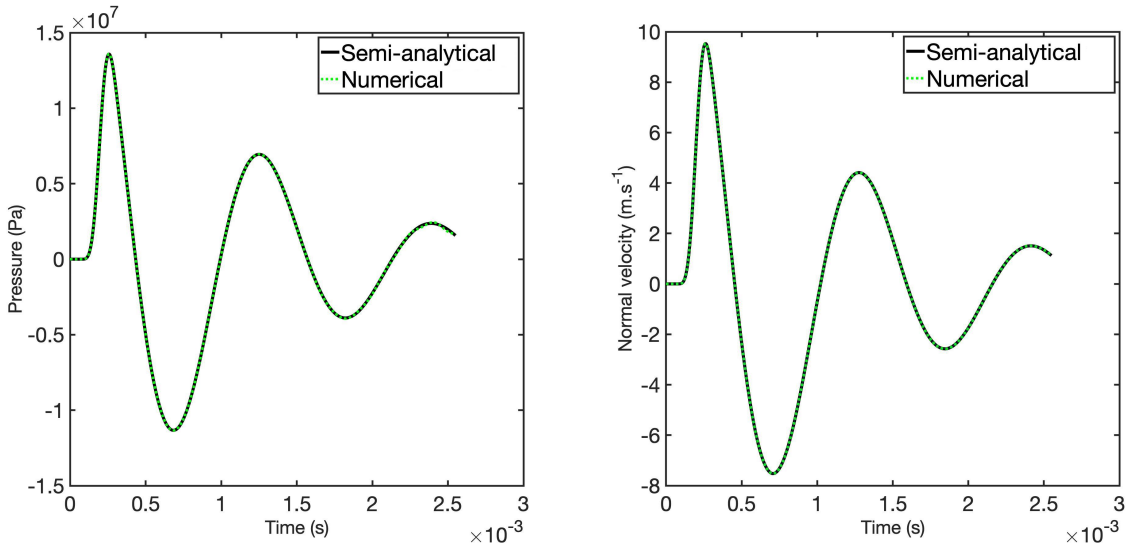

(a) *(b)*

Figure 3.5: *(a) Fluid pressure p at a node $\in \Gamma^{ext}$ obtained with a semi-analytical method and a global-in-time FEM/Z-BEM iterative algorithm ($\Delta t = 1.7\ 10^{-6}, N_t = 1500$, El=2336). Relative error : e_p^{sol} =0.50%. (b) Normal fluid velocity at a node $\in \Gamma^{ext}$ obtained with a semi-analytical method and a global-in-time FEM/Z-BEM iterative algorithm ($\Delta t = 1.7\ 10^{-6}, N_t = 1500$, El=2336). Relative error : e_v^{res} =0.05%.*

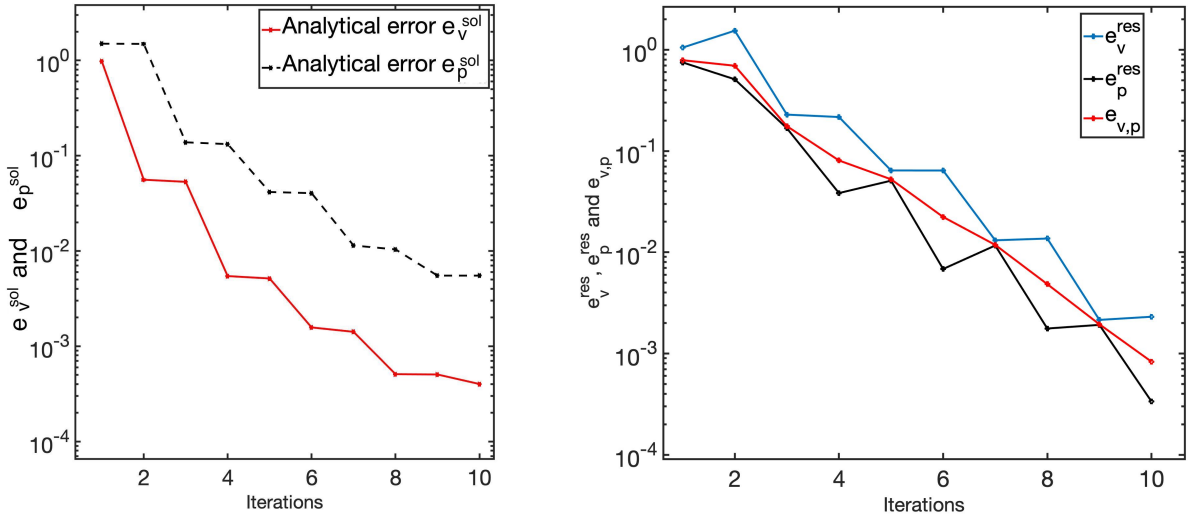

(a) *(b)*

Figure 3.6: *(a) e_v^{res} and e_p^{res} with respect to the analytic solution versus the number of iterations ($\Delta t = 1.7\ 10^{-6}, N_t = 1500$, El=2336). (b) e_v^{sol}, e_p^{sol} and $e_{v,p}$ on transmission residuals versus the number of iterations ($\Delta t = 1.7\ 10^{-6}, N_t = 1500$, El=2336).*

3.3.2 Comparison of algorithms based on Robin, Neumann and Dirichlet boundary conditions

In domain decomposition methods, when using transient step-by-step iterative methods it is common to use Neumann boundary conditions at the interface (see [82] for example). However for global-in-time iterative procedures we have shown (Section 2.3.2) that the loss of space-time regularity of the solutions of Neumann evolution problems do not allow the boundary traces to remain in a fixed regularity space and that it prevents the construction of a convergent iterative algorithm. As an illustration, we perform a few global-in-time iterations with the algorithm based on Neumann BCs as described in Section 2.3.2 on the radially-symmetric 2D problem (Figure 3.4). We consider a high-frequency 2D radially-symmetric problem as schematised in Figure 3.4 with the same material properties (Table 3.1). The time interval $[0, T]$ is discretised with N_t= 2000 time steps ($\Delta t = 7.0\ 10^{-7}$s) and the causal signal defined by (3.16) has a time parameter $T_p = 50\Delta t = 3.5\ 10^{-5}$s.

Figure 3.7 shows the relative error on the analytical solution e_p^{sol} with respect to the iterations when using three types of boundary conditions. When Robin conditions are used the error (in black) converges within 10 iterations. On the other hand, using Neumann (in blue) or Dirichlet (in red) boundary conditions does not enable e_p^{sol} to converge.

The fluid pressure evaluated on a point of the boundary is represented as a function of time at three different Neumann-based iterations in Figure 3.8a. It clearly illustrates the loss of regularity. At each iteration the solution p becomes less and less regular. For similar reasons global-in-time iterations based on Dirichlet conditions do not allow convergence either. We also perform a few iterations with the algorithm based on Dirichlet BCs in both subdomains. A loss of regularity at each iteration is also found by observing the evolution of the fluid pressure with respect to time in Figure 3.8b.

We have transmission conditions for three kinds of conditions (Robin in black, Neumann in blue and Dirichlet in red). These results obtained for a very simple configuration show that the algorithm based on Robin boundary conditions is better than the others for step-by-step iterative procedures. Some "mixed" algorithms have been proposed in the literature based on Robin and Neumann conditions or on Robin and Dirichlet conditions [6, 7, 76]. The Robin and Dirichlet boundary conditions are in particular sometimes used as it is the easiest to implement [56, 188]. However, for global-in-time iterative procedures however, only the numerical scheme based on Robin boundary conditions has a guaranteed convergence.

3.3.3 Optimal parameters for the Robin boundary conditions

In the previous example we have used a Robin coupling parameter equal to the acoustic impedance ($k_c = \rho_f c_f$). It is justified first by a dimensional analysis because the parameter k_c carries impedance unit. In addition for a high frequency radiation problem, the behaviour of the fluid pressure on an elastic surface can be described by $p = \rho_f c_f u(t)$ (with u the fluid velocity) [146]. The aim of this section is to check if another value could be more efficient. An option is to consider two distinct coupling parameters, the first noted k_a for the acoustic domain and the other noted

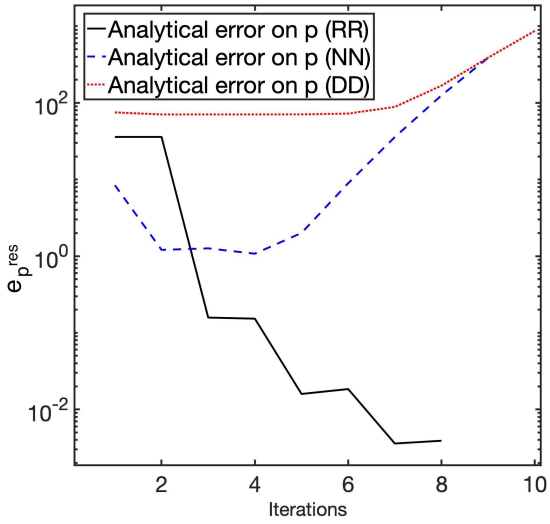

Figure 3.7: *Relative error on pressure e_p^{sol} compared to the semi-analytical solution with the iterations for different numerical schemes, for a 2D radially-symmetric problem (Δt=7.0e-07, El=2336, $k_c = \rho_f c_f$).*

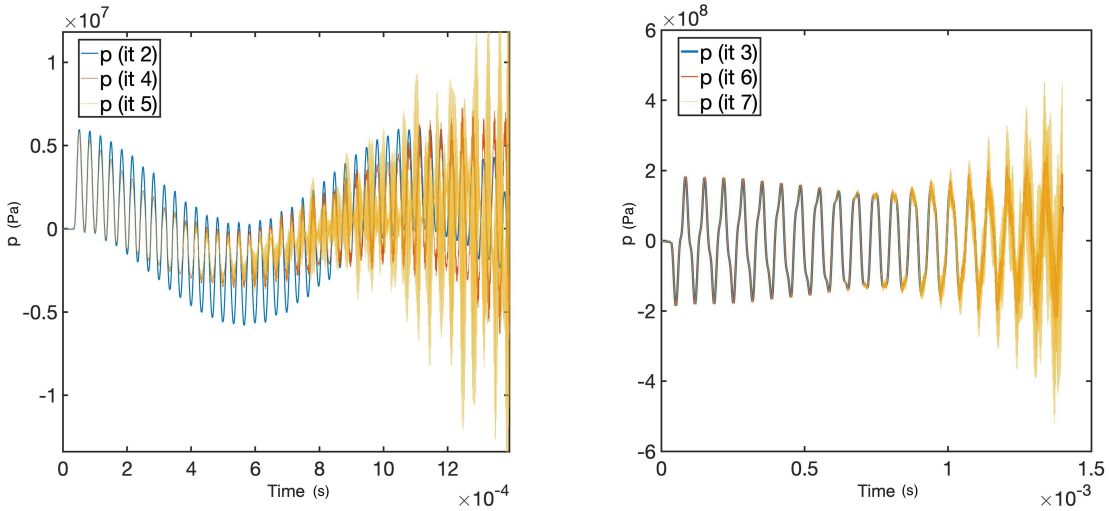

(a) *Neumann boundary conditions.* ***(b)*** *Dirichlet boundary conditions.*

Figure 3.8: *Pressure evaluated on a point of Γ with respect to time at three iterations for the algorithm based on Neumann transmission conditions (a) and on Dirichlet transmission conditions (b) ($\Delta t = 7.0\ 10^{-7}$, $N_t = 2000$, El=2336).*

k_s for the elastic structure. To answer this question, it is possible on this simple radially-symmetric problem to semi-analytically estimate the value of the coupling parameter that maximises the convergence speed. The iterative procedure is based now on two Robin transmission conditions of the form

$$\begin{cases} k_a \partial_n \phi^{i+1}(t) - \rho_f \partial_t \phi^{i+1}(t) = g_f^i(t) \\ \mathbf{t}[\mathbf{u}^{i+1}](t) + k_s \partial_t \mathbf{u}^{i+1} = \mathbf{g_s}^i(t) \end{cases}$$

where k_a and k_s are the coupling parameters and g_f and $\mathbf{g_s}$ are the boundary terms depending on the variables obtained at the previous iterate according to the definition (2.40). Another well-known approach to speed up the convergence is to consider relaxed transmission conditions of the form

$$\begin{cases} k_a \partial_n \phi^{i+1}(t) - \rho_f \partial_t \phi^{i+1}(t) = (1-r) g_f^{i-1}(t) + r g_f^i(t) \\ \mathbf{t}[\mathbf{u}^{i+1}](t) + k_s \partial_t \mathbf{u}^{i+1} = (1-r) \mathbf{g_s}^{i-1}(t) + r \mathbf{g_s}^i(t) \end{cases}$$

with $r \in]0,1[$. For the 2D radially-symmetric problem, the coupling parameters values to optimise the convergence rate can be evaluated with a semi-analytical analysis.

Theoretical convergence speed for the radially-symmetric FSI problem. To evaluate the theoretical convergence speed of the global-in-time iterations depending on the coupling and relaxation parameters, we consider the semi analytical-solution (Appendix A) and the matrix system (9) defined in Appendix A. This matrix system defines three coefficients A, B and C, characterising the acoustic-elastic semi-analytical solution. The convergence of the error of the coupled problem is estimated by expressing, at a fixed frequency s, the matrix relation between the errors on the coefficients at two successive iterations, in the form

$$\begin{bmatrix} A_1 - A_{ext} \\ B_1 - B_{ext} \\ C_1 - C_{ext} \end{bmatrix} = [M] \begin{bmatrix} A_0 - A_{ext} \\ B_0 - B_{ext} \\ C_0 - C_{ext} \end{bmatrix}.$$

We aim at determining the matrix $[M]$. For a fixed frequency s, we express the variables of the radiated problem with modified Bessel functions. The Robin radiated problem verifies the internal pressure condition on the inner surface ($r = a$) and possibly relaxed Robin conditions on the exterior interface ($r = b$). These three relations link the variables of iterations 0 and 1:

$$\begin{cases} \bar{t}_1(a,s) = 0 \\ (\bar{p}_1 + k_a \bar{v}_1)(b,s) = h - (\bar{\mathbf{t}}_0 - k_a s \bar{\mathbf{u}}_0).\mathbf{n} + \nu)(b,s) \\ (\bar{\mathbf{t}}_1 + k_s s \bar{\mathbf{u}}_1)(b,s) = \mathbf{n}(h - \bar{p}_0 + k_s(\bar{v}_0 - \nu))(b,s) \end{cases} \tag{3.18}$$

To rewrite these relations with the modified Bessel functions, we use $K_0'(z) = -K_1(z), I_1'(z) = I_0(z) - \frac{1}{z} I_1(z)$ and $K_1'(z) = -K_0(z) - \frac{1}{z} K_1(z)$. We also introduce the short-hand notations

$$T_i(r) := \left[l \frac{s}{c} I_1'(\frac{sr}{c}) + \frac{\lambda}{r} I_1(\frac{sr}{c}) \right] \quad \text{and} \quad T_k(r) := \left[l \frac{s}{c} K_1'(\frac{sr}{c}) + \frac{\lambda}{r} K_1(\frac{sr}{c}) \right].$$

$$\begin{cases} A_1 T_i(a) + B_1 T_k(a) = 0 & \\ C_1 \left[-\rho_f s K_0(\frac{sb}{c_f}) - \frac{k_a s}{c_f} K_1(\frac{sb}{c_f}) \right] & = h + \nu + A_0[-T_i(b) + k_a s I_1(\frac{sb}{c})] \\ & \quad + B_0[-T_k(b) + k_a s K_1(\frac{sb}{c})] \\ A_1 \left[T_i(b) + k_s s I_1(\frac{sb}{c}) \right] \mathbf{n} + & B_1 \left[T_k(b) + k_s s K_1(\frac{sb}{c}) \right] \mathbf{n} = h\mathbf{n} - \nu\mathbf{n} \\ & \quad + C_0 \left[\rho_f s K_0(\frac{sb}{c_f}) - k_s \frac{s}{c_f} K_1(\frac{sb}{c_f}) \right] \mathbf{n} \end{cases}$$

As these relations are verified by the coefficients of the converged solution A_{ext}, B_{ext} and C_{ext}, it is also verified by the differences $A_0 - A_{ext}$, $B_0 - B_{ext}$ and $C_0 - C_{ext}$. We have a system of the form

$$\left[Rg\right] \begin{bmatrix} A_1 - A_{ext} \\ B_1 - B_{ext} \\ C_1 - C_{ext} \end{bmatrix} = \left[Rd\right] \begin{bmatrix} A_0 - A_{ext} \\ B_0 - B_{ext} \\ C_0 - C_{ext} \end{bmatrix}. \tag{3.19}$$

Subtracting the two matrix systems entails the elimination of the boundary terms h and ν which are independent of the iteration number n. As the modified Bessel functions admit the large-argument expansions (8), when one subtract the converged solution, the matrix $[R_g]$ and $[R_d]$ have the form:

$$\left[Rg\right] = \begin{bmatrix} T_i(a) & T_k(a) & 0 \\ 0 & 0 & -s\left(\rho_f K_0(\frac{sb}{c_f}) + \frac{k_a}{c_f} K_1(\frac{sb}{c_f})\right) \\ T_i(b) + k_s s I_1(\frac{sb}{c}) & T_k(b) + k_s s K_1(\frac{sb}{c}) & 0 \end{bmatrix}$$

$$\left[Rd\right] = \begin{bmatrix} 0 & 0 & 0 \\ -T_i(b) + k_a s I_1(\frac{sb}{c}) & -T_k(b) + k_a s K_1(\frac{sb}{c}) & 0 \\ 0 & 0 & \left[\rho_f s K_0(\frac{sb}{c_f}) - k_s \frac{s}{c_f} K_1(\frac{sb}{c_f})\right] \mathbf{n} \end{bmatrix}$$

The spectral radius of $[M] = \left[Rg\right]^{-1} \left[Rd\right]$ is the convergence factor of the algorithm and must be smaller than 1 to ensure the convergence of the iterations. The smaller it is, the larger the convergence rate of the iterative algorithms. It is defined by

$$\varrho_s(s) = \max \left(\lambda \left(\left[Rg\right]^{-1} \left[Rd\right] \right) \right)$$

where λ are the eigenvalues of $\left[Rg\right]^{-1} \left[Rd\right]$. To determine an optimal value of k_a and k_s taking into account all the complex frequencies, we consider as the spectral radius, the maximum of all eigenvalues for all the complex frequencies.

$$\boxed{\varrho(k_a, k_s) = \max_s \varrho_s(s)} \tag{3.20}$$

This convergence factor ϱ does not depend on the mesh discretisation or on the impulsion (T_p value for example).

Relaxation. Taking the relaxation into account, the three equations (14) defined in Appendix A linking two successive iterations become

$$\begin{cases} \overline{t}_1(a,s) = 0 \\ (\overline{p}_1 + k_a\overline{v}_1)(b,s) = (1-r)(\overline{p}_0 + k_a\overline{v}_0)(b,s) + r\left[h - (\overline{\mathbf{t}}_0 - k_a s\overline{\mathbf{u}}_0).\mathbf{n} + \nu)(b,s)\right] \\ (\overline{\mathbf{t}}_1 + k_s s\overline{\mathbf{u}}_1)(b,s) = (1-r)(\overline{\mathbf{t}}_0 + k_s s\overline{\mathbf{u}}_0)(b,s) + r\left[\mathbf{n}(h - \overline{p}_0 + k_s(\overline{v}_0 - \nu))(b,s)\right] \end{cases}$$

and only the matrix $[R_d]$ changes. It has then the form:

$$\begin{bmatrix} 0 & 0 & 0 \\ r\left(-T_i(b) + sk_a I_1\left(\frac{sb}{c}\right)\right) & r\left(-T_k(b) + sk_a K_1\left(\frac{sb}{c}\right)\right) & \alpha\left[\rho_f s K_0\left(\frac{sb}{c_f}\right) + \frac{sk_a}{c_f} K_1\left(\frac{sb}{c_f}\right)\right] \\ -\alpha\left[T_i(b) + sk_s I_1\left(\frac{sb}{c}\right)\right] & -\alpha\left[T_k(b) + sk_s K_1\left(\frac{sb}{c}\right)\right] & r\left[\rho_f s K_0\left(\frac{sb}{c_f}\right) - \frac{sk_s}{c_f} K_1\left(\frac{sb}{c_f}\right)\right] \end{bmatrix}$$

(with $\alpha = r - 1$).

Using the analytical definition, the global-in-time iterative algorithm theoretical convergence factor is determined by assessing the value of (3.20). We first consider one coupling parameter k_c ($k_s = k_a = k_c$). Figure 3.9a shows the spectral radius value depending on the coupling parameter k_c and on the complex frequency s. The algorithm convergence factor is then the maximal value of $\varrho_s(s)$ taking all the complex frequencies into account. Figure 3.9b shows the convergence factor for the radially-symmetric example (with $L = 2N_t = 3000$ frequencies) as a function of the value of the coupling parameter k_c. In this case, Figure 3.9b shows that choosing the coupling parameter as $k_c = 0.9\rho_f c_f$ allows to minimise the spectral radius of the system (15) linking two successive iterations ($\varrho = 0.24$) and thus to maximise the convergence speed of the iterative algorithm. This optimal value is close to the physical value of the acoustic impedance which was thus a good a priori choice.

Similarly Figure 3.10 shows the iterative algorithm convergence factor ϱ depending on the coupling parameter value k_c and the relaxation parameter r. This semi-analytical calculation highlights the convergence factor high sensitivity to the choice of k_c and the existence of a relaxation parameter value that minimises system (15) spectral radius for each value of k_c. For example with $k_c = \rho_f c_f$, the spectral radius is minimal (ϱ =0.28) without relaxation (r=1). Relaxation might however be useful in some cases, as for $k_c = 7\rho_f c_f$, a relaxation parameter r=0.8 reduces the spectral radius to ϱ =0.78 instead of 0.86 without relaxation. In conclusion, in the absence of physical information enabling a good a priori choice of the value of $k_c = k_a = k_s$, using relaxation might improve the convergence. But otherwise choosing k_c according to the physics or to an analytical analysis is more efficient. Figure 3.10 also shows the convergence factor evolution when k_c tends to 0. The fluid pressure (or elastic traction) is then enforced as a Neumann condition and the convergence factor tends to 1, slowing down the convergence excessively (as illustrated in Section 3.4).

This simplified FSI problem with a radially-symmetric geometry allows to derive an a priori suggestion for the optimal choice of k_c, depending on some physical parameters. This estimation might then be used for other transient FSI problems. This is the usual approach to determine a priori optimal values of the coefficients in the Robin transmission conditions that minimise the number of iterations in partitioned algorithms [6, 37, 86, 161].

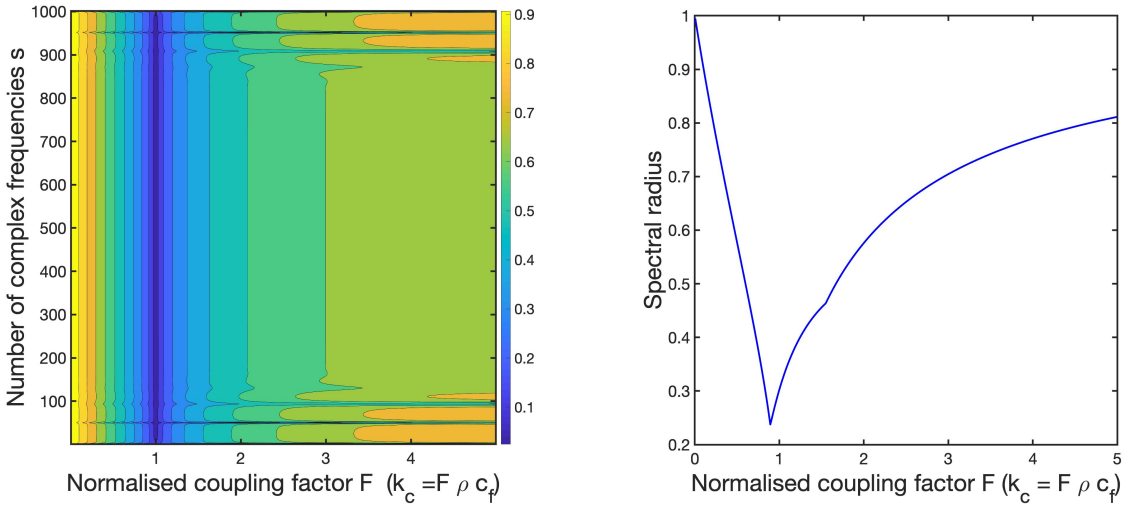

(a) *(b)*

Figure 3.9: *(a) Spectral radius of* $\left[Rg\right]^{-1}\left[Rd\right]$ *depending on the coupling parameter, for several complex frequencies.(b) Spectral radius of* $\left[Rg\right]^{-1}\left[Rd\right]$ *taking all the complex frequencies into account.*

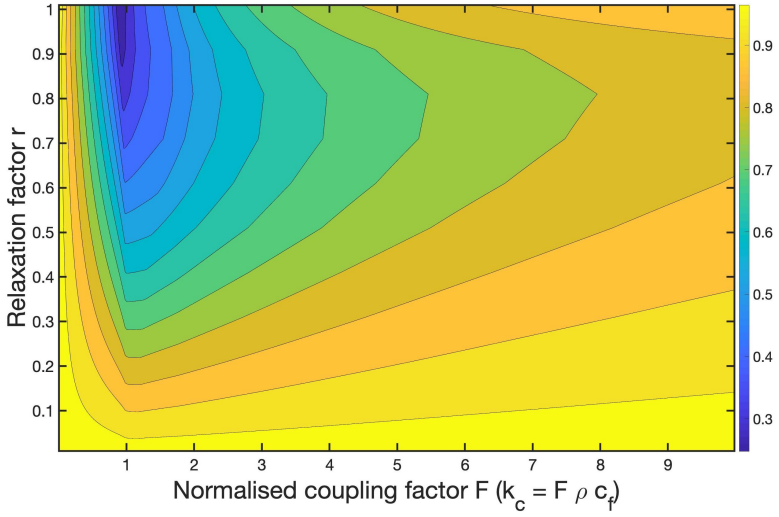

Figure 3.10: *Semi-analytical convergence factor depending on the coupling parameter* k_c *and the relaxation parameter* r *(*$\Delta t = 1.7\ 10^{-6}, N_t = 1500$*, El=2336). (b) Spectral radius of* $\left[Rg\right]^{-1}\left[Rd\right]$ *taking all the complex frequencies into account.*

Fully numerical validation. These semi-analytical observations are validated by numerical experiments, summarised in Table 3.2. For several pairs of parameters (k_c, r) we show the number of iterations needed to reach the convergence. We consider the convergence reached when the relative error on the transmission residuals $e_{v,p} < 10^{-3}$, with $e_{v,p}$ defined by (2.17).The number of iterations is in agreement with the expected spectral radius values. We show on Figure 3.11a that the iterative algorithm based on Robin boundary conditions converges with a larger convergence rate for a value of $k_c = 0.9\rho_f c_f$, without relaxation, as predicted by the theoretical spectral radius value. We also observe that the relaxation only slightly improves the convergence speed when $k_c = 7\rho_f c_f$ (reduction by three iterations), as predicted by the convergence factor values. A bad choice of the relaxation parameter value can however have a drastic negative effect on the convergence as illustrated by the example $k_c = \rho_f c_f$. By adding a relaxation with $r = 0.2$ the number of iterations is multiplied by 4 compared to the case without relaxation (see Figure 3.11b). The optimal relaxation parameter value highly depends on the chosen coupling parameter k_c.

From this analysis we can conclude that if a good guess of the Robin k_c coefficient is known, either from the physics or from an analytical analysis (such as here $k_c = \rho_f cf$), the iterative algorithm is more efficient without relaxation. However, if a good guess is not available the relaxation might improve the convergence rate. For general cases where no semi-analytical solution can be determined, it is therefore preferable to choose another acceleration method whose efficiency does not depend on the choice of coupling parameters (for example the Aitken acceleration, see Section 3.4.2).

Coupling factor f (k_c =f$\rho_f c_f$)	0.2	0.2	1	1	1	0.9	7	7
Relaxation parameter r	1	0.2	1	0.5	0.2	1	1	0.8
Spectral radius ϱ	0.83	0.96	0.28	0.54	0.80	0.24	0.86	0.78
Numerical iterations	44	>100	10	19	40	9	45	42

Table 3.2: *Theoretical values of spectral radius ϱ and number of iterations to reach convergence ($e_{v,p} < 10^{-3}$) for couples of parameters (k_c, r).*

Remark. It is worth noticing that the optimal value for the Robin coupling parameter k_c does not depend on the time discretisation. Previous studies have shown that time-stepping iterative procedures based on Robin's transmission conditions generally have an optimal value of coupling parameter that depends on the time discretisation [6, 86, 159] in contrast to our global-in-time iterative procedure. This optimal value does not depend on the spatial discretisation either. This is similar to the step-by-step iterative procedures used for transient FSI problems where the optimal k_c value is independent on the mesh parameter size [86], but contrasts with the Robin optimal parameter values for harmonic problems [79].

Two-sided Robin iterations. We now relax the constraint that the same Robin condition has to be used in the acoustic and elastic problems. It is the approach used for time-harmonic problems in [79] for example. The semi-analytical values of the

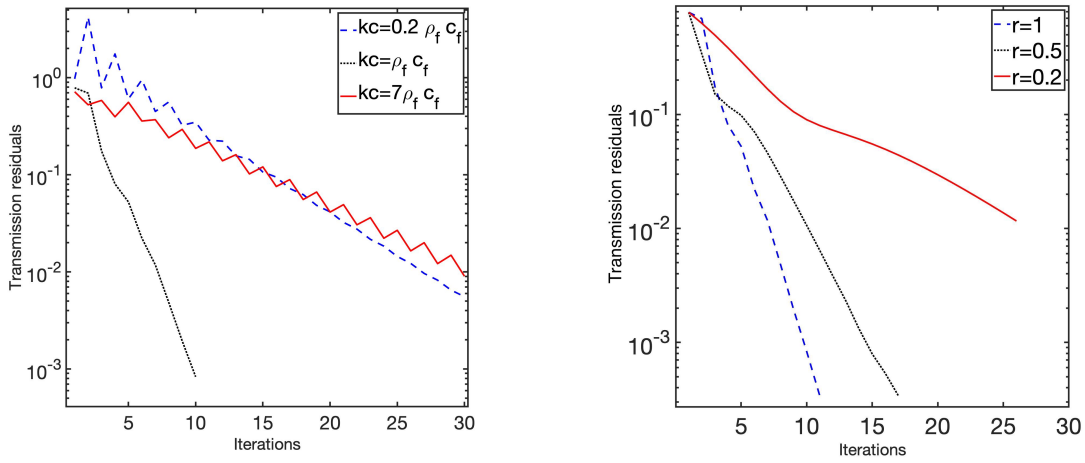

(a) *(b)*

Figure 3.11: *(a) Convergence of the indicator $e_{v,p}$ on interfacial residuals for three values of k_c ($\Delta t = 1.7\ 10^{-6}, N_t = 1500$, El=2336). (b) Convergence of the indicator $e_{v,p}$ on interfacial residuals for $k_c = \rho_f c_f$ and three values of r ($\Delta t = 1.7\ 10^{-6}, N_t = 1500$, El=2336).*

convergence factor (3.20) depending on k_a and k_s are shown in Figure 3.12. These semi-analytical results on the convergence factor are numerically validated as they are consistent with respect to the number of numerical iterations needed to reach convergence presented in Table 3.3. By minimising the convergence factor of the iterations, the optimal value for the coupling parameters is found to be very close to the physical acoustic impedance ($k_a = k_s = \rho_f c_f$) and entails a convergence factor $\varrho = 0.24$. Choosing distinct values for k_a and k_s does not seems to be interesting in this case. Similar Robin conditions on both sides of the interface ($k_a = k_s$) seems to be an optimal choice when one of the two values is imposed (e.g. k_a), especially as the convergence factor is quite robust to the variations of k_s. However this

Coupling factor f (k_a =f$\rho_f c_f$)	0.2	0.2	1	1	3	3	3
Coupling factor f$_s$ (k_s =f$_s\rho_f c_f$)	1	0.2	1	0.2	3	1	0.2
Spectral radius ϱ	0.93	0.83	0.28	0.66	0.70	0.71	0.74
Numerical iterations	>100	44	10	20	25	26	32

Table 3.3: *Theoretical values of convergence factor ϱ and number of iterations to reach convergence ($e_{v,p} < 10^{-3}$) for couples of parameters (k_a, k_s).*

depends on the problem parameters. Table 3.4 shows the theoretical convergence factor ϱ depending on the thickness of the elastic part ($e = R_{\text{ext}} - R_{\text{int}}$). It shows that when the geometry changes and the thickness increases, the choice $k_a = Z_c$ and $k_s = Z_s$ might becomes optimal. For thicker elastic obstacles, for example e=10, $k_a = k_s = Z_c$ is still a good choice as the convergence factor is then 0.12, but choosing $k_a = Z_c$ and $k_s = Z_s$ entails an optimal convergence factor $\varrho = 0.01$

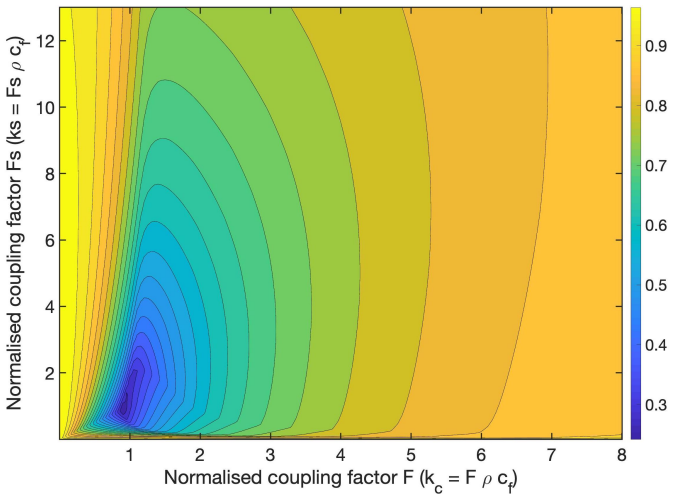

Figure 3.12: *Semi-analytical convergence factor depending on the coupling parameters k_a and k_s ($\Delta t = 1.7\ 10^{-6}, N_t = 1500$, El=2336).*

(2 iterations). For very thin elastic obstacles, the elastic domain has a smaller influence on the coupling and the influence of the acoustic domain is predominant. For thick obstacles the influences of both domains have to be taken into account, so the acoustic and elastic impedances have to be include in the Robin boundary conditions in each subdomain. This observation is consistent with the physics and also with the literature on FSI coupling with Robin conditions [7, 159, 161]. This literature highlights some cases where it makes sense to take different k_a and k_s. It is especially common to choose both parameters equal to the elastic and acoustic impedances ($k_s = \rho_{\text{mat}} c_{\text{mat}}$ and $k_a = \rho_f c_f$), as they both carry impedance units [161].

Table 3.4 shows that the choice of k_a and k_s highly depends on the geometry and especially on the structure thickness. When the structure is thick enough ($e \geq 2$ for this example), it is preferable to choose the acoustic and elastic Robin coupling parameters equal to the acoustic and elastic impedances, according to the physics. However, when the structure is thin, its impact on fluid-structure coupling is limited and choosing the both Robin coupling parameters equal to the acoustic impedance is preferable.

Tables 3.5 and 3.6 show the theoretical convergence factor depending on the ratio of both domains densities, for a fixed thickness $e = 0.1$ (Table 3.5) or $e = 9$ (Table 3.6). For both thin and thick geometries the convergence factor only slightly varies with the fluid and structure densities ratio. For a thin structure, Table 3.5 shows that the optimised nature of the choice $k_a = k_s = \rho_f c_f$ is robust to the values of the densities. We observe that the convergence factor improves when the structure density decreases and becomes closer to the density of a fluid. For a thick structure, Table 3.6 also shows that choosing $k_a = Zc$ and $k_s = Z_s$ entails the lowest convergence factor and that the densities ratio does not have a great influence on ϱ.

Finally the theoretical convergence factor ϱ is evaluated depending on the Young modulus value E for two different geometries in Tables 3.7 ($e = 0.1$) and 3.8 ($e = 9$). For both thin and thick geometries the convergence factor is seen to be independent

Coupling parameter k_a	0.2 Zc	0.2 Zc	0.2 Zc	Zc	Zc	3Zc	Zc	Zs
Coupling parameter k_s	Zc	0.5 Zc	0.2Zc	Zc	0.5Zc	0.2Zc	Zs	Zs
e=0.01 ($R_{ext} = 1.01$)	0.93	0.89	0.82	0.20	0.34	0.79	0.93	0.96
e=0.1 ($R_{ext} = 1.1$)	0.93	0.89	0.82	0.28	0.34	0.74	0.87	0.93
e=1 ($R_{ext} = 2$)	0.92	0.88	0.81	0.25	0.33	0.74	0.44	0.66
e=2 ($R_{ext} = 3$)	0.90	0.	0.88	0.81	0.21	0.32	0.21	0.46
e=4 ($R_{ext} = 5$)	0.89	0.87	0.81	0.16	0.32	0.72	0.05	0.22
e=9 ($R_{ext} = 10$)	0.89	0.87	0.81	0.12	0.32	0.71	0.01	0.09

Table 3.4: *ϱ variation depending on the thickness e (R_{int}=1, $\frac{\rho_f}{\rho_{\text{mat}}} = 0.128$).*

Coupling parameter k_a	0.2 Zc	0.2 Zc	0.2 Zc	Zc	Zc	3Zc	Zc	Zs
Coupling parameter k_s	Zc	0.5 Zc	0.2Zc	Zc	0.5Zc	0.2Zc	Zs	Zs
$\frac{\rho_f}{\rho_{\text{mat}}} = 0.01$	0.93	0.89	0.81	0.32	0.37	0.73	0.92	0.87
$\frac{\rho_f}{\rho_{\text{mat}}} = 0.128$	0.93	0.89	0.82	0.28	0.35	0.71	0.87	0.93
$\frac{\rho_f}{\rho_{\text{mat}}} = 0.5$	0.93	0.89	0.82	0.20	0.34	0.75	0.73	0.85

Table 3.5: *Theoretical values of convergence factor ϱ for couples of parameters (k_a, k_s) and different physical parameters values ($Z_c = \rho_f c_f$, $Z_s = \rho_{\text{mat}} c_{\text{mat}}$ and e=0.1).*

Coupling parameter k_a	0.2 Zc	0.2 Zc	0.2 Zc	Zc	Zc	3Zc	Zc	Zs
Coupling parameter k_s	Zc	0.5 Zc	0.2Zc	Zc	0.5Zc	0.2Zc	Zs	Zs
$\frac{\rho_f}{\rho_{\text{mat}}} = 0.01$	0.93	0.89	0.82	0.12	0.33	0.72	0.01	0.09
$\frac{\rho_f}{\rho_{\text{mat}}} = 0.128$	0.89	0.87	0.81	0.12	0.32	0.71	0.01	0.09
$\frac{\rho_f}{\rho_{\text{mat}}} = 0.5$	0.76	0.81	0.80	0.11	0.30	0.70	0.01	0.08

Table 3.6: *Theoretical values of convergence factor ϱ for couples of parameters (k_a, k_s) and different physical parameters values ($Z_c = \rho_f c_f$, $Z_s = \rho_{\text{mat}} c_{\text{mat}}$ and e=0.1).*

on this material parameter.

Coupling parameter k_a	0.2Zc	0.2Zc	0.2Zc	Zc	Zc	3Zc	Zc	Zs
Coupling parameter k_s	Zc	0.5Zc	0.2Zc	Zc	0.5Zc	0.2Zc	Zs	Zs
E=390.10^9 kg.m^{-1}s $^{-2}$	0.93	0.89	0.82	0.27	0.34	0.74	0.90	0.95
E=210.10^9 kg.m^{-1}s $^{-2}$	0.93	0.88	0.81	0.28	0.35	0.71	0.87	0.93
E=69.10^9 kg.m^{-1}s $^{-2}$	0.93	0.89	0.82	0.25	0.34	0.74	0.86	0.93

Table 3.7: *ϱ variation depending on E (0.1, $\frac{\rho_f}{\rho_{\text{mat}}} = 0.128$).*

Coupling parameter k_a	0.2Zc	0.2Zc	0.2Zc	Zc	Zc	3Zc	Zc	Zs
Coupling parameter k_s	Zc	0.5Zc	0.2Zc	Zc	0.5Zc	0.2Zc	Zs	Zs
E=390.10^9 kg.m^{-1}s $^{-2}$	0.90	0.88	0.81	0.11	0.32	0.70	0.02	0.15
E=210.10^9 kg.m^{-1}s $^{-2}$	0.89	0.87	0.81	0.12	0.32	0.71	0.01	0.09
E=69.10^9kg.m^{-1}s $^{-2}$	0.85	0.86	0.81	0.11	0.32	0.68	0.01	0.05

Table 3.8: *ϱ variation depending on E ($e = 9$, $\frac{\rho_f}{\rho_{mat}} = 0.128$).*

From this analysis on a simple radially-symmetric FSI problem, we validate the convergence of the global-in-time FEM/Z-BEM iterations based on Robin boundary conditions. We conclude that a good guess for the Robin coupling coefficient can be derived on this simplified problem. For our test case with a thin elastic object, choosing $k_a = k_s = \rho_f c_f$ minimises the convergence factor and maximises the convergence rate. For thicker obstacles, the elastic domain influence on the coupling increases and choosing $k_s = \rho_{\text{mat}} c_{\text{mat}}$ and $k_a = \rho_f c_f$ becomes an optimal choice. This is in agreement with the physics and the literature on FSI coupling. Moreover, the optimised aspect of this choice is robust with respect to the time step Δt, the mesh discretisation, the excitation T_p, the elastic obstacle thickness e and the material parameters. In the absence of a simplified semi-analytical solution providing an indication of the optimal choice of k_a and k_s, choosing k_a and k_s according to the physical impedances seems to be a good default choice. In the next section we consider a different 2D FSI problem to test whether this optimised value of the coupling parameters can be efficiently used.

3.4 Convergence acceleration

We now consider another two-dimensional FSI problem with the aim of (i) testing the optimised values for parameters k_a and k_s on a fully 2D FSI problem with a different geometry, and (ii) defining a problem-independent acceleration.

In contrast to the semi-analytical analysis in Section 3.3, for which the radially-symmetric geometry was necessary to derive the conclusion on the analytical rate of convergence, the observations regarding the coupling parameters and the rate of convergence in this section are independent of the problem parameters and geometry.

We consider the scattering of a wave by a non radially-symmetric 2D cylinder as described in Section 2.6 and illustrated in Figure 3.13. We use the same fluid and structure physical parameters and the same discretisation parameters as listed in Table 2.1. We consider a smooth incident causal signal ϕ_{inc} of the form of

$$\phi_{\text{inc}}(t, \mathbf{x}) = f(t - \frac{1}{c}\widehat{\mathbf{p}}.\mathbf{x})$$

where the function $t \to f(t)$ defines the time modulation of the propagating pulse. It is assumed to have a compact support T. f is defined by (2.61) with $\gamma = 3$. A HFA is used and for this 2D problem 70 harmonic BEM problems corresponding to the lowest frequencies are computed (see Section 3.5).

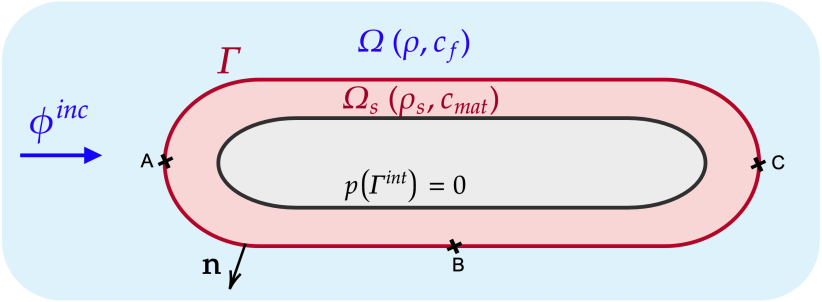

Figure 3.13: *Schematic representation of a fluid-structure interaction problem between an incident acoustic plane wave ϕ_{inc} in an acoustic domain $\Omega(\rho, c_f)$ and an elastic domain $\Omega_s(\rho_s, c_s)$.*

3.4.1 Optimised Robin coupling parameters

The numbers of global-in-time iterations to reach the convergence ($e_{v,p} < 10^{-3}$) are reported in Table 3.9 for different values of k_a and k_s. As no semi-analytical solution is available for this non radially symmetric example, the convergence is evaluated with the relative $L2$ error $e_{v,p}$ on transmission residuals (2.17). Moreover, it is not possible to evaluate the semi-analytical convergence factor nor to predict the values of the coupling and relaxation parameters that optimise the convergence rate. We therefore choose coupling parameter values similar to those in Table 3.3 to verify if $k_a = k_s = \rho_f c_f$ is still a good choice regarding the convergence rate. While the

Coupling factor f (k_a =f$\rho_f c_f$)	1	1	3	3
Coupling factor f$_s$ (k_s =f$_s\rho_f c_f$)	1	0.2	3	0.2
Numerical iterations	49	96	> 100	> 100

Table 3.9: *Number of numerical iterations to converge ($e_{v,p} < 10^{-3}$) for couples of parameters (k_a, k_s), with $e = 1.5$ and $\frac{\rho_f}{\rho_{\text{mat}}} = 0.128$.*

algorithm converges for all coupling parameters values, choosing $k_a = k_s = \rho_f c_f$ considerably reduces the number of global-in-time iterations needed to reach the convergence. The pressure and velocity solutions at convergence are evaluated at three different locations A, B and C of the structure surface Γ (see Figure 3.13). The fluid pressure and the elastic stress in A, B and C are given on Figure 3.14a, Figure 3.15a and Figure 3.16a as functions of time. The fluid and elastic normal velocities in A, B and C are given on Figure 3.14b, Figure 3.15b and Figure 3.16b. All the Figures have been obtained with $k_a = k_s = \rho_f c_f$ after 49 iterations.

3.4.2 Aitken's acceleration

As observed in Section 3.3.3, adding a relaxation with a fixed parameter r does not systematically improve the algorithm convergence rate and sometimes even bring along a drastic decrease in efficiency. As the optimal value of the relaxation parameter (which depends on the coupling parameters k_a and k_s) is initially unknown, an

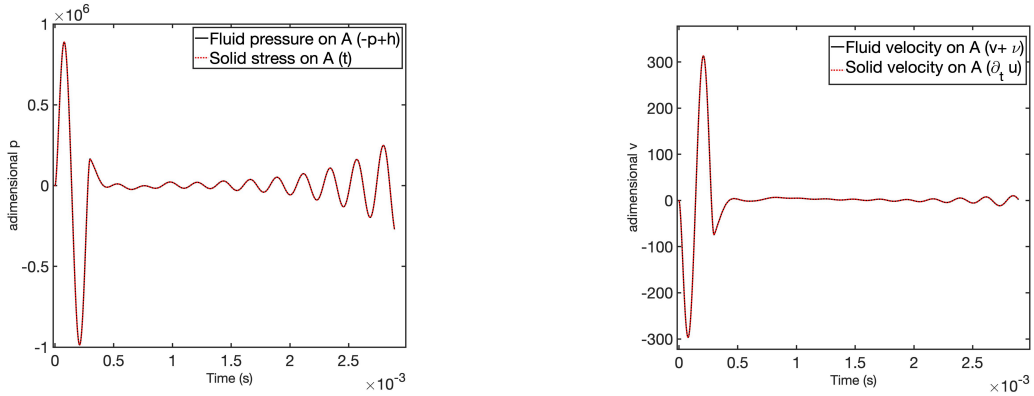

(a) *(b)*

Figure 3.14: *(a) Normalised fluid pressure and elastic stress evaluated on point A. (b) Normalised fluid and elastic velocities evaluated on point A.*

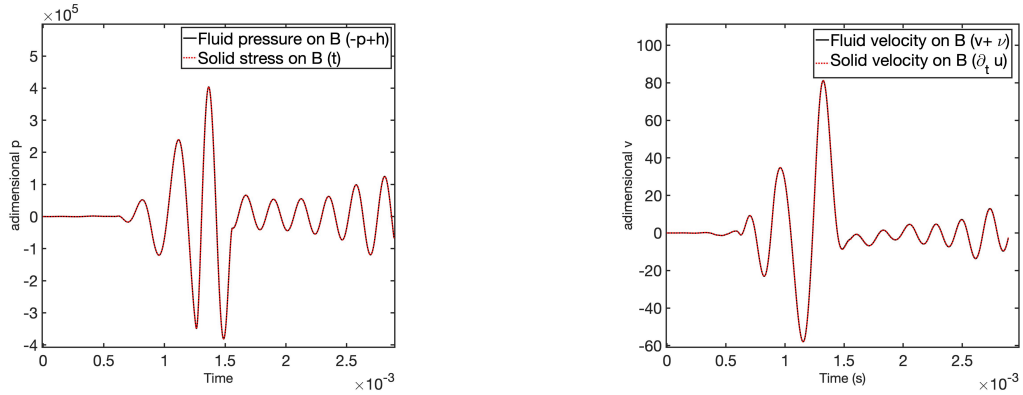

(a) *(b)*

Figure 3.15: *(a) Normalised fluid pressure and elastic stress evaluated on point B. (b) Normalised fluid and elastic velocities evaluated on point B.*

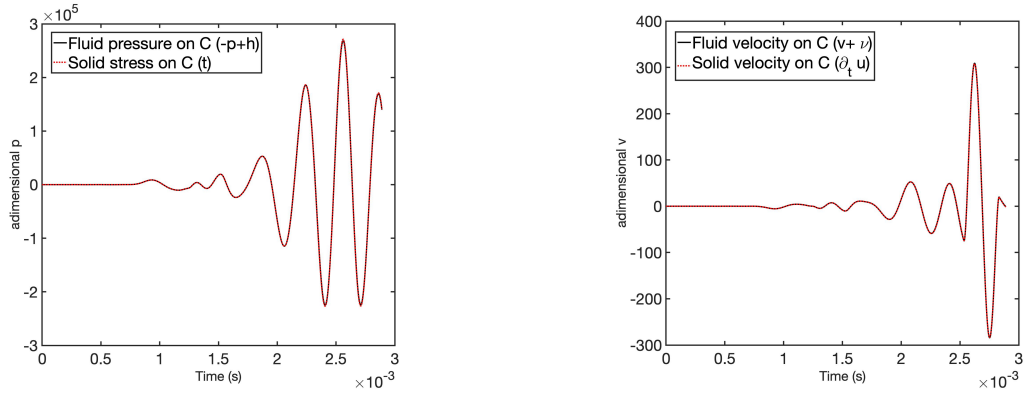

(a) *(b)*

Figure 3.16: *(a) Normalised fluid pressure and elastic stress evaluated on point C. (b) Normalised fluid and elastic velocities evaluated on point C.*

adaptive method is proposed to redefine an optimal relaxation parameter value at each iteration. We consider Aitken's Δ^2 dynamic relaxation proposed by [111]. This acceleration is classically employed for the determination of an iteration dependent relaxation parameter r_i^*. This method provides a simple procedure to determine r_i^*, based on the results of two subsequent iterations. Despite its simplicity, Aitken's relaxation significantly speeds up convergence of fixed-point iterative algorithms and it is often applied in the literature, especially for fluid–structure interaction problems [6, 119, 188].

At each iteration, a coefficient r_i^* is defined and used in a linear combination of g and $\mathbf{g}$ (the boundary terms depending on the variables obtained at the previous iterate in Section 2.4) to define modified transmissions conditions. The idea is that the iterations can be viewed as fixed-point iterations for the incoming traces $\mathbb{B}$. We note $F(\mathbb{B})$ the solution of two Robin IBVPs in each subdomain, for a given incoming trace $\mathbb{B}$. The iterations thus takes the form

$$\mathbb{B}_{n+1} = F(\mathbb{B}_n), \qquad \text{with } F(\mathbb{B}) := \mathbb{X}\mathbb{S}\mathbb{B} + \mathbb{H} = \mathbb{X}\overline{\mathbb{B}} + \mathbb{H}.$$

At each iteration we consider two candidate $\mathbb{B}_0$ and $\mathbb{B}_1$ and set $F_0 := F(\mathbb{B}_0)$, $F_1 := F(\mathbb{B}_1)$. Next we linearly interpolate $(\mathbb{B}_0, \mathbb{B}_1)$ by defining

$$\mathbb{B}(r) := \mathbb{B}_1 + r(\mathbb{B}_0 - \mathbb{B}_1), \quad F(r) := F_1 + r(F_0 - F_1)$$

and seek to define the next iterate $\mathbb{B}_2$ as $\mathbb{B}_2 = \mathbb{B}(r)$, choosing r such that $\mathbb{B}(r)$ is the closest to a fixed point:

$$r^* = \operatorname*{arglim}_r \|F(r) - \mathbb{B}(r)\|_2^2$$

which is easily found to be given by

$$r^* = \frac{(\Delta_1, \Delta_1 - \Delta_0)}{\|\Delta_1 - \Delta_0\|_2^2}, \quad \Delta_0 := \mathbb{B}_0 - F_0, \Delta_1 := \mathbb{B}_1 - F_1$$

The next iterate is hence

$$\mathbb{B}_2 = \mathbb{B}(r^*) = \mathbb{B}_1 + r^*(\mathbb{B}_0 - \mathbb{B}_1)$$

The iterative process becomes

- Choose an initial guess $\mathbb{B}_0$, evaluate $F_0 := F(\mathbb{B}_0)$.
- Set $\mathbb{B}_1 := F_0$ (this iterate thus coincides with the one produced by classical iterations), evaluate $F_1 := F(\mathbb{B}_1)$.
- For $n \geq 1$, generate subsequent iterates using

$$\mathbb{B}_{n+1} = \mathbb{B}_n + r_n^*(\mathbb{B}_{n-1} - \mathbb{B}_n) \quad \text{with } r_n^* = \frac{(\Delta_n, \Delta_n - \Delta_{n-1})}{\|\Delta_n - \Delta_{n-1}\|_2^2}.$$

For a FSI problem and iterations based on Robin BCs, the condition in each subdomain is modified to

$$\begin{cases} k_a \partial_n \phi^{i+1}(t) - \rho_f \partial_t \phi^{i+1}(t) = g^i(t) + r_i^* \left(g^{i-1}(t) - g^i(t)\right) \\ \mathbf{t}[\mathbf{u^{i+1}}](t) + k_s \partial_t \mathbf{u^{i+1}}(t) = \mathbf{g}^i(t) + r_i^* \left(\mathbf{g}^{i-1}(t) - \mathbf{g}^i(t)\right) \end{cases}$$

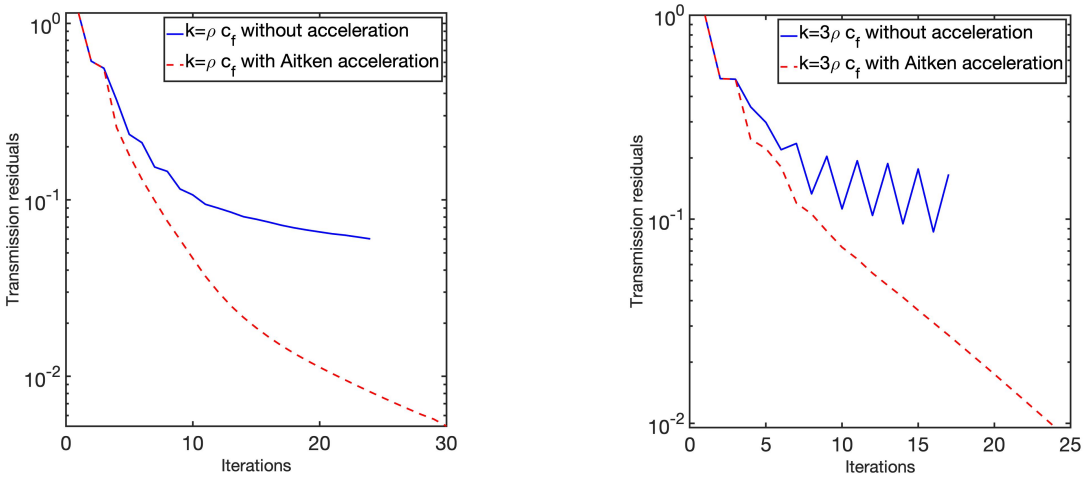

(a) *(b)*

Figure 3.17: *(a) Convergence of the indicator $e_{v,p}$ on interfacial residuals with and without Aitken acceleration ($\Delta t = 1.7\ 10^{-6}, k_c = \rho_f c_f$). (b) Convergence of the indicator $e_{v,p}$ on interfacial residuals with and without Aitken acceleration ($\Delta t = 1.7\ 10^{-6}, k_c = 3\rho_f c_f$).*

We compare in Figures 3.17a and 3.17b the transmission residuals convergence for the 2D acoustic-elastic problem (Figure 3.4) with Aitken acceleration and without any acceleration for two values of coupling parameter k_c ($k_a = k_s = kc$). These two comparisons show that the Aitken acceleration systematically optimises the convergence rate. At least, this Aitken acceleration will never imply a slower convergence than the algorithm without acceleration, as it provides at each iteration an optimised r^*. The positive effect is especially seen in Figure 3.17b. The convergence for $k_c = 3\rho_f c_f$ without acceleration is very oscillating and becomes almost linear with the Aitken algorithm.

3.5 High-frequency approximations for an efficient FSI Robin problem

Another important strategy to improve the algorithm efficiency is to reduce the number of harmonic BEM problems solved, independently of the problem geometry and physical parameters as well as of the choice of values of the coupling parameters k_a and k_s. The Z-BEM procedure allows to treat time-domain problems by solving frequency domain BIEs. These resolutions can be accelerated using fast-BEM methods. However [146] shows that the procedure, still lacks efficiency when dealing with rapid transient problems. A high frequency approximation (HFA) is proposed to drastically reduce the number of frequency BEM problems to solve. In fact, using small time steps Δt implies that some of the complex frequencies $s_k(\xi_k) = \frac{p(\xi_k)}{\Delta t}$ have a high amplitude. The idea is thus to rely on an asymptotic HFA of solutions to the boundary integral equation. When $|s_k| = \frac{|p(\xi_k)|}{\Delta t} > f_{\text{HFA}}$ some threshold frequency f_{HFA}, the HFA is used. Otherwise the fast BEM is used (when $|s_k| \leq f_{\text{HFA}}$). The

main issue is to define the HFA and its validity frequency range. In [146] a high frequency approximations is formulated according to the decomposition (2) of the fluid variables into three variables: an incident field, a Neumann-reflected field and a radiated field. The pressure is decomposed as

$$p = p^{\text{inc}} + p_N^{\text{ref}} + p^{\text{rad}} \tag{3.21}$$

This decomposition is described in Section 2.1. For this specific decomposition, two HFA are defined for the two types of problems arising during the resolution of a FSI problem with a monolithic approach or with an iterative Neumann-Neumann coupling procedure: one for the reflected problem and one for the radiation problem.

Radiated problem. To derive a high frequency approximation, we consider the case of a surface Γ vibrating at a high frequency. The radiated pressure is created at a point $\mathbf{x}$ by the interactions between this point and the nearby points, which can be considered as belonging to the tangent plane at Γ in $\mathbf{x}$. The radiated pressure created by this tangent plane can therefore be approximated by the pressure radiated by a high frequency plane: $p = \rho_f c u$ [146]. Thus, from a sufficiently high frequency f_{HFA}, it is no longer necessary to solve the frequency domain BEM problems to determine p. When an explicit HFA is available, allowing to evaluate p_{HFA}, the cut-off frequency f_{HFA} is set by considering the ratio:

$$\delta(s) = \frac{||p_{BEM}(s) - p_{HFA}(s)||_2}{||p_{BEM}(s)||_2}$$

where p_{BEM} is the BEM computation result and p_{HFA} is the pressure evaluated with the HFA. When $\delta(s_k)$ is smaller than a chosen tolerance, the HFA is used for all the higher frequencies $s > s_k$.

Reflected problem. Constructing a high frequency approximation for the reflected problem is more complex, as the fluid velocity remains unknown before p^{Ref} is calculated. The first idea proposed by [8] is called the Kirchhoff high frequency approximation. It consists in choosing at each point $\mathbf{x}$ of the boundary Γ, a reflected value depending on the incident wave and on the normal to Γ. The reflected pressure p^{ref} can first be simply approximated by:

$$\begin{cases} p_{HFA}(\mathbf{x}, t) = 0 & \text{si } \mathbf{d}(\mathbf{x}).\mathbf{n} > 0 \\ p_{HFA}(\mathbf{x}, t) = 2p^{\text{inc}}(\mathbf{x}, t) & \text{si } \mathbf{d}(\mathbf{x}).\mathbf{n} < 0 \end{cases}$$

This simple approximation gives correct results near the surface Γ, where $|\mathbf{d}(\mathbf{x}).\mathbf{n}| \sim 1$ but not in the vicinity of $|\mathbf{d}(\mathbf{x}).\mathbf{n}| \sim 0$. There is a discontinuity between two mesh points. The idea proposed in [146] is to consider a variable coefficient $\mathbf{R}(\mathbf{x})$ linking the Z-transforms of p_{HFA} and p^{inc}. We introduce the ratio

$$R(\mathbf{x}, s) := \frac{P(\mathbf{x}, s)}{P^{inc}(\mathbf{x}, s)}$$

For a convex obstacle, it is shown that as $|s|$ increases, this ratio becomes constant [44]. We can therefore consider that from a cut-off frequency f_{HFA},

$$R(\mathbf{x}, s) = R(\mathbf{x}, f_{HFA}) \qquad \forall s, |s| > f_{HFA}$$

and so

$$P_{HFA}(\mathbf{x}, s) = R(\mathbf{x}, f_{HFA})P^{inc}(\mathbf{x}, s) \qquad \forall s, |s| > f_{HFA}$$

Improvement if the efficiency. The Z-BEM method without HFA allows to reach a spatial complexity of O(NlogN), with N the number of DOF. The complexity in time is O($N_t$logN_t). However, using the HFA, the Z-BEM method reaches a O(1) complexity in time, since for any number N_t of time steps in the problem, only a small fixed number of frequency problems is solved. For all complex frequencies $s = \frac{p(\xi)}{\Delta t}$ such as

$$s \geq f_{\text{HFA}}$$

the HFA is used. Thanks to this approximation, the Z-BEM is a very competitive method to solve time-domain boundary integral equations. The method efficiency is illustrated in [146] on some examples: the radiation of an acoustic wave into a fluid by a deformable structure with prescribed velocity, and the scattering of an abrupt wave by simple and realistic geometries.

Extension to Robin conditions. When using a different decomposition for the fluid variables or a problem with another type of boundary condition, it is necessary to define a new HFA. For example, the Robin-Robin iterative coupling procedure is based on the decomposition (1) and on Robin IBVPs. In order to improve this iterative Robin-Robin coupling procedure, we propose here a different high-frequency asymptotic approximation, adapted for Robin BCs. We consider the decomposition (3.21) (also described in Section 2.1). For a Robin radiation problem, the Robin BC on the acoustic-elastic interface Γ at a time $t > 0$, with two positive parameters k_a and k_s, is written

$$(p + k_a\partial_n\phi)(t,.) = \underbrace{h(t) + (-\mathbf{t}(t,.) + k_s\partial_t\mathbf{u}(t,.)).\mathbf{n}}_{g(t)} \quad \text{on } \Gamma \tag{3.22}$$

where ϕ and $p := -\rho\partial_t\phi$ are the fluid variables, and $\mathbf{u}$ and $\mathbf{t}$ are the solid displacement and stress. h is the pressure jump related to the incident pressure according to (2.5) ($\nu = 0$ in this case). We thus denote the right hand-side member $g(t)$ defined on the interface Γ. We note r the characteristic length of the obstacle. Using a Laplace transform, with s as the Laplace variable, (3.22) becomes

$$(-\rho s\overline{\phi} + k_a\partial_r\overline{\phi})(s,r) = (\overline{h} + k_s s\overline{u} - \frac{\lambda}{\nu}(1-\nu)\frac{\partial\overline{u}}{\partial r} - \frac{\lambda}{r}\overline{u})(s,r). \tag{3.23}$$

We introduce the notation

$$R(s) := (-\rho s + k_a\partial_r)$$

and (3.23) becomes

$$R(s)\overline{\phi}(s,r) = \overline{g}(s)$$

In the case of an acoustic-elastic problem such as (2.4), the fluid and solid variables verify second-order homogeneous differential equations (the wave equation and the elastodynamic equation). They thus are linear combinations of the modified Bessel functions of order 1 and 0 (see A). In particular, the fluid velocity potential yields

$$\overline{\phi}(s,r) = C(s)K_0(s,r) \text{ and } \partial_r\overline{\phi}(s,r) = -sC(s)K_1(s,r).$$

In order to derive an HFA we also introduce $\overline{\phi}_0(s,r)$, the fluid velocity potential for an unit excitation

$$\begin{cases} R(s)\overline{\phi}(s,r) = R(s)C(s)K_0(s,r) = \overline{g}(s) \\ R(s)\overline{\phi}_0(s,r) = R(s)C_0(s)K_0(s,r) = 1 \end{cases}$$

with $\overline{\phi}$ and $\overline{\phi}_0$ which verify the linear relation

$$\overline{\phi}(s,r) = \overline{\phi}_0(s,r)\overline{g}(s).$$

By linearity, the coefficient C_0 is given by

$$C_0(s) = \frac{1}{R(s)K_0(s,r) - k_a s K_1(s,r)} = \frac{1}{-\rho s K_0(s,r) - k_a s K_1(s,r)}$$

such that

$$\overline{\phi}(s,r) = C_0(s)K_0(s,r)\overline{g}(s) = \frac{-K_0(s,r)}{\rho s K_0(s,r) + k_a s K_1(s,r)}\overline{g}(s)$$

The limiting case $|s| \to +\infty$ yields the high-frequency behaviour of the surface velocity potential:

$$\begin{aligned} \lim_{|s|\to+\infty} \frac{\overline{\phi}}{\overline{g}}(s,r) = & \lim_{|s|\to+\infty} \frac{-K_0(s,r)}{\rho s K_0(s,r) + k_a s K_1(s,r)} \\ = & \frac{-\pi e^{-s}}{\sqrt{2\pi s}\left[\frac{\rho s \pi e^{-s}}{\sqrt{2\pi s}} + \frac{k_a s \pi e^{-s}}{\sqrt{2\pi s}}\right]} \\ = & \frac{-1}{s} \times \frac{1}{\rho + k_a} \end{aligned}$$

The explicit HFA for the radiated pressure field on the surface in the case of a Robin FSI problem is then

$$\boxed{\overline{p}(s) = -\rho s \overline{\phi}(s) = \frac{1}{1 + \frac{k_a}{\rho}}\overline{g}(s)}. \tag{3.24}$$

The approximated time synthesis procedure then relies on the evaluation of relative differences

$$\delta_{HFA}(s) = \frac{\left\|\overline{\phi}_{BEM}(s) - \overline{\phi}_{HFA}(s)\right\|_{L^2}}{\left\|\overline{\phi}_{BEM}(s)\right\|_{L^2}}$$

until it becomes smaller than a chosen tolerance tol_{HFA}. When $\delta_{HFA}(s) < \text{tol}_{HFA}$, solving the frequency BEM problems are not necessary anymore and the Robin HFA (3.24) is used for all the higher complex frequencies.

Remark. This HFA for a FSI interaction with Robin boundary condition also allows to retrieve the HFA proposed by [146] for a Neumann problem. The limiting case $k_a \to +\infty$ in the Robin BC (3.23) is an asymptotic approximation of the Neumann boundary condition:

$$\begin{aligned} \lim_{k_a\to+\infty} \quad (-\rho s\overline{\phi} + k_a \partial_r \overline{\phi}) = & \lim_{k_a\to+\infty} \quad (\overline{h} + k_a s\overline{u} - \tfrac{\lambda}{\nu}(1-\nu)\tfrac{\partial \overline{u}}{\partial r} - \tfrac{\lambda}{r}\overline{u}) \\ \Rightarrow \lim_{k_a\to+\infty} \quad k_a \partial_r \overline{\phi} = & \lim_{k_a\to+\infty} \quad k_a s\overline{u} \end{aligned}$$

The HFA (3.24) then becomes

$$\lim_{k_a \to +\infty} \frac{k_a \overline{p}}{\overline{g}} = \lim_{k_a \to +\infty} \frac{k_a}{1 + \frac{k_a}{\rho}} = \rho$$

The radiated pressure for a Robin problem can then be asymptotically approximated by

$$\overline{p}(b, s) = \rho \frac{\overline{g}}{k_a} = \rho s \overline{u}(b, s).$$

This is the simple HFA for radiation problem. Physically this HFA express the radiated pressure as the pressure locally radiated by a vibrating infinite plate [126].

Numerical verification. We consider again the 2D elastic cylinder Ω_s immersed in an acoustic fluid domain Ω_f (see Section 3.3). We use the same parameters and the incident load has an exponent $\gamma = 3$. We solve a time-domain Robin radiation problem on the exterior surface, with the Z-BEM procedure with and without the Robin high-frequency approximation (3.24). Table 3.10 shows the relative error with respect to the number of frequency BEM solutions computed. For this example, 70 BEM resolutions are needed for the error to be smaller than 10^{-2}. Figure 3.18 hows the fluid pressure evaluated on a point of the coupling interface Γ_e with the time, for different HFA approximations.

Computed BEM solutions	5	35	50	60	70	150	2706
Relative space-time L2 error	1.05	0.063	0.021	0.011	0.008	0.003	0
Percentage of BIEs solved (%)	0.2	1.3	1.8	2.2	2.6	5.5	100

Table 3.10: *Relative space-time L^2 error between the numerical solutions computed with and without HFA, depending on the number of computed frequency BEM problems.*

3.6 Global-in-time FEM/Z-BEM coupling for UNDEX

We have applied the global-in-time iterative method with a FEM/Z-BEM coupling and validated its convergence on 2D examples. The next objective is to use this method to solve realistic UNDEX problems. As explained in Section 2.1, a classic approach in FSI is to decompose the fluid variables into three components, one incident component, one reflected component and one radiated component:

$$p = p^{\text{inc}} + p^{\text{ref}} + p^{\text{rad}}$$

where p^{inc} is the incident pressure field. The reflected field p^{ref} is defined so that the fluid motion for a rigid and motionless solid is given by adding the incident and reflected component $(p^{\text{inc}} + p^{\text{ref}})$. The radiated field p^{rad} is the additive correction to the fluid motion induced by the interfacial motion. For an acoustic shock wave problem in time domain, [146] presents an efficient Z-BEM/FEM/FEM method to

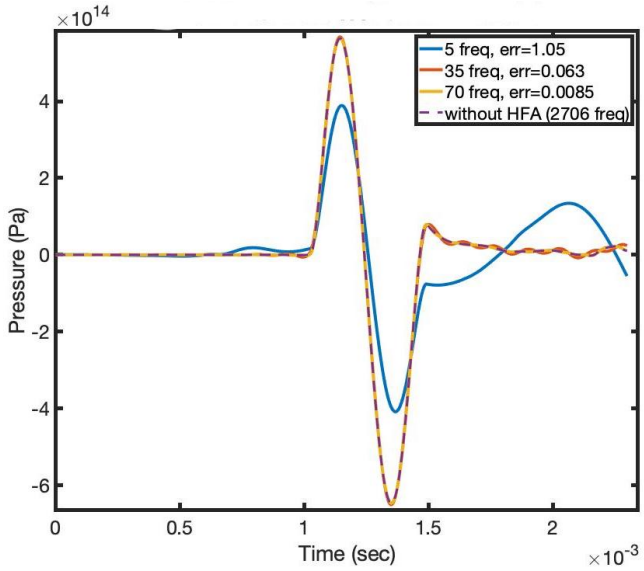

Figure 3.18: *HFA validation for the radiation problem with Robin BCs. Comparison between the Z-BEM fluid pressure and the Z-BEM-HFA fluid pressure on a point of* Γ_e *(*$\Delta t = 1.7\ 10^{-6}$*,* $El = 1778$*).*

compute the solution of the transient coupled FSI problem in three steps, (i) the reflected pressure p^{ref} is computed on the whole time interval and on the whole fluid domain, using the Z-BEM procedure; (ii) the nodal forces $\mathbf{f}$ associated to the pressure $p^{\text{inc}} + p^{\text{ref}}$ are computed on each point of interface Γ, for each time step of the whole interval, and (iii) the structure deformation and the radiated fluid pressure p^{rad} are computed with a monolithic FEM/FEM resolution of the FSI problem, between the structure and a truncated 3D volume mesh for the exterior water, that is refined only near the FSI interface. The nodal forces $\mathbf{f}$ are used on the interface Γ as an input. This strategy allows to successfully solve a rapid transient UNDEX problem. As only the radiated pressure is computed with finite elements, the whole fluid domain doesn't have to be discretised and only a small part of the 3D fluid domain needs is meshed. This makes it possible to solve rapid transient problems involving large structures, with relatively reasonable computation times. Both solvers are used as black boxes, without internal modification. This algorithm is then easily usable to solve realistic problems in an industrial context. It is for example now directly usable by Naval Group. However, the method described in [146] has still some drawbacks compared to a global-in-time FEM/Z-BEM iterative coupling based on Robin boundary conditions as described in Chapter 2:

- A non-uniform complex 3D volume mesh has to be generated for the fluid volume around the structure, with a geometrically complex internal boundary (submarine surface). This might entail the creation of a very refined mesh and increase the computation time.
- The volume mesh has be truncated and an approximation of the radiation condition has to be imposed, which may entail unwanted reflections.

These two drawbacks can be overcome by using the global-in-time FEM/Z-BEM

iterative coupling. Meshing a part of the acoustic domain is no longer necessary with the FEM/Z-BEM procedure and the boundary element method intrinsically model the radiation condition correctly, so the absence of unwanted reflections is guaranteed. It is also possible to use plate or shell elements to model the elastic domain behaviour and thus completely avoid any volume mesh. It should however be noted that in the case of shell elements, the transmission conditions have to be reformulated to take account of the plate theory. We also highlight the following additional benefits:

- The coupling is very efficient, especially since the frequency BEM operators can be reused at each iteration. When combined with the HFA, only a few BEM operators have to be computed once and store. Moreover, the FEM and Z-BEM resolutions are performed in parallel at each iteration. The total computation time of the resolution is therefore only limited by the FEM resolution time at each iteration.

- It is no longer necessary to carry out a preliminary computation of the reflected pressure before the radiated pressure calculation, as only a scattered component is considered, which also reduces the computation time.

- The use of the Z-BEM method allows the total acoustic solution to be computed in the whole fluid domain, including far away from the ship. This can not be done with the FEM/FEM/Z-BEM method used in [146] because in this case the Z-BEM is only used to calculate the reflected component of the acoustic solution. For example this is useful to accurately evaluate the influence of the explosion on the acoustic signature of the submarine without refining a fluid mesh far away from the structure.

- Using a global-in-time iterative procedure with guaranteed convergence allows the use of fixed point acceleration methods (as Aitken's Δ^2 acceleration) to optimise the choice of the coupling parameters value in order to minimise the number of iterations, even on complex problems.

3.7 Conclusion

We have proposed and discussed the efficiency of a global-in-time iterative coupling based on Robin boundary conditions. This coupling implemented with a FEM/Z-BEM method has been validated on 2D examples and the coupling parameters values have been optimised by using a simplified 2D problem for which a semi-analytical solution is available. An Aitken fixed-point acceleration strategy has been used as well as a high frequency approximation adapted for Robin evolution problems. In this way we derived an efficient numerical method for solving high frequency transient FSI problems.

In the context of UNDEX, the iterative global-in-time method based on Robin BCs is a promising alternative to overcome the drawbacks of an Z-BEM/FEM/FEM method, as it neither requires the imposition of radiation boundary conditions, nor the pre-calculation of the reflected pressure by finite elements, and increases the

efficiency of resolution. We have shown that the use of Robin BCs is essential for the convergence of this kind of coupling. The main problem that could prevent the industrial use of such an iterative procedure is the need to use a FEM solver offering the possibility to impose non-homogeneous Robin BCs. Commercial solvers do not always propose this kind of boundary conditions. In such a case, a possible solution would be to consider an alternative iterative coupling strategy, involving an acoustic-acoustic interface. This strategy, developed in Chapter 4, will avoid the use of a Robin elastic condition.

CHAPTER 4

A convergent global-in-time acoustic/acoustic-elastic coupling

Our goal is to study all the possible configurations where a black box coupling can be used. For this reason, we design in this chapter an iterative global-in-time coupling with guaranteed convergence that solves transient acoustic-elastodynamic problems and that does not use non-homogeneous Robin boundary conditions in the elastic domain. We recall in Section 4.1 the importance of this alternative coupling and its advantages. Section 4.3 introduces the problem definition and the notations. Then, in Section 4.3.2, we present the global-in-time iterations based on the solutions of well-posed Robin IBVPs. The Robin boundary conditions are imposed in the acoustic domain only. We prove the iterations convergence in Section 4.4. We numerically validate our procedure with a FEM/Z-BEM numerical method in Section 4.5 on simple 2D problems before considering more complex 3D geometries in Chapter 5.

Contents

4.1 Why another coupling algorithm? 112

4.2 Acoustic/acoustic-elastic coupling definition 113

4.3 Global-in-time iterative procedure based on acoustic/acoustic Robin boundary conditions 115

4.3.1 General acoustic/acoustic iterative method for transient FSI problems 116

4.3.2 Acoustic/acoustic iterative method with Robin boundary conditions 117

4.3.3 Robin boundary conditions definition. 117

4.3.4 Solvability of acoustic and acoustic-elastic Robin IBVPs. . 120

4.4 Proof of convergence of the acoustic-acoustic iterative algorithm 122

4.5 Validation and optimisation of the acoustic-acoustic FEM/Z-BEM coupling 127

4.5.1 Coupling validation: 2D test case 127

4.5.2 Coupling parameter optimisation 128
4.6 Conclusion 132

4.1 Why another coupling algorithm?

We want to consider all the possible options to use a FEM solver in non-intrusive fashion in our coupling strategy. In particular, Robin boundary conditions (BCs) are not available in some FE solvers. For example in Abaqus, non-homogeneous Robin BCs are not accessible for the modelling of the structure, preventing the implementation of the acoustic/elastic coupling procedure detailed of Chapter 2. An alternative way to solve the coupled FSI problem is to decompose differently the domains, in order to perform an acoustic/acoustic coupling with acoustic/acoustic transmission conditions. As illustrated in Figure 4.1, the idea is to model the structure and a small region of fluid around the structure, using the FEM, while the remainder of the fluid domain is treated with a BEM. The iterative global-in-time FEM/Z-BEM coupling based on an acoustic/acoustic coupling interface, hereafter named acoustic-acoustic FEM/Z-BEM, presents three main additional advantages compared to the previous approach:

1. Inhomogeneous Robin impedance-like boundary conditions might be available for an acoustic domain in some finite element solvers while it might not for an elastic domain.

2. Modelling part of the fluid domain with the FEM allows to introduce nonlinearities. For example in the context of UNDEX, the phenomenon of cavitation appears in the vicinity of the hull for surface ships, when the shock wave reflects on the free surface and creates an important pressure drop. Since the BEM is only suitable for linear equations, it is natural to take this phenomena into account in the FEM solver.

3. In the case of the acoustic/elastic global-in-time coupling, the physical boundary of the ship is the support of the coupling interface and the mesh for the BEM. The frequency-domain BEM resolutions therefore have a high computational cost due to the large number of boundary elements to model the geometry complexity. In the case of an acoustic/acoustic-elastic coupling, the coupling interface is a boundary that has no physical meaning and it can be arbitrary chosen. The use of a very smooth coupling interface (for example a sphere) reduces the number of boundary elements, and thus the computational cost of the frequency-domain BEM resolutions. From a mathematical point of view, it is then easier to satisfy the criterion of minimum spatial regularity needed to obtain useful data-to-solution mappings and solvability results.

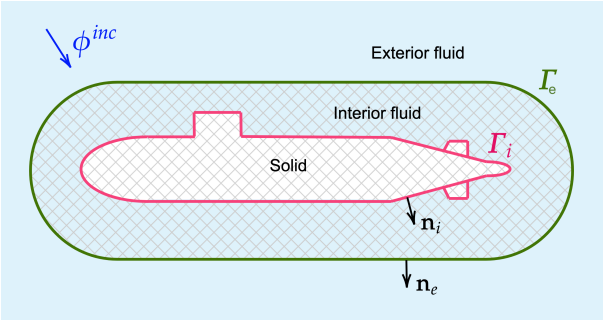

Figure 4.1: *Domain decomposition for an acoustic-acoustic coupling: FEM (solid and interior fluid), and BEM (exterior fluid) parts.*

4.2 Acoustic/acoustic-elastic coupling definition

We consider again an elastic solid immersed in an acoustic fluid, but the coupling interface is now moved inside the fluid domain. We define a unbounded fluid sub-domain Ω_e and the complementary fluid-structure sub-domain $\Omega_i := \Omega_i^s \cap \Omega_i^f$, composed of a bounded elastic solid Ω_i^s and a bounded fluid region Ω_i^f surrounding the solid. The sub-domains Ω_e and Ω_i have a shared interface $\Gamma_e = \partial\Omega_e = \overline{\Omega_i^f} \cap \overline{\Omega_e}$ and the sub-domain Ω_i has an internal boundary $\Gamma_i = \partial\Omega_i^s = \overline{\Omega_i^s} \cap \overline{\Omega_i^f}$. In this model, Ω_i^s and Ω_e do not share any interface (Figure 4.2). We denote by $\mathbf{n_e}$ the unit outward normal to Γ_e and $\mathbf{n_i}$ the unit outward normal to Γ_i.
In both sub-domains, the fluid has the same physical properties. We distinguish the notation for the physical quantities as follows

- Exterior fluid: velocity potential ϕ_e, velocity $v_e = \nabla\phi_e$, pressure $p_e = -\rho_f \partial_t \phi_e$
- Interior fluid: velocity potential ϕ_i, velocity $v_i = \nabla\phi_i$, pressure $p_i = -\rho_f \partial_t \phi_i$
- Solid: displacement $\mathbf{u}$, Cauchy stress $\sigma[\mathbf{u}]$

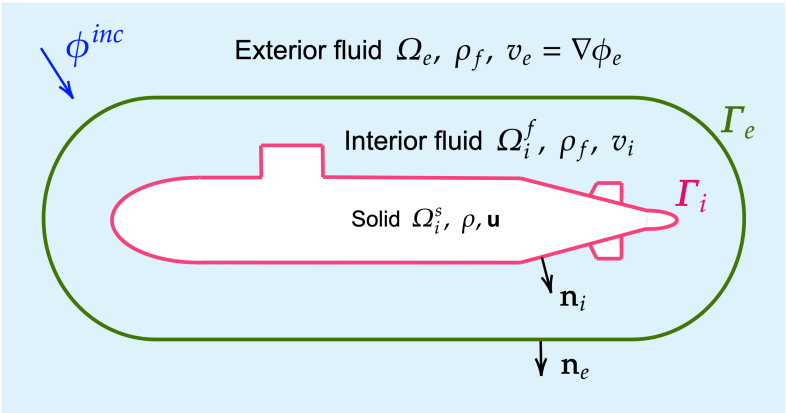

Figure 4.2: *Domain decomposition for an acoustic-acoustic coupling : notations.*

The incident wave is defined by the velocity potential ϕ^{inc}, which solves at all times the homogeneous wave equation and is perturbed by the presence of the solid. The FSI between Ω_s^i and Ω_f^i occurs due to the kinematic and dynamical transmission conditions (2.2) defined on Γ_i as described in Section 2.1. They express the continuity across Γ_i of the normal velocity and the traction vector. In addition, we introduce another exterior boundary Γ_e and two transmission conditions:

$$\text{a) } \rho_f \partial_t \phi_i = \rho_f \partial_t \phi_e \qquad \text{b) } \partial_n \phi_i = \partial_n \phi_e \qquad \text{on } \Gamma_e \times [0,T] \tag{4.1}$$

which express the continuity of the fluid pressure and fluid velocity across the fluid-fluid interface Γ_e. We described the FSI problem with the velocity potential ϕ. As for the acoustic/elastic procedure in Section 2.1, ϕ_e is decomposed with one of the following possible decompostions:

1. The simpliest additive decomposition consists in introducing a scattered field and to decompose ϕ_e according to $\phi_e = \phi_e^{\text{inc}} + \phi_e^{\text{sca}}$. In this case, the transmission conditions (4.1) expressed in terms of ϕ_e^{sca} read

$$\rho_f \partial_t \phi_i = \rho_f \partial_t \phi_e^{\text{sca}} + \rho_f \partial_t \phi_e^{\text{inc}}, \qquad \partial_n \phi_i = \partial_n \phi_e^{\text{inc}} + \partial_n \phi_e^{\text{sca}} \qquad \text{in } \Gamma_e \times [0,T].$$

2. Introducing a Neumann-reflected field and a radiated field $\phi_e = \phi_e^{\text{inc}} + \phi_e^{\text{ref}} + \phi_e^{\text{rad}}$. The reflected fluid motion is defined by the reflection IBVP

$$-\Delta \phi_e^{\text{ref}} + \frac{1}{c_f^2} \partial_t^2 \phi_e^{\text{ref}} = 0 \quad \text{in } \Omega_e \times [0,T], \qquad \begin{cases} \partial_n \phi_e^{\text{ref}} = -\partial_n \phi_e^{\text{inc}} & \text{in } \Gamma_e \times [0,T] \\ \phi_e^{\text{ref}}(\cdot,0) = \partial_t \phi_e^{\text{ref}}(\cdot,0) = 0 & \text{in } \Omega_e. \end{cases}$$

3. Introducing a Robin-reflected field and a radiated field $\phi_e = \phi_e^{\text{inc}} + \phi_e^{\text{ref}} + \phi_e^{\text{rad}}$. The reflected fluid motion is defined by a reflection IBVP with a Robin BC:

$$-\Delta \phi_e^{\text{ref}} + \frac{1}{c_f^2} \partial_t^2 \phi_e^{\text{ref}} = 0 \quad \text{in } \Omega_e \times [0,T],$$

$$\begin{cases} \left(k_e \partial_n - \rho_f \partial_t\right) \phi_e^{\text{ref}} = \left(-k_e \partial_n + \rho_f \partial_t\right) \phi_e^{\text{inc}} & \text{in } \Gamma_e \times [0,T] \\ \phi_e^{\text{ref}}(\cdot,0) = \partial_t \phi_e^{\text{ref}}(\cdot,0) = 0 & \text{in } \Omega_e, \end{cases}$$

   where k_e is a positive factor.

Using either of these additive decompositions, the coupled FSIP (4.2) is formulated with ϕ_e as the main unknown, referring either to the scattered ϕ_e^{sca} or to the radiated variable ϕ_e^{rad}, depending on the chosen decomposition.

In this chapter, we focus on an equivalent non-dimensional version of the FSIP, obtained by expressing the coordinates $\mathbf{x}, t$, field variables, $\phi_e, \phi_i, \mathbf{u}, \mathbf{t}$ and material parameters as

$$\mathbf{x} = b\widehat{\mathbf{x}}, \quad t = \frac{b\widehat{t}}{c_f}, \quad \phi_e = bc_f\widehat{\phi}_e, \quad \phi_i = bc_f\widehat{\phi}_i, \quad \mathbf{u} = b\widehat{\mathbf{u}}, \quad \mathbf{t} = \rho_f c_f^2 \widehat{\mathbf{t}}, \quad \rho_s = \rho_f \widehat{\rho}_s$$

where b is a characteristic length. We hence consider the dimensionless IBVP (4.2). It consists of the standard exterior Helmholtz problem (4.2c), an interior Helmholtz

problem (4.2b) and the elastodynamic equation (4.2a) governing the equilibrium of an elastic scatterer. The equations are coupled through a dynamic and a kinematic interface conditions (4.2d) defined on the acoustic/elastic interface Γ_i. They are imposed to ensure the continuity of the stress and of the normal component of the velocity. The acoustic equations are coupled through two transmission conditions (4.2e) defined on Γ_e.

$$\begin{cases} -\boldsymbol{\Delta}_{\mathbf{s}}\mathbf{u} + \rho\partial_t^2\mathbf{u} = \mathbf{0} & \text{in } \Omega_i^s \times [0,T], \quad \mathbf{u}(0) = \partial_t\mathbf{u}(0) = \mathbf{0} \quad \text{in } \Omega_i^s & \text{(a)} \\ \Delta\phi_i - \partial_t^2\phi_i = 0 & \text{in } \Omega_i^f \times [0,T], \quad \phi_i(0) = \partial_t\phi_i(0) = 0 \quad \text{in } \Omega_i^f & \text{(b)} \\ \Delta\phi_e - \partial_t^2\phi_e = 0 & \text{in } \Omega_e \times [0,T], \quad \phi_e(0) = \partial_t\phi_e(0) = 0 \quad \text{in } \Omega_e & \text{(c)} \\ \mathbf{t} = \partial_t\phi\mathbf{n_i}, & \partial_n\phi = \partial_t\mathbf{u}.\mathbf{n_i} \quad \text{in } \Gamma_i \times [0,T] & \text{(d)} \\ -\partial_t\phi_i = -\partial_t\phi_e - s_p, & \partial_n\phi_i = s_v + \partial_n\phi_e \quad \text{in } \Gamma_e \times [0,T] & \text{(e)} \end{cases} \tag{4.2}$$

In the TCs (4.2e), s_v and s_p are prescribed time-dependent normal velocity and pressure jumps across Γ_e. These terms depend on the chosen decomposition of ϕ_e

1. $s_p = \partial_t\phi_e^{\text{inc}}$ $\quad s_v = \partial_n\phi_e^{\text{inc}}$ $\quad \left(\phi = \phi_e^{\text{inc}} + \phi_e^{\text{sca}}\right)$
2. $s_p = \partial_t\phi_e^{\text{Ref}} = \partial_t(\phi_e^{\text{inc}} + \phi_e^{\text{ref}})$ $\quad s_v = 0$ $\quad \left(\phi = \phi_e^{\text{inc}} + \phi_e^{\text{ref}} + \phi_e^{\text{rad}}\right)$
3. $s_p = \partial_t\phi_e^{\text{Ref}} = \partial_t(\phi_e^{\text{inc}} + \phi_e^{\text{ref}})$ $\quad s_v = \dfrac{1}{k_e}\partial_n(\phi_e^{\text{inc}} + \phi_e^{\text{ref}})$ $\quad \left(\phi = \phi_e^{\text{inc}} + \phi_e^{\text{ref}} + \phi_e^{\text{rad}}\right)$

As in Section 2.1, the system is assumed to be at rest at the beginning and homogeneous initial conditions are prescribed. The decomposition in a scattering and a radiation problem allows to deal with compactly supported variables in the coupled problem. To simplify the notations, we omit thereafter the superscript “rad” (or "sca"), with all the fluid variables understood to pertain to the radiated motion in Ω_e (the complete fluid motion being recovered by adding back the relevant “Ref” quantities), ϕ_e now refers to ϕ_e^{rad} (or ϕ_e^{sca}).

Remark. Since the fluid is at initial rest and is excited only by the interface motion, the radiated variable ϕ_e has a bounded support at any finite time. Thanks to the decomposition into a reflected and a radiated problems, the infinite exterior domain does not need to be artificially truncated and the introduction of a DtN operator, such as proposed in [13], is not necessary.

4.3 Global-in-time iterative procedure based on acoustic/acoustic Robin boundary conditions

In this section we introduce an iterative global-in-time method to solve a transient FSI problem. As in Section 2.3, we construct sequences $(\phi_e^n, \phi_i^n, \mathbf{u}^n)_{n\geq 0}$ which converge to the solution $(\phi_e, \phi_i, \mathbf{u})$ of problem (4.2) as $n \to \infty$, each iterate $(\phi_e^n, \phi_i^n, \mathbf{u}^n)$ solving a pair of decoupled IBVPs in $\Omega_e \times [0,T]$ and $\Omega_i \times [0,T]$. We then justify with mathematical arguments how the choice of the IBVPs boundary conditions influence the iterations convergence.

4.3.1 General acoustic/acoustic iterative method for transient FSI problems

The resolution of the coupled problem (4.2) with a partitioned approach leads to study two boundary value problems defined in each subdomain. We consider one acoustic initial boundary value problem in the Ω_e fluid domain and one acoustic/elastodynamic IBVP in the domain $\Omega_f^i \cap \Omega_s^i$. The exterior acoustic IBVP at each iteration $n \geq 1$ is assumed to have the form:

$$\begin{cases} \Delta\phi_e^n - \partial_t^2\phi_e^n = 0 & \text{in } \Omega_e \times [0,T] \\ \Pi_e^n\left[\phi_e^n\right] = G_e[\phi_e^{n-1}, \phi_i^{n-1}] & \text{on } \Gamma_e \times [0,T], \\ \phi_e^n(0) = \partial_t\phi_e^n(0) = 0 & \text{in } \Omega_e. \end{cases} \tag{4.3}$$

Similarly, the acoustic/elastodynamic IBVP at each iteration $n \geq 1$ is assumed to have the form:

$$\begin{cases} -\boldsymbol{\Delta}_\mathbf{s}\mathbf{u}^n + \rho_s\partial_t^2\mathbf{u}^n = \mathbf{0} & \text{in } \Omega_i^s \times [0,T], \\ \Delta\phi_i^n(t,\mathbf{x}) - \partial_t^2\phi_i^n(t,\mathbf{x}) = 0 & \text{in } \Omega_i^f \times [0,T], \\ \Pi_i^n\left[\phi_i^n\right] = G_i[\phi_e^{n-1}, \phi_i^{n-1}] & \text{on } \Gamma_e \times [0,T], \\ \phi_i^n(0) = \partial_t\phi_i^n(0) = 0 & \text{in } \Omega_i^f, \\ \mathbf{u}^n(0) = \partial_t\mathbf{u}^n(0) = \mathbf{0} & \text{in } \Omega_i^s. \end{cases} \tag{4.4}$$

Π_e and Π_i are boundary operators such that $\phi_e^n \to \Pi_e[\phi_e^n]$ and $\phi_i^n \to \Pi_i[\phi_i^n]$, to be specified. At iteration n, $G_e[\phi_e^{n-1}, \phi_i^{n-1}]$ and $G_i[\phi_e^{n-1}, \phi_i^{n-1}]$ are boundary data that depend on interfacial quantities for the previous iterate $n-1$ and possibly on their normal or time derivatives. We will note

$$g_e^n := G_e[\phi_e^{n-1}, \phi_i^{n-1}], \quad \text{and} \quad g_i^n := G_i[\phi_e^{n-1}, \phi_i^{n-1}].$$

With the notations $\phi_e = \phi_e[g_e]$ and $\phi_i = \phi_i[g_i]$ emphasising the dependence of these solutions on the respective boundary data, the iterative DDM consists in an algorithm defining a data sequence $(g_e^n, g_i^n)_{n\geq 0}$ such that the solution iterates verify the transmission conditions of the coupled FSIP (4.2e) in $\Gamma_e \times [0,T]$, in the limit $n \to \infty$, i.e.:

$$\text{(a)}\ \ (-\partial_t\phi_i[g_i^n] + \partial_t\phi_e[g_e^n] + s_p) \to 0, \qquad \text{(b)}\ \ (\partial_n\phi_i[g_i^n] - s_v - \partial_n\phi_e[g_e^n]) \to 0. \tag{4.5}$$

To satisfy these TCs in the limit, the sequence (g_e^n, g_i^n) of data must have a different definition depending on the boundary operators Π_e and Π_i. Indeed, the boundary operators and data must be such that if the iterative process converges, the limiting equalities

$$\Pi_e\left[\phi_e\right] = G_e\left[\phi_e, \phi_i\right], \quad \text{and} \quad \Pi_i\left[\phi_i\right] = G_i\left[\phi_e, \phi_i\right] \tag{4.6}$$

are equivalent to the transmission conditions (4.2e) of the original FSIP. The regularity results on Neumann IBVPs and the observations regarding the loss of space-time regularity of their solutions in Section 2.3.2, prompt us to directly consider an iterative procedure based on Robin IBVPs.

4.3.2 Acoustic/acoustic iterative method with Robin boundary conditions

We choose a linear combination of interfacial varibales for the boundary operators in the IBVPs (4.3) and (4.4):

$$\Pi_e[\phi_e] := -\partial_t\phi_e + K_e\partial_n\phi_e \qquad \text{and} \qquad \Pi_i[\phi_i] := \partial_t\phi_i + K_i\partial_n\phi_i \tag{4.7}$$

where $K_e : L^2(\Gamma_e) \to L^2(\Gamma_e)$ and $K_i : L^2(\Gamma_e) \to L^2(\Gamma_e)$ are time-independent symmetric, positive and boundedly invertible operators. The exterior acoustic IBVP (4.3) becomes, at each iteration $n \geq 1$

$$\begin{cases} \Delta\phi_e^n - \partial_t^2\phi_e^n = 0 & \text{in } \Omega_e \times [0,T] \\ -\partial_t\phi_e^n + K_e\partial_n\phi_e^n = g_e^n & \text{on } \Gamma_e \times [0,T], \\ \phi_e^n(0) = \partial_t\phi_e^n(0) = 0 & \text{in } \Omega_e. \end{cases} \tag{4.8}$$

The interior acoustic/elastodynamic IBVP (4.4) becomes at each iteration $n \geq 1$

$$\begin{cases} -\boldsymbol{\Delta}_{\mathbf{s}}\mathbf{u}^n + \rho_s\partial_t^2\mathbf{u}^n = \mathbf{0} & \text{in } \Omega_i^s \times [0,T], \\ \Delta\phi_i^n(t,\mathbf{x}) - \partial_t^2\phi_i^n(t,\mathbf{x}) = 0 & \text{in } \Omega_i^f \times [0,T], \\ \partial_t\phi_i^n + K_i\partial_n\phi_i^n = g_i^n & \text{on } \Gamma_e \times [0,T], \\ \phi_i^n(0) = \partial_t\phi_i^n(0) = 0 & \text{in } \Omega_i^f, \\ \mathbf{u}^n(0) = \partial_t\mathbf{u}^n(0) = \mathbf{0} & \text{in } \Omega_i^s. \end{cases} \tag{4.9}$$

If the iterations are convergent, the solution iterates $(\phi_e^n, \phi_i^n, \mathbf{u}^n)$ are required to verify the TCs (4.2e) in $\Gamma_e \times [0,T]$, in the limit $n \to \infty$. To derive the form of the Robin boundary data for the Robin IBVPs (4.8) and (4.9), adapt the methodology used to derive and justify the acoustic/elastic iterations in Section 2.4.2.

4.3.3 Robin boundary conditions definition.

We now aim at defining the exact form of the Robin boundary data G_e and G_i. Still inspired by [49] where iterations with Robin boundary conditions are proved to be convergent and used to solve Helmholtz equations, we first introduce incoming and outgoing trace operators to formulate the Robin iterations based on BCs of the form (4.7).

Incoming and outcoming trace operators.

The incoming trace operators B_e and B_i are defined by

$$B_e(\phi_e) = -\partial_t\phi_e + K_e\partial_n\phi_e \qquad B_i(\phi_i) = \partial_t\phi_i + K_i\partial_n\phi_i \tag{4.10}$$

As in Section 2.4.2, these trace operators can be understood as incoming operators on Γ_e in the sense that acoustic motions satisfying $B_e(\phi_e) = 0$ or $B_i(\phi_i) = 0$ are incoming relative to Ω_e and Ω_i^f respectively. Still following [49], we also introduce two outgoing trace operators $\overline{B}_e$ and $\overline{B}_i$:

$$\overline{B}_e(\phi_e) = \partial_t\phi_e + K_e\partial_n\phi_e \qquad \overline{B}_i(\phi_i) = -\partial_t\phi_i + K_i\partial_n\phi_i. \tag{4.11}$$

They are "outgoing" traces in the sense that motions satisfying $\overline{B}_e(\phi_e) = 0$ or $\overline{B}_i(\phi_i) = 0$ are outgoing relative to Ω_e and Ω_i^f. All boundary traces involved in Robin BCs (4.7) can be formulated as combinations of incoming and outgoing traces: relations (4.10) and (4.11) can readily be inverted and any set of velocity and Neumann traces on Γ_e are given in terms of the incoming and outgoing traces by

$$\begin{aligned} \partial_n\phi_e &= \tfrac{1}{2}K_e^{-1}\left(\overline{B}_e(\phi_e) + B_e(\phi_e)\right); \quad \partial_t\phi_e = \tfrac{1}{2}\left(\overline{B}_e(\phi_e) - B_e(\phi_e)\right) \\ \partial_n\phi_i &= \tfrac{1}{2}K_i^{-1}\left(B_i(\phi_i) + \overline{B}_i(\phi_i)\right); \quad \partial_t\phi_i = \tfrac{1}{2}\left(B_i(\phi_i) - \overline{B}_i(\phi_i)\right). \end{aligned} \tag{4.12}$$

With these notations and choosing

$$\Pi_e[\phi_e] = B_e(\phi_e), \qquad \text{and} \qquad \Pi_i[\phi_i] = B_i(\phi_i)$$

the Robin conditions (4.7) at iteration n are written

$$B_e(\phi_e^n) = G_e[\phi_e^{n-1}, \phi_i^{n-1}] \quad \text{and} \quad B_i(\phi_i^n) = G_i[\phi_e^{n-1}, \phi_i^{n-1}], \tag{4.13}$$

The left-hand side quantities are the incoming traces of ϕ_e^{n-1} and ϕ_i^{n-1} through Γ_e, while the right hand side quantities are the Robin boundary data depending on the traces ϕ_e^{n-1} and ϕ_i^{n-1} of the previous iterate. Moreover at convergence, the transmission conditions (4.2e) have to be verified. Expressed using the incoming and outgoing traces, they are given by

$$\begin{aligned} \left(B_i(\phi_i) - \overline{B}_i(\phi_i)\right) + \left(B_e(\phi_e) - \overline{B_e}(\phi_e)\right) &= 2s_p, \qquad \text{(a)} \\ K_i^{-1}\left(B_i(\phi_i) + \overline{B_i}(\phi_i)\right) - K_e^{-1}\left(B_e(\phi_e) + \overline{B}_e(\phi_e)\right) &= 2s_v. \qquad \text{(b)} \end{aligned} \tag{4.14}$$

These equations will help defining appropriate choices for G_e and G_i.

Derivation of RR iterations.

The Robin global-in-time iterations for the FSIP (4.2) are, again, formulated by means of the LATIN heuristic [122, 155].

Let then (g_e^{n-1}, g_i^{n-1}) be some Robin datum. Let $\phi_e[g_e^{n-1}], \phi_i[g_i^{n-1}]$ solve the Robin IBVPs (4.8) and (4.9), and have well-defined velocity and Neumann traces (or, equivalently, incoming and outgoing traces) on Γ_e. We then define the next datum iterate (g_e^n, g_i^n), and resulting solution iterate $(\phi_e^n, \phi_i^n) = (\phi_e[g_e^n], \phi_i[g_i^n])$, by requiring that the transmission conditions (4.2e) be verified by the final incoming traces and the initial outgoing traces. We accordingly set

$$(B_e(\phi_e), B_i(\phi_i)) = (B_e(\phi_e^n), B_i(\phi_i^n)),$$

and

$$(\overline{B}_e(\phi_e), \overline{B}_i(\phi_i)) = (\overline{B}_e(\phi_e^{n-1}), \overline{B}_i(\phi_i^{n-1}))$$

in (4.14) and solve the resulting equations for $(B_e(\phi_e^n), B_i(\phi_i^n))$. This results in the final incoming traces being given by

$$B_e(\phi_e^n) = G_e[\phi_e^{n-1}, \phi_i^{n-1}], \quad \text{and} \quad B_i(\phi_i^n) = G_i[\phi_e^{n-1}, \phi_i^{n-1}] \tag{4.15}$$

with

$$\begin{aligned} G_e[\phi_e,\phi_i] &= 2K_eH^{-1}\overline{B}_i + (K_e-K_i)H^{-1}\overline{B}_e + 2K_eH^{-1}(s_p - K_is_v),\\ G_i[\phi_e,\phi_i] &= 2K_iH^{-1}\overline{B}_e + (K_i-K_e)H^{-1}\overline{B}_i + 2K_iH^{-1}(s_p + K_es_v), \end{aligned} \tag{4.16}$$

in terms of the initial outgoing traces (with $H := K_e + K_i$). Equations (4.15), (4.16) constitute the proposed iterations based on Robin conditions. These iterations thus consist in (i) evaluating the datum (g_e^n, g_i^n) and (ii) solving the Robin IBVPs (4.4) and (4.3) with that datum. In this work, we will implement these iterations in a simpler form, by using the particular values $K_e = k_eI$, $K_i = k_iI$. Choosing adapted values for the positive parameters k_e and k_i can improve the convergence rate, as we will study later (see Section 3.3.3). Iterations can be started by solving problems (2.10) and (2.11) with arbitrarily chosen (g_e^0, g_i^0). The simplest choice is to set $(g_e^0, g_i^0) = (0,0)$, yielding $\overline{B}_e(\phi_e^0) = 0$ and $\overline{B}_i(\phi_i^0) = 0$ in formulas (4.16).

Matrix notation.

Still following [49] and transposing the approach of Chapter 2, we introduce matrix notations in order to express G_e and G_i in a compact form. These notations will be very helpful for studying the convergence of Robin acoustic:acoustic coupling iterations thereafter. We set

$$\mathbb{B} = \begin{Bmatrix} B_e(\phi_e)\\ B_i(\phi_i)\end{Bmatrix}, \qquad \overline{\mathbb{B}} = \begin{Bmatrix} \overline{B}_e(\phi_e)\\ \overline{B}_i(\phi_i)\end{Bmatrix} \quad \text{and} \quad \mathbb{H} = \begin{Bmatrix} s_p\\ s_v\end{Bmatrix}. \tag{4.17}$$

The corresponding L^2 scalar product and norm on $\Gamma_e \times [0,T]$ are then

$$(\mathbb{B},\mathbb{B}')_{\Gamma_e,T} := (B_e,B_e')_{\Gamma_e,T} + (B_i,B_i')_{\Gamma_e,T}, \quad \|\mathbb{B}\|^2_{\Gamma_e,T} := (\mathbb{B},\mathbb{B})_{\Gamma_e,T}.$$

With the weighting operator matrix

$$\mathbb{K} = \begin{bmatrix} k_e^{-1} & 0\\ 0 & k_i^{-1}\end{bmatrix},$$

we define the weighted versions of the $L^2_T(\Gamma_e)$ space-time scalar product and norm by

$$(\mathbb{B},\mathbb{B}')_{\Gamma,T,\mathbb{K}} := (\mathbb{B},\mathbb{K}\mathbb{B}')_{\Gamma_e,T}, \quad \|\mathbb{B}\|^2_{\Gamma_e,T,\mathbb{K}} := (\mathbb{B},\mathbb{K}\mathbb{B})_{\Gamma_e,T}.$$

We denote $\mathbb{L}^2_T(\Gamma_e)$ the space of sets of boundary traces $\mathbb{B}$ with finite norm $\|\mathbb{B}\|^2_{\Gamma_e,T}$ or $\|\mathbb{B}\|^2_{\Gamma_e,T,\mathbb{K}}$. Using these notations, the transmission conditions (4.14) take the compact form

$$\mathbb{B} = \mathbb{X}\overline{\mathbb{B}} + \mathbb{L}\mathbb{H}, \tag{4.18}$$

while the iterative procedure based on Robin acoustic/acoustic iteration equations (4.13) becomes

$$\mathbb{B}_n = \mathbb{X}\overline{\mathbb{B}}_{n-1} + \mathbb{L}\mathbb{H} \tag{4.19}$$

where the operator matrices $\mathbb{X}$ and $\mathbb{L}$ are given by

$$\mathbb{X} = \begin{bmatrix} (K_e-K_i)H^{-1} & 2K_eH^{-1}\\ (K_i-K_e)H^{-1} & 2K_iH^{-1}\end{bmatrix}, \quad \mathbb{L} = \begin{bmatrix} 2K_eH^{-1} & -2K_eK_iH^{-1}\\ 2K_iH^{-1} & 2K_eK_iH^{-1}\end{bmatrix}.$$

This operator has the same two main properties as the acoustic-elastic $\mathbb{X}$ operator in Section 2.4.2, namely:

$$\mathbb{X}\mathbb{X} = \mathbb{I} \text{ and } \mathbb{X}'\mathbb{K}\mathbb{X} = \mathbb{K}$$

so that $\mathbb{X}$ defines an isometry for the $\|\cdot\|_{\Gamma_e,T,\mathbb{K}}$ norm:

$$\|\mathbb{X}\mathbb{B}\|^2_{\Gamma_e,T,\mathbb{K}} = \|\mathbb{B}\|^2_{\Gamma_e,T,\mathbb{K}} \quad \forall \mathbb{B} \in \mathbb{L}^2_T(\Gamma_e).$$

The iteration equation (4.19) can therefore be inverted giving the identity

$$\overline{\mathbb{B}}_{n-1} = \mathbb{X}\left(\mathbb{B}_n - \mathbb{L}\mathbb{H}\right)$$

which plays a key role in the convergence proof for the iterative process. If iterations (4.19) converge, their limit satisfies the transmission conditions (4.18).

Relaxed iterations. We also consider a relaxed version of iterations (4.19). Introducing a relaxation parameter $r \in [0,1]$, the Robin data iterates are defined by:

$$\begin{aligned} B_e(\phi_e^n) &= (1-r)B_e(\phi_e^{n-1}) + rG_e[\phi_e^{n-1},\phi_i^{n-1}], \\ B_i(\phi_i^n) &= (1-r)B_i(\phi_i^{n-1}) + rG_i[\phi_e^{n-1},\phi_i^{n-1}], \end{aligned} \tag{4.20}$$

instead of (4.15), with $G_e[\phi_e^{n-1},\phi_i^{n-1}]$ and $G_i[\phi_e^{n-1},\phi_i^{n-1}]$ still given by (4.16). Iterations (4.15) then correspond to (4.20) with $r = 1$. Using the matrix notation, the relaxed Robin iteration equation (4.18) becomes

$$\mathbb{B}_n = (1-r)\mathbb{B}_{n-1} + r\left[\mathbb{X}\overline{\mathbb{B}}_{n-1} + \mathbb{L}\mathbb{H}\right]$$

instead of (4.19). This iteration equation can be inverted as well, yielding

$$\overline{\mathbb{B}}_{n-1} = \mathbb{X}(1-r) + r\left[\frac{1}{r}\mathbb{B}_n + (1-\frac{1}{r})\mathbb{B}_{n-1} - \mathbb{L}\mathbb{H}\right]. \tag{4.21}$$

This reformulation of the transmission conditions and the Robin-Robin iterations in terms of incoming and outgoing traces is crucial for proving the convergence of the proposed Robin acoustic/acoustic iterations (see Section 4.4).

4.3.4 Solvability of acoustic and acoustic-elastic Robin IBVPs.

For an iterative procedure based on sequentially solving Robin IBVPs, it is necessary to verify the IBVPs well-posedness. The generic exterior Robin IBVP has the form

$$\begin{cases} -\Delta\phi_e + \partial_t^2\phi_e = 0 & \text{in } \Omega_e \times [0,T] \\ -\partial_t\phi_e + k_e\partial_n\phi_e = g_e & \text{on } \Gamma_e \times [0,T] \\ \phi_e(0) = \partial_t\phi_e(0) = 0 & \text{in } \Omega_e. \end{cases} \tag{4.22}$$

Likewise, the generic FSI interior IBVP has the form

$$\begin{cases} -\Delta\phi_i + \partial_t^2\phi_i = 0 & \text{in } \Omega_i^f \times [0,T] \\ -\mathbf{\Delta_s}[\mathbf{u}] + \rho_s\partial_t^2\mathbf{u} = \mathbf{0} & \text{in } \Omega_i^s \times [0,T] \\ \partial_n\phi_i = \partial_t\mathbf{u}.\mathbf{n_i} \quad \text{and } \mathbf{t} = \partial_t\phi_i\mathbf{n_i} & \text{on } \Gamma_i \times [0,T] \\ \partial_t\phi_i + k_i\partial_n\phi_i = g_i & \text{on } \Gamma_e \times [0,T] \\ \phi_i(0) = \partial_t\phi_i(0) = 0 \quad \text{in } \Omega_i^f \quad \text{and} \quad \mathbf{u}(0) = \partial_t\mathbf{u}(0) = \mathbf{0} \text{ in } \Omega_i^s \end{cases} \tag{4.23}$$

We choose to define the scalar $L^2(\Omega_e)$, $L^2(\Omega_i^f)$, $H^1(\Omega_e)$ and $H^1(\Omega_i^f)$ norms using the bilinear forms a, b of the acoustic weak formulation (2.6):

$$\|\phi\|_\Omega^2 = b(\phi,\phi), \quad \|\phi\|_{1,\Omega}^2 = a(\phi,\phi) + b(\phi,\phi). \tag{4.24}$$

We do likewise for the norms of vector fields in the elastic domain Ω_i^s, using the bilinear forms A, B of the elastodynamic weak formulation (2.6). We choose to equip the spaces $\mathbf{L^2}(\Omega_i^s) := L^2\left(\Omega_i^s, \mathbb{R}^d\right)$ and $\mathbf{H^1}(\Omega_i^s) := H^1\left(\Omega_i^s, \mathbb{R}^d\right)$ of vector-valued functions with the norms defined by

$$\|\mathbf{u}\|_{\Omega_i^s}^2 = B(\mathbf{u},\mathbf{u}), \quad \|\mathbf{u}\|_{1,\Omega_i^s}^2 = A(\mathbf{u},\mathbf{u}) + B(\mathbf{u},\mathbf{u}). \tag{4.25}$$

To write (4.22) and (4.23) in a weak form, we also introduce the bilinear forms

$$c_e(\phi,\widetilde{\phi}) = \frac{1}{k_e}\int_{\Gamma_e} \phi\widetilde{\phi}d\Gamma_e \quad \text{and } c_i(\phi,\widetilde{\phi}) = \frac{1}{k_i}\int_{\Gamma_e} \phi\widetilde{\phi}d\Gamma_e.$$

With time-independent test functions $\widetilde{\phi}$ and using the bilinear forms a, b, A, B (2.6), the acoustic Robin IBVP in variational form is:
Find ϕ_e such that, $\forall\widetilde{\phi} \in H^1(\Omega_e), t \in [0,T]$:

$$\begin{cases} a(\phi_e(t),\widetilde{\phi}) + b(\partial_t^2\phi_e(t),\widetilde{\phi}) + c_e\left(\partial_t\phi_e(t),\widetilde{\phi}\right) = -\dfrac{1}{k_e}(g_e(t),\widetilde{\phi})_{\Gamma_e} \\ \phi_e(0) = \partial_t\phi_e(0) = 0. \end{cases} \tag{4.26}$$

and in Ω_i, the acoustic/elastic Robin IBVP has the form:
Find $(\phi_i, \mathbf{u})$ such that, $\forall\widetilde{\phi} \in H^1(\Omega_i^f), \widetilde{\mathbf{u}} \in \mathbf{H}^1(\Omega_i^s), t \in [0,T]$:

$$\begin{cases} a(\phi_i,\widetilde{\phi}) + b(\partial_t^2\phi_i,\widetilde{\phi}) + c_i(\partial_t\phi_i(t),\widetilde{\phi}) \\ \qquad + A(\mathbf{u},\widetilde{\mathbf{u}}) + B(\partial_t^2\mathbf{u},\widetilde{\mathbf{u}}) = -(\partial_n\phi_i(t),\widetilde{\phi})_{\Gamma_i} - \dfrac{1}{k_i}(g_i(t),\widetilde{\phi})_{\Gamma_e} + (\mathbf{t}(t),\widetilde{\mathbf{u}})_{\Gamma_i} \\ \phi_i(0) = \partial_t\phi_i(0) = 0 \quad \text{and} \quad \mathbf{u}(0) = \partial_t\mathbf{u}(0) = 0. \end{cases} \tag{4.27}$$

These Robin IBVPs have the same forms as the acoustic and elastic Robin IBVPs in Section 2.4.3 and thus behave in the same way. The solvabilty results are obtained following the same proof steps as described in Appendix D. They read:

Theorem 4.3.1 (solvability of Robin IBVPs)**.** *Let Γ be a Lipschitz closed surface. Let $g_e \in L_T^2(\Gamma_e)$ and $g_i \in L_T^2(\Gamma_e)$. Then:*

1. The acoustic Robin IBVP (4.22) has a unique solution ϕ_e verifying (continuously in g_e)

$$\phi_e \in L^2_T(H^1(\Omega_e)), \qquad \phi'_e \in L^2_T(\Omega_e), \qquad \phi'_e|_{\Gamma_e} \in L^2_T(\Gamma_e). \tag{4.28}$$

2. The acoustic/elastic Robin IBVP (4.23) has a unique solution ϕ_i verifying (continuously in g_i)

$$\phi_i \in L^2_T(H^1(\Omega_i^f)), \qquad \phi'_i \in L^2_T(\Omega_i^f), \qquad \phi'_i|_{\Gamma_e} \in L^2_T(\Gamma_e). \tag{4.29}$$

These Robin evolution problems preserve the space-time regularity of their trace solutions compared to the data. Robin data $g_e \in L^2_T(\Gamma_e)$ and $g_i \in L^2_T(\Gamma_e)$ produce solutions which belong to

$$\begin{aligned} \phi_e \in L^2_T\left(H^1(\Omega_e)\right), \quad \partial_t\phi_e \in L^2_T\left(L^2(\Omega_e)\right), \\ \phi_i \in L^2_T\left(H^1(\Omega_i^f)\right), \quad \partial_t\phi_i \in L^2_T\left(L^2(\Omega_i^f)\right), \end{aligned}$$

and the boundary traces of the velocities verify

$$\partial_t\phi_e\,|_{\Gamma_e}, \partial_t\phi_i\,|_{\Gamma_e} \in L^2_T\left(\Gamma_e\right).$$

The iterative method based on the successive solutions of Robin IBVPs (4.26) and (4.27) will thus preserve the $L^2_T(\Gamma_e)$ regularity of all the interfacial variables as iterations progress.

4.4 Proof of convergence of the acoustic-acoustic iterative algorithm

Like for the acoustic/elastic coupling in Section 2.5, the proof of convergence for the global-in-time iterations is based on establishing that the error between an iterate and the converged solution vanishes in the limit of infinitely many iterations.

The proof is based on establishing that the error between an iterate and the exact FSI solution has a vanishing norm in the limit of infinitely many iterations. We consider the interface traces ϕ_e, ϕ_i, $v_e := \partial_n\phi_e$ and $v_i := \partial_n\phi_i$ on Γ_e (which solve the governing system (4.2a)- (4.2c) for the FSI problem). We introduce error fields $\phi_e^q - \phi_e, v_e^q - v_e, \phi_i^q - \phi_i$ and $v_i^q - v_i$ at the q-th iteration. Notations $\phi_e^q, v_e^q, \phi_i^q, v_i^q$ will refer to those error fields, rather than to the absolute iterates, for the remainder of this section. The errors ϕ_e^q verify the homogeneous wave equation in Ω_e, while ϕ_i^q solve the homogeneous wave equation in Ω_i^f. We introduce likewise the error fields $\mathbf{t}^q - \mathbf{t}$ and $\mathbf{u}^q - \mathbf{u}$, which will hereon be denoted as $\mathbf{t}^q$ and $\mathbf{u}^q$ and verify the homogeneous elastic equation. In particular, we assume that $\mathbb{H} = 0$, which means that the velocity and pressure jumps s_v and s_p are equal to zero.

Using the weak equalities (4.26) and (4.27), with the test functions set equal to the time derivative of the corresponding primary variable at the same time instant, the error variables (ϕ_e^q, v_e^q) verify the identities

$$a(\phi_e^q(t), \partial_t\phi_e^q(t)) + b(\partial_t^2\phi_e^q(t), \partial_t\phi_e^q(t)) = -(v_e^q(t), \partial_t\phi_e^q(t))_{\Gamma_e} \quad t \in [0, T]$$

while the variables $\phi_i^q, v_i^q, \mathbf{t}_i^q, \mathbf{u}_i^q$, similarly verify

$$a(\phi_i^q, \partial_t\phi_i^q) + b(\partial_t^2\phi_i^q, \partial_t\phi_i^q) + A(\mathbf{u}^q, \partial_t\mathbf{u}^q) + B(\partial_t^2\mathbf{u}^q, \partial_t\mathbf{u}^q) \\ = -(v_i^q, \partial_t\phi_i^q)_{\Gamma_i} + (v_i^q, \partial_t\phi_i^q)_{\Gamma_e} + (\mathbf{t}^q, \partial_t\mathbf{u}^q)_{\Gamma_i}, \quad t \in [0,T]. \tag{4.30}$$

The transmission conditions verified on Γ_i by the error fields $\partial_n\phi_i^q, \partial_t\phi_i^q, \mathbf{t}^q$ and $\partial_t\mathbf{u}^q$ imply that the term $(\mathbf{t}^q(t), \partial_t\mathbf{u}^q(t))_{\Gamma_i}$ is written

$$(\mathbf{t}^q(t), \partial_t\mathbf{u}^q(t))_{\Gamma_i} = (\partial_t\phi_i^q(t), \mathbf{n}.\partial_t^q\mathbf{u}(t))_{\Gamma_i} = (\partial_t\phi_i^q(t), v_i^q(t))_{\Gamma_i} \tag{4.31}$$

We then introduce the energy $E^q(s)$ of the q-th iterate error at time s, given by

$$E^q(s) := \frac{1}{2}\mathcal{E}\left(\phi_e^q(s), \phi_i^q(s)\right) \tag{4.32}$$

where the energy functional $\mathcal{E}$ is defined, for any $(\phi_e, \phi_i, \mathbf{u}) \in C_T^0\left(H^1(\Omega_e) \times H^1(\Omega_i^f) \times H^1(\Omega_i^s)\right)$ satisfying (4.2a,b,c), by

$$\mathcal{E}\left(\phi_e(s), \phi_e(s)\right) := a(\phi_e(s), \phi_e(s)) + b(\phi_e'(s), \phi_e'(s)) + a(\phi_i(s), \phi_i(s)) \\ + b(\phi_i'(s), \phi_i'(s)) + A(\mathbf{u}(s), \mathbf{u}(s)) + B(\mathbf{u}'(s), \mathbf{u}'(s)). \tag{4.33}$$

$E^q(s)$ is obtained by integrating (4.30) over t$\in [0, s]$ (where $s \in [0,T]$ is arbitrary). Using the identity (4.31) to eliminate $(\mathbf{t}^q(t), \partial_t\mathbf{u}^q(t))_{\Gamma_i}$ and $-(v_i^q, \partial_t\phi_i^q)_{\Gamma_i}$ in the right hand side, we also get

$$E^q(s) = -(v_e^q, \partial_t\phi_e^q)_{\Gamma_e,s} + (v_i^q, \partial_t\phi_i^q)_{\Gamma_e,s}. \tag{4.34}$$

$E^q(s)$ is the sum of the potential and kinetic energies reached in the solid domain and in both fluid domains, from a state of initial rest; in particular $E(s) \geq 0$. The proof of convergence follows the same ideas as the proof of convergence for acoustic-elastic iterations (Section 2.5). We start by showing that $E^q(s) \to 0$ as $q \to \infty$, and we then show that the error fields vanish in energy norm in the respective domains with the number q of iterations, for any choice of positive coupling parameters k_e, k_i and of relaxation parameter r.

Lemma 4.4.1. *For any set of fluid and solid variables solving the field equations, the energy $E^q(s)$ at any finite time $s \leq T$ is related to the incoming and outgoing traces by*

$$E^q(s) = \frac{1}{4}\left\|\mathbb{B}^q\right\|^2_{\Gamma_e,s,\mathbb{K}} - \frac{1}{4}\left\|\overline{\mathbb{B}^q}\right\|^2_{\Gamma_e,s,\mathbb{K}}$$

Moreover, let N be any integer, and assume $\mathbb{H} = 0$. The energies, incoming and outgoing traces of the first N relaxed RR iterates verify the identity

$$\sum_{q=0}^{N-1}\left\{E^q(s) + \frac{1}{r}(\frac{1}{r} - 1)\left\|\mathbb{X}\overline{\mathbb{B}}^q - \mathbb{B}^q\right\|^2_{\Gamma_e,s,\mathbb{K}}\right\} + \frac{1}{r}\left\|\mathbb{B}^N\right\|^2_{\Gamma_e,s,\mathbb{K}} = \frac{1}{r}\left\|\mathbb{B}^0\right\|^2_{\Gamma_e,s,\mathbb{K}} \tag{4.35}$$

Proof. (4.10) and (4.11) can readily be inverted, any set of Dirichlet and Neumann traces on Γ_e being given in terms of the incoming and outgoing traces by

$$\begin{cases} \partial_t\phi_e &= -\frac{1}{2}(B_e - \overline{B}_e) \\ v_e &= \frac{1}{2k_e}(B_e + \overline{B}_e) \\ \partial_t\phi_i &= \frac{1}{2}(B_i - \overline{B}_i) \\ v_i &= \frac{1}{2k_i}(B_i + \overline{B}_i) \end{cases}$$

These formulas allow to express the right-hand side of identity (4.35) in terms of the incoming and outgoing traces, following the trace notations (4.17),

$$[-(v_e^q,\partial_t\phi_e^q)_{\Gamma_e,s}+(v_i^q,\partial_t\phi_i^q)_{\Gamma_e,s}] = \frac{1}{4}\left((B_e+\overline{B}_e),\frac{(B_e-\overline{B}_e)}{k_e}\right)_{\Gamma_e,s,\mathbb{K}}+\frac{1}{4}\left((B_i+\overline{B}_i),\frac{(B_i-\overline{B}_i)}{k_i}\right)_{\Gamma_e,s,\mathbb{K}}$$
$$=\frac{1}{4}\left\|\mathbb{B}^q\right\|^2_{\Gamma_e,s,\mathbb{K}}-\frac{1}{4}\left\|\overline{\mathbb{B}}^q\right\|^2_{\Gamma_e,s,\mathbb{K}}$$

Using the above equality in (4.35) yields the first identity of the Lemma 4.4.1. Then, since the traces of successive iterates of the error fields satisfy (4.21) with $\mathbb{H}=0$, we rewrite $\overline{\mathbb{B}}^q$ in terms of $\mathbb{B}^q$ and $\mathbb{B}^{q+1}$, to obtain

$$\begin{aligned}-(v_e^q,\partial_t\phi_e^q)_{\Gamma_e,s}+(v_i^q,\partial_t\phi_i^q)_{\Gamma_e,s} &= \frac{1}{4}\left\|\mathbb{B}^q\right\|^2_{\Gamma_e,s,\mathbb{K}}-\frac{1}{4}\left\|\mathbb{X}\left[\frac{1}{r}\mathbb{B}^{q+1}+(1-\frac{1}{r})\mathbb{B}^q\right]\right\|^2_{\Gamma_e,s,\mathbb{K}}\\ &=\frac{1}{4}\left\|\mathbb{B}^q\right\|^2_{\Gamma_e,s,\mathbb{K}}-\frac{1}{4}\left\|\frac{1}{r}\mathbb{B}^{q+1}+(1-\frac{1}{r})\mathbb{B}^q\right\|^2_{\Gamma_e,s,\mathbb{K}}\end{aligned} \tag{4.36}$$

with the second equality stemming from the isometry property of $\mathbb{X}$. The Hilbert space identity

$$\left\|\frac{1}{r}a+\left(1-\frac{1}{r}\right)b\right\|^2=\frac{1}{r}\left\|a\right\|^2+\left(1-\frac{1}{r}\right)\left\|b\right\|^2-\frac{1}{r}\left(1-\frac{1}{r}\right)\left\|a-b\right\|^2$$

can then be applied in the above right-hand side. We have

$$\left\|\frac{1}{r}\mathbb{B}^{q+1}+\left(1-\frac{1}{r}\right)\mathbb{B}^q\right\|^2_{\Gamma_e,s,\mathbb{K}}=\frac{1}{r}\left\|\mathbb{B}^{q+1}\right\|^2_{\Gamma_e,s,\mathbb{K}}+\left(1-\frac{1}{r}\right)\left\|\mathbb{B}^q\right\|^2_{\Gamma_e,s,\mathbb{K}}$$
$$-\frac{1}{r}\left(1-\frac{1}{r}\right)\left\|\mathbb{B}^{q+1}-\mathbb{B}^q\right\|^2_{\Gamma_e,s,\mathbb{K}}.$$

After noticing that the transition equation (4.21) with $\mathbb{H}=0$ gives

$$\mathbb{B}^{q+1}-\mathbb{B}^q=r(\mathbb{X}\overline{\mathbb{B}}^q-\mathbb{B}^q),$$

the identity (4.36) becomes

$$-(v_e^q,\partial_t\phi_e^q)_{\Gamma_e,s}+(v_i^q,\partial_t\phi_i^q)_{\Gamma_e,s}=\frac{1}{4r}\left\|\mathbb{B}^q\right\|^2_{\Gamma_e,s,\mathbb{K}}-\frac{1}{4r}\left\|\mathbb{B}^{q+1}\right\|^2_{\Gamma_e,s,\mathbb{K}}$$
$$+\frac{1}{4}(1-\frac{1}{r})\left\|\mathbb{X}\overline{\mathbb{B}}^q-\mathbb{B}^q\right\|^2_{\Gamma_e,s,\mathbb{K}}$$

Using the above equality in the right-hand side of (4.34) and rearranging so that the left and right-hand sides of the resulting identity feature only positive terms, we obtain

$$E^q(s)+\frac{1}{4r}\left\|\mathbb{B}^{q+1}\right\|^2_{\Gamma_e,s,\mathbb{K}}+\frac{1}{4}\left(\frac{1}{r}-1\right)\left\|\mathbb{X}\overline{\mathbb{B}}^q-\mathbb{B}^q\right\|^2_{\Gamma_e,s,\mathbb{K}}=\frac{1}{4r}\left\|\mathbb{B}^q\right\|^2_{\Gamma_e,s,\mathbb{K}} \tag{4.37}$$

(noticing that $\frac{1}{r}(\frac{1}{r}-1)>0$ for any $0<r\leq 1$). We finally perform N successive RR iterations (with $0<q\leq N-1$), sum the energy equalities (4.37) for each iteration and notice a telescopic sum effect (the same terms $\frac{1}{4r}\left\|\mathbb{B}^q\right\|^2_{\Gamma_e,s,\mathbb{K}}$ appearing in the left- and right-hand sides of the sum for $1<q\leq N-1$ and cancelling each other), and this results in the second identity claimed in the Lemma 4.4.1. □

Since the right-hand side in (4.35) does not depend on N while all terms are positive, the sum has a finite limit as $N \to \infty$, implying that

$$\lim_{q\to\infty} \left\{ E^q(s) + \frac{1}{r}(\frac{1}{r} - 1) \left\| \mathbb{X}\overline{\mathbb{B}}^q - \mathbb{B}^q \right\|^2_{\Gamma_e,s,\mathbb{K}} \right\} = 0, \quad s \in [0,T]. \tag{4.38}$$

Considering the energy defined at each iteration q as a function of the error fields, lemma 4.4.1 reformulates it as a function of the incoming and outgoing trace operators. The summation of the energies at each iteration shows that the error fields, and then the energy, tend towards 0 in the limit of the number of iterations.

Theorem 4.4.2. *The two-operator global-in-time acoustic/acoustic Robin iterations are convergent:* $\|\phi_e^q(s)\|_{H^1(\Omega_e)}$, $\|\partial_t\phi_e^q(s)\|_{L^2(\Omega_e)}$, $\|\phi_i^q(s)\|_{H^1(\Omega_i^f)}$, $\|\partial_t\phi_i^q(s)\|_{L^2(\Omega_i^f)}$, $\|\mathbf{u}^q(s)\|_{\mathbf{H}^1(\Omega_i^s)}$ *and* $\|\partial_t\mathbf{u}^q(s)\|_{\mathbf{L}^2(\Omega_i^s)}$ *all vanish in the limit* $q \to \infty$ *for the error fields, uniformly in time.*

Proof of theorem 4.4.2. The identity (4.37) holds for any choice of final time $s \leq T$. In particular, we have

$$\sum_{q=0}^{N-1} E^q(s) \leq \frac{1}{r} \left\| \mathbb{B}^0 \right\|^2_{\Gamma_e,s,\mathbb{K}} = B(s) \tag{4.39}$$

We notice that $s \to B(s)$ is continuous, positive and non-decreasing, it is hence bounded above by $B(T)$. Recalling the definition (4.32) of $E^q(s)$ and (4.24), (4.25) of norms, we first have

$$\|\partial_t\phi_e^q(s)\|^2_{\Omega_e} \leq E^q(s), \qquad \|\partial_t\phi_i^q(s)\|^2_{\Omega_i^f} \leq E^q(s), \qquad \|\partial_t\mathbf{u}^q(s)\|^2_{\Omega_i^s} \leq E^q(s).$$

Inequality (4.39) provides

$$\sum_{q=0}^{N-1} \|\partial_t\phi_e^q(s)\|^2_{\Omega_e} \leq B(s) \leq B(T), \quad \sum_{q=0}^{N-1} \|\partial_t\phi_i^q(s)\|^2_{\Omega_i^f} \leq B(T), \quad \sum_{q=0}^{N-1} \|\partial_t\mathbf{u}^q(s)\|^2_{\Omega_i^s} \leq B(T) \tag{4.40}$$

implying that $\|\partial_t\phi_e^q(s)\|^2_{\Omega_e}$, $\|\partial_t\phi_i^q(s)\|^2_{\Omega_i^f}$ and $\|\partial_t\mathbf{u}^q(s)\|^2_{\Omega_i^s}$ vanish in the limit $q \to \infty$. Moreover, taking into account the relevant initial conditions, we have $\phi_e^q(t) = \int_0^t \partial_t\phi_e^q(s)ds$, for $t \in [0,T]$ so that

$$\|\phi_e^q(s)\|^2_{\Omega_e} \leq T \int_0^s \|\partial_t\phi_e^q(t)\|^2_{\Omega_e}\, dt$$

and likewise for $\phi_i^q(t)$ and $\mathbf{u}^q(t)$. We hence have

$$\begin{gathered}(\text{a}) \sum_{q=0}^{N-1} \|\phi_e^q(s)\|^2_{\Omega_e} \leq T \int_0^s B(t)dt, \quad (\text{b}) \sum_{q=0}^{N-1} \|\phi_i^q(s)\|^2_{\Omega_i^f} \leq T \int_0^s B(t)dt, \\ (\text{c}) \sum_{q=0}^{N-1} \|\mathbf{u}^q(s)\|^2_{\Omega_i^s} \leq T \int_0^s B(t)dt.\end{gathered} \tag{4.41}$$

Next, we note $\alpha(s) := B(s) + T\int_0^s B(t)dt$ and we add inequality (4.41a), (4.41b) or (4.41c) to (4.39). Recalling the definition (4.32) of $E(s)$, we deduce, $\forall t \leq T$:

$$\text{(a)} \sum_{q=0}^{N-1} \|\nabla\phi_e^q(t)\|_{\Omega_e}^2 + \|\phi_e^q(t)\|_{\Omega_e}^2 = \sum_{q=0}^{N-1} \|\phi_e^q(t)\|_{1,\Omega_e}^2 \leq \alpha(s)$$

$$\text{(b)} \sum_{q=0}^{N-1} \|\nabla\phi_i^q(t)\|_{\Omega_i^f}^2 + \|\phi_i^q(t)\|_{\Omega_i^f}^2 = \sum_{q=0}^{N-1} \|\phi_i^q(t)\|_{1,\Omega_i^f}^2 \leq \alpha(s)$$

and

$$\text{(c)} \sum_{q=0}^{N-1} \|\nabla\mathbf{u}^q(t)\|_{\Omega_i^s}^2 + \|\mathbf{u}^q(t)\|_{\Omega_i^s}^2 = \sum_{q=0}^{N-1} \|\mathbf{u}^q(t)\|_{1,\Omega_i^s}^2 \leq \alpha(s).$$

As α is a positive and increasing function, we find the the uniform (in time) bounds:

$$\sum_{q=0}^{N-1} \|\phi_e^q(s)\|_{1,\Omega_e}^2 \leq \alpha(T), \quad \sum_{q=0}^{N-1} \|\phi_i^q(s)\|_{1,\Omega_i^f}^2 \leq \alpha(T), \quad s \in [0,T], \tag{4.42}$$

as well as

$$\sum_{q=0}^{N-1} \|\mathbf{u}^q(s)\|_{1,\Omega_i^s}^2 \leq C_K\alpha(T), \quad s\text{ß}[0,T], \tag{4.43}$$

applying the Korn's inequality [46, Thm 6.15], which gives a majoration of $\|\mathbf{u}^q(s)\|_{1,\Omega_i^s}^2$ for some $C_K > 0$ for the elastic component. Therefore $\|\phi_e^q(s)\|_{1,\Omega_e}^2$, $\|\phi_i^q(s)\|_{1,\Omega_i^f}^2$ and $\|\mathbf{u}^q(s)\|_{1,\Omega_i^s}^2$ also vanish in the limit $q \to \infty$. Moreover, integrating the estimates (4.42) and (4.43) over $s \in [0,T]$ implies that the corresponding $L^2([0,T])$ norms of the error fields also vanish in the limit $q \to \infty$. □

Conclusion. Similarly to the result presented in Chapter 2 for the acoustic-elastic coupling based on Robin boundary conditions and on a acoustic-elastic coupling interface, we have shown for the new acoustic/acoustic-elastic coupling that the error fields vanish in energy norm in the respective domains with the number of iterations, for any choice of positive coupling parameters k_e and k_i and of relaxation parameter r. This result comes from the fact that the Robin problems solved in each subdomain preserve the regularity during the resolution. As detailed in Section 2.4.3, the Robin evolution problems involved in the acoustic/acoustic-elastic global-in-time iterations have velocity interfacial variables with the same regularity as the datum. The proof of the guaranteed algorithm's convergence is due to this important and original result, provided a minimum regularity assumption on this datum, so that the definition of the interfacial solution traces is possible. This procedure presents significant advantages compared to the two previous ones. In particular Robin impedance-like boundary conditions might be easier to impose in a fluid domain in a black box context (as for example in `Code_Aster` software [64]). Moreover treating a part of the fluid domain by a finite element method will allow to introduce nonlinearities in this part, and thus to treat more easily the cavitation phenomenon.

4.5 Validation and optimisation of the acoustic-acoustic FEM/Z-BEM coupling

The goal of this section is to validate the convergence of our global-in-time acoustic/acoustic-elastic iterations based on Robin boundary conditions and on an acoustic/acoustic coupling interface. We therefore solve the simple 2D acoustic-elastic problem introduced in Section 3.3.1. As the algorithm convergence does not depend on the used numerical method, we choose a FEM/Z-BEM coupling accelerated with a high-frequency approximation as described in Section 3.5. In addition to the validation of our procedure, this example also permits to (i) optimise the values for the Robin coupling parameters k_i and k_e, (ii) compare the acoustic/acoustic-elastic procedure convergence rate to the acoustic/elastic one, and (iii) investigate the influence of the size of the interior fluid domain Ω_i^f on the overall algorithm convergence.

4.5.1 Coupling validation: 2D test case

To validate our iterative global-in-time coupling procedure, we now consider the 2D problem represented on Figure 4.3. A bounded elastic ring Ω_i^s is immersed in a acoustic fluid (mass density ρ_f, acoustic wave velocity c_f) occupying the unbounded fluid region. The fluid domain is separated into two parts: Ω_i^f is the interior fluid domain bounded by a circular boundary Γ_e and Ω_e is the exterior fluid domain such as $\Omega_e := \mathbb{R}^2 \setminus \left(\overline{\Omega_i^s} \cap \overline{\Omega_i^f}\right)$. A uniform normal pressure $p^{int}(t)$ is applied to the solid interior surface Γ_i, which creates a deformation in the elastic solid and a radiated FSI problem on the exterior interface. The physical and numerical parameters are the same as for the example in Section 3.3.1 and the fluid and structure physical parameters are listed in Table 3.1. The interior and exterior surface are set at $R_{\text{int}} = 0.9\text{m}$ and $R_{\text{ext}} = 1\text{m}$ respectively. The acoustic-acoustic interface Γ_e is set at a distance d=1.1m. The coupled solution is evaluated on the interface Γ_e. For this first test, the iterations are performed without acceleration and with the coupling parameters $k_e = k_i = \rho_f c_f$. Since we know the semi-analytical solution for this

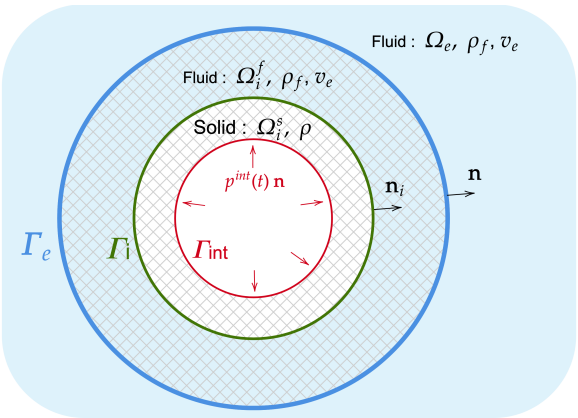

Figure 4.3: *Radially-symmetric pressurised annulus with a finite element mesh for the interior acoustic-elastic domain and BEM elements for the exterior acoustic domain.*

acoustic/acoustic-elastic problem (see Appendix A.2), we can validate the iterative acoustic/acoustic-elastic algorithm with a FEM/Z-BEM numerical procedure, by evaluating the convergence of the transmission residuals on the acoustic-acoustic boundary Γ_e and the relative L^2 error between the analytical and computed solutions. The iterative procedure consists in solving the IBVPs (4.3) and (4.4) until the difference between two successive iterates is small enough (stagnation criterion). For a given tolerance ϵ, the satisfaction of the criterion

$$\frac{\|(\partial_t\phi_e^n - \partial_t\phi_e^{n-1})\|^2_{L^2_T(\Gamma_e)} + \left\|\left(\partial_t\phi_i^n - \partial_t\phi_i^{n-1}\right)\right\|^2_{L^2_T(\Gamma_e)}}{\|\partial_t\phi_e^{n-1}\|^2_{L^2_T(\Gamma_e)} + \left\|\partial_t\phi_i^{n-1}\right\|^2_{L^2_T(\Gamma_e)}} \leq \epsilon \tag{4.44}$$

indicates that the solution has converged. In case of convergence, the transmission residual quantities associated with given boundary trace solutions also have to converge towards zero:

$$e_p^{\text{sol}} = \frac{\|(-\partial_t\phi_e - s_p) + \partial_t\phi_i\|_{L^2([0,T],\Gamma_e)}}{\|\partial_t\phi_i\|_{L^2([0,T],\Gamma_e)}}, \tag{4.45}$$

and

$$e_v^{\text{sol}} = \frac{\|\partial_n\phi_i - (\partial_n\phi_e + s_v)\|_{L^2([0,T],\Gamma_e)}}{\|\partial_n\phi_i\|_{L^2([0,T],\Gamma_e)}}. \tag{4.46}$$

We also consider a global dimensionless transmission residual $e_{v,p}$, combining the two interfacial transmission residuals, defined on Γ_e by

$$e_{v,p} := \sqrt{\frac{\|(-\partial_t\phi_e - s_p) + \partial_t\phi_i\|^2_{L^2([0,T],\Gamma_e)} + \|\partial_n\phi_i - (\partial_n\phi_e + s_v)\|^2_{L^2([0,T],\Gamma_e)}}{\|\partial_n\phi_i\|^2_{L^2([0,T],\Gamma_e)} + \|\partial_t\phi_i\|^2_{L^2([0,T],\Gamma_e)}}} \tag{4.47}$$

Figure 4.4a shows the coupled velocity and pressure solutions of the FSI problem at iteration 12 compared to the semi-analytical solutions. At this iteration, the transmission residuals are $e_v^{\text{sol}} = 4\ 10^{-4}$ and $e_p^{\text{sol}} = 2\ 10^{-4}$, and the global dimensionless transmission residual is $e_{v,p}$ =3 10^{-4}. The convergence of the errors e_v^{sol}, e_p^{sol} and of the global transmission residual $e_{v,p}$ are displayed on Figure 4.4b. As in Section 3.4 for the acoustic/acoustic-elastic algorithm, here the new acoustic-elastic algorithm based convergence rate can be improved with an Aitken's Δ^2 acceleration. This example confirms the verification of the transmission conditions and thus, the convergence and the correctness of the method.

4.5.2 Coupling parameter optimisation

We first used a Robin coupling parameter equal to the acoustic impedance on both subdomains ($k_e = k_i = \rho_f c_f$). As in Section 3.3.3 for RR acoustic/elastic iterations, we now look for an *a priori* optimal values for k_e and k_i that minimises the number of global-in-time iterations to reach a given accuracy. We consider the radially-symmetric 2D acoustic/acoustic-elastic problem described in Section 4.5.1 which admits a semi-analytical solution (see Appendix A.2). The Robin BCs for the acoustic/acoustic-elastic iterations are defined by (4.15) and (4.16). To estimate

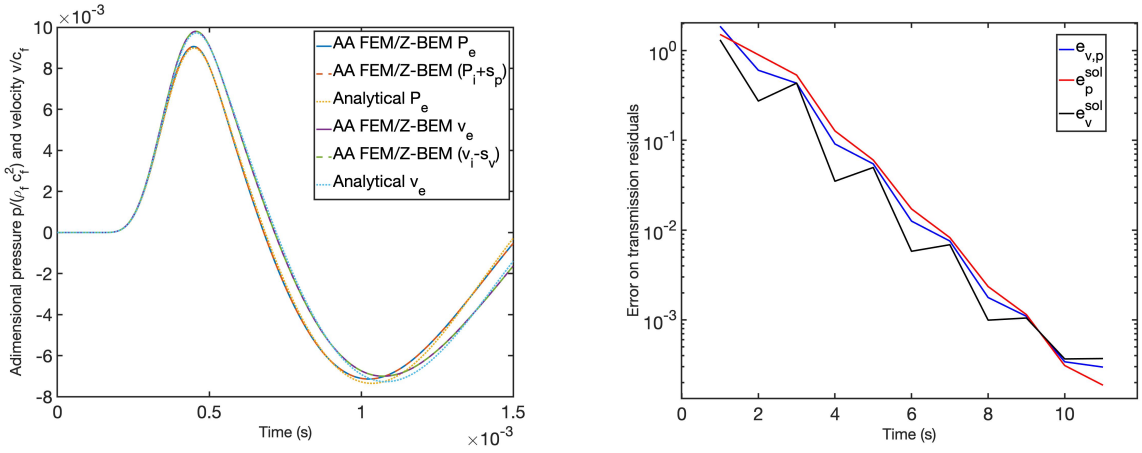

(a) *(b)*

Figure 4.4: *(a) Dimensionless radially-symmetric scattered pressures p_e, p_i and velocities v_e, v_i on Γ_e. Numerical results obtained using the acoustic/acoustic Robin-Robin coupling method are compared to semi-analytical reference values, $e_{v,p} = 3.10^{-4}$. (b) Errors e_v^{sol}, e_p^{sol} and $e_{v,p}$ on the transmission residuals for an acoustic/acoustic-elastic radially-symmetric problem.*

the convergence factor, we evaluate the spectral radius ϱ of the matrix linking two successive iterations. We described in Appendix B the semi-analytical analysis to determine ϱ for this radially symmetric problem. The method is similar to the one in Section 3.3.3 for acoustic/elastic Robin iterations. The evolution of the convergence factor ϱ depending on k_e and k_i is shown in Figure 4.5 and some values are provided in Table 4.1.

Figure 4.5 clearly illustrates the minimisation of the convergence factor ϱ when both Robin coupling parameters are equal to the acoustic impedance, $k_e = k_i = \rho_f c_f$. This optimal value for k_i and k_e is similar to the one for the acoustic-elastic iterations as it is shown in Section 3.3.3 for a similar radially-symmetric problem. Moreover, the optimised convergence factor takes the same value for both algorithms ($\varrho = 0.255$ for the acoustic/acoustic-elastic iterations and $\varrho = 0.24$ for acoustic/elastic iterations), which implies a similar number of global-in-time iterations to reach the convergence. As for the acoustic/elastic iterations in Chapter 3, using a simplified problem and a semi-analytical solution helps to determine an optimal a priori value for the coupling parameters to improve the algorithm convergence rate.

Coupling factor f_i ($k_i = f_i \rho_f c_f$)	0.2	0.2	1	1	1	3	7
Coupling factor f_e ($k_e = f_e \rho_f c_f$)	1	0.2	1	0.5	0.2	3	0.5
Convergence factor ϱ	0.64	0.63	0.26	0.61	0.76	0.59	0.93

Table 4.1: *Theoretical values of the convergence factor ϱ for couples of parameters (k_e, k_i).*

Influence of the distance of Γ_e to the elastic domain. We now investigate the influence of the acoustic-acoustic coupling interface position on the algorithm

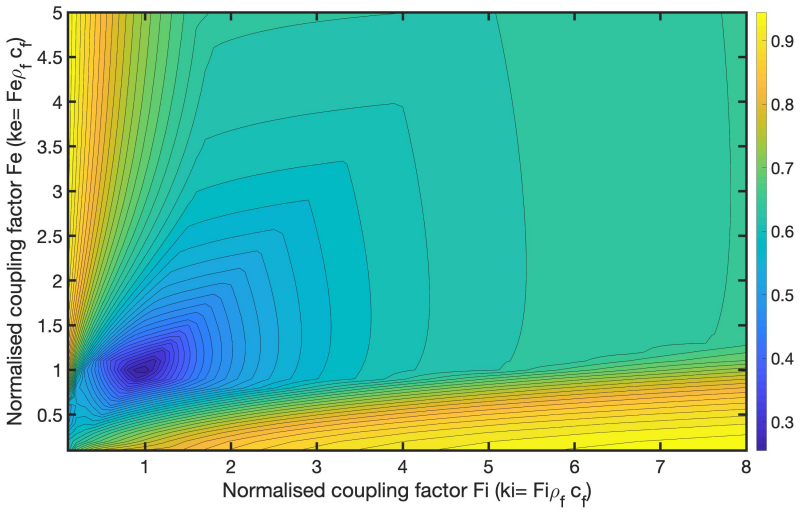

Figure 4.5: *Semi-analytical convergence factor depending on the coupling parameters k_e and k_i (Δt = 1.7 10^{-6}, a=0.9, b=1, d=1.1).*

efficiency in the case of FEM/Z-BEM coupling. It has already been shown for FSI problem solved with finite elements, that the size of the fluid mesh and the fluid thickness from the ship surface to the exterior boundary of fluid are of great importance to improve the numerical efficiency and accuracy [169]. These observations are however specific to the numerical method we use and have not been previously studied for a FEM/Z-BEM coupling.

Table 4.2 provides semi-analytical convergence factor ϱ values for different values of k_e and k_i, for different positions of the coupling interface Γ_e (d is the radius of the spherical acoustic-acoustic interface and is strictly greater than the radius of the acoustic-elastic boundary b=1). The optimal ϱ (evaluated at $k_i = k_e = \rho_f c_f$) is shown to be only slightly affected by the radius d of the spherical coupling interface. But increasing this distance d reduces the convergence factor taken for all the other values of k_i and k_e, up to a certain distance. In our example, from d=3, the values taken by ϱ are almost no longer affected. In addition, from $d = 3$ the optimal convergence factor ϱ is not only reached for $k_i = k_e = \rho_f c_f$, but also for a large part of the values that k_e and k_i can take. In Table 4.2 from d=3 we find ϱ=0.25 for almost all k_e and k_i values. Figures 4.6a and 4.6b illustrate that when the coupling interface distance increases, the choice of coupling parameters values has a smaller impact on the convergence factor and therefore on the speed of convergence. This can be physically interpreted as when the distance between the acoustic/acoustic coupling interface and the elastic obstacle increases, the obstacle has less influence on the coupling. The fluid behaviour is predominant in the interior acoustic/elastic domain Ω_i. The iterative coupling algorithm thus behaves as if two identical homogeneous fluids were on either side of the interface.

Furthermore, the optimised ϱ is then the same as for RR iterations ($\varrho = 0.25$), which means that adding an acoustic-acoustic interface does not increase the number of iterations required to achieve convergence. As the distance d has no influence on the number of iterations required to reach the convergent, d should be minimised.

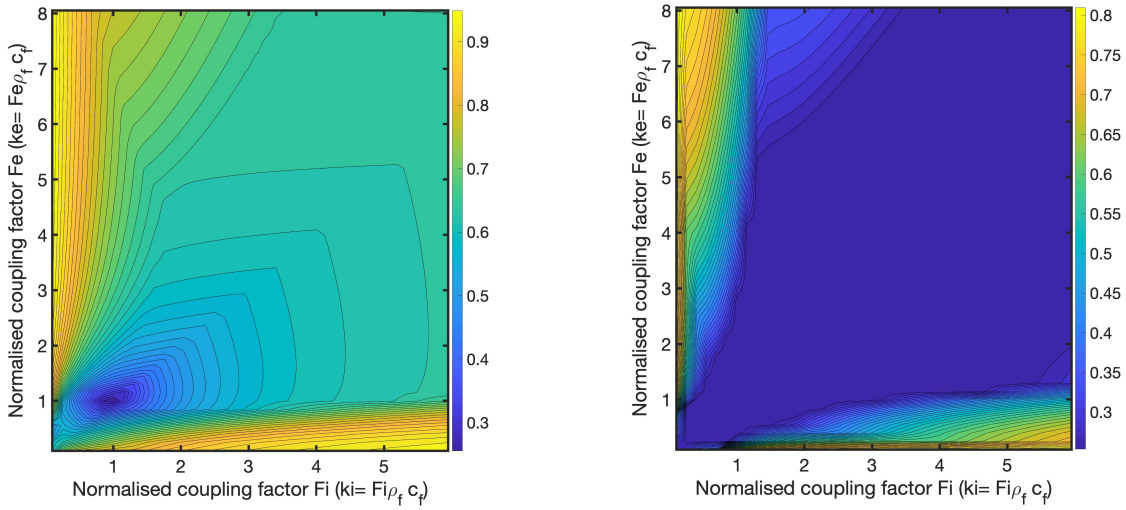

Figure 4.6: *Semi-analytical convergence factor depending on the coupling parameters for (a) d=1.1 and (b) for d=7.*

When the optimal coupling factor is known (here $k_i = k_e = \rho_f c_f$), the interface then has to be as close as possible to the elastic obstacle in order to minimise the volume of fluid to be meshed, maximise the domain treated with the Z-BEM and accelerate the computation.

Coupling factor f_i ($k_i = f_i \rho_f c_f$)	0.2	0.2	1	1	1	3	3
Coupling factor f_e ($k_e = f_e \rho_f c_f$)	1	0.2	1	0.5	0.2	3	1
d=1.1	0.64	0.63	0.26	0.61	0.76	0.59	0.58
d=1.2	0.60	0.59	0.27	0.57	0.68	0.47	0.49
d=1.5	0.54	0.32	0.25	0.36	0.57	0.35	0.38
d=2	0.51	0.28	0.25	0.27	0.48	0.27	0.27
d=3	0.49	0.25	0.25	0.25	0.45	0.25	0.25
d=7	0.47	0.25	0.25	0.25	0.44	0.25	0.25

Table 4.2: *Convergence factor value for various acoustic-acoustic interface radius values d and k_e and k_i values ($\Delta t = 1.7\ 10^{-6}$, $N_t = 1500$, a=0.9, b=1).*

We perform some numerical acoustic/acoustic Robin iterations to verify the algorithm behaviour depending on the value of ϱ. The convergence of the transmission residual $e_{v,p}$ is displayed on Figure 4.7. We show that the iterative algorithm converges with a larger convergence rate for a value of $k_e = k_i = \rho_f c_f$, as predicted by the theoretical spectral radius value. The number of iterations is seen to be in agreement with the expected spectral radius values of Table 4.1.

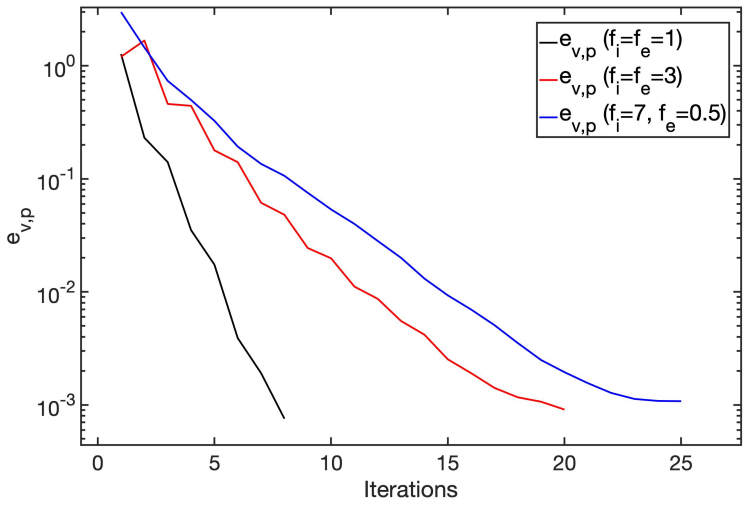

Figure 4.7: *Convergence of the indicator $e_{v,p}$ on interfacial residuals for three couples of Robin parameters (k_e, k_i).*

4.6 Conclusion

The main purpose of this chapter was to design and validate an alternative global-in-time iterative algorithm to solve an acoustic-elastodynamic transient problem, based on an acoustic-acoustic coupling interface and Robin coupling conditions. The convergence of the global-in-time acoustic/acoustic-elastic iterations has been proved in Section 4.4. We have then validated the convergence of the algorithm by implementing it with a FEM/Z-BEM coupling and using a HFA. We have improved the algorithm convergence rate by choosing optimal values of Robin coupling parameter and an adapted coupling interface distance from the elastic obstacle. We have shown that choosing the coupling parameters equal to the acoustic impedance improves the convergence. Finally we have shown that increasing the acoustic-acoustic interface distance improves the convergence speed, up to a fixed distance from which the convergence rate is not influenced anymore.

The goal of Chapter 5 is now to use the capabilities of this convergent iterative algorithm to solve more realistic transient rapid 3D problems with more complex geometries.

CHAPTER 5

Non-intrusive coupling in an industrial context. Application to underwater explosions.

The purpose of this chapter is to demonstrate that the domain decomposition iterative algorithm we have developed, based on the successive solutions of Robin evolution problems in each subdomain, allows to deal with complex phenomena taking place in the context of underwater explosions. In practice, we aim at coupling two 3D solvers in a black box manner, according to the acoustic/acoustic-elastic iterative procedure detailed in Chapter 4. To treat the finite element interior acoustic/elastic part of the problem, we use the open-source FEM software `Code_Aster`, developed by EDF (Électricité de France) [64]. To deal with the unbounded exterior acoustic domain, we use an in-house 3D Z-BEM solver.
In Section 5.1 we detail the validation of the non-intrusive acoustic/acoustic-elastic coupling when an industrial FEM solver is used in a black box manner. We insist on some additional implementation difficulties related to the solver architecture. The coupling procedure is then validated on the simple 3D FSI problem of an elastic sphere in a uniform time-dependent incident acoustic field. To simulate the hydroacoustic sound radiation of surface ships, the free surface boundary condition has to be taken into account. In Section 5.2 we consider half-space Green functions to improve the Z-BEM solver in the context of free-surface boundary condition. Section 5.3 is dedicated to an overview of the characteristics of an underwater explosion and especially of its primary acoustic shock wave. The final goal is to deal with a realistic case of a submarine subjected to a shock wave produced by a far-field underwater explosion. Finally in Section 5.4, we give some ideas for future studies and numerical developments.

Contents

5.1 Non-intrusive 3D FEM/Z-BEM coupling validation . . . 134

5.1.1 Finite element model for a time-domain elastic-acoustic problem . . . 134

5.1.2 `Code_Aster` for domain decomposition methods and vibroacoustic problems . . . 136

5.1.3 Validation of the 3D FEM/Z-BEM coupling using Code Aster 141
5.2 Free surface 142
5.2.1 Fast Z-BEM with half-space Green's functions 143
5.2.2 Z-BEM for partially emerged ships 149
5.3 Modelling the interaction between a shock wave and a submarine 152
5.4 Conclusion 156

5.1 Non-intrusive 3D FEM/Z-BEM coupling validation

In Chapters 2, 3 and 4 we have considered the design, implementation and validation of two convergent domain decomposition iterative procedures. The first one (acoustic/elastic Robin iterations see Section 2.4) requires inhomogeneous Robin boundary conditions (BC) to be imposed on acoustic and elastic subdomains. This is not possible with some industrial FEM solvers. For this reason, we consider only the second algorithm (acoustic/acoustic-elastic Robin iterations detailed in Section 4.3) in this chapter. It has the advantage of only requiring inhomogeneous Robin BCs to be imposed on acoustics subdomains. The notations used in this chapter are presented in Figure 5.1.

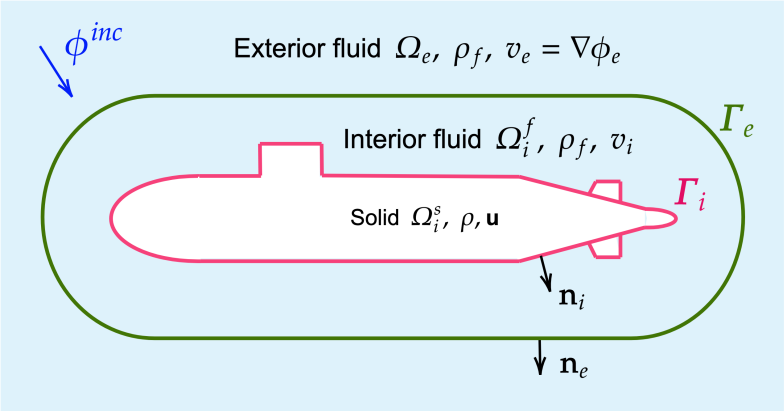

Figure 5.1: *Domain decomposition for an acoustic-acoustic coupling : notations.*

5.1.1 Finite element model for a time-domain elastic-acoustic problem

Depending on the choice of the variables to describe the state of the fluid, different numerical formulations of the vibro-acoustic coupling can be found in the literature

[70, 183]. The pressure p, the fluid velocity potential ϕ, or both variable can be chosen, and each choice corresponds to a coupling formulation $(\mathbf{u}_s, p)$, $(\mathbf{u}_s, \phi)$ or $(\mathbf{u}_s, p, \phi)$ [115, 183]. The three formulations are equivalent, but they all have advantages and drawbacks. In particular, the formulation $(\mathbf{u}_s, \phi)$ has the advantage to correspond to the form of the fluid equations we expressed in Section 2.1 in terms of velocity potential [70]. As described in [115], this formulation allows the definition of symmetric matrices. Its main drawback is generally the presence of an additional coupling term K_c in the global damping matrix (see (5.1)). It is a problem for modal analysis, as the resolution of a quadratic eigenvalue problem is needed in this case. However, for time-domain analysis, the form of the global damping matrix does not add any complexity. The formulation in $(\mathbf{u_s}, \phi)$ is thus a symmetric formulation that does not introduce more degrees of freedom as it would be the case with a formulation in $(\mathbf{u}_s, p, \phi)$.

In the context of underwater explosions, the incident shock wave is discontinuous (see Section 5.3). To avoid regularity problems related to this pressure discontinuity, it is possible to use regularised models to represent the shock wave. However, even regularised, these incident wave models have low regularities in time. The fluid equations should thus preferably be written in terms of velocity potential ϕ only, instead of pressure variable p, to gain a degree of regularity in time.

$(\mathbf{u}_s, \phi)$ **formulation.** The weak formulation in $(\mathbf{u_s}, \phi)$ of the fluid-structure interior problem with a Robin boundary condition is given by (4.27). Considering an external force g_i applied on the boundary of the fluid domain through a Robin BC of the form (4.7), we have

$$\rho_f \partial_t \phi_i + k_i \partial_n \phi_i = g_i \quad \text{ on } \Gamma_e \times [0, T].$$

The fluid-structure conditions at the interface Γ_i are defined by (2.2) as Neumann conditions:

$$\partial_n \phi_i = \partial_t \mathbf{u}.\mathbf{n} \qquad \text{and} \qquad \mathbf{t}[\mathbf{u}] = \rho_f \partial_t \phi_i \mathbf{n} \quad \text{ on } \Gamma_i \times [0, T].$$

The dynamic of the spatially discretised coupled problem using FEM is then described by a system of ordinary differential equations:

$$\begin{bmatrix} M_s & 0 \\ 0 & \rho_f M_f \end{bmatrix} \begin{bmatrix} \ddot{\mathbf{U}}_\mathbf{s}(t) \\ \ddot{\phi}_\mathbf{i}(t) \end{bmatrix} + \begin{bmatrix} K_s & 0 \\ 0 & \rho_f K_f \end{bmatrix} \begin{bmatrix} \mathbf{U_s}(t) \\ \phi_i(t) \end{bmatrix} + \begin{bmatrix} 0 & -\rho_f K_c \\ -\rho_f K_c & Q \end{bmatrix} \begin{bmatrix} \dot{\mathbf{U}}_\mathbf{s}(t) \\ \dot{\phi}_i(t) \end{bmatrix} = \begin{bmatrix} 0 \\ G(t) \end{bmatrix} \tag{5.1}$$

where the vectors $\mathbf{U_s}$ and ϕ contain respectively the nodal values of the structural displacements and fluid velocity potentials. The block matrices M_s, M_f , K_s, K_f and the right-hand side F are defined by:

$$
\begin{aligned}
(M_s)_{ij} = \int_{\Omega_s} \rho_s \mathbf{N}_i^s.\mathbf{N}_j^s, \quad (K_s)_{ij} = \int_{\Omega_s} \epsilon_{\mathbf{s}}\left(\mathbf{N_j^s}\right) : \mathbf{C} : \epsilon_{\mathbf{s}}\left(\mathbf{N_i^s}\right) \\
(M_f)_{ij} = \int_{\Omega_f} \frac{1}{c^2} \mathrm{N}_i^f.\mathrm{N}_j^f, \quad (K_f)_{ij} = \int_{\Omega_f} \nabla \mathrm{N}_i^f.\nabla \mathrm{N}_j^f, \\
(K_c)_{ij} = \int_{\Gamma_e} \mathrm{N}_j^f(\mathbf{N}_i^s.\mathbf{n}_s), \qquad (G)_i = \int_{\Gamma_e} g_i.N_i^f, \\
(Q)_{ij} = -\frac{\rho_f^2}{k_i} \int_{\Gamma_e} N_i^f.N_j^f,
\end{aligned}
\tag{5.2}
$$

where $(\mathbf{N}_i^s)_{i=1,\dots,n_s}$ and $(N_i^f)_{i=1,\dots,n_f}$ are the finite element basis functions in the structural part and in the fluid part, respectively. The matrices M_s, M_f are the mass matrices of the structural and fluid parts, respectively, and are symmetric positive definite. The matrices K_s, K_f are the stiffness matrices of the structural and fluid parts and are symmetric positive semi-definite. There are three additional matrices. Two mass matrix defined on the boundary Γ_i are related to the terms $-\rho_f(v_i, \widetilde{\mathbf{u}})_{\Gamma_i}$ and $(\mathbf{t}, \widetilde{\phi})_{\Gamma_i}$ and represent the fluid-structure coupling. The third matrix Q is linked to the Robin condition added on the boundary Γ_e of the truncated fluid domain and represents the term $\frac{\rho_f^2}{k_i}(\partial_t \phi_i, \widetilde{\phi})_{\Gamma_e}$. Finally, the vector G is the right-hand side related to the load g_i, imposed on the boundary.

5.1.2 `Code_Aster` for domain decomposition methods and vibroacoustic problems

The `Code_Aster` software is available on the website "`www.code-aster.org`". One of the strengths of this software is the integration in a single environment of many physical phenomena (thermal, acoustic, hydration, drying, etc.), types of finite elements, and constitutive models (steel, concrete, geomaterials, etc.) related to mechanics. It enables a wide range of static and dynamic analyses, including multi-physics, multi-scale, non-linear or coupled system modelling (fluid-structure, soil-structure, soil-fluid-structure...). It is often used for transient fluid-structure interaction studies [72, 105, 192], and in particular for vibroacoustic applications [20, 115, 171].

The introduction of different fluid-structure formulations and of the Robin boundary conditions (inhomogeneous impedance conditions) on the boundary of an acoustic domain is a recent feature of `Code_Aster` 2022. Previous versions only included the $(\mathbf{u}_s, p, \phi)$ formulation. The formulation in $(\mathbf{u}_s, \phi)$, which is needed to implement the Robin acoustic/acoustic global-in-time iterations described in Chapter 4, has been implemented in `Code_Aster` 2022 and validated as part of L. Khoun's PhD work [115].

Another advantage of `Code_Aster` is the possibility to use non-homogeneous Robin boundary conditions in an acoustic domain. These conditions enable for example to use `Code_Aster` within non-invasive domain decomposition coupling methods [92, 165]. The non-homogeneous acoustic Robin boundary conditions in `Code_Aster` have been developed in [115]. This recent development allows to use

an impedance Q defined by:

$$Q = -\frac{\rho_f^2}{Z_c} C = -\frac{\rho_f^2}{k_i} C$$

where C is the boundary mass matrix. The user has to pay attention to the coefficient used in the code: the calculation of the impedance matrix Q is done with the functions `AFFE_CHAR_MECA`, and the user can choose the impedance value Z_c. To impose the Robin boundary condition (4.7), $\mathbf{Z_c} = \mathbf{k_i}$ has to be chosen.

In `Code_Aster` the impedance matrix Q associated with a Robin impedance condition applied on a surface "surfaceA" is assembled with the commands [115]:

```
Char_Q = AFFE_CHAR_MECA( MODELE    = Model,
                         IMPE_FACE = _F(GROUP_MA = 'surfaceA',
                                        IMPE = ki,),);
El_Q   = CALC_MATR_ELEM( OPTION    = 'IMPE_MECA',
                         MODELE    = Model,
                         CHARGE    = Char_Q,
                         CHAM_MATER = MATER,)
Q      = ASSE_MATRICE( MATR_ELEM = El_Q, NUME_DDL = N_DDL)
```

Validation of `Code_Aster` inhomogeneous Robin conditions. We first verify these conditions on a 2D radially-symmetric acoustic-elastic example, represented on Figure 5.2. A 2D elastic annulus Ω_s of interior radius R^{int} and exterior radius R^{ext} is immersed in a circular acoustic fluid domain Ω_f of radius R_a, bounded by a boundary Γ_e. The physical and numerical parameters are the same as for the example in Section 3.3.1 and the fluid and structure physical parameters are listed in Table 3.1. The interior and exterior surface are set at $R_{\text{int}} = 0.9$m and $R_{\text{ext}} = 1$m respectively. The acoustic-acoustic interface Γ_e is set at a distance d=1.1m. A transient Robin condition is imposed on Γ_e:

$$[p + k_i v_n](t, R_a) = g(t)$$

$$\text{with } \begin{cases} g(t) = a(2t/T_p)^\gamma \times (2 - 2t/T_p)^\gamma & \text{if } t \in [0, T_p], \\ g(t) = 0 & \text{if } t > T_p \end{cases}$$

with a time parameter $T_p = 4.67\ 10^{-4}$s, a Robin coupling parameter $k_i = \rho_f c_f$ and an exponent $\gamma = 3$. The problem is entirely modelled by finite elements (quadratic elements in `Code_Aster`). The problem is representative of an acoustic-elastic problem that would be solved with a global-in-time FEM/Z-BEM iterative coupling. The fluid pressure evaluated on the fluid-structure interface obtained using `Code_Aster` is compared with the pressure obtained by a FEM solution with the in-house Matlab finite element solver (Figure 5.3). The relative difference between both numerical transient solutions is evaluated by

$$e_p^{\text{num}} := \frac{\|v^i - v_{\text{analytic}}\|_{L^2([0,T],\Gamma^i)}}{\|v_{\text{analytic}}\|_{L^2([0,T],\Gamma^i)}},$$

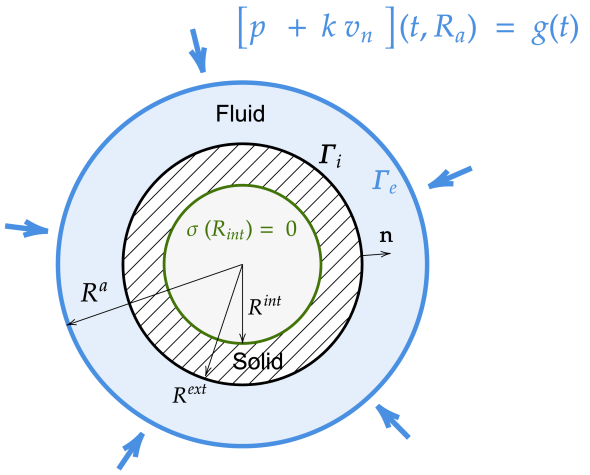

Figure 5.2: *2D elastic annulus immersed in a circular fluid domain of radius R^a, bounded by a circular boundary Γ_e on which a Robin boundary condition is imposed.*

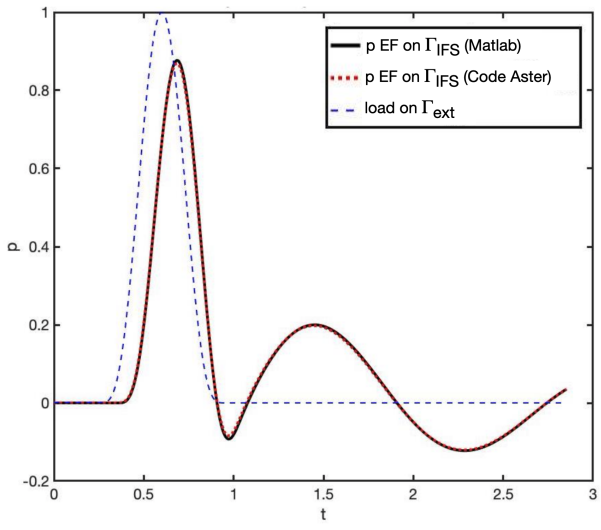

Figure 5.3: *Fluid pressure p evaluated on a point of the coupling interface Γ_i computed with* `Code_Aster` *and compared with the Matlab FEM result ($e_p^{num} = 0.013$).*

Mesh elements	1665	3418	13727	28297	222360
e_p^{num}	$1.37\ 10^{-2}$	$1.18\ 10^{-2}$	$1.12\ 10^{-2}$	$1.10\ 10^{-2}$	$1.09\ 10^{-2}$

Table 5.1: *Error e_p^{num} against the number of FEM elements.*

and we verify the convergence of the error with the mesh discretisation. With second-order quadratic finite elements, the errors e_p^{num} are given in Table 5.1. The comparison allows to validate the accuracy of the Robin condition imposed via `Code_Aster`. The availability of this condition makes it possible to consider the implementation of an acoustic/acoustic-elastic FEM/Z-BEM coupling, with the FEM contribution performed using `Code_Aster`.

Space-time variable pressure load in `Code_Aster`.

Another difficulty comes from the space-time nature of the pressure load in the context of global-in-time iterations. In order to execute global-in-time iterations, the information exchanged at each iteration between the FEM and Z-BEM solvers consists of the values of a surface variable, on the nodes of the coupling surface, for the entire time interval. For a surface Γ_e with N nodes and a time interval containing N_t time steps, the Z-BEM solution of an acoustic problem (4.8) allows to find a Robin boundary data g_i^n defined on Γ_e with $N \times N_t$ values. This boundary data is imposed as N nodal forces defined by (5.2). The FEM solver solves a general second-order ordinary differential equation of the form:

$$\begin{cases} M\ddot{X}(t) + Q\dot{X}(t) + KX(t) = G(t) \\ X(t=0) = X_0 \\ \dot{X}(t=0) = \dot{X}_0 \end{cases}$$

where the matrices M, Q and K are defined by (5.1), $X(t) = \{\mathbf{U}_s(t); \phi_i(t)\}$ is the time dependent vector of unknowns and the right-hand side G is a time dependent vector of nodal forces.

To solve this equation with `Code_Aster`, the dynamical vibration analysis are usually done with the operator `DYNA_VIBRA` (see `Code_Aster` documentation). The classical way of calling this operator is to provide the assembled mass matrix M, stiffness matrix K and damping matrix Q, as well as the characteristics of the numerical scheme (in this case a Newmark scheme) and the chosen solver (in this case MUMPS). The command is finally:

```
MY_RESU = DYNA_VIBRA(TYPE_CALCUL  = 'TRAN',
    BASE_CALCUL  = 'PHYS',
    MATR_MASS    = M,
    MATR_RIGI    = K,
    MATR_AMOR    = Q,
    SCHEMA_TEMPS = _F(SCHEMA='NEWMARK',
                      BETA=0.25*(1.0-alpha)*(1.0-alpha),
                      GAMMA = 0.5-alpha),
    INCREMENT    = (_F(INST_INIT = 0,
                       INST_FIN = T,
                       PAS = dt,)),
```

```
12          SOLVEUR         = _F(METHODE='MUMPS',),
13          EXCIT           = (_F(VECT_ASSE = G),  ),
14      )
```

However in this case, the excitation is imposed on the surface by the operator `VECT_ASSE` and it consists in a vector `G` containing N nodal forces imposed on each node of the coupling surface. This `G` does not depend on the time and cannot describe the temporal evolution of surface stress. It is possible to impose a variable stress over time using an optional time-dependent function `FT`, describing the temporal variation of the vector `G`:

```
1       EXCIT      = (_F(VECT_ASSE = G,  FONC_MULT = FT) ,) ,
```

this time variation must be described by an explicit function and applied uniformly to all the nodal forces. In the case of a global-in-time FEM/Z-BEM coupling, it is necessary to impose different nodal forces on each node of the coupling surface, whose variation in time is not described by an explicit function, but is the result of a Z-BEM calculation. It cannot be done in the classical way in `Code_Aster`. One alternative option is to use pressure loads of type `evol_char`. In this case, the dynamic load is imposed in `DYNA_VIBRA` by means of the command

```
1       EXCIT      = (_F(CHARGE = resuChar) ,) ,
```

where `resuChar` is a data structure of type `evol_char`. This structure can only be created by the operators `LIRE_RESU` or `CREA_RESU`. The inconvenient of `LIRE_RESU` is that this operator only reads two formats: IDeas or MED. In our case, we choose to use `CREA_RESU`, to create a result file in ASTER format directly with `Code_aster`. `CREA_RESU` is used as:

```
1   resuChar=CREA_RESU(OPERATION ='AFFE',
2                      TYPE_RESU ='EVOL_CHAR',
3                      NOM_CHAM  ='PRES',
4                      AFFE      =( _F(CHAM_GD=presOne,    INST=0.0,),
5                                   _F(CHAM_GD=presTwo,    INST=1.0,),
6                                   _F(CHAM_GD=presThree,  INST=2.0,),
7                                  )
8                       )
```

where `AFFE` contains N_t lines. The arguments presOne, presTwo, presThree... are vectors containing the N nodal forces at a time step. These fields of type `cham_no` have to be created in `Code_aster` with `CREA_CHAMP` and read with `LIRE_TABLE`. It has the advantage of being able to read any data format, unlike `LIRE_RESU`. The manipulation of space-time data files is difficult to implement and the resulting procedure is very time-consuming. There is currently no simple alternative for imposing a space-time variable pressure load in `Code_aster`, which may be an important limitation to its use in an industrial context.

Future developments regarding the table manipulations are planned in `Code_aster`.

It will probably be possible to use Python functions and numpy tables in the future versions of `Code_aster`. It will significantly simplify and speed up this part of the procedure.

5.1.3 Validation of the 3D FEM/Z-BEM coupling using Code Aster

The first numerical model consists in an elastic hollow sphere Ω_i^s of exterior radius R_{ext} and interior radius R_{int}, immersed in an acoustic unbounded domain. The shell and fluid are both at initial rest, and a source point is located inside the sphere (see Figure 5.4). The source point creates a radially-symmetric incident field ϕ^{inc} equal to the 3D transient fundamental solution

$$\phi^{\text{inc}}(r,t|f) := f(t-\frac{r}{c_f}) \quad \text{with } f(t|a) = \begin{cases} a(\frac{2t}{T_{\text{pulse}}})^3(2-\frac{2t}{T_{\text{pulse}}})^3 \text{ if } t \in [0, T_{\text{pulse}}] \\ 0 \qquad \text{otherwise} \end{cases}$$

where a is the amplitude and $T_{\text{pulse}} = 1.1$ is the width of the pulse. We look for the induced acoustic pressure in the fluid domain, evaluated for example, on the spherical acoustic/acoustic coupling surface $\Gamma_e = \{r = R_{\text{AA}}\}$. To solve the exterior fluid part of the problem, we use the in-house 3D Z-BEM Matlab solver described in Appendix E.3. The time interval is discretised with $N_t = 176$ time steps ($\Delta t = 2\ 10^{-2}$). $El = 33750$ BEM elements are used to discretise the boundary and 30 frequency BEM problems are solved before using the HFA. The geometrical and physical parameters are listed in Table 5.2. The coupling parameters used

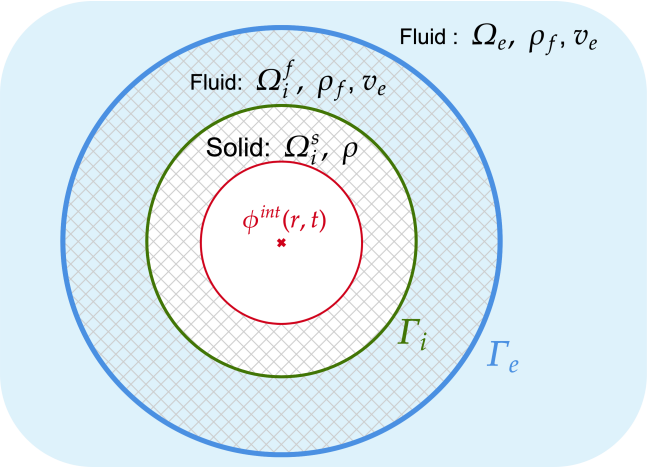

Figure 5.4: *Schematic radially-symmetric 3D pressurised sphere with a finite element mesh for the interior acoustic-elastic domain and BEM elements for the exterior acoustic domain.*

in the Robin boundary conditions are chosen according to the acoustic impedance: $k_e = k_i = \rho_f * c_f = 1500\text{kg.s}^{-1}m^{-2}$. The convergence is evaluated with the evaluation of the error e_r on the transmission residuals:

$$e_r := \sqrt{\frac{\|p_i - (p_e - s_p)\|^2_{L^2([0,T],\Gamma^e)} + \|v_i - (v_e + s_v)\|^2_{L^2([0,T],\Gamma^e)}\,\rho_f^{-1}}{\|v_i\|^2_{L^2([0,T],\Gamma^e)} + \|p_i\|^2_{L^2([0,T],\Gamma^e)}\,\rho_f^{-1}}}$$

Name	c_f	ρ_f	c_{mat}	ρmat	E	R_{int}	R_{ext}	R_{AA}
Value	1.5	1000	1.1602	1000	1000	0.9	1.2	2.2
Unity	m.s^{-1}	kg.m^{-3}	m.s^{-1}	kg.m^{-3}	$\text{kg.m}^{-1}.s^{-2}$	m	m	m

Table 5.2: *Physical properties of the structure and the fluid in the first study case 5.1.3.*

where s_p and s_v are the pressure and velocity jumps evaluated on the acoustic/acoustic interface Γ_e. Figure 5.5a shows the convergence of e_r with respect to the number of iterations, with and without Aitken acceleration (see Section 3.4.2). The Aitken algorithm is shown to be more efficient for this 3D test case than for the 2D tests in Section 4.5.2. The convergence is reached ($e_r < 10^{-3}$) within 10 iterations performed with the acoustic/acoustic-elastic coupling, which validate the coupling procedure. Figure 5.5b shows that the pressure p_e evaluated on Γ_e computed using the FEM/Z-BEM procedure verifies the transmission condition $p_i = p_e - s_p$.

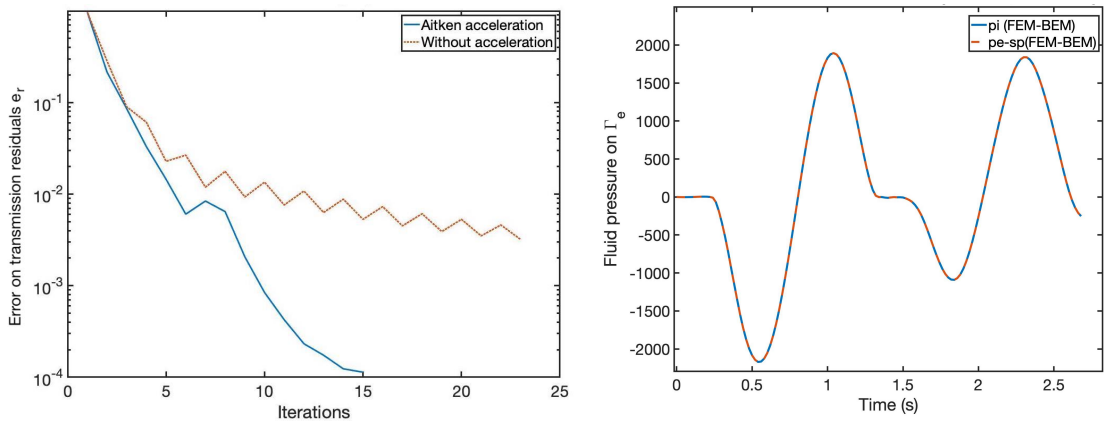

(a) ***(b)***

Figure 5.5: *3D pressurised sphere: (a) error on transmission residuals e_r computed with the 3D FEM/Z-BEM coupling, with and without Aitken acceleration, as a function of the iterations. (b) pressure induced on the surface Γ_e. $e_p^{sol} = 1.2\ 10^{-4}$.*

5.2 Free surface

So far, we have only considered structures submerged at a sufficient depth for the effect of the free surface to be neglected. However, there are also industrial demands for modelling surface vessels or submarines emerging at the surface as well as submarines submerged close to the sea bed. To simulate the hydro-acoustic sound radiation of surface ships, the free surface boundary condition has to be taken into account. In acoustics, half-space problems are problems where an infinite plane divides a whole acoustic domain into two half-space domains, with the source and the object located above the infinite plane, as illustrated in Figure 5.6. When using a classical boundary element method, with an infinite space Green function, the

free surface has to be discretised and truncated. In this case, the surface integration within the boundary integral equation must be done over the whole surface boundaries bounding the acoustic domain. This will inevitably increase the computation time. An alternative approach consists in using the method of images and introducing an half-space Green's function (HSGF) [150, 181, 185]. The HSGF will account analytically for the boundary condition on the plane and it will thus limit the support of the boundary mesh to the surface of the finite vibrating obstacle [181]. HSGF are extensively used in the context of BEMs and integral equations for scattering or radiating boundaries [14, 31, 32, 134, 202]. [162] provides different methods to construct half-space Green's functions, based on the boundary condition of the infinite plane. For the perfectly reflecting plane, the Green's function must satisfy the Neumann condition on the plane, i.e. $\partial_n G = 0$. We introduce $\widetilde{G} = G(x,y) + G(x,\widehat{y})$, where $\widehat{y}$ is the image point of y, when reflected through the plane [73, 182]. Similarly, if a homogeneous Dirichlet boundary condition is considered on the plane then the revised Green's function is $\widetilde{G} = G(x,y) - G(x,\widehat{y})$. More generally, the modified Green's function is $\widetilde{G} = G(x,y) + \beta G(x,\widehat{y})$ with β representing the reflection coefficient of the plane ($-1 \leq \beta \leq 1$).

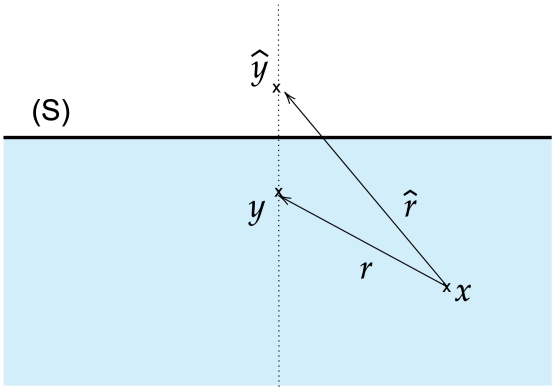

Figure 5.6: *Impulsive point source in a domain Ω, bounded by a surface (S); Notations.*

In the case of an air-liquid free surface, the Green's function for an half-space is given by

$$\widetilde{G}(\mathbf{r},\hat{\mathbf{r}}) = \left(\frac{1}{\mathbf{r}} + \beta\frac{1}{\hat{\mathbf{r}}}\right) \qquad \text{with } \beta = 1. \tag{5.3}$$

5.2.1 Fast Z-BEM with half-space Green's functions

The Z-BEM is based on the solution of time-harmonic acoustic boundary integral equations. The use of HSGFs for time-harmonic problems is well-documented [31, 103, 134].

As described in Section 3.2.2, solving a time-harmonic boundary integral equation consists, after discretisation, in solving a matrix system of the form

$$[\mathbf{K}]\,\{\phi\} = \{f\} \tag{5.4}$$

where $\{\phi\}$ represents the N unknown degrees of freedom, $\{f\}$ is a N-vector containing the discretised traces of the data on the boundary, while the N $\times$ N matrix of influence coefficients $[\mathbf{K}]$ contains evaluations of the boundary integrals. Unlike for FEM, the matrix $[\mathbf{K}]$ is fully populated. Solving this system with a direct solver entails a $O(N^3)$ complexity. It is thus impossible to solve large-scale problems with such solvers. An efficient way to solve large BEM problems consists in using iterative algorithms such as the Generalised Minimal RESidual method (GMRES) [174]. This iterative method is based on the construction of Krylov subspaces that are expanded at each new iteration. In this method, the main time-consuming task is the evaluation of the matrix-vector product $[\mathbf{K}]\{\mathbf{v}\}$ at each GMRES iteration. The complexity of such a matrix-vector product is $\mathrm{O}(N^2)$ if either the matrix is stored or if it is re-evaluated at each GMRES iteration using standard BEMs.

The goal of accelerated BEMs is therefore to speed up the evaluations of $[\mathbf{K}]\{\mathbf{v}\}$ without actually forming the full matrix $[\mathbf{K}]$. Two families of acceleration methods are often used. On the one hand, hierarchical matrix (H-matrix) based solvers have been developed. They partition the dense linear system, and approximate it into a data-sparse system. Sub-blocks in the matrix are accurately estimated by low-rank matrices to reduce storage and computational costs. It is a fully algebraic method [43, 97]. Alternatively, the Fast Multipole Method (FMM) is based on a reformulation of the fundamental solution with a plane wave expansion in order to factorise some operations [53, 157]. It is known that the FMM can reduce the computational and memory complexity of the BEM from $\mathrm{O}(N^2)$ to O(NlogN) for oscillatory kernels such as the Helmholtz kernel [200]. Acoustic FMM formulations in the frequency domain have been investigated for example in [42, 77, 118].

H-matrix and fast multipole method

[146] has shown that, in the context of UNDEX, both methods are useful and have their advantages and drawbacks. FMM is very efficient and flexible for wave propagation problems. It has been used in [146] to accelerate the Z-BEM computation of the reflected fluid pressure resulting from the interaction of the shock wave and the submarine. H-matrices have been used to accelerate the solution of the oscillating bubble problem.

An important aspect to decide if we use FMM or H-matrix it that, when performing global-in-time FEM/Z-BEM iterations, the same transient BEM problem has to be solved at each iteration n, with a different transient right-hand side member g^n. It implies to solve a set of frequency-BEM problems of the form:

$$[H](s)\{\Phi^n\} = [G](s)\{\overline{g}^n\}$$

with right-hand side member $\overline{g}^n$ depending on the frequency s and on the iteration n, while the BEM matrices $[H]$ and $[G]$ are fixed. Such problems are termed multiple right-hand side, as only the data g^n (and of course the solution Φ^n) is changing from one iteration to another [184]. Even though hierarchical matrix are known to be suboptimal for wave problems, they are still efficient and they are very appropriate for multiple right-hand sides problems. In the present work, we thus choose to use H-matrix to accelerate the Z-BEM computation.

An efficient way to deal with multiple right-hand side problems is to compute and store the H-matrix representations once and for all when solving the first BEM system and reuse them at each iteration, to compute the matrix-vector product required in the GMRES method [18]. Moreover, since we use a high-frequency approximation (as described in Section 3.5), only a few H-matrix representations have to be stored. On the contrary, the FMM does not assemble nor store the matrices, implying that matrix-vector product sequences must be computed again for each BEM problem.

Finally, a third advantage for the H-matrix method is that it is a purely algebraic approach. Unlike other methods such as FMM, it is therefore independent of the form of the fundamental solution. It is thus easy to adapt the method with the half-space Green function and to take the free surface into account in the FEM/Z-BEM global-in-time iterations.

Remark. In the same way, it is possible to use an half-space fundamental solution to take the sea bed into account in the case of a submarine in shallow water. The procedure is the same, but the boundary condition changes. The sea bed is represented with a Dirichlet boundary condition instead of a Neumann one. It is however not possible with this method to take both a free surface and the sea-bed into account at the same time.

Validation: Z-BEM with a half-space Green's function

We first validate the Z-BEM when the method of images is used. The free surface is defined by a homogeneous Neumann condition imposed on a plane with normal $\overrightarrow{e_z}$. The 3D Z-BEM solver described in Appendix E.3 is used with a half-space Green's function. We consider the same 3D problem as in Appendix E.3 and we add a free surface ($\mathcal{S}$) which refers to the plan (x, y) (Figure 5.7). We consider a sphere Ω with a boundary $\partial\Omega = \Gamma$, immersed in an acoustic domain $\Omega_f := \mathbb{R}^2 \setminus \overline{\Omega}$, and a point source fixed in the interior domain Ω. The point source produces an acoustic field ϕ equal to the 3D transient fundamental acoustic solution

$$\phi(x,y,z,t|f) := G(x,y,z,t|f) = \frac{f(t-r/c_f)}{4\pi r}$$
$$\text{with } f(t|a) = \begin{cases} at^3(T_{\text{pulse}}-t)^3 \text{ if } t \in [0, T_{\text{pulse}}] \\ 0 \qquad\qquad \text{otherwise} \end{cases}$$

where a is the amplitude and T_{pulse} is the width of the pulse. As G is the fundamental solution for a point source, it verifies the boundary integral equation for an exterior Dirichlet problem:

$$\mathcal{H}\{\phi\}(\mathbf{x},t) = -\mathcal{G}\{\partial_n\phi\}(\mathbf{x},t) \quad \forall \mathbf{x} \in \Gamma$$

In Appendix E.3, the Z-BEM solver behaviour without free surface is validated by solving this equation with a datum ϕ and an unknown $q = \partial_n\phi$, and verifying that $q = \partial_n\phi = \partial_n G$. To validate the 3D Z-BEM solver with a free surface, we now solve the boundary integral equation

$$\widetilde{\mathcal{H}}\left\{\widetilde{\Phi}\right\}(\mathbf{x}) = -\widetilde{\mathcal{G}}\{\widetilde{q}\}(\mathbf{x}) \quad \forall \mathbf{x} \in \Gamma$$

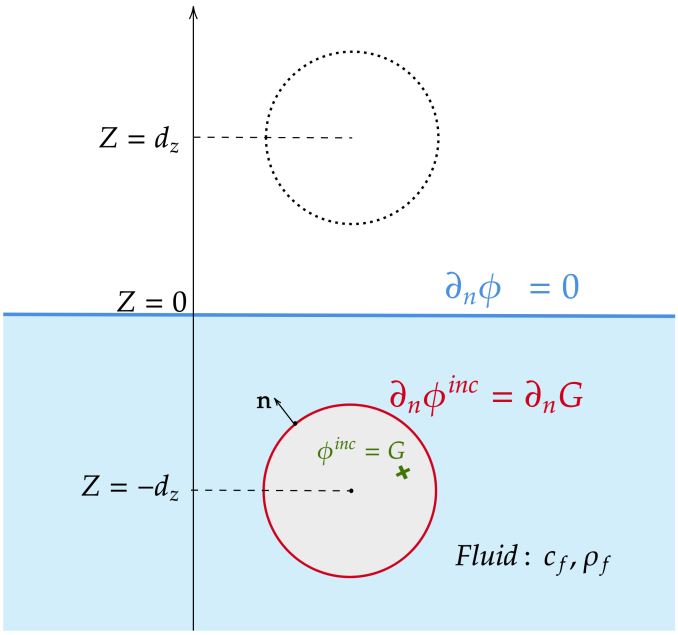

Figure 5.7: *Sketch of a sphere with an interior point source, immersed in a fluid domain bounded by a free surface.*

where $\widetilde{\mathcal{H}}$ and $\widetilde{\mathcal{G}}$ are the boundary operators modified with the half-space Green's function, $\widetilde{\Phi} := \left(\phi + \widehat{\phi}\right)$ is the datum evaluated on both the surface Γ and its symmetric $\widehat{\Gamma}$, and q is the unknown. We verify that $q = \left(\partial_n\phi + \partial_n\widehat{\phi}\right) \simeq \left(\partial_n G + \partial_n\widehat{G}\right)$. The HFA does not change and is still defined by (51). The geometrical and physical parameters are listed in Table 5.3. $N_t = 234$ time steps are used to discretised the time interval, $El = 33750$ BEM elements are used to discretise the boundary and 40 frequency BEM problems are solved before using the HFA. We first place the

Name	c_f	ρ_f	$\mathbf{x}_{\text{centre}}$	$\mathbf{x}_{\text{source}}$	Δt	$T_{\max}$
Value	1	1000	$[0; 0; -2.5]$	$[0.2; -0.4; -2.8]$	$6\ 10^{-2}$	14
Unity	m.s^{-1}	kg.m^{-3}	m	m	s	s

Table 5.3: *Fast Z-BEM with half-space Green function: physical properties for the validation case 5.2.1.*

sphere Ω at a depth of $Z_{\text{depth}} = -2.5\text{m}$. Figure 5.8a shows the normal derivative $\partial_n\phi$ evaluated with the 3D Z-BEM solver on a point of the boundary Γ as a function of the time. This numerical solution is compared to the analytical solution $\partial_n G$. We evaluate the relative L_2 error between the analytical and the numerical solutions. The relative error is $1.0\ 10^{-3}$. As a comparison, the black curve shows the solution $\partial_n G$ in the case where the free surface is not taken into account. As illustrated in Figure 5.8b, a similar test, but for a sphere placed at a deeper depth $Z_{\text{depth}} = -10\text{m}$,

yields the same transient solution as in the case where the free surface is not taken into account. The deeper the depth of the sphere, the less influence the free surface has on the diffracted solution field.

In Table 5.4 we show the convergence of the relative error with the number of frequency BEM problems solved before using the HFA. When 40 BEM problems are solved, the relative error is 1.0 10^{-3}. From 80 frequency BEM problems solved, the error converges and reaches 4.4 10^{-4}.

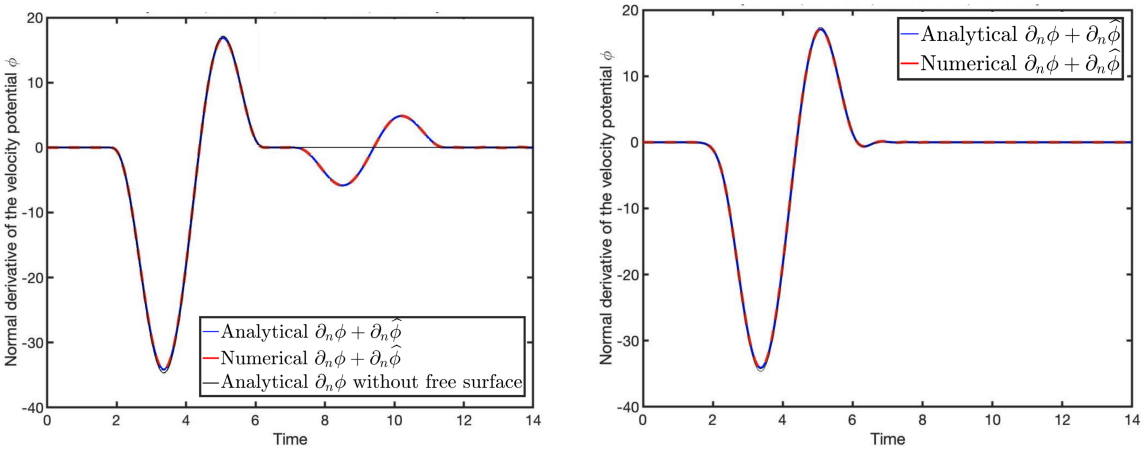

Figure 5.8: *Numerical solution $\partial_n\phi$ and analytical $\partial_n G$ evaluated on a point of Γ for an acoustic scattering problem with a free surface (a) $Z_{depth} = -2.5m$, err =1.0 10^{-3}. (b) $Z_{depth} = -10m$, err =1.0 10^{-3}.*

BEM problems solved	20	40	50	70	80	100
Relative error	1.3 10^{-2}	1.0 10^{-3}	6.9 10^{-4}	4.5 10^{-4}	4.4 10^{-4}	4.4 10^{-4}

Table 5.4: *Relative error with the number of frequency BEM problems solved in the Z-BEM before using the HFA.*

Test case: spherical elastic hull immersed in an acoustic domain with a free surface

We now validate the FEM/Z-BEM coupling procedure when a free-surface is added by considering a simple 3D study case. An elastic sphere immersed in an acoustic domain. The acoustic domain is bounded by an horizontal infinite plane located at $Z = 0$. The sphere is submitted to a radial exterior excitation ϕ^{inc}, as illustrated in Figure 5.9. As for the first 3D validation cases in Section 5.1.3, we use a fast FEM/Z-BEM method with `Code_Aster` for the FEM part and Matlab for the Z-BEM part, and the global-in-time acoustic/acoustic-elastic coupling method. For the numerical illustration, the loading under consideration is a radially symmetric

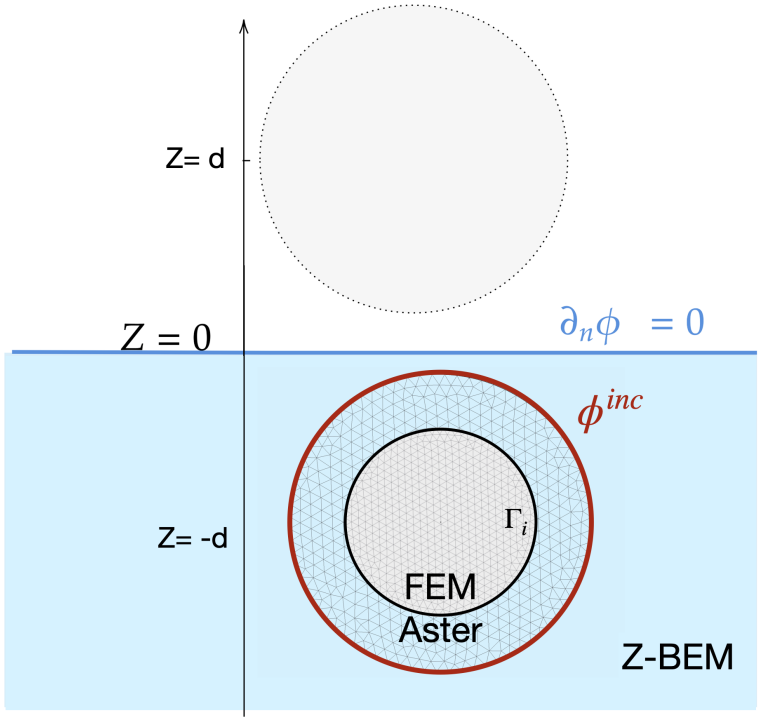

Figure 5.9: *Sketch of an elastic sphere immersed in an acoustic half-space.*

incident wave, whose profile is given by:

$$\phi(r,t|f) = f(t + r/c_f) \quad \text{with } f(t|a) = \begin{cases} at^3(T_{\text{pulse}} - t)^3 \text{ if } t \in [0, T_{\text{pulse}}] \\ 0 \qquad \text{otherwise} \end{cases}$$

where $a = 10^3$ is the amplitude and $T_{\text{pulse}} = 1.1$s is the width of the pulse. The elastic spherical hull is placed at $Z_{\text{depth}} = -10$m, the Robin coupling parameters are $k_e = k_i = c_f\rho_f = 10^4$ kg.s^{-1}m^{-2}. The geometrical and physical parameters are listed in Table 5.5. El=33750 BEM elements are used to mesh the acoustic/acoustic spherical interface and 30 frequency BEM problems are solved before using the HFA. We also use an Aitken acceleration to improve the convergence rate. Figure 5.10a

Name	c_f	ρ_f	c_{mat}	ρmat	E	R_{int}	R_{ext}	R_{AA}
Value	10	1000	1.1602	1000	1000	0.9	1.2	2.2
Unity	m.s^{-1}	kg.m^{-3}	m.s^{-1}	kg.m^{-3}	kg.m^{-1}.s^{-2}	m	m	m

Table 5.5: *Spherical elastic hull with a free-surface: physical properties.*

illustrates the convergence of the error indicator $e_{v,p}$ defined by (4.47) on Γ_e, which combines the two interfacial variables (velocity and pressure). 28 global-in-time Robin iterations are needed for the error to reach $e_{v,p} < 10^{-2}$. The numerical solutions in velocity p_i and $p_e - s_p$ are evaluated on a point of the acoustic/acoustic interface Γ_e after 28 iterations, and displayed in Figure 5.10b as functions of the time. They are shown to verify the transmission condition $p_i = p_e - s_p$.

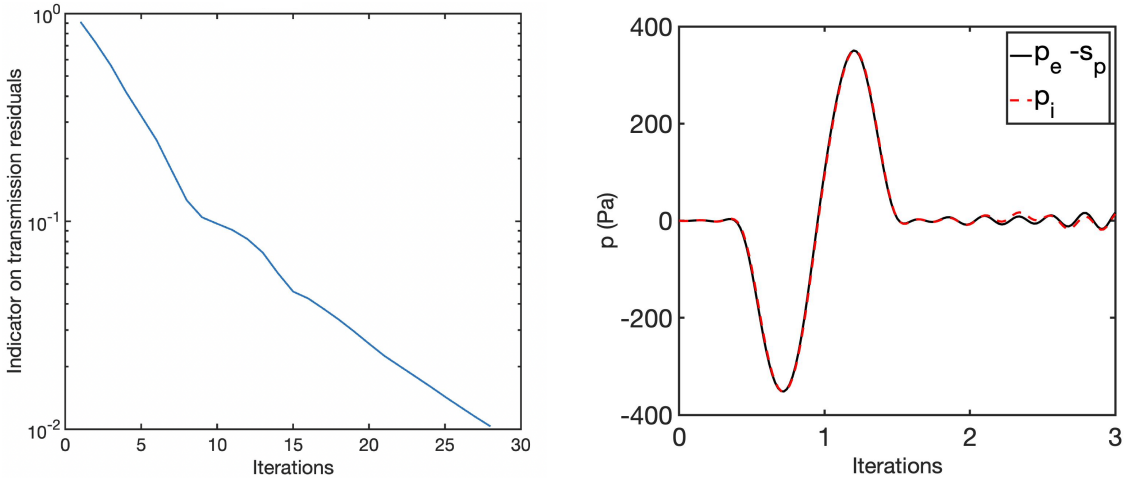

(a) *(b)*

Figure 5.10: *(a) Convergence of $e_{v,p}$ on transmission residuals with the number of iterations for a 3D FSI problem with a free surface. (b) Numerical solutions $p_e - s_p$ and p_i evaluated on a point of Γ_e. $e_p^{sol} = 5\ 10^{-2}$.*

5.2.2 Z-BEM for partially emerged ships

We have dealt so far with elastic hulls immersed in (bounded) acoustic domains, taking the presence of a free-surface (or a sea bed) into account. We now aim at considering partially emerged objects and still using the method of images. The method requires some adaptations but the general principle is the same as described in Section 5.2.1.

For a partially emerged object of boundary Γ, some degrees of freedom of the boundary also belong to the free surface (S). They are thus in Γ and in the symmetric boundary $\widehat{\Gamma}$, as illustrated in Figure 5.11. Unlike when the structure is completely immersed and no point is common to both boundaries (Section 5.2.1), in this case, the half-space fundamental solution is singular at these points. If $\mathbf{x} \in (S)$ the evaluation of $\widehat{G}(\widehat{\mathbf{r}}) = (4\pi \|\mathbf{x} - \widehat{\mathbf{y}}\|)^{-1}$ is singular for $\mathbf{y} = \widehat{\mathbf{x}} = \mathbf{x}$. A simple way to treat this singularity consists in making a distinction between the positions of the degrees of freedom of Γ and evaluating:

$$\begin{aligned} &\text{If } \mathbf{x} \notin (S), \quad \widetilde{G}(\mathbf{r}, \widehat{\mathbf{r}}) = G(\mathbf{r}) + \widehat{G}(\widehat{\mathbf{r}}), \\ &\text{If } \mathbf{x} \in (S), \quad \widetilde{G}(\mathbf{r}, \widehat{\mathbf{r}}) = 2G(\mathbf{r}). \end{aligned}$$

We thus evaluate $G(\mathbf{r}) = (4\pi \|\mathbf{x} - \mathbf{y}\|)^{-1}$ instead of $\widehat{G}(\widehat{\mathbf{r}}) = (4\pi \|\mathbf{x} - \widehat{\mathbf{y}}\|)^{-1}$. Using this trick, we avoid the evaluation of the additional singular terms due to the method of images.

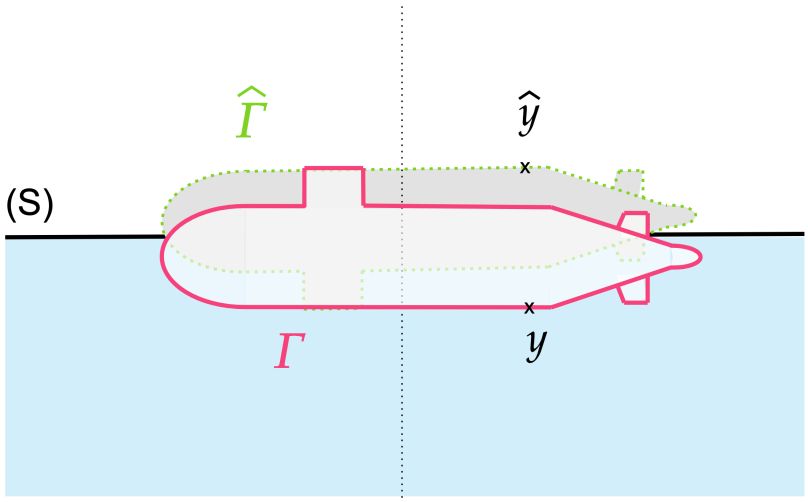

Figure 5.11: *Sketch of a partially emerged ship and its image with respect to surface (S).*

Validation: Z-BEM with a partially emerged sphere.

We first validate the Z-BEM for an acoustic scattering problem in the case where an obstacle is partially emerged. We consider a similar 3D validation case as in Section 5.2.1. A sphere Ω of radius $R = 0.8$m with a boundary $\partial\Omega = \Gamma$, is partially immersed in an acoustic domain Ω_f, as schematised in Figure 5.12. The centre of the sphere is placed at $Z_{\text{depth}} = 0.4$m (above the free surface (S)). A point source fixed in the interior domain Ω. The point source produces an acoustic field ϕ equal to the 3D transient fundamental acoustic solution G. We solve the boundary integral equation for an exterior Dirichlet problem:

$$\widetilde{\mathcal{H}}\left\{\widetilde{\Phi}\right\}(\mathbf{x}) = -\widetilde{\mathcal{G}}\left\{\widetilde{q}\right\}(\mathbf{x}) \quad \forall \mathbf{x} \in \Gamma$$

where $\widetilde{\mathcal{H}}$ and $\widetilde{\mathcal{G}}$ are the boundary operators modified with the half-space Green's function, $\widetilde{\Phi} := \left(\phi + \widehat{\phi}\right)$ is the datum evaluated on both the surface Γ and its symmetric $\widehat{\Gamma}$, and $\widetilde{q}$ is the unknown. We verify that $\widetilde{q} = \left(\partial_n G + \partial_n \widehat{G}\right)$. The HFA does not change and is still defined by (51). The geometrical and physical parameters are listed in Table 5.6. $N_t = 234$ time steps are used to discretised the time interval, $El = 9049$ BEM elements are used to discretise the boundary and 40 frequency BEM problems are solved before using the HFA.

Name	c_f	ρ_f	$\mathbf{x}_{\text{centre}}$	$\mathbf{x}_{\text{source}}$	Δt	$T_{\max}$
Value	1	1000	$[0; 0; 0.4]$	$[0; -0.05; -0.05]$	$6\ 10^{-2}$	14
Unity	m.s^{-1}	kg.m^{-3}	m	m	s	s

Table 5.6: *Fast Z-BEM with half-space Green function: physical properties for the validation case 5.2.1.*

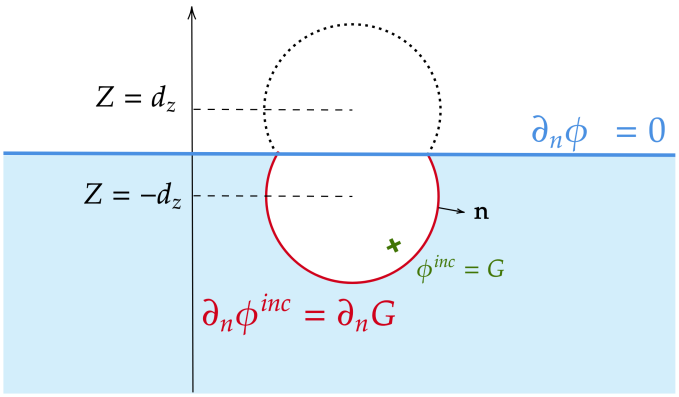

Figure 5.12: *Sketch of a sphere with an interior point source, partially immersed in a fluid domain bounded by a free surface.*

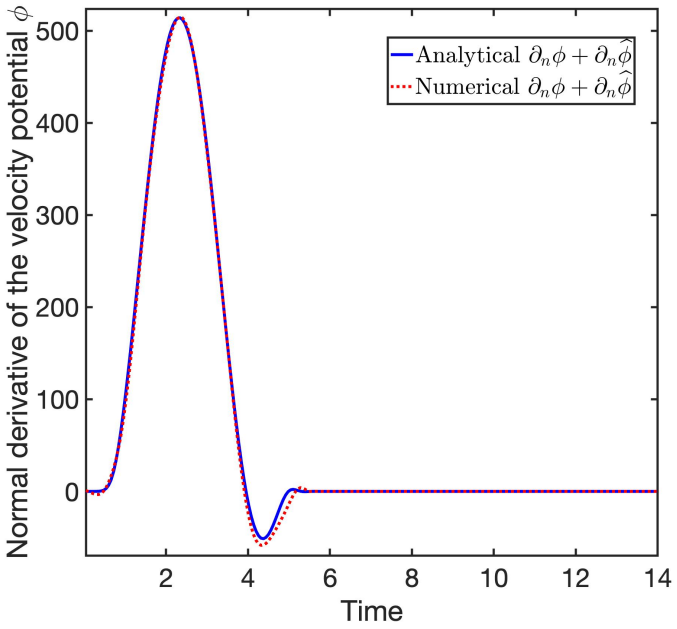

Figure 5.13: *Numerical solution $\partial_n\phi$ and analytical $\partial_n G$ evaluated on a point of Γ for an acoustic scattering problem with an emerged sphere.*

Figure 5.13 shows the normal derivative $\partial_n \phi$ evaluated with the 3D Z-BEM solver on a point of the boundary Γ as a function of the time. This numerical solution is compared to the analytical solution $\partial_n G$. The relative error evaluated on the time interval $[0, T]$ is 3 10^{-2}. Although further work will be required to assess the convergence and efficiency of this Z-BEM procedure adapted for a partially emerged structure, this first numerical example enables to validate the method. The next step will be to implement this modified Z-BEM in a FEM/Z-BEM coupling and to solve simple FSI problems with partially emerged structures. In the future, it will also be interesting to compare the results obtained for a industrial model of submarine facing a shock wave, while fully immersed in the water and partially emerged.

5.3 Modelling the interaction between a shock wave and a submarine

This last section aims at solving an industrial problem related to the main application of this PhD work: the fluid-structure interaction between the shock wave emitted by a far-field underwater explosion and a realistic submarine hull. The purpose is to demonstrate that the numerical coupling method we developed is robust in an industrial context.

As described in the introduction, a conventional underwater explosion produces two physical phenomena. It generates first a *shock wave*, propagating in the water at almost the sound speed. And in a second time, an *oscillating gas bubble* is produced. Its oscillations, due to a difference between its internal and external pressures, generates flows of heavy fluid, and secondary pressure waves are created when the bubble is the most contracted, as schematised in Figure 2. During a far-field explosion, the explosion charge is smaller or it is located far enough from the ship so that the primary impact of the explosion comes from the shock wave, and the ship's structural response is limited to elastic deformations. For a far-field explosion, the bubble migrates to the free surface without having its movement disturbed by the presence of the structure. As a remark, we stress out that the term "far-field" is distinct from the notion of "far" in classical wave propagation theory.

When modelling the far-field UNDEX, there are two important assumptions: (i) the shock wave and the oscillations of gas bubbles are far enough from the submerged structure, so that they can be modelled without taking into account the presence of the structure, and (ii) they occur on sufficiently distinct time scales and thus affect the ship separately.

In this work we focus on the first phenomenon, the *primary shock wave* and on its simulation. However, it should be remembered that the two phenomena are physically linked because they are due to the same explosion and that it is essential to consider both to obtain a realistic model of the total impact of an explosion on a naval structure [85, 94]. To model the shock wave, we use a common approximation used in the naval industry, which is recalled in the next section.

Modelling of the primary acoustic shock wave

An underwater explosion generally consists in a sudden release of a large quantity of energy of a chemical nature and immediately releases a shock wave which propagates in the surrounding water domain at a speed equal to several times the speed of propagation of acoustic waves in water. After a very short distance, the wave velocity decays and stabilises at the speed of sound in water ($c_f = 1500$ m/s). During the first brief supersonic phase, the energy carried by the wave reduces before reaching a quasi-stable value. Once this stabilised phase is reached, the shock wave is called *primary shock wave*. This shock wave occurs at a short time-scale and in the high frequencies (between 3 and 7 kHz for $c_f = 1500$ m/s). As discussed in [146], a first approximation of the shock wave model consists in considering that the supersonic shock wave turns into an acoustic wave that propagates in the fluid at a constant speed according to the wave equation (2.1). Moreover, the deformations and the displacements are considered small and the water is a perfect fluid, homogeneous, isotropic, where the flow is non-viscous and irrotational [48]. The fluid flow admits a velocity potential $\phi = \phi(\mathbf{x}, t)$, defined at any time t and any point $\mathbf{x}$ by:

$$v(\mathbf{x}, t) = -\nabla\phi(\mathbf{x}, t)$$

where v is the fluid velocity field. Under these hypotheses, it is shown in [146] that the dynamic pressure p is simply reduced to

$$p = -\rho_f \partial_t \phi.$$

Experimental measurements have been used to determine an expression of the incident pressure $p_{\text{inc}} = -\rho_f \partial_t \phi_{\text{inc}}$, associated with the primary wave. Different profiles have been proposed and compared, with large variations in the evaluation of the shock wave energy [116, 196]. In particular, [85] described the shock wave as a sudden jump, within less than 10^{-7} seconds, to a pressure peak p_m of 1 to 10 MPa. This jump is followed by a double-exponential decay of time constant τ between 10^{-3} and 10^{-4} seconds:

$$\begin{cases} p_{\text{inc}}(t) = 0, & t < 0 \\ p_{\text{inc}}(t) = p_m e^{-t/\tau}, & 0 \leq t \leq \tau \\ p_{\text{inc}}(t) = \alpha_1 e^{-\beta_1 t/\tau} + \alpha_2 e^{-\beta_2 t/\tau}, & \tau \leq t \leq 7\tau \end{cases} \tag{5.5}$$

$\alpha_1, \alpha_2, \beta_1$ and β_2 are numerical coefficients, obtained from experimental data, that depend on the type of the explosive material. We adopt this model for our last numerical example in this section.

Discontinuous shock wave

The shock wave models (5.5) and (5.5) are discontinuous in time and it could cause regularity problems as a minimal space-time regularity is needed for the global-in-time iterative algorithm to converge (see Chapter 2). For the acoustic IBVP as (2.20) to be well-posed, ϕ has to be of sufficient regularity for the variational form of the problem to be meaningful in the sense of distributions. As the double-exponential model chosen for the pressure is discontinuous, in practice the incident pressure is

regularised by considering that the jump to the magnitude p_m is smoothly performed during a very short time. In this work, we will then consider a double-exponential model of the shock wave with well-chosen coefficients so it verifies the wave equation, and we will slightly regularise the pressure jump in order to gain some regularity in time. For example, we will modify the incident pressure given by (5.5) to make it vary smoothly from zero to its maximum during a small time interval of $\tau/20$.

Numerical case study: a submarine facing a shock wave

The example we want to consider is an elastic submarine. The geometry is derived from a modern generic submarine, the BB2, based on a variant of the "Joubert" hull form design [166]. The mesh, provided by Naval Group Research, is modified to add a structural volume and also a volume of acoustic FEM elements around the boundary (see Figure 5.14). The acoustic/elastic finite element mesh has 3 10^5 elements. The incident pressure wave is described by (5.5). While all the numerical tools needed to

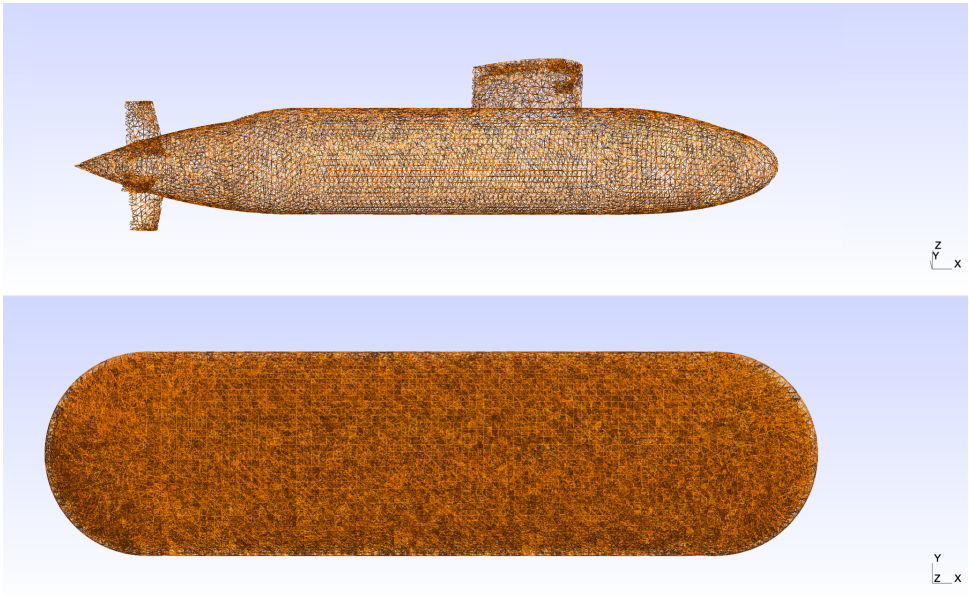

Figure 5.14: *3D view of the finite element mesh used for the acoustic/acoustic-elastic FEM/Z-BEM coupling.*

solve this industrial problem have now been validated and are available, the analyses are still in progress.

Limitations of the present FEM/Z-BEM iterative coupling for UNDEX

The main limitation of the acoustic/acoustic-elastic iterative coupling presented here is the need to mesh an arbitrary truncated volume of fluid around the elastic structure. As the thickness of this finite element fluid part can be very small, the impact on the FEM calculation cost is limited. However, this additional finite element mesh increases the difficulty to generate adapted refined meshes when dealing with complex interface shapes Γ. This difficulty already highlighted in [146] is not overcome by the global-in-time FEM/Z-BEM coupling method presented here.

The iterative coupling method is based on FEM and Z-BEM solvers, both able to analyse complex geometries. `Code_Aster` can treat complex mechanical materials. The Z-BEM solver is limited to linear fluid models and is not adapted for complex fluid flow. This is not an important limitation, first because in the context of a far-field UNDEX, during the shock wave propagation, considering the shock wave as an ideal acoustic wave is propagating in a linear fluid is a fair approximation. Moreover, one part of fluid around the structure is treated with the FEM. This fluid part treated with `Code_Aster` enables to add some local non-linear phenomena as cavitation. However, as `Code_Aster` is not a CFD code, it is limited to linear acoustic models or added matrices models based on a potential fluid approach, and complex cavitation models are not available. Finally, since the acoustic/acoustic-elastic global-in-time coupling convergence does not depend on the chosen numerical methods, this limitation could be overcome by using a different FEM solver instead of `Code_Aster`.

Regarding our numerical implementation, `Code_Aster` has many advantages, including the possibility of using a very large number of material behaviour models, which is very useful to model the structure response to an UNDEX. In addition, as it is a free software, it is highly modular and improvements adapted to user requests are constant. Finally, the possibility of using non-homogeneous Robin boundary conditions in an acoustic domain is essential to implement a global-in-time iterative FEM/Z-BEM coupling. However, a major drawback is the imposition of non-homogeneous variable loads. As detailed in Section 5.1, the manipulation of space-time data files is difficult to implement and the resulting procedure is very time-consuming. The communication step between the two solvers at each iteration is therefore limiting and cannot currently be improved. The method proposed in this chapter does allow `Code_Aster` to be coupled with a Z-BEM solver, but the manipulation of space-time data files is difficult to implement and the resulting procedure is very time-consuming. The communication step between the two solvers at each iteration is therefore limiting and cannot currently be improved. In an industrial context, it will be essential to improve and speed up this part. Future python functions are planned to be added to `Code_Aster`, which would probably make it easier to manipulate data arrays.

5.4 Conclusion

Based on the algorithms developed in Chapters 2 to 4, this Chapter presented some improvements and industrial applications of the global-in-time acoustic/acoustic-elastic iterative method.

We have shown the capabilities of the algorithm to treat realistic industrial FSI problems. We have shown that it allows to use solvers in a black-box manner. We have used the FEM solver `Code_Aster` as an illustration and detailed a way to couple it with a Z-BEM solver. We have also shown that the algorithm enables to treat large and complex problems involving complex geometries and high frequency loading. The iterative FEM/Z-BEM coupling has these characteristics thanks to an optimal choice of the Robin coupling parameter in each subdomain, of acceleration methods in the Z-BEM solver (H-matrices, HFA, parallel solution of the frequency BEM problems, re-use of the BEM operators at each iteration) and of an optimal definition of the acoustic/acoustic coupling interface, allowing to reduce the volumic FEM mesh to the minimal distance. A first numerical proof of concept for the FEM/Z-BEM coupling is given by considering a pressurised elastic hollow sphere immersed in a linear fluid domain.

To model submarines located near the free-surface and also partially emerged ships, we have extended the method to the case of an half-space. Using the method of images, we have modified the Green's function in the Z-BEM solver to take into account the free surface boundary condition. We have validated this improved Z-BEM combined with the H-matrix method by simulating the behaviour of a deformable spherical elastic hull immersed in an acoustic domain.

Conclusions and perspectives

This work proposes a global-in-time domain decomposition method well-suited for FSI problems. The main application we have in mind is the design of naval structures subjected to underwater explosion. This work has been supported by fundings from the French company Naval Group Research and the Direction Générale de l'Armement (DGA) (through the Agence de l'Innovation de Défense (AID)). We first emphasise our contributions both in terms of theoretical and numerical developments.

Main algorithmic and theoretical results.

Chapter 1 highlights the existence of various domain decomposition methods for transient problems. We stress that the use of modified boundary conditions generally improves the algorithm convergence and we highlight in particular the advantages of the Robin boundary conditions. It is nowadays clear that the use of Robin boundary conditions in each subdomain improves the convergence rate compared to Neumann or Dirichlet ones. But the challenge is to determine the optimal coupling parameters in these Robin conditions. Different methods exist and there are still a lot of ongoing research on how to choose the coupling parameters. Our literature review also shows that, until this work, there was no global-in-time iterative domain decomposition method adapted to the modelling of transient acoustic/elastic problems.

Chapter 2 is one of our most significant contribution. It concerns the mathematical analysis of a general time-domain acoustic–elastic interaction problem. We consider the scattering of a time-domain acoustic wave by a bounded elastic obstacle which is immersed in a homogeneous fluid and we provide existence and uniqueness results, as well as continuous data-to-solution maps. Solvability results are established for three cases, which differ by the assumed regularity in space of the transmission data on the acoustic-elastic interface. We then introduce a Robin-Robin global-in-time iterative procedure, inspired from Schwarz Waveform Relaxation methods, adapted to acoustic/elastic transient problems and based on Robin boundary conditions in each subdomain. We also provide the convergence proof of the iterative method. These Robin-Robin global-in-time iterations have a guaranteed convergence, which does not depend in practice on the chosen numerical methods.

We propose a proof of concept of the method for coupled FSI problems using a global-in-time FEM/Z-BEM coupling in Chapter 3. We numerically solve simple 2D scattering problems to illustrate the algorithm convergence and optimise its behaviour. Semi-analytical solutions enable to validate the global-in-time algorithm, but also to explicitly characterise the algorithm convergence speed in a particular case, and thus to optimise it. In particular, we show that optimal Robin coupling parameters can be defined according to the physics, in terms of acoustic and elastic impedances. The Robin parameters are easy to choose and do not require complicated tuning to get an efficient convergence rate. It is a major advantage compared to many classical step-by-step DDMs. We also propose a high-frequency approximation adapted to Robin boundary conditions, that allows to considerably improve the Z-BEM procedure.

We then propose an acoustic/acoustic-elastic global-in-time iterative method based on Robin boundary conditions in each subdomain. We provide the convergence proof of the iterative method. This alternative method has a guaranteed convergence and allows to solve FSI problems with a different domain decomposition.

We finally carry out more realistic 3D simulations. The underwater explosions applications presented in Chapter 5 confirm the efficiency of the FEM/Z-BEM global-in-time coupling and the possibility to use it in an industrial context, with commercial solvers. To be able to consider more realistic configurations, the iterative method are improved by introducing the possibility to treat surface ships or partially emerged submarines thanks to the use of an half-space Green function in the Z-BEM method.

Main numerical developments.

Even though this work was not started from scratch, important numerical developments have been done to illustrate the efficiency of the proposed algorithm.

A FEM/Z-BEM code has been developed in Matlab to obtain the 2D results presented in Chapters 2 and 3. This program solves 2D transient acoustic-elastic problems using a FEM solver and a Z-BEM solver accelerated by the H-matrix method. The main software development contributions are:

- The 2D FEM program used is the one of [25]. We have nevertheless implemented some improvements to allow the use of a boundary mass matrix, of Robin boundary conditions and the solution of acoustic-elastic FEM problems. Two versions of the solver are available, either to solve elastic FEM problems (in the context of an acoustic/elastic iterative coupling method as described in Chapter 2) or acoustic/elastic FEM problems (in the context of an acoustic/acoustic-elastic iterative coupling method as described in Chapter 4).

- A fast 2D Z-BEM solver has been implemented from scratch. It is based on a fast frequency domain BEM solver for Helmholtz problems (accelerated with the H-matrix method). The Z-BEM algorithm has then been implemented to recover the time-domain solution (see Appendix E). To improve the program

efficiency, the frequency BEM solutions are computed in parallel and a high-frequency approximation is implemented.

- The coupling FEM/Z-BEM procedure consists in an initialisation script which computes and stores the H-matrix structures for the complex frequencies lower than the cut-off frequency chosen for the HFA. Then a second script calls both solvers in parallel and computes at each iteration the new Robin boundary data. There are two versions for this procedure, for the acoustic/elastic iterative method and for the acoustic/acoustic-elastic iterative method respectively. The user can use both versions with or without an Aitken's acceleration algorithm.

The 3D results presented in Chapter 5 have been obtained through a coupling between a Matlab BEM solver and `Code_Aster` for the FEM part.

- A 3D Z-BEM solver has been developed from an existing fast frequency BEM solver for Laplace problems. This solver has been adapted for Helmholtz equations, and the Z-BEM algorithm has then been implemented to recover the time-domain solution. We have also added a free-surface option, allowing to use this solver for half-space problems.

- In `Code_Aster`, a python routine has been developed to take into account non-homogeneous space-time pressure loading (see Section 5.1.2).

- The coupling FEM/Z-BEM procedure has been developed with Matlab and Python. It consists of an initialisation script which defines two mesh files, one volumic mesh readable by `Code_Aster` and one surface mesh of the coupling interface. The program then contains a second bash script that calls in parallel and in command line, the command files for each FEM and Z-BEM solvers. This script also computes at each iteration the new Robin boundary data and saves it as text format.

Although the efficiency of the mentioned codes can be improved in many ways, these developements enabled us to derive a concrete proof of concept of the Robin-Robin global-in-time iterative methods, which is promising for future use in industrial applications.

Directions for future work.

This work results in two efficient convergent iterative methods to solve transient fluid-structure interaction problems. A first application of this work consists in an efficient iterative FEM/Z-BEM method. Even though it is already an efficient algorithm, there are still room for improvement.

Numerical improvements of the FEM/Z-BEM procedure. To use this FEM/Z-BEM coupling procedure in an industrial context, some improvements can be proposed. Among the possibilities, we could consider non-matching volume and

surface meshes for the FEM and the Z-BEM part, in order to avoid an overly refined FEM mesh. This can be done with a mesh interpolation procedure. Finally the current manipulation of space-time data files in `Code_Aster` results in a very time-consuming procedure. Future python functions are planned to be added to `Code_Aster`, which will probably make it easier to manipulate data arrays and open new possibilities to accelerate this part of the procedure.

A very interesting prospect is also to consider a Z-BEM adapted to non-zero initial conditions. This improvement would enable to consider a problem over a long time interval in several short sub-intervals and to solve them in parallel. By choosing the time discretisation of these sub-problems with the same time step and the same number of time steps, the same complex frequencies and therefore the same H-mat structures could be reused in the Z-BEM. This would considerably reduce the computational cost. Further work is still needed in this direction to adapt the Z-BEM procedure.

Industrial application to underwater explosions. We aim at integrating the results of this research in an internal tool for the structural design of the fluid-structure interaction between a far-field underwater explosion and submarines or surface ships, which would be used by Naval Group to treat the whole UNDEX phenomena, i.e. the shock wave and the bubble movement, in an unified way. This implies to work on the junction between the two phenomena. Numerical smoothing procedures can be used [146], but there is still no clear method to blend the two phases for realistic configurations.

We developed a FEM/Z-BEM solver to model scattering problems caused by the shock waves of far-field underwater explosions. In this context, we could improve the model to consider more realistic underwater explosion problems. Unlike the submarines, in the case of a surface ship the shock wave also creates a non-linear cavitation phenomenon in the fluid near the hull. It can severely damage the structure. Cavitation consists in a rapid formation and collapse of gas bubbles in the water, which occurs when the pressure of the water drops below the vaporisation pressure. In this case, the boiling temperature can decrease to the ambient temperature of

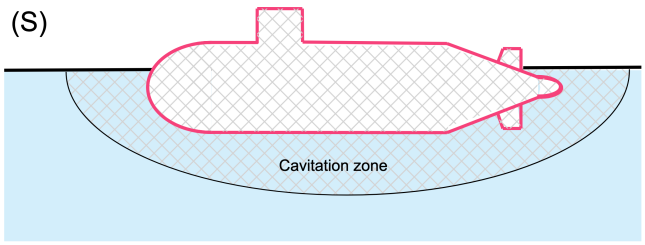

Figure 5.15: *Cavitation region treated with finite elements in an underwater explosion event.*

the liquid, which leads to the formation of gas bubbles. In the case of submarines the pressure of the surrounding fluid is high enough to prevent cavitation. But for

surface vessels or submarines stationed near the surface, this phenomenon cannot be neglected [201]. An implementation of this phenomena in the fluid FEM part within the acoustic/acoustic-elastic iterative method would be a useful addition to this work. To achieve this, a non-linear behaviour law has to be considered for the fluid in the acoustic domain modelled with acoustic finite elements. We could choose a non-linear fluid pressure model as described for example in [138]. The distance between the acoustic/acoustic coupling interface and the boundary of the ship would then be defined physically, as the region in which cavitation usually occurs (Figure 5.15).

Bibliography

[1] A. Aimi and M. Diligenti. "A new space–time energetic formulation for wave propagation analysis in layered media by BEMs". In: *International journal for numerical methods in engineering* 75.9 (2008), pp. 1102–1132.

[2] A. Aimi, M. Diligenti, C. Guardasoni, and S. Panizzi. "A space-time energetic formulation for wave propagation analysis by BEMs". en. In: *Rivista di Matematica della Universita di Parma* (2008), pp. 171–207.

[3] X. Antoine and E. Lorin. "An analysis of Schwarz waveform relaxation domain decomposition methods for the imaginary-time linear Schrödinger and Gross-Pitaevskii equations". In: *Numerische Mathematik* 137 (2017), pp. 923–958.

[4] X. Antoine and E. Lorin. "Explicit determination of Robin parameters in pptimized Schwarz waveform relaxation methods for Schrödinger equations based on pseudodifferential operators". In: *Communications in Computational Physics* 27 (2020), pp. 1032–1052.

[5] A. Arnoult, C. Japhet, and P. Omnes. "Discrete-time analysis of optimized Schwarz waveform relaxation with Robin parameters depending on the targeted iteration count". In: *ESAIM: Mathematical Modelling and Numerical Analysis* 57.4 (2023), pp. 2371–2396.

[6] S. Badia, F. Nobile, and C. Vergara. "Fluid-structure partitioned procedures based on Robin transmission conditions". In: *Journal of Computational Physics* 227.14 (2008), pp. 7027–7051.

[7] S. Badia, F. Nobile, and C. Vergara. "Robin-Robin preconditioned Krylov methods for fluid-structure interaction problems". In: *Computer Methods in Applied Mechanics and Engineering* 198.33-36 (2009), pp. 2768–2784.

[8] B.B. Baker and E.T. Copson. *The Mathematical Theory of Huygens' Principle*. AMS Chelsea Publishing. American Mathematical Society, 2003.

[9] A. Bamberger, R. Glowinski, and Q. H. Tran. "A domain decomposition method for the acoustic wave equation with discontinuous coefficients and grid change". In: *SIAM Journal on Numerical Analysis* 34.2 (1997), pp. 603–639.

[10] A. Bamberger and T. Ha Duong. "Formulation variationnelle espace-temps pour le calcul par potentiel retardé de la diffraction d'une onde acoustique (I)". In: *Mathematical Methods in the Applied Sciences* 8.1 (1986), pp. 405–435.

[11] L. Banjai, M. Messner, and M. Schanz. "Runge-Kutta convolution quadrature for the Boundary Element Method". In: *Computer Methods in Applied Mechanics and Engineering* 245-246 (2012), pp. 90–101.

[12] L. Banjai and S. Sauter. "Rapid solution of the wave equation in unbounded domains". In: *SIAM Journal on Numerical Analysis* 47.1 (2009), pp. 227–249.

[13] G. Bao, Y. Gao, and P. Li. "Time-Domain Analysis of an Acoustic–Elastic Interaction Problem". In: *Archive for Rational Mechanics and Analysis* 229.2 (2018), pp. 835–884.

[14] M.S. Bapat, L. Shen, and Y.J. Liu. "Adaptive fast multipole boundary element method for three-dimensional half-space acoustic wave problems". In: *Engineering Analysis with Boundary Elements* 33.8-9 (2009), pp. 1113–1123.

[15] G. Barras. "Interaction fluide-structure : application aux explosions sous-marines en champ proche". PhD thesis. 2012.

[16] H. Barucq, R. Djellouli, and E. Estecahandy. "On the existence and the uniqueness of the solution of a fluid-structure interaction scattering problem". In: *Journal of Mathematical Analysis and Applications* 412.2 (2014), pp. 571–588.

[17] K.J. Bathe, H. Zhang, and M.H. Wang. "Finite element analysis of incompressible and compressible fluid flows with free surfaces and structural interactions". In: *Computers & Structures* 56.2 (1995), pp. 193–213.

[18] M. Bebendorf. *Hierarchical matrices, volume 63 of Lecture Notes in Computational Science and Engineering*. 2008.

[19] D. Bennequin, M. J. Gander, L. Gouarin, and L. Halpern. "Optimized Schwarz waveform relaxation for advection reaction diffusion equations in two dimensions". In: *Numerische Mathematik* 134 (2016), pp. 513–567.

[20] M. Berton. "Modélisation de la réponse vibro-acoustique d'une structure excitée par une couche limite turbulente en présence d'un gradient de pression statique". PhD thesis. Ecole Centrale de Lyon, 2014.

[21] T. Betcke, N. Salles, and W. Smigaj. "Overresolving in the Laplace domain for convolution quadrature methods". In: *SIAM Journal on Scientific Computing* 39.1 (2017).

[22] M. Bjørhus. "A note on the convergence of discretized dynamic iteration". In: *BIT Numerical Mathematics* 35 (1995), pp. 291–296.

[23] M. Bonnet. *Boundary integral equation methods in solids and fluids*. John Wiley & sons, 1999.

[24] M. Bonnet, S. Chaillat, and A. Nassor. "Solvability results for the transient acoustic scattering by an elastic obstacle". In: *Journal of Mathematical Analysis and Applications* 536.1 (2024), p. 128198.

[25] M. Bonnet, A. Frangi, and C. Rey. *The Finite Element Method in Solid Mechanics*. McGraw-Hill Education, 2014.

[26] M. Bonnet, G. Maier, and C. Polizzotto. "Symmetric galerkin boundary element methods". In: *Applied Mechanics Reviews* 51.11 (1998), pp. 669–704.

[27] S. Börm and L. Grasedyck. "Hybrid cross approximation of integral operators". In: *Numerische Mathematik* 101 (2005), pp. 221–249.

[28] C. Brezinski. "Convergence Acceleration During the 20th Century". In: *J. Comput. Appl. Math* 122 (2000), pp. 1–21.

[29] H. Brezis. *Functional analysis, Sobolev spaces and partial differential equations*. Springer, 2011.

[30] K. Brochard. "Modélisation analytique de la réponse d'un cylindre immergé à une explosion sous-marine". PhD thesis. 2018.

[31] D. Brunner, M. Junge, C. Cabos, and L. Gaul. "Vibroacoustic simulation of partly immersed Bodies by a coupled fast BE-FE approach". In: *The Journal of the Acoustical Society of America* 123 (June 2008), p. 3418.

[32] D. Brunner, G. Of, M. Junge, O. Steinbach, and L. Gaul. "A fast BE-FE coupling scheme for partly immersed bodies". In: *International Journal for Numerical Methods in Engineering* 81.1 (2010), pp. 28–47.

[33] A. Buchau, W. Rucker, O. Rain, V. Rischmuller, S. Kurz, and S. Rjasanow. "Comparison between different approaches for fast and efficient 3-D BEM computations". In: *Magnetics, IEEE Transactions on* 39 (June 2003), pp. 1107–1110.

[34] M. Bukač, G. Fu, A. Seboldt, and C. Trenchea. "Time-adaptive partitioned method for fluid-structure interaction problems with thick structures". In: *Journal of Computational Physics* 473 (2023), p. 111708.

[35] K. Burrage. *Parallel and sequential methods for ordinary differential equations*. Clarendon Press, 1995.

[36] X.-C. Cai. "Multiplicative Schwarz methods for parabolic problems". In: *SIAM Journal on Scientific Computing* 15.3 (1994), pp. 587–603.

[37] S. Cao, A. Main, and K. G. Wang. "Robin-Neumann transmission conditions for fluid-structure coupling: embedded boundary implementation and parameter analysis". In: *International Journal for Numerical Methods in Engineering* 115.5 (2018), pp. 578–603.

[38] S. Cao, G. Wang, and K. G. Wang. "A spatially varying robin interface condition for fluid-structure coupled simulations". In: *International Journal for Numerical Methods in Engineering* 122.19 (2021), pp. 5176–5203.

[39] B. Caudron. "Couplages FEM-BEM faibles et optimisés pour des problèmes de diffraction harmoniques en acoustique et en électromagnétisme". PhD thesis. Université de Lorraine; Université de Liège, 2018.

[40] P. Causin, J.-F. Gerbeau, and F. Nobile. "Added-mass effect in the design of partitioned algorithms for fluid-structure problems". In: *Computer methods in applied mechanics and engineering* 194.42-44 (2005), pp. 4506–4527.

[41] S. Chaillat. "Fast Multipole Method for 3-D elastodynamic boundary integral equations . Application to seismic wave." PhD thesis. Ecole des Ponts ParisTech, 2008.

[42] S. Chaillat and F. Collino. “A wideband Fast Multipole Method for the Helmholtz kernel: Theoretical developments”. In: *Computers & Mathematics with Applications* 70.4 (2015), pp. 660–678.

[43] S. Chaillat, L. Desiderio, and P. Ciarlet. “Theory and implementation of $\mathcal{H}$-matrix based iterative and direct solvers for Helmholtz and elastodynamic oscillatory kernels”. In: *Journal of Computational Physics* (Sept. 2017).

[44] S. Chandler-Wilde and S. Langdon. “A Galerkin Boundary Element Method for High Frequency Scattering By Convex Polygons”. In: *SIAM Journal on Numerical Analysis* 45 (Jan. 2007), pp. 610–640.

[45] D. J. Chappell. “Convolution quadrature Galerkin boundary element method for the wave equation with reduced quadrature weight computation”. In: *IMA Journal of Numerical Analysis* 31.2 (2011), pp. 640–666.

[46] P. G. Ciarlet. *Linear and nonlinear functional analysis with applications*. SIAM, 2013.

[47] S. Clement, F. Lemarié, and E. Blayo. “Discrete analysis of Schwarz waveform relaxation for a diffusion reaction problem with discontinuous coefficients”. In: *SMAI Journal of Computational Mathematics* 8 (2022), pp. 99–124.

[48] R. H. Cole. *Underwater explosions*. Princeton University Press, 1948, p. 468.

[49] F. Collino, P. Joly, and M. Lecouvez. “Exponentially convergent non overlapping domain decomposition methods for the Helmholtz equation”. In: *ESAIM M2AN* 54 (2020), pp. 775–810.

[50] M. Costabel and F.-J. Sayas. “Time-Dependent Problems with the Boundary Integral Equation Method”. In: *Encyclopedia of Computational Mechanics Second Edition* (2017), pp. 1–24.

[51] T. Courvoisier and M. J. Gander. “Optimization of Schwarz waveform relaxation over short time windows”. In: *Numerical Algorithms* 64 (2013), pp. 221–243.

[52] T.A. Cruse. “Numerical solutions in three dimensional elastostatics”. In: *International Journal of Solids and Structures* 5.12 (1969), pp. 1259–1274.

[53] E. Darve. “The Fast Multipole Method: Numerical Implementation”. In: *Journal of Computational Physics* 160.1 (2000), pp. 195–240.

[54] R. Dautray and J-L. Lions. *Mathematical analysis and numerical methods for science and technology: Volume 5: Evolution problems 1*. Ed. by Springer Science & Business Media. 1988.

[55] P. Davies and D. Duncan. “Numerical stability of collocation schemes for time domain boundary integral equations”. In: *Computational Electromagnetics: Proceedings of the GAMM Workshop on Computational Electromagnetics, Kiel, Germany, January 26–28, 2001*. Springer. 2003, pp. 51–67.

[56] J. Degroote. “On the similarity between Dirichlet-Neumann with interface artificial compressibility and Robin-Neumann schemes for the solution of fluid-structure interaction problems”. In: *Journal of computational physics* 230.17 (2011), pp. 6399–6403.

[57] J. Degroote, K.-J. Bathe, and J. Vierendeels. "Performance of a new partitioned procedure versus a monolithic procedure in fluid–structure interaction". In: *Computers & Structures* 87.11-12 (2009), pp. 793–801.

[58] N. Delaissé, T. Demeester, R. Haelterman, and J. Degroote. "Quasi-Newton Methods for Partitioned Simulation of Fluid–Structure Interaction Reviewed in the Generalized Broyden Framework". In: *Archives of Computational Methods in Engineering* (2023), pp. 1–30.

[59] B. Després. "Domain decomposition method and the Helmholtz problem." In: *Mathematical and Numerical Aspects of Wave Propagation Phenomena* (1991), pp. 44–52.

[60] B. Després. "Méthodes de décomposition de domaine pour la propagation d'ondes en régime harmonique. Le théorème de Borg pour l'équation de Hill vectorielle". PhD thesis. 1991.

[61] B. Després. "Domain decomposition method and the Helmholtz problem. II." In: *Second international conference on mathematical and numerical aspects of wave propagation* (1993), pp. 197–206.

[62] B. Després, P. Joly, and J. E. Roberts. "A domain decomposition method for the harmonic Maxwell equations". In: *Iterative methods in linear algebra* (1992), pp. 475–484.

[63] M. Discacciati and T. Vanzan. "Optimized Schwarz methods for the time-dependent Stokes-Darcy coupling". In: *arXiv preprint arXiv:2305.07379* (2023).

[64] EDF R&D Code Aster documentation. *Code Aster Open Source. General FEA software*. Open source on www.code-aster.org. 2020. URL: https://www.code-aster.org/V2/doc/default/en/index.php?man=commande.

[65] V. Dolean, M. J. Gander, and L. Gerardo-Giorda. "Optimized Schwarz methods for Maxwell's equations". In: *SIAM Journal on Scientific Computing* 31.3 (2009), pp. 2193–2213.

[66] V. Dolean, P. Jolivet, and F. Nataf. "An Introduction to Domain Decomposition Methods: algorithms, theory and parallel implementation". Master. Lecture. France, Jan. 2015.

[67] T. Ha-Duong, B. Ludwig, and I. Terrasse. "A Galerkin BEM for transient acoustic scattering by an absorbing obstacle". In: *International Journal for Numerical Methods in Engineering* 57.13 (2003), pp. 1845–1882.

[68] B. Engquist and A. Majda. "Absorbing boundary conditions for numerical simulation of waves". In: *Proceedings of the National Academy of Sciences* 74.5 (1977), pp. 1765–1766.

[69] L. C. Evans. *Partial differential equations*. Vol. 19. American Mathematical Society, 2022.

[70] G. C. Everstine. "A symmetric potential formulation for fluid-structure interaction". In: *Journal of Sound and Vibration* 79 (1981), pp. 157–160.

[71] G. C. Everstine and F. M. Henderson. "Coupled finite element/boundary element approach for fluid–structure interaction". In: *The Journal of the Acoustical Society of America* 87.5 (1990), pp. 1938–1947.

[72] T. Fabbri. “Développement d’un solveur haute fidélité d’interaction fluide-structure: vers la simulation de profils flexibles”. PhD thesis. Université Grenoble Alpes, 2022.

[73] J. A. Fawcett. “A scattering-chamber approach for solving finite rough surface scattering problems”. In: *The Journal of the Acoustical Society of America* 118.3 (2005), pp. 1348–1357.

[74] C. A. Felippa, K. C. Park, and C. Farhat. “Partitioned analysis of coupled mechanical systems”. In: *Computer Methods in Applied Mechanics and Engineering* 190 (2001), pp. 3247–3270.

[75] M. A. Fernández. “Coupling schemes for incompressible fluid-structure interaction: implicit, semi-implicit and explicit”. In: 55.1 (2011), pp. 59–108.

[76] M. A. Fernández, J. Mullaert, and M. Vidrascu. “Explicit Robin–Neumann schemes for the coupling of incompressible fluids with thin-walled structures”. In: *Computer Methods in Applied Mechanics and Engineering* 267 (2013), pp. 566–593.

[77] M. Fischer, U. Gauger, and L. Gaul. “A multipole Galerkin boundary element method for acoustics”. In: *Engineering analysis with boundary elements* 28.2 (2004), pp. 155–162.

[78] M. Gander. “Schwarz methods over the course of time”. In: *ETNA. Electronic Transactions on Numerical Analysis [electronic only]* 31 (Jan. 2008).

[79] M. Gander, L. Halpern, and F. Magoules. “An optimized Schwarz method with two-sided Robin transmission conditions for the Helmholtz equation”. In: *International journal for numerical methods in fluids* 55.2 (2007), pp. 163–175.

[80] M. Gander, L. Halpern, and F. Nataf. “Optimal Schwarz waveform relaxation for the one dimensional wave equation”. In: *SIAM Journal on Numerical Analysis* 41.5 (2003), pp. 1643–1681.

[81] M. J. Gander, L. Halpern, and F. Nataf. “Optimal convergence for overlapping and non-overlapping Schwarz waveform relaxation”. In: *Eleventh international Conference of Domain Decomposition Methods. ddm. org*. 1999.

[82] M. J. Gander, F. Kwok, and B. Mandal. “Dirichlet-Neumann and Neumann-Neumann waveform relaxation algorithms for parabolic problems”. In: *arXiv preprint arXiv:1311.2709* (2013).

[83] M. J. Gander and V. Martin. “Why Fourier mode analysis in time is different when studying Schwarz Waveform Relaxation”. In: *Journal of Computational Physics* 491 (2023), p. 112316.

[84] M. J. Gander and A. M. Stuart. “Space-time continuous analysis of waveform relaxation for the heat equation”. In: *SIAM Journal on Scientific Computing* 19.6 (1998), pp. 2014–2031.

[85] T. L. Geers and K. S. Hunter. “An integrated wave-effects model for an underwater explosion bubble”. In: *Journal of the Acoustical Society of America* 111.4 (2002), pp. 1584–1601.

[86] L. Gerardo-Giorda, F. Nobile, and C. Vergara. "Analysis and optimization of Robin-Robin partitioned procedures in fluid-structure interaction problems". In: *SIAM Journal on Numerical Analysis* 48.6 (2010), pp. 2091–2116.

[87] G. Gigante, M. Pozzoli, and C. Vergara. "Optimized Schwarz methods for the diffusion-reaction problem with cylindrical interfaces". In: *SIAM Journal on Numerical Analysis* 51.6 (2013), pp. 3402–3430.

[88] G. Gigante, G. Sambataro, and C. Vergara. "Optimized Schwarz Methods for Spherical Interfaces With Application to Fluid-Structure Interaction". In: *SIAM Journal on Scientific Computing* 42.2 (2020), A751–A770.

[89] G. Gigante and C. Vergara. "On the choice of interface parameters in Robin-Robin loosely coupled schemes for fluid–structure interaction". In: *Fluids* 6.6 (2021), p. 213.

[90] E. Giladi and H. B. Keller. "Space-time domain decomposition for parabolic problems". In: *Numerische Mathematik* 93 (2002), pp. 279–313.

[91] J. A. Goldstein. *Semigroups of linear operators and applications*. Oxford University Press, 1985.

[92] P. Gosselet, M. Blanchard, O. Allix, and G. Guguin. "Non-invasive global–local coupling as a Schwarz domain decomposition method: acceleration and generalization". In: *Advanced Modeling and Simulation in Engineering Sciences* 5.1 (2018), p. 4.

[93] P. Gosselet and C. Rey. "Non-overlapping domain decomposition methods in structural mechanics". In: *Archives of computational methods in engineering* 13 (2006), pp. 515–572.

[94] D. Graham, J. Hobson, P. Murphy, C. Toole, S. Cross, and J. Farnworth. "Efficient modelling of the structural response of submarine pressure hulls to underwater explosions". In: *Warship 2017: Naval Submarines & UUVs, The Royal Institution of Naval Architects* 9 (2017), p. 81.

[95] L. Greengard and V. Rokhlin. "A fast algorithm for particle simulations". In: *Journal of computational physics* 73.2 (1987), pp. 325–348.

[96] S. Güttel. "A parallel overlapping time-domain decomposition method for ODEs". In: *Domain decomposition methods in science and engineering XX*. Springer, 2013, pp. 459–466.

[97] W. Hackbusch. "Sparse matrix arithmetic based on H-matrices. Part I: Introduction to H-matrices". In: *Computing (Vienna/New York)* 62.2 (1999), pp. 89–108.

[98] W. Hackbusch, W. Kress, and S. A. Sauter. "Sparse convolution quadrature for time domain boundary integral formulations of the wave equation". In: *IMA journal of numerical analysis* 29.1 (2009), pp. 158–179.

[99] L. Halpern, C. Japhet, and J. Szeftel. "Optimized Schwarz waveform relaxation and discontinuous Galerkin time stepping for heterogeneous problems". In: *SIAM Journal on Numerical Analysis* 50.5 (2012), pp. 2588–2611.

[100] L. Halpern and J. Szeftel. “Optimized and quasi-optimal Schwarz waveform relaxation for the one-dimensional Schrödinger equation”. In: *Mathematical Models and Methods in Applied Sciences* 20.12 (2010), pp. 2167–2199.

[101] M. A. Hamdi and P. Jean. “A Mixed Functional for the Numerical Resolution of Fluid-Structure Interaction Problems”. In: *Aero- and Hydro-Acoustics*. Ed. by Geneviève Comte-Bellot and John E. Ffowcs Williams. Berlin, Heidelberg: Springer Berlin Heidelberg, 1986, pp. 269–276.

[102] R. D. Haynes and K. Mohammad. “Fully discrete Schwarz waveform relaxation on two bounded overlapping subdomains”. In: *Domain Decomposition Methods in Science and Engineering XXV 25*. Springer. 2020, pp. 159–166.

[103] R. O. Hein Hoernig. “Green’s functions and integral equations for the Laplace and Helmholtz operators in impedance half-spaces”. PhD thesis. Ecole Polytechnique, 2010.

[104] T. Hoang, J. Jaffré, C. Japhet, M. Kern, and J. E. Roberts. “Space-time domain decomposition methods for diffusion problems in mixed formulations”. In: *SIAM Journal on Numerical Analysis* 51.6 (2013), pp. 3532–3559.

[105] S. Hoerner. “Caractérisation d’interaction fluide-structure pour une hydrolienne à voilure déformable”. PhD thesis. Université Grenoble Alpes, 2020.

[106] G. Horton, S. Vandewalle, and P. Worley. “An algorithm with polylog parallel complexity for solving parabolic partial differential equations”. In: *SIAM Journal on Scientific Computing* 16.3 (1995), pp. 531–541.

[107] G. C. Hsiao. “On the boundary-field equation methods for fluid-structure interactions”. In: *Problems and methods in mathematical physics* (1994), pp. 79–88.

[108] G. C. Hsiao, R. E. Kleinman, and G. F. Roach. “Weak solutions of fluid–solid interaction problems”. In: *Mathematische Nachrichten* 218.1 (2000), pp. 139–163.

[109] G. C. Hsiao, F.-J. Sayas, and R. J. Weinacht. “Time-dependent fluid-structure interaction”. In: *Mathematical Methods in the Applied Sciences* 40.2 (2017), pp. 486–500.

[110] S. Imperiale. “Modélisation mathématique et numérique de capteurs piézoélectriques”. PhD thesis. Paris 9, 2012.

[111] B. M. Irons and R. C. Tuck. “A version of the Aitken accelerator for computer iteration”. In: *International Journal for Numerical Methods in Engineering* 1.3 (1969), pp. 275–277.

[112] C. Japhet and F. Nataf. “The best interface conditions for domain decomposition methods: absorbing boundary conditions”. In: *Absorbing boundaries and layers, domain decomposition methods* (2001), pp. 348–373.

[113] C. Japhet, F. Nataf, and F. Rogier. “The optimized order 2 method: Application to convection–diffusion problems”. In: *Future generation computer systems* 18.1 (2001), pp. 17–30.

[114] P. Joly. *Analyse et approximation de modèles de propagation d’ondes. Analyse mathématique. Lecture notes,Ecole polytechnique, Palaiseau, France*. 2002.

[115] L. Khoun. “Réduction de modèles pour les problèmes vibro-acoustique transitoires paramétriques. Application aux problèmes de pré-dimensionnement de structures immergées aux ondes de choc d’explosion”. PhD thesis. 2021.

[116] R. Kiciński and B. Szturomski. “Pressure wave caused by trinitrotoluene (TNT) underwater explosion—short review”. In: *Applied Sciences* 10.10 (2020), p. 3433.

[117] Y. Kim, K.-H. Kim, and Y. Kim. “Analysis of hydroelasticity of floating shiplike structure in time domain using a fully coupled hybrid BEM-FEM”. In: *Journal of Ship Research* 53.01 (2009), pp. 31–47.

[118] S. Koc and W. C. Chew. “Calculation of acoustical scattering from a cluster of scatterers”. In: *The Journal of the Acoustical Society of America* 103.2 (1998), pp. 721–734.

[119] U. Küttler and W. A. Wall. “Fixed-point fluid–structure interaction solvers with dynamic relaxation”. In: *Computational Mechanics* 43 (2008), pp. 61–72.

[120] I. Labarca, L. M Faria, and C. Pérez-Arancibia. “Convolution quadrature methods for time-domain scattering from unbounded penetrable interfaces”. In: *Proceedings of the Royal Society A* 475.2227 (2019), p. 20190029.

[121] J. C. Lachat and J. O. Watson. “Effective numerical treatment of boundary integral equations: A formulation for three-dimensional elastostatics”. In: *International Journal for Numerical Methods in Engineering* 10.5 (1976), pp. 991–1005.

[122] P. Ladevèze, J. C. Passieux, and D. Néron. “The LATIN multiscale computational method and the Proper Generalized Decomposition”. In: *Computer Methods in Applied Mechanics and Engineering* 199.21-22 (2010), pp. 1287–1296.

[123] I. Lasiecka, J.-L. Lions, and R. Triggiani. “Non homogeneous boundary value problems for second order hyperbolic operators”. In: *J. Math. Pures Appl.* 65 (1986), pp. 149–192.

[124] I. Lasiecka and R. Triggiani. “Sharp regularity theory for second order hyperbolic equations of Neumann type - Part I. -L2 nonhomogeneous data”. In: *Annali di Matematica Pura ed Applicata* 157.1 (1990), pp. 285–367.

[125] I. Lasiecka and R. Triggiani. “Regularity theory of hyperbolic equations with non-homogeneous Neumann boundary conditions. II. General boundary data”. In: *Journal of Differential Equations* 94.1 (1991), pp. 112–164.

[126] C. Leblond. “Modélisation de phénomènes fortement instationnaires en milieux couplés: application au dimensionnement de structures immergées aux explosions sous-marines”. PhD thesis. Nantes, 2007.

[127] M. Lecouvez. “Méthodes itératives de décomposition de domaine sans recouvrement avec convergence géométrique pour l’equation de Helmholtz”. PhD thesis. Ecole Polytechnique, 2015.

[128] E. Lelarasmee, A. E. Ruehli, and A. L. Sangiovanni-Vincentelli. "The waveform relaxation method for time-domain analysis of large scale integrated circuits". In: *IEEE transactions on computer-aided design of integrated circuits and systems* 1.3 (1982), pp. 131–145.

[129] P. Li and L. Zhang. "Analysis of transient acoustic scattering by an elastic obstacle". In: *arXiv preprint arXiv:1811.12480* (2018).

[130] J. L. Lions. *Contrôlabilité exacte. Perturbation et stabilisation de systèmes distribués. Tome 1: contrôlabilité exacte*. Masson, 1984.

[131] J.L. Lions and E. Magenes. *Non-homogeneous boundary value problems and applications: Vol. 1*. Grundlehren der mathematischen Wissenschaften. Springer Berlin Heidelberg, 2012.

[132] P. L. Lions. "On the Schwarz Alternating Method III: A Variant for Nonoverlapping Subdomains". In: *Third International Symposium on Domain Decomposition Methods for Partial Differential Equations*. Ed. by T. Chan, R. Glowinski, J. Périaux, and O. Widlund. SIAM Philadelphia. 1990. Chap. 11, pp. 202–223.

[133] P.L. Lions. "On the Schwartz alternating method 1." In: *First international symposium on domain decomposition methods for partial differential equations* (1988).

[134] X. Liu, H. Wu, R. Sun, and W. Jiang. "A fast multipole boundary element method for half-space acoustic problems in a subsonic uniform flow". In: *Engineering Analysis with Boundary Elements* 137 (2022), pp. 16–28.

[135] B. Lizé. "Résolution directe rapide pour les éléments finis de frontière en électromagnétisme et acoustique: -Matrices. Parallélisme et applications industrielles". PhD thesis. Université Paris-Nord-Paris XIII, 2014.

[136] P. Longère, A.-G. Geffroy-Grèze, B. Leblé, and A. Dragon. "Ship structure steel plate failure under near-field air-blast loading: Numerical simulations vs experiment". In: *International Journal of Impact Engineering* 62 (2013), pp. 88–98.

[137] M. Lopez-Fernandez and S. Sauter. "Generalized convolution quadrature with variable time stepping". In: *IMA Journal of Numerical Analysis* 33.4 (2013), pp. 1156–1175.

[138] Z. Lu and A. Brown. "Application of the Spectral Element Method in a Surface Ship Far-Field UNDEX Problem". In: *Shock and Vibration* (July 2019), pp. 1–16.

[139] C. Lubich. *Convolution quadrature and discretized operational calculus I. Numer.* Math, 52 :129 – 145, 1988.

[140] C. Lubich and R. Schneider. "Time discretization of parabolic boundary integral equations". In: *Numerische Mathematik* 63.1 (1992), pp. 455–481.

[141] C. J. Luke and P. A. Martin. "Fluid-solid interaction: acoustic scattering by a smooth elastic obstacle". In: *SIAM Journal on Applied Mathematics* 55.4 (1995), pp. 904–922.

[142] F. Magoules, P. Iványi, and B. H. V. Topping. "Non-overlapping Schwarz methods with optimized transmission conditions for the Helmholtz equation". In: *Computer Methods in Applied Mechanics and Engineering* 193.45-47 (2004), pp. 4797–4818.

[143] W. J. Mansur. "A time-stepping technique to solve wave propagation problems using the boundary element method". PhD thesis. University of Southampton, 1983.

[144] N. Marsic, C. Waltz, J.-F. Lee, and C. Geuzaine. "Domain decomposition methods for time-harmonic electromagnetic waves with high-order Whitney forms". In: *IEEE Transactions on Magnetics* 52.3 (2015), pp. 1–4.

[145] V. Martin. "Méthodes de décomposition de domaine de type relaxation d'ondes pour des équations de l'océanographie". PhD thesis. Université Paris-Nord-Paris XIII, 2003.

[146] D. Mavaleix-Marchessoux. "Modelling the fluid-structure coupling caused by a far-field underwater explosion". PhD thesis. Hadamard Doctoral School of Mathematics (EDMH), 2020.

[147] D. Mavaleix-Marchessoux, M. Bonnet, S. Chaillat, and B. Leblé. "A fast boundary element method using the Z-transform and high-frequency approximations for large-scale 3D transient wave problems". In: *International Journal for Numerical Methods in Engineering* 121 (2020), pp. 4734–4767.

[148] W. McLean. *Strongly elliptic systems and boundary integral equations*. Cambridge university press, 2000.

[149] M. Merta and J. Zapletal. "A parallel library for boundary element discretization of engineering problems". In: *Mathematics and Computers in Simulation* 145 (2018), pp. 106–113.

[150] A. Messaoudi, R. Cottereau, and C. Gomez. "Boundary effects in radiative transfer of acoustic waves in a randomly fluctuating half-space". In: *Multiscale Modeling & Simulation* 21.3 (2023), pp. 1299–1321.

[151] T. Moyer, J. Stergiou, G. Reese, J. Luton, and N. Abboud. "Navy enhanced sierra mechanics (NESM): toolbox for predicting navy shock and damage". In: *Computing in Science & Engineering* 18.6 (2016), pp. 10–18.

[152] F. Nataf. *Absorbing boundary conditions and perfectly matched layers in wave propagation problems*. 2013.

[153] F. Nataf, F. Rogier, and E. de Sturler. "Optimal interface conditions for domain decomposition methods". PhD thesis. CMAP Ecole Polytechnique, 1994.

[154] J.C. Nédélec, T. Abboud, and J. Volakis. "Stable solution of the retarded potential equations, Applied Computational Electromagnetics Society (ACES) Symposium Digest". In: *17th Annual Review of Progress, Monterey* (2001).

[155] D. Néron. "Sur une stratégie de calcul pour les problèmes multiphysiques". PhD thesis. École normale supérieure de Cachan, 2004.

[156] M. Neumüller. "Space-Time methods: fast solvers and applications". PhD thesis. University of Graz, 2013.

[157] N. Nishimura. "Fast multipole accelerated boundary integral equation methods". In: *Applied Mechanics Reviews* 55.4 (2002), pp. 299–324.

[158] F. Nobile, M. Pozzoli, and C. Vergara. "Time accurate partitioned algorithms for the solution of fluid–structure interaction problems in haemodynamics". In: *Computers & Fluids* 86 (2013), pp. 470–482.

[159] F. Nobile and C. Vergara. "An effective fluid-structure interaction formulation for vascular dynamics by generalized Robin conditions". In: *SIAM Journal on Scientific Computing* 30.2 (2008), pp. 731–763.

[160] F. Nobile and C. Vergara. "Partitioned algorithms for fluid-structure interaction problems in haemodynamics". In: *Milan journal of mathematics* 80.2 (2012), pp. 443–467.

[161] O. O'Reilly, E. M. Dunham, and J. Nordström. "Simulation of Wave propagation along fluid-filled cracks using high-order summation-by-parts operators and implicit-explicit time stepping". In: *SIAM Journal on Scientific Computing* 39.4 (2017).

[162] A. R. Okoyenta, H. Wu, X. Liu, and W. Jiang. "A short survey on Green's function for acoustic problems". In: *Journal of Theoretical and Computational Acoustics* 28.02 (2020), p. 1950025.

[163] F.W.J. Olver, D. W. Lozier, R. F. Boisvert, and C. W. Clark. *NIST handbook of mathematical functions*. Cambridge university press, 2010.

[164] B. W. Ong and J. B. Schroder. "Applications of time parallelization". In: *Computing and Visualization in Science* 23 (2020), pp. 1–15.

[165] P. Oumaziz, P. Gosselet, P.-A. Boucard, and S. Guinard. "A parallel non-invasive mixed domain decomposition-Implementation and applications to mechanical assemblies". In: *Finite Elements in Analysis and Design* 156 (2019), pp. 24–33.

[166] B. Overpelt, B. Nienhuis, B. Anderson, et al. "Free running manoeuvring model tests on a modern generic SSK class submarine (BB2)". In: *Pacific International Maritime Conference*. 2015, pp. 1–14.

[167] E. Parolin. "Non-overlapping domain decomposition methods with non-local transmission operators for harmonic wave propagation problems". PhD thesis. Hadamard Doctoral School of Mathematics (EDMH), 2020.

[168] E. Picard. "Sur l'application des méthodes d'approximations successives à l'étude de certaines équations différentielles ordinaires". In: *Journal de mathématiques pures et appliquées* 9 (1893), pp. 217–271.

[169] J. Qiankun and D. Gangyi. "A finite element analysis of ship sections subjected to underwater explosion". In: *International Journal of Impact Engineering* 38.7 (2011), pp. 558–566.

[170] A. Quarteroni and A. Valli. *Domain decomposition methods for partial differential equations*. BOOK. Oxford University Press, 1999.

[171] Q. Rakotomalala, C. Leblond, G. Dolo, J.-F. Deü, and L. Rouleau. "Approche fluide-structure pour l'analyse vibratoire des pales d'un propulseur". In: *15ème colloque national en calcul des structures*. 2022.

[172] F. J. Rizzo. "An integral equation approach to boundary value problems of classical elastostatics". In: *Quarterly of Applied Mathematics* 25.1 (1967), pp. 83–95.

[173] Y. Saad. *Iterative Methods for Sparse Linear Systems: Second Edition*. Other Titles in Applied Mathematics. SIAM, Philadelphia, PA, 2003.

[174] Y. Saad and M. H. Schultz. "GMRES: A Generalized Minimal Residual Algorithm for Solving Nonsymmetric Linear Systems". In: *SIAM Journal on Scientific and Statistical Computing* 7.3 (July 1986), pp. 856–869.

[175] P. Saha, J. Stadel, and S. Tremaine. "A parallel integration method for solar system dynamics". In: *arXiv preprint astro-ph/9605016* (1996).

[176] T. K. Sarkar, W. Lee, and S. M. Rao. "Analysis of transient scattering from composite arbitrarily shaped complex structures". In: *IEEE Transactions on Antennas and Propagation* 48.10 (2000), pp. 1625–1634.

[177] S. Sauter and A. Veit. "A Galerkin method for retarded boundary integral equations with smooth and compactly supported temporal basis functions". In: *Numerische Mathematik* 123.1 (2013), pp. 145–176.

[178] F.J. Sayas. *Retarded Potentials and Time Domain Boundary Integral Equations: A Road Map*. Springer Series in Computational Mathematics. Springer International Publishing, 2016.

[179] M. Schanz and H. Antes. "A new visco- and elastodynamic time domain boundary element formulation". In: *Computational Mechanics* 20.5 (1997), pp. 452–459.

[180] H. A. Schwarz. *Ueber einen Grenzübergang durch alternirendes Verfahren*. Zürcher u. Furrer, 1870.

[181] A. F. Seybert and B. Soenarko. "Radiation and scattering of acoustic waves from bodies of arbitrary shape in a three-dimensional half space". In: (1988).

[182] R. Seznec. "Diffraction of sound around barriers: use of the boundary elements technique". In: *Journal of sound and vibration* 73.2 (1980), pp. 195–209.

[183] J.-F. Sigrist. *Fluid-Structure interaction - An introduction to finite element coupling*. Vol. 4. 3. John Wiley & Sons, Ltd, 2015, pp. 57–71.

[184] V. Simoncini and E. Gallopoulos. "An iterative method for nonsymmetric systems with multiple right-hand sides". In: *SIAM Journal on Scientific Computing* 16.4 (1995), pp. 917–933.

[185] V. Sladek, J. Sladek, and M. Tanaka. "Numerical integration of logarithmic and nearly logarithmic singularity in BEMs". In: *Applied Mathematical Modelling* 25.11 (2001), pp. 901–922.

[186] H. G. Snay. "Hydrodynamics of underwater explosions". In: *Symposium on naval hydrodynamics*. Vol. 515. 1957, pp. 325–346.

[187] T. Spenke, N. Delaissé, J. Degroote, and N. Hosters. "On the number of subproblem iterations per coupling step in partitioned fluid-structure interaction simulations". In: *arXiv preprint arXiv:2303.08513* (2023).

[188] T. Spenke, M. Make, and N. Hosters. "A Robin-Neumann scheme with quasi-Newton acceleration for partitioned fluid-structure interaction". In: *International Journal for Numerical Methods in Engineering* 124.4 (2023), pp. 979–997.

[189] B. Stupfel. "Improved transmission conditions for a one-dimensional domain decomposition method applied to the solution of the Helmholtz equation". In: *Journal of Computational Physics* 229.3 (2010), pp. 851–874.

[190] A. Sutradhar, G. Paulino, and L. J Gray. *Symmetric Galerkin boundary element method*. Springer Science & Business Media, 2008.

[191] T. Takahashi, N. Nishimura, and S. Kobayashi. "A fast BIEM for three-dimensional elastodynamics in time domain". In: *Engineering analysis with boundary elements* 27.5 (2003), pp. 491–506.

[192] V. Temtching Temou, B. Augier, and B. Paillard. "Hydro-elastic response of composite hydrofoil with FSI". In: *Ocean Engineering* 221 (2021), p. 108230.

[193] S. Thery. "On the links between observed and theoretical convergence rates for Schwarz waveform relaxation algorithm for the time-dependent problems". In: *Domain Decomposition Methods in Science and Engineering XXVI*. Springer, 2023, pp. 571–578.

[194] R. Triggiani. "Sharp regularity theory of second order hyperbolic equations with Neumann boundary control non-smooth in space." In: *Evolution Equations & Control Theory* 5.4 (2016).

[195] S. Vandewalle and E. Van de Velde. "Space-time concurrent multigrid waveform relaxation". In: *Annals of Numerical Mathematics* 1.1 (1994), pp. 335–346.

[196] F. Vannucchi de Camargo. "Survey on experimental and numerical approaches to model underwater explosions". In: *Journal of Marine Science and Engineering* 7.1 (2019), p. 15.

[197] E. Veron. "Calcul numérique des grandes déformations de structures minces en contact avec des fluides lourds". PhD thesis. 2016.

[198] A. Vion and C. Geuzaine. "Parallel double sweep preconditioner for the optimized Schwarz algorithm applied to high frequency Helmholtz and Maxwell equations". In: *Domain Decomposition Methods in Science and Engineering XXII*. Springer. 2016, pp. 239–247.

[199] K. G. Wang, P. Lea, A. Main, O. McGarity, and C. Farhat. "Predictive simulation of underwater implosion: Coupling multi-material compressible fluids with cracking structures". In: *International Conference on Offshore Mechanics and Arctic Engineering*. Vol. 45509. American Society of Mechanical Engineers. 2014.

[200] D. R. Wilkes, A. J. Duncan, and S. Marburg. "A Parallel and Broadband Helmholtz FMBEM Model for Large-Scale Target Strength Modeling". In: *Journal of Theoretical and Computational Acoustics* 28.03 (2020), p. 2050001.

[201] S. L Wood. *Cavitation Effects on a Ship-Like Box Structure Subjected to an Underwater Explosion.* Tech. rep. Naval Postgraduate school Monterey, 1998.

[202] H. Wu, Y. Liu, W. Jiang, and W. Lu. “A fast multipole boundary element method for three-dimensional half-space acoustic wave problems over an impedance plane”. In: *International Journal of Computational Methods* 12.01 (2015), p. 1350090.

Appendices

A Semi-analytical solution for a radially symmetric 2D test case

A.1 Acoustic-elastic analytical solution

In Section 3.3, we consider the radially symmetric 2D annular elastic solid represented on Figure 3.4. This elastic ring Ω_s of interior and exterior radius R_{int} and R_{ext} is immersed in a acoustic fluid (mass density ρ_f, acoustic wave velocity c_f) occupying the unbounded fluid region $\Omega_f := \mathbb{R}^2 \setminus \overline{\Omega_s}$. We assume 2D conditions and plane strain deformations for the solid. Both media are at initial rest. A uniform internal pressure $p^{int}(t)$ is prescribed on the interior surface Γ_{int}, which creates a deformation in the elastic solid and a radiated FSI problem on the exterior interface. This coupled FSI problem admits a known semi-analytical solution. The potential fluid has a time dependent velocity potential $\phi(t)$, a velocity $\mathbf{v}(t) = \nabla\phi(t)$ and a pressure $p(t) = -\rho_f \partial_t \phi(t)\ \forall t \in [0, T]$. The solid variables are the displacement $\mathbf{u}$ and the stress vector $\mathbf{t} := \sigma[\mathbf{u}].\mathbf{n}$.

Semi-analytical coupled solution. Semi-analytical solutions are often used in the UNDEX field. The method consists in solving a wave equation with a decomposition of the solution on an infinite base of Bessel's functions. Each coefficient of the decomposition verifies the equation, and the solution is then approximated with a truncated summation. An example in the context of UNDEX is given by [126]. For an elastic annulus of interior and exterior radius a and b, embedded in an unbounded acoustic fluid, the solid displacement u and fluid velocity potential ϕ verify the following system of equations:

$$\begin{cases} \Delta\phi - \dfrac{1}{c_f^2}\partial_{tt}\phi = 0 & \text{in } \Omega_f \times [0,T] \\ \dfrac{\partial^2 u}{\partial r^2} + \dfrac{1}{r}\dfrac{\partial u}{\partial r} - \dfrac{u}{r^2} = \dfrac{1}{c_1^2}\dfrac{\partial^2 u}{\partial t^2} & \text{in } \Omega_s \times [0,T] \\ \left[\dfrac{\lambda}{\nu}\left((1-\nu)\dfrac{\partial u}{\partial r} + \nu\dfrac{u}{r}\right)\right](a,t) = -p^{int}(t) & \text{on } \Gamma^{int} \times [0,T] \\ \left[\dfrac{\lambda}{\nu}\left((1-\nu)\dfrac{\partial u}{\partial r} + \nu\dfrac{u}{r}\right)\right](b,t) = -\rho_f \partial_t\phi(b,t) & \text{on } \Gamma \times [0,T] \\ \partial_t u(b,t) = \partial_r \phi(b,t) & \text{on } \Gamma \times [0,T] \end{cases}$$

where λ, μ are the Lamé elastic constants, $c_1 = \sqrt{(\lambda + 2\mu)/\rho_s}$ is the compression

wave velocity. By taking the Laplace transform, the system becomes

$$\begin{cases} \Delta\overline{\phi} - \dfrac{1}{c_f^2}s^2\overline{\phi} = 0 & \text{in } \Omega_f \qquad (a) \\ \dfrac{\partial^2\overline{u}}{\partial r^2} + \dfrac{1}{r}\dfrac{\partial\overline{u}}{\partial r} - \dfrac{\overline{u}}{r^2} = \dfrac{1}{c_1^2}s^2\overline{u} & \text{in } \Omega_s \qquad (b) \\ \left[\dfrac{\lambda}{\nu}\left((1-\nu)\dfrac{\partial\overline{u}}{\partial r} + \nu\dfrac{\overline{u}}{r}\right)\right](a,s) = -\overline{p}^{int}(s) & \text{on } \Gamma^{\text{int}} \qquad (c) \\ \left[\dfrac{\lambda}{\nu}\left((1-\nu)\dfrac{\partial\overline{u}}{\partial r} + \nu\dfrac{\overline{u}}{r}\right)\right](b,s) = -\rho_f s\overline{\phi}(b,s) & \text{on } \Gamma \qquad (d) \\ s\overline{u}(b,s) = \partial_r\overline{\phi}(b,s) & \text{on } \Gamma \qquad (e) \end{cases}$$

where $\overline{p}, \overline{u}$ and $\overline{\phi}$ are the Laplace transforms of p, u and ϕ. The second-order homogeneous differential equations (a) and (b) are the modified Bessel equations of order 1 and 0, respectively, such that

$$\overline{u}(r,s) = A(s)I_1(\frac{rs}{c}) + B(s)K_1(\frac{sr}{c}), \quad \overline{\phi}(r,s) = C(s)K_0(\frac{sr}{c}) \tag{6}$$

with $\overline{\phi}$ containing no term with I_0 to enforce its decay as $r \to \infty$ and where I_1, K_1, K_0 are modified Bessel functions. The variables of the coupled problem expressed with the modified Bessel functions are:

$$\begin{cases} \overline{u}_0(r,s) = A_0 I_1(\frac{sr}{c}) + B_0 K_1(\frac{sr}{c}) \\ \overline{p}_0(r,s) = -\rho_f s C_0 K_0(\frac{sr}{c_f}) \\ \overline{v}_0(r,s) = \partial_r\overline{\phi}(r,s) = -\frac{s}{c_f}C_0 K_1(\frac{sr}{c_f}) \\ \overline{t}_0(r,s) = A_0[\frac{\lambda}{\nu}(1-\nu)\frac{s}{c}I_1'(\frac{sr}{c}) + \frac{\lambda}{r}I_1(\frac{sr}{c})] + B_0[\frac{\lambda}{\nu}(1-\nu)\frac{s}{c}K_1'(\frac{sr}{c}) + \frac{\lambda}{r}K_1(\frac{sr}{c})] \end{cases}$$

with $c^2 = \frac{\lambda(1-\nu)}{\lambda\rho_s}$. The boundary condition (c) and kinematic and dynamic conditions (d) and (e) imply that the constants A, B and C solve the equations:

$$\begin{cases} \frac{\lambda}{\nu}(1-\nu)\left[A(s)\frac{s}{c}I_1'\left(\frac{sa}{c}\right) + B(s)\frac{s}{c}K_1'(\frac{sa}{c})\right] + \frac{\lambda}{a}\left[A(s)I_1\left(\frac{sa}{c}\right) + B(s)K_1\left(\frac{sa}{c}\right)\right] = -\overline{p}^{int}(s) \\ \frac{\lambda}{\nu}(1-\nu)\left[A(s)\frac{s}{c}I_1'\left(\frac{sb}{c}\right) + B(s)\frac{s}{c}K_1'(\frac{sb}{c})\right] + \frac{\lambda}{b}\left[A(s)I_1\left(\frac{sb}{c}\right) + B(s)K_1\left(\frac{sb}{c}\right)\right] = -\rho_f C(s)\frac{b}{c_f}K_1\left(\frac{sb}{c_f}\right) \\ sA(s)I_1(\frac{sb}{c}) + sB(s)K_1\left(\frac{sb}{c}\right) = -C(s)\frac{s}{c_f}K_1\left(\frac{sb}{cf}\right) \end{cases}$$

that correspond to the matrix system:

$$[M]\begin{bmatrix} A(s) \\ B(s) \\ C(s) \end{bmatrix} = \begin{bmatrix} -\overline{p}^{int}(s)) \\ 0 \\ 0 \end{bmatrix} \tag{7}$$

with $[M]$ defined by

$$[M] = \begin{bmatrix} \frac{\lambda}{\nu}(1-\nu)\frac{s}{c}I_1'\left(\frac{sa}{c}\right) + \frac{\lambda}{a}I_1\left(\frac{sa}{c}\right) & \frac{\lambda}{\nu}(1-\nu)\frac{s}{c}K_1'\left(\frac{sa}{c}\right) + \frac{\lambda}{a}K_1\left(\frac{sa}{c}\right) & 0 \\ \frac{\lambda}{\nu}(1-\nu)\frac{s}{c}I_1'\left(\frac{sb}{c}\right) + \frac{\lambda}{b}I_1\left(\frac{sb}{c}\right) & \frac{\lambda}{\nu}(1-\nu)\frac{s}{c}K_1'\left(\frac{sb}{c}\right) + \frac{\lambda}{b}K_1\left(\frac{sb}{c}\right) & -s\rho_f K_0\left(\frac{sb}{c_f}\right) \\ c_f I_1\left(\frac{sb}{c}\right) & c_f K_1\left(\frac{sb}{c}\right) & K_1\left(\frac{sb}{c_f}\right) \end{bmatrix}$$

We will denote $[P] := \left\{-\overline{p}^{int}(s); 0; 0\right\}$. We then use the relations

$$K_0'(z) = -K_1(z), I_1'(z) = I_0(z) - \frac{1}{z}I_1(z) \text{ and } K_1'(z) = -K_0(z) - \frac{1}{z}K_1(z)$$

Moreover, the modified Bessel functions admit the large-argument expansions (see [163], Sec 10.40):

$$I_n(z) = \frac{e^z}{(2\pi z)^{1/2}}\left(1 + O\left(\frac{1}{z}\right)\right), K_n(z) = \frac{\pi e^{-z}}{(2\pi z)^{1/2}}\left(1 + O\left(\frac{1}{z}\right)\right) \quad |z \to \infty| \quad (8)$$

For large values of the argument z when $|z| \to \infty$, $I_n(z)$, $K_n(z)$ can't be numerically evaluated with a good accuracy because of the exponential behaviour. To address this problem, let normalise the versions $\widehat{I_n}, \widehat{K_n}$ of I_n and K_n be defined by

$$\widehat{I_n}(z) := e^{-Re(z)}I_n(z), \quad \widehat{K_n}(z) := e^z K_n(z)$$

where we rely on the assumption that Re(z) ≥ 0. Expressing the asymptotic expansions (8) in terms of $\widehat{I_n}, \widehat{K_n}$, we obtain

$$\widehat{I_n}(z) = \frac{e^{iIm(z)}}{(2\pi z)^{1/2}}\left(1 + O\left(\frac{1}{z}\right)\right), \quad \widehat{K_n}(z) = \left(\frac{\pi}{2z}\right)^{1/2}\left(1 + O\left(\frac{1}{z}\right)\right) \quad |z| \to \infty$$

These expressions depend on $z^{1/2}$ which is smoother and thus allows to evaluate large values of the argument z. The system (7) can then be recast in terms of $\widehat{I_n}, \widehat{K_n}$ with normalised coefficients $\widehat{A}, \widehat{B}$ and $\widehat{C}$:

$$\widehat{A}(s) := e^{Re(\frac{sb}{c})}A(s), \quad \widehat{B}(s) := e^{-\frac{sa}{c}}B(s), \quad \widehat{C}(s) := e^{-\frac{sb}{c_f}}C(s)$$

With these definitions and denoting $l = \frac{\lambda}{\nu}(1-\nu)$, $z_a = \frac{sa}{c}$ and $z_b = \frac{sb}{c}$ the system (7) becomes:

$$\begin{bmatrix} e^{Re(za-zb)}\left[l\frac{s}{c}\widehat{I_1}'(z_a) + \frac{\lambda}{a}\widehat{I_1}(z_a)\right] & l\frac{s}{c}\widehat{K_1}'(z_a) + \frac{\lambda}{a}\widehat{K_1}(z_a) & 0 \\ l\frac{s}{c}\widehat{I_1}'(z_b) + \frac{\lambda}{b}\widehat{I_1}(z_b) & e^{(za-zb)}\left[l\frac{s}{c}\widehat{K_1}'(z_b) + \frac{\lambda}{b}\widehat{K_1}(z_b)\right] & -s\rho_f\widehat{K_0}\left(\frac{sb}{c_f}\right) \\ \widehat{I_1}(z_b) & e^{(za-zb)}\widehat{K_1}(z_b) & \frac{1}{c_f}\widehat{K_1}\left(\frac{sb}{c_f}\right) \end{bmatrix} \begin{bmatrix} \widehat{A}(s) \\ \widehat{B}(s) \\ \widehat{C}(s) \end{bmatrix} = [P] \quad (9)$$

and the solutions take the form:

$$\overline{u}(r,s) = \widehat{A}e^{-Re(\frac{s(r-b)}{c})}\widehat{I_1}\left(\frac{sr}{c}\right) + \widehat{B}e^{\frac{s(a-r)}{c}}\widehat{K_1}\left(\frac{sr}{c}\right) \quad (10)$$

$$\overline{\phi}(r,s) = \widehat{C}e^{\frac{s(b-r)}{c_f}}\widehat{K_0}\left(\frac{sr}{c_f}\right) \quad (11)$$

These solutions in the Laplace domain are used to proceed the synthesis of the corresponding time-domain solution. (9) shows that the coefficients (A,B,C) are proportional to the Laplace transform $\overline{P}(s)$, for every complex frequency s. From expression (6) there exist functions $\overline{U}(r,s)$ and $\overline{\Phi}(r,s)$ such that

$$\overline{u}(r,s) = \overline{U}(r,s)\overline{P}(s) \quad \text{and} \quad \overline{\phi}(r,s) = \overline{\Phi}(r,s)\overline{P}(s)$$

with $\overline{U}(r,s)$ and $\overline{\Phi}(r,s)$ that depend on reference coefficients (A_0, B_0, C_0) according to

$$\overline{U}(r,s) = A_0(s)\widehat{I_1}\left(\frac{sr}{c}\right) + B_0(s)\widehat{K_1}\left(\frac{sr}{c}\right) \quad \text{and} \quad \overline{\Phi}(r,s) = C_0(s)\widehat{K_0}\left(\frac{sr}{c_f}\right)$$

$$\begin{cases} A(s) = A_0(s)p(s) \\ B(s) = B_0(s)p(s) \\ C(s) = C_0(s)p(s) \end{cases}$$

With this decomposition the solution (6) is thus the Laplace image of a time convolution. It can then be numerically evaluated at discrete times using the inverse $\mathcal{Z}$-transform. This semi-analytical solution will be used as a reference validation solution for checking the numerical iterative coupling algorithms, for example in Section 3.3 and 4.5.1.

In the case where a decomposition of the fluid variables into reflected and radiated components is used ($\phi = \phi^{\text{inc}} + \phi^{\text{ref}} + \phi^{\text{rad}}$), the reflected solution can be obtained with a similar method and different boundary condition, and the radiated solution is then obtained by linear superposition, subtracting the reflected solution from the complete coupling solution.

Reflected semi-analytic solution. The reflected solution is used for example to validate the acoustic-elastic FEM solver on a reflection FSI problem in Section 3.3. Let u^r denote the displacement in the annular solid domain subjected to the same incident pressure. We now impose a zero displacement on the exterior surface Γ. The solution to this problem is a reflected solution by analogy to the decomposition of the acoustic field used for solving FSI problems generated by incident shock waves. After a Laplace transform, the reflected solution satisfies:

$$\begin{cases} \left[\dfrac{\partial^2 \overline{u}^r}{\partial r^2} + \dfrac{1}{r}\dfrac{\partial \overline{u}^r}{\partial r} - \dfrac{\overline{u}^r}{r^2}\right](r,s) = \dfrac{1}{c_1^2}s^2\overline{u}^r(r,s) & \text{in } \Omega_s & (a) \\ \left[\dfrac{\lambda}{\nu}\left((1-\nu)\dfrac{\partial \overline{u}^r}{\partial r} + \nu\dfrac{\overline{u}^r}{r}\right)\right](a,s) = -\overline{p}^{int}(s) & \text{on } \Gamma^{\text{int}} & (b) \\ \overline{u}^r(b,s) = 0 & \text{on } \Gamma & (c) \end{cases}$$

It is therefore given by

$$\overline{u}^r(r,s) = A_R(s)I_1(\frac{rs}{c}) + B(s)K_1(\frac{rs}{c})$$

where the constants A_R, B_R solve the equation

$$\begin{bmatrix} \frac{\lambda}{\nu}(1-\nu)\frac{s}{c}I_1'(\frac{as}{c}) + \frac{\lambda}{a}I_1(\frac{as}{c}) & \frac{\lambda}{\nu}(1-\nu)\frac{s}{c}K_1'(\frac{as}{c}) + \frac{\lambda}{a}K_1(\frac{as}{c}) \\ I_1(\frac{bs}{c}) & K_1(\frac{bs}{c}) \end{bmatrix} \begin{Bmatrix} A_R \\ B_R \end{Bmatrix} = \{P\}$$

with $\{P\} := \begin{Bmatrix} -\overline{p}^{\text{int}}(s) \\ 0 \end{Bmatrix}$. On setting the normalised coefficients $\widehat{A}_R, \widehat{B}_R$ to

$$\widehat{A}_R(s) := e^{Re(\frac{sb}{c})}A_R(s), \quad \widehat{B}_R(s) := e^{-\frac{sa}{c}}B_R(s)$$

and using again the normalised modified Bessel functions, the system becomes

$$\begin{bmatrix} e^{\mathrm{Re}(\frac{s(a-b)}{c})}\left[\frac{\lambda}{\nu}(1-\nu)\frac{s}{c}\widehat{I_1}'(\frac{as}{c})+\frac{\lambda}{a}\widehat{I_1}(\frac{as}{c})\right] & \frac{\lambda}{\nu}(1-\nu)\frac{s}{c}\widehat{K_1}'(\frac{as}{c})+\frac{\lambda}{a}\widehat{K_1}(\frac{as}{c}) \\ \widehat{I_1}(\frac{bs}{c}) & e^{\frac{s(a-b)}{c}}\widehat{K_1}(\frac{bs}{c}) \end{bmatrix} \begin{Bmatrix} \widehat{A_R} \\ \widehat{B_R} \end{Bmatrix} = \{P\}$$

while the solution $\overline{u}^r(r,s)$ is given by

$$\overline{u}^r(r,s) = e^{\mathrm{Re}(\frac{s(r-b)}{c})}\widehat{A_R}(s)\widehat{I_1}(\frac{sr}{c}) + e^{(\frac{s(a-r)}{c})}\widehat{B_R}(s)\widehat{K_1}(\frac{sr}{c}) \tag{12}$$

Radiated semi-analytical solution. Finally, we define $u^{\mathrm{rad}}(r,s) := u - u^r$, a radiating displacement responsible for setting the fluid into (radiating) motion. In the Laplace domain and by virtue of linear superposition, the radiated solution is obtained by subtracting the reflected solution (12) from the complete solution (10). The reflected elastic displacement is thus given in the solid domain ($0 < r < b$) by

$$\overline{u}^{\mathrm{rad}}(r,s) = e^{\mathrm{Re}(\frac{s(r-b)}{c})}\left(\widehat{A}-\widehat{A_R}\right)\widehat{I_1}\left(\frac{sr}{c}\right) + e^{(\frac{s(a-r)}{c})}\left(\widehat{B}-\widehat{B_R}\right)\widehat{K_1}\left(\frac{sr}{c}\right)$$

and in the same way, in the fluid domain, for any $r > b$:

$$\overline{\phi}^{\mathrm{rad}}(r,s) = e^{\frac{s(b-r)}{c_f}}\widehat{C}\widehat{K_0}\left(\frac{sr}{c_f}\right)$$

A.2 Acoustic/acoustic-elastic analytical solution

In Section 4.5, we consider another configuration: the radially symmetric 2D annular elastic solid represented is immersed in a fluid and a coupling acoustic-acoustic interface is at a distance $r = d$ from the elastic boundary as represented on Figure 16. This elastic ring Ω_i^s of interior and exterior radius R_{int} and R_{ext} is immersed in a acoustic interior fluid Ω_i^f (mass density ρ_f, acoustic wave velocity c_f) bounded by $\Gamma_i \bigcap \Gamma_e$. An unbounded fluid region is defined $\Omega_e := \mathbb{R}^2 \setminus (\overline{\Omega_s} \bigcap \overline{\Omega_i^f})$. We assume 2D conditions and plane strain deformations for the solid. Both media are at initial rest. A uniform internal pressure $p^{int}(t)$ is prescribed on the interior surface Γ_{int}. Two time dependent velocity potentials are defined for the interior and exterior fluid domains : $\phi_i(t)$ and $\phi_e(t)$, two velocities $\mathbf{v_i}(t) = \nabla\phi_i(t)$, $\mathbf{v_e}(t) = \nabla\phi_e(t)$, and two pressures $p_i(t) = -\rho_f\partial_t\phi_i(t)$ and $p_ie(t) = -\rho_f\partial_t\phi_e(t)\ \forall t \in [0,T]$. The solid variables are the displacement $\mathbf{u}$ and the stress vector $\mathbf{t} := \sigma[\mathbf{u}].\mathbf{n}$.

Semi-analytical coupled solution. Following the same method as in the previous section for an elastic annulus of interior and exterior radius a and b, embedded in an unbounded acoustic fluid and with an acoustic-acoustic interface of radius d, the solid displacement $\mathbf{u}$ and fluid velocity potentials ϕ_i and ϕ_e verify the following

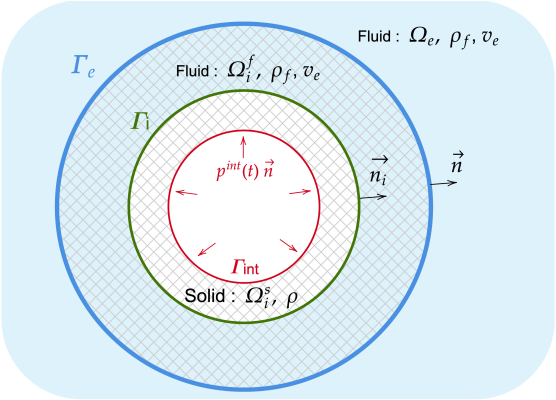

Figure 16: *Radially-symmetric pressurised annulus with a finite element mesh for the interior acoustic-elastic domain and BEM elements for the exterior acoustic domain.*

system of equations:

$$
\begin{cases}
\Delta\phi_i - \dfrac{1}{c_f^2}\partial_t^2\phi_i = 0 & \text{in } \Omega_i^f \times [0,T] \\
\Delta\phi_e - \dfrac{1}{c_f^2}\partial_t^2\phi_e = 0 & \text{in } \Omega_e \times [0,T] \\
\dfrac{\partial^2 u}{\partial r^2} + \dfrac{1}{r}\dfrac{\partial u}{\partial r} - \dfrac{u}{r^2} = \dfrac{1}{c_1^2}\dfrac{\partial^2 u}{\partial t^2} & \text{in } \Omega_i^s \times [0,T] \\
\left[\dfrac{\lambda}{\nu}\left((1-\nu)\dfrac{\partial u}{\partial r} + \nu\dfrac{u}{r}\right)\right](a,t) = -p^{int}(t) & \text{on } \Gamma^{int} \times [0,T] \\
\left[\dfrac{\lambda}{\nu}\left((1-\nu)\dfrac{\partial u}{\partial r} + \nu\dfrac{u}{r}\right)\right](b,t) = -p_i(b,t) & \text{on } \Gamma_i \times [0,T] \\
\partial_t u(b,t) = \partial_r\phi_i(b,t) & \text{on } \Gamma_i \times [0,T] \\
-\rho_f\partial_t\phi_i(d,t) = -\rho_f\partial_t\phi_e(d,t) & \text{on } \Gamma_e \times [0,T] \\
\partial_r\phi_i(d,t) = \partial_r\phi_e(d,t) & \text{on } \Gamma_e \times [0,T]
\end{cases}
$$

where λ, μ are the Lamé elastic constants, $c = \sqrt{(\lambda+2\mu)/\rho_s}$ is the compression

wave velocity. By taking the Laplace transform, the system becomes

$$\begin{cases} \Delta\overline{\phi_i} - \dfrac{1}{c_f^2}s^2\overline{\phi_i} = 0 & \text{in } \Omega_i^f \quad (a) \\ \Delta\overline{\phi_e} - \dfrac{1}{c_f^2}s^2\overline{\phi_e} = 0 & \text{in } \Omega_e \quad (b) \\ \dfrac{\partial^2\overline{u}}{\partial r^2} + \dfrac{1}{r}\dfrac{\partial\overline{u}}{\partial r} - \dfrac{\overline{u}}{r^2} = \dfrac{1}{c_1^2}s^2\overline{u} & \text{on } \Omega_i^s \quad (c) \\ \left[\dfrac{\lambda}{\nu}\left((1-\nu)\dfrac{\partial\overline{u}}{\partial r} + \nu\dfrac{\overline{u}}{r}\right)\right](a,s) = -\overline{p}^{int}(s) & \text{on } \Gamma^{\text{int}} \quad (d) \\ \left[\dfrac{\lambda}{\nu}\left((1-\nu)\dfrac{\partial\overline{u}}{\partial r} + \nu\dfrac{\overline{u}}{r}\right)\right](b,s) = \rho_f s\overline{\phi_i}(b,s) & \text{on } \Gamma_i \quad (e) \\ s\overline{u}(b,s) = \partial_r\overline{\phi_i}(b,s) & \text{on } \Gamma_i \quad (f) \\ -\rho_f s\overline{\phi_i}(d,s) = -\rho_f s\overline{\phi_e}(d,s) & \text{on } \Gamma_e \quad (g) \\ \partial_r\overline{\phi_i}(d,s) = \partial_r\overline{\phi_e}(d,s) & \text{on } \Gamma_e \quad (h) \end{cases}$$

where $\overline{p_i}, \overline{p_e}, \overline{u}, \overline{\phi_i}, \overline{\phi_e}$ and are the Laplace transforms of p_i, p_e, u, ϕ_i and ϕ_e. The second-order homogeneous differential equations (a), (b) and (c) are modified Bessel equations of order 1 and 0, respectively, such that

$$\overline{u}(r,s) = A(s)I_1\left(\frac{sr}{c}\right) + B(s)K_1\left(\frac{sr}{c}\right),$$

$$\overline{\phi_i}(r,s) = C(s)K_0\left(\frac{sr}{c_f}\right) + D(s)I_0\left(\frac{sr}{c_f}\right), \text{ and } \overline{\phi_e}(r,s) = E(s)K_0\left(\frac{sr}{c_f}\right)$$

with $\overline{\phi_e}$ containing no term with I_0 to enforce its decay as $r \to \infty$ and where I_1, K_1, K_0 are modified Bessel functions. The variables of the coupled problem expressed with the modified Bessel functions are:

$$\begin{cases} \overline{u}^0(r,s) = A_0 I_1(\frac{sr}{c}) + B_0 K_1(\frac{sr}{c}) \\ \overline{p}_i^0(r,s) = -\rho_f s C_0 K_0\left(\frac{sr}{c_f}\right) - \rho_f s D_0 I_0\left(\frac{sr}{c_f}\right) \\ \overline{p}_e^0(r,s) = -\rho_f s E_0 K_0\left(\frac{sr}{c_f}\right) \\ \overline{v}_i^0(r,s) = -\frac{s}{c_f}C_0 K_1\left(\frac{sr}{c_f}\right) + \frac{s}{c_f}D_0 I_1\left(\frac{sr}{c_f}\right) \\ \overline{v}_e^0(r,s) = -\frac{s}{c_f}E_0 K_1\left(\frac{sr}{c_f}\right) \\ \overline{t}^0(r,s) = A_0[\frac{\lambda}{\nu}(1-\nu)\frac{s}{c}I_1'(\frac{sr}{c}) + \frac{\lambda}{r}I_1(\frac{sr}{c})] + B_0[\frac{\lambda}{\nu}(1-\nu)\frac{s}{c}K_1'(\frac{sr}{c}) + \frac{\lambda}{r}K_1(\frac{sr}{c})] \end{cases}$$

with $c^2 = \frac{\lambda(1-\nu)}{\lambda\rho_s}$. The boundary condition (d), (e), (f) and the kinematic and dynamic conditions (g) and (h) imply that the constants A, B, C, D and E solve

the five equations:

$$\begin{cases} l\left[A(s)\frac{s}{c}I_1'\left(\frac{sa}{c}\right)+B(s)\frac{s}{c}K_1'(\frac{sa}{c})\right]+\frac{\lambda}{a}\left[A(s)I_1\left(\frac{sa}{c}\right)+B(s)K_1\left(\frac{sa}{c}\right)\right]=-\overline{p}^{int}(s) & \\ l\left[A(s)\frac{s}{c}I_1'\left(\frac{sb}{c}\right)+B(s)\frac{s}{c}K_1'(\frac{sb}{c})\right]+\frac{\lambda}{b}\left[A(s)I_1\left(\frac{sb}{c}\right)+B(s)K_1\left(\frac{sb}{c}\right)\right]= & \rho_f sC(s)K_0\left(\frac{sb}{c_f}\right) \\ & +\rho_f sD(s)I_0\left(\frac{sb}{c_f}\right) \\ sA(s)I_1(\frac{sb}{c})+sB(s)K_1\left(\frac{sb}{c}\right)=-C(s)\frac{s}{c_f}K_1\left(\frac{sb}{cf}\right)+D(s)\frac{s}{c_f}I_1\left(\frac{sb}{cf}\right) & \\ -\rho_f sC(s)K_0\left(\frac{sd}{c_f}\right)-\rho_f sD(s)I_0\left(\frac{sd}{c_f}\right)=-\rho_f sE(s)K_0\left(\frac{sd}{c_f}\right) & \\ -C(s)\frac{s}{c_f}K_1\left(\frac{sd}{cf}\right)+D(s)\frac{s}{c_f}I_1\left(\frac{sd}{cf}\right)=-E(s)\frac{s}{c_f}K_1\left(\frac{sd}{cf}\right) & \end{cases}$$

with $l := \frac{\lambda}{\nu}(1-\nu)$. This corresponds to the matrix system

$$[M]\begin{bmatrix} A(s) \\ B(s) \\ C(s) \\ D(s) \\ E(s) \end{bmatrix} = \begin{bmatrix} -\overline{p}^{int}(s)) \\ 0 \\ 0 \\ 0 \\ 0 \end{bmatrix} \tag{13}$$

with $[M]$ being

$$\begin{bmatrix} l\frac{s}{c}I_1'\left(\frac{sa}{c}\right)+\frac{\lambda}{a}I_1\left(\frac{sa}{c}\right) & l\frac{s}{c}K_1'\left(\frac{sa}{c}\right)+\frac{\lambda}{a}K_1\left(\frac{sa}{c}\right) & 0 & 0 & 0 \\ l\frac{s}{c}I_1'\left(\frac{sb}{c}\right)+\frac{\lambda}{b}I_1\left(\frac{sb}{c}\right) & l\frac{s}{c}K_1'\left(\frac{sb}{c}\right)+\frac{\lambda}{b}K_1\left(\frac{sb}{c}\right) & -s\rho_f K_0\left(\frac{sb}{c_f}\right) & -s\rho_f I_0\left(\frac{sb}{c_f}\right) & 0 \\ c_f I_1\left(\frac{sb}{c}\right) & c_f K_1\left(\frac{sb}{c}\right) & K_1\left(\frac{sb}{c_f}\right) & I_1\left(\frac{sb}{c_f}\right) & 0 \\ 0 & 0 & \rho_f sK_0\left(\frac{sd}{c_f}\right) & -\rho_f sI_0\left(\frac{sd}{c_f}\right) & \rho_f sK_0\left(\frac{sd}{c_f}\right) \\ 0 & 0 & -\frac{s}{c_f}K_1\left(\frac{sd}{cf}\right) & \frac{s}{c_f}I_1\left(\frac{sd}{cf}\right) & \frac{s}{c_f}K_1\left(\frac{sd}{cf}\right) \end{bmatrix}$$

We use the relations $K_0'(z) = -K_1(z), I_0'(z) = I_1(z), I_1'(z) = I_0(z) - \frac{1}{z}I_1(z)$ and $K_1'(z) = -K_0(z) - \frac{1}{z}K_1(z)$, the large-argument expansions for the modified Bessel functions and the normalised the versions $\widehat{I_n}, \widehat{K_n}$ of I_n and K_n as defined in Appendix A.1. The system (13) can then be recast in terms of $\widehat{I_n}, \widehat{K_n}$ with normalised coefficients $\widehat{A}, \widehat{B}, \widehat{C}, \widehat{D}$ and $\widehat{E}$:

$$\widehat{A}(s) := e^{Re(\frac{sb}{c})}A(s), \quad \widehat{B}(s) := e^{\frac{sa}{c}}B(s)$$

$$\widehat{C}(s) := e^{\frac{sb}{c_f}}C(s), \quad \widehat{D}(s) := e^{-Re(\frac{sd}{c_f})}D(s), \quad \widehat{E}(s) := e^{\frac{sd}{c_f}}E(s)$$

With these definitions and denoting $\alpha := e^{Re(za-zb)}\left[l\frac{s}{c}\widehat{I_1}'(z_a)+\frac{\lambda}{a}\widehat{I_1}(z_a)\right]$, $z_a = \frac{sa}{c}$, $z_b = \frac{sb}{c}$, and $z_d = \frac{sd}{c_f}$, $[M]$ in (13) becomes:

$$\begin{bmatrix} \alpha & l\frac{s}{c}\widehat{K_1}'(z_a)+\frac{\lambda}{a}\widehat{K_1}(z_a) & 0 & 0 & 0 \\ l\frac{s}{c}\widehat{I_1}'(z_b)+\frac{\lambda}{b}\widehat{I_1}(z_b) & e^{(za-zb)}\left[l\frac{s}{c}\widehat{K_1}'(z_b)+\frac{\lambda}{b}\widehat{K_1}(z_b)\right] & -s\rho_f\widehat{K_0}\left(\frac{sb}{c_f}\right) & -s\rho_f e^{Re(\frac{s(b-d)}{c_f})}\widehat{I_0}\left(\frac{sb}{c_f}\right) & 0 \\ \widehat{I_1}(z_b) & e^{(za-zb)}\widehat{K_1}(z_b) & \frac{1}{c_f}\widehat{K_1}\left(\frac{sb}{c_f}\right) & e^{Re(\frac{s(b-d)}{c_f})}\widehat{I_1}\left(\frac{sb}{c_f}\right) & 0 \\ 0 & 0 & e^{\frac{s(b-d)}{c_f}}\rho_f s\widehat{K_0}\left(\frac{sd}{c_f}\right) & -\rho_f s\widehat{I_0}\left(\frac{sd}{c_f}\right) & \rho_f s\widehat{K_0}\left(\frac{sd}{c_f}\right) \\ 0 & 0 & -e^{\frac{s(b-d)}{c_f}}\frac{s}{c_f}\widehat{K_1}\left(\frac{sd}{cf}\right) & \frac{s}{c_f}\widehat{I_1}\left(\frac{sd}{cf}\right) & \frac{s}{c_f}\widehat{K_1}\left(\frac{sd}{cf}\right) \end{bmatrix}$$

and the solutions take the form

$$\overline{u}(r,s) = \widehat{A}e^{-Re(\frac{s(r-b)}{c})}\widehat{I}_1\left(\frac{sr}{c}\right) + \widehat{B}e^{\frac{s(a-r)}{c}}\widehat{K_1}\left(\frac{sr}{c}\right)$$

$$\overline{\phi_i}(r,s) = \widehat{C}e^{\frac{s(b-r)}{c_f}}\widehat{K_0}\left(\frac{sr}{c_f}\right) + \widehat{D}e^{Re(\frac{sr}{c_f})-Re(\frac{sd}{c_f})}\widehat{I}_0\left(\frac{sr}{c_f}\right)$$

and

$$\overline{\phi_e}(r,s) = \widehat{E}e^{\frac{s(r-d)}{c_f}}\widehat{K_0}\left(\frac{sr}{c_f}\right)$$

These solutions in the Laplace domain are used to proceed the synthesis of the corresponding time-domain solution. (9) shows that the coefficients (A,B,C,D,E) are proportional to the Laplace transform $\overline{P}(s)$, for every complex frequency s. From (6) there exist functions $\overline{U}(r,s)$, $\overline{\Phi_i}(r,s)$ and $\overline{\Phi_e}(r,s)$ such that

$$\overline{u}(r,s) = \overline{U}(r,s)\overline{P}(s), \quad \overline{\phi_i}(r,s) = \overline{\Phi_i}(r,s)\overline{P}(s) \quad \text{and} \quad \overline{\phi_e}(r,s) = \overline{\Phi_e}(r,s)\overline{P}(s)$$

with $\overline{U}(r,s)$ and $\overline{\Phi}(r,s)$ that depend on reference coefficients $(A_0, B_0, C_0, D_0, E_0)$ according to

$$\overline{U}(r,s) = A_0(s)\widehat{I_1}\left(\frac{sr}{c}\right) + B_0(s)\widehat{K_1}\left(\frac{sr}{c}\right),$$

$$\overline{\Phi_i}(r,s) = C_0(s)\widehat{K_0}\left(\frac{sr}{c_f}\right) + D_0(s)\widehat{I_0}\left(\frac{sr}{c_f}\right) \quad \text{and} \quad \overline{\Phi_e}(r,s) = E_0(s)\widehat{K_0}\left(\frac{sr}{c_f}\right)$$

$$\begin{cases} A(s) = A_0(s)p(s) \\ B(s) = B_0(s)p(s) \\ C(s) = C_0(s)p(s) \\ D(s) = D_0(s)p(s) \\ E(s) = E_0(s)p(s) \end{cases}$$

With this decomposition with modified Bessel functions the solution is the Laplace image of a time convolution. It can then be numerically evaluated at discrete times using the inverse $\mathcal{Z}$-transform. This semi-analytical solution will be used as a reference validation solution for checking the numerical iterative coupling algorithms in Section 4.5.1 and Chapter 5.

In the case where a decomposition of the fluid variables with reflected and radiated components is used ($\phi = \phi^{\text{inc}} + \phi^{\text{ref}} + \phi^{\text{rad}}$), the reflected solution can be obtained with a similar method and different boundary condition, and the radiated solution is then obtained by linear superposition, subtracting the reflected solution from the complete coupling solution.

B Convergence factor evaluation for acoustic/ acoustic-elastic iterations

In Section 4.5.2 we consider a simple radially-symmetric problem to semi-analytically estimate the values of the coupling parameters k_e and k_i that maximises the iterative

algorithm speed of convergence. At each iteration i, the acoustic/acoustic-elastic procedure is based on two Robin transmission conditions of the form

$$\begin{cases} -\rho_f \partial_t \phi_e^{i+1}(t) + k_e \partial_n \phi_e^{i+1}(t) = g_e^i(t) \\ -\rho_f \partial_t \phi_i^{i+1}(t) - k_i \partial_n \phi_i^{i+1}(t) = g_i^i(t) \end{cases}$$

where k_e and k_i are the coupling parameters, g_e and g_i are the boundary terms depending on the variables obtained at the previous iterate. To evaluate the theoretical convergence speed of the Robin-Robin iterations depending on the coupling and relaxation parameters values, we consider the semi analytical-solution (Appendix A) and the matrix system (13). This matrix system defines five coefficients A, B, C, D and E characterising the semi-analytical solution. The convergence of the error of the coupled problem is estimated by expressing, at a fixed frequency s, the matrix relation between the errors on the coefficients at two successive iterations, in the form :

$$\begin{bmatrix} A_1 - A_{ext} \\ B_1 - B_{ext} \\ C_1 - C_{ext} \\ D_1 - D_{ext} \\ E_1 - E_{ext} \end{bmatrix} = [M] \begin{bmatrix} A_0 - A_{ext} \\ B_0 - B_{ext} \\ C_0 - C_{ext} \\ D_0 - D_{ext} \\ E_0 - E_{ext} \end{bmatrix}$$

and we aim at determining the matrix $[M]$. For a fixed frequency s, we express the variables of the radiated problem with the modified Bessel functions. The Robin radiated problem verifies the internal pressure condition on the inner surface ($r = a$), the kinematical and dynamical transmission conditions on the acoustic-elastic interface ($r = b$) and possibly relaxed Robin conditions on the exterior acoustic-acoustic interface ($r = d$). For each complex frequency s these five relations link the variables of iterations 0 and 1:

$$\begin{aligned} \overline{\mathbf{t}}^1.\mathbf{n} &= \mathbf{0} && \text{on } r = a \\ \overline{\mathbf{t}}^1.\mathbf{n} &= -\overline{p}_i^0 && \text{on } r = b \\ \overline{v}_i^1 &= s\overline{\mathbf{u}}^0 && \text{on } r = b \\ -\rho_f \partial_t \phi_i^1 - k_i \partial_n \phi_i^1 &= -\rho_f \partial_t \phi_i^0 + k_i v_i^0 - \\ &\quad \frac{2k_i}{k_i + k_e} \left[s_p + k_e(v_e^0 + s_v) + k_i v_i^0 - \rho_f \partial_t \phi_i^0 + \rho_f \partial_t \phi_e^0 \right] && \text{on } r = d \\ -\rho_f \partial_t \phi_e^1 + k_e \partial_n \phi_e^1 &= -\rho_f \partial_t \phi_e^0 - k_e v_e^0 + \\ &\quad \frac{2k_e}{k_e + k_i} \left[s_p + k_i(v_i^0 - s_v) + k_e v_e^0 - \rho_f \partial_t \phi_i^0 + \rho_f \partial_t \phi_e^0 \right] && \text{on } r = d \end{aligned} \tag{14}$$

To rewrite these relations with the modified Bessel functions, we use $K_0'(z) = -K_1(z), I_0'(z) = I_1(z), I_1'(z) = I_0(z) - \frac{1}{z} I_1(z)$ and $K_1'(z) = -K_0(z) - \frac{1}{z} K_1(z)$. At iteration i the elastic displacement $\mathbf{u}$ and the fluid velocity potentials ϕ_i, ϕ_e on each side of the acoustic-acoustic interface are:

$$\begin{aligned} \mathbf{u}^i(s,r) &= A_i(s) I_1(\tfrac{sr}{c}) + B_i(s) K_1(\tfrac{sr}{c}) \\ \phi_i^i(s,r) &= C_i(s) K_0(\tfrac{sr}{c_f}) + D_i(s) I_0(\tfrac{sr}{c_f}) \\ \phi_e^i(s,r) &= E_i(s) K_0(\tfrac{sr}{c_f}) \end{aligned}$$

We also introduce the short-hand notations

$$T_i(r) := \left[l\frac{s}{c} I_1'(\frac{sr}{c}) + \frac{\lambda}{r} I_1(\frac{sr}{c}) \right] \quad \text{and} \quad T_k(r) := \left[\frac{s}{c} K_1'(\frac{sr}{c}) + \frac{\lambda}{r} K_1(\frac{sr}{c}) \right].$$

$$\begin{aligned}
A_1 T_i(a) + B_1 T_k(a) &= 0 \\
A_1 T_i(b) + B_1 T_k(b) &= C_0 \rho_f s K_0\left(\frac{sb}{c_f}\right) + D_0 \rho_f s I_0\left(\frac{sb}{c_f}\right) \\
-C_1 \frac{s}{c_f} K_1\left(\frac{sb}{c_f}\right) + D_1 \frac{s}{c_f} I_1\left(\frac{sb}{c_f}\right) &= A_0 s I_1\left(\frac{sb}{c}\right) + B_0 s K_1\left(\frac{sb}{c}\right) \\
C_1 \left[-\rho_f s K_0\left(\frac{sd}{c_f}\right) + \frac{sk_i}{c_f} K_1\left(\frac{sd}{c_f}\right) \right] + & \\
D_1 \left[-\rho_f s I_0\left(\frac{sd}{c_f}\right) - \frac{sk_i}{c_f} I_1\left(\frac{sd}{c_f}\right) \right] &= C_0 \left[-\rho_f s K_0\left(\frac{sd}{c_f}\right) - k_i \frac{s}{c_f} K_1\left(\frac{sd}{c_f}\right) + \frac{2k_i}{k_e + k_i} \left(k_i \frac{s}{c_f} K_1\left(\frac{sd}{c_f}\right) + \rho_f s K_0\left(\frac{sd}{c_f}\right) \right) \right] \\
&\quad + D_0 \left[-\rho_f s I_0\left(\frac{sd}{c_f}\right) + k_i \frac{s}{c_f} I_1\left(\frac{sd}{c_f}\right) - \frac{2k_i}{k_e + k_i} \left(k_i \frac{s}{c_f} I_1\left(\frac{sd}{c_f}\right) - \rho_f s I_0\left(\frac{sd}{c_f}\right) \right) \right] \\
&\quad + E_0 \left[\frac{-2k_i}{k_e + k_i} \left(-k_e \frac{s}{c_f} K_1\left(\frac{sd}{c_f}\right) + \rho_f s K_0\left(\frac{sd}{c_f}\right) \right) \right] \\
E_1 \left[-\rho_f s K_0(\frac{sd}{c_f}) - \frac{sk_e}{c_f} K_1(\frac{sd}{c_f}) \right] &= C_0 \left[\frac{-2k_e}{k_e + k_i} \left(s \frac{k_i}{c_f} K_1\left(\frac{sd}{c_f}\right) + \rho_f s K_0\left(\frac{sd}{c_f}\right) \right) \right] \\
&\quad + D_0 \left[\frac{2k_e}{k_e + k_i} \left(s \frac{k_i}{c_f} I_1\left(\frac{sd}{c_f}\right) - \rho_f s I_0\left(\frac{sd}{c_f}\right) \right) \right] \\
&\quad + E_0 \left[-\rho_f s K_0\left(\frac{sd}{c_f}\right) + k_e \frac{s}{c_f} K_1\left(\frac{sd}{c_f}\right) + \frac{2k_e}{k_e + k_i} \left(\rho_f s K_0\left(\frac{sd}{c_f}\right) - k_e \frac{s}{c_f} K_1\left(\frac{sd}{c_f}\right) \right) \right]
\end{aligned}$$

As these relations are verified by the coefficients of the converged solution A_{ex}, B_{ex}, C_{ex}, D_{ex} and E_{ex}, they are also verified by the differences $A_0 - A_{ex}$, $B_0 - B_{ex}$, $C_0 - C_{ex}$, $D_0 - D_{ex}$ and $E_0 - E_{ex}$ such that we have a system of the form

$$\left[R_g\right] \begin{bmatrix} A_1 - A_{ext} \\ B_1 - B_{ext} \\ C_1 - C_{ext} \\ D_1 - D_{ext} \\ E_1 - E_{ext} \end{bmatrix} = \left[R_d\right] \begin{bmatrix} A_0 - A_{ext} \\ B_0 - B_{ext} \\ C_0 - C_{ext} \\ D_0 - D_{ext} \\ E_0 - E_{ext} \end{bmatrix} \tag{15}$$

Subtracting the two matrix systems entails the elimination of the boundary terms h and ν which are independent of the iteration number. As the modified Bessel functions admit the large-argument expansions (8), when one subtract the converged solution, it gives the forms of the matrix $[R_g]$ and $[R_d]$. Then the spectral radius of $[M] = \left[R_g\right]^{-1} \left[R_d\right]$ is the convergence factor of the algorithm and must be smaller than 1 to ensure the convergence of the iterations. In fact, the smaller it is, the faster the convergence rate of the iterative algorithm is

$$\varrho_s(s) = \max \left(\lambda \left(\left[R_g\right]^{-1} \left[R_d\right] \right) \right)$$

To determine an optimal value of k_e and k_i that take into account all the complex frequencies, we consider as the spectral radius, the maximum of all eigenvalues for all the complex frequencies. For the acoustic/acoustic-elastic iterations the procedure

is similar to the acoustic-elastic iterations in Section 3.3.3. Here the theoretical convergence factor is

$$\boxed{\varrho(k_e, k_i) = \max_s \varrho_s(s)} \tag{16}$$

This convergence factor ϱ does not depend on the mesh discretisation or on the impulsion (T_p value for example).

Relaxation. Taking the relaxation into account, the three equations (14) linking two successive iterations become

$$\begin{cases} \overline{\mathbf{t}}^1.\mathbf{n}((a,s) = \mathbf{0} \\ \overline{\mathbf{t}}^1.\mathbf{n}(b,s) = -\overline{p}^0(b,s) \\ \overline{v}^1(b,s) = s\overline{\mathbf{u}}^0(b,s) \\ \left(-\rho_f \partial_t \phi_i^1 - k_i \partial_n \phi_i^1\right)(d,s) = (1-r)\left[-\rho_f \partial_t \phi_i^0 - k_i \partial_n \phi_i^0\right](d,s) + r g_i^0(d,s) \\ \left(-\rho_f \partial_t \phi_e^1 + k_e \partial_n \phi_e^1\right)(d,s) = (1-r)\left[-\rho_f \partial_t \phi_e^0 + k_e \partial_n \phi_e^0\right](d,s) + r g_e^0(d,s) \end{cases}$$

and only the matrix $[R_d]$ changes.

C Proof of solvability for Neumann IBVPs

We prove the well-posedness for the acoustic and elastic Neumann IBVPs (2.20) and (2.19) given by Theorem 2.3.2. The approach follows the same steps as that of the FSIP (2.4) in Section 2.7. We first assume a sufficient regularity in the data with respect to time to allow the existence of classical time derivatives wherever needed. We reformulate the evolution problem as a first-order in time, and prove the existence and uniqueness of the strong solution using the Hille-Yosida theorem. We then use energy identities to extend the solvability results to a problem in weak form, assuming lower data regularity. To illustrate the steps of the proof of solvability we consider an acoustic Neumann IBVP of the form

$$\begin{aligned} -\Delta\phi + \partial_t^2\phi &= 0 \quad \text{in } \Omega \times [0,T], \\ \partial_n\phi &= g \quad \text{in } \Gamma \times [0,T], \\ \phi(0) = \partial_t\phi(0) &= 0 \quad \text{in } \Omega. \end{aligned} \tag{17}$$

Initial rest is assumed since the FSIP of interest is to be solved under that assumption and we use the same space and norm definitions as introduced in Section 2.2. We prove the well-posedness of problem (17) and focus on how the solvability depends on the Neumann datum g.

Existence and uniqueness of a strong solution.

(i) First-order form of the Neumann IBVP.
In preparation to applying the Hille-Yosida theorem, we begin by recasting the IBVP (17) in first-order form, setting $\psi := \partial_t\phi$ to treat the velocity as a separate unknown. The system (17) yields the following first-order system for $\mathbb{U}(t) := (\phi, \psi)(t)$:

$$\mathbb{U}' + A\mathbb{U} = 0 \text{ in } \Omega \times [0,T], \qquad \mathbb{U}(0) = 0 \text{ in } \Omega, \qquad B\mathbb{U} = g \text{ in } \Gamma \times [0,T]. \tag{18}$$

where g is the boundary data. The unbounded differential operator A in $\Omega \times \Omega$ and the boundary operator B are defined by

$$A\mathbb{U} = \begin{Bmatrix} -\psi \\ -\Delta\phi \end{Bmatrix} \quad \text{and} \quad B\mathbb{U} = \partial_n\phi. \tag{19}$$

Due to the form of $\mathbb{U}$, we define the Hilbert space $\mathcal{H}$ by

$$\mathcal{H} := H^1(\Omega) \times L^2(\Omega)$$

equipped with the scalar product

$$(\mathbb{U}, \widetilde{\mathbb{U}})_{\mathcal{H}} := a(\phi, \widetilde{\phi}) + b(\phi, \widetilde{\phi}) + b(\psi, \widetilde{\psi}), \tag{20}$$

using the bilinear forms (2.6). We note that the norm $\|\cdot\|_{\mathcal{H}}$ arising from (20) is equivalent to the standard Sobolev product norm of $H^1(\Omega) \times L^2(\Omega)$ and that relevant Sobolev norms in Ω can be expressed in terms of the bilinear forms as (2.68). Let also the space $\mathcal{H}_A$ and its scalar product $(\cdot,\cdot)_{\mathcal{H}_A}$ be defined by

$$\begin{aligned} \mathcal{H}_A &:= \{\mathbb{U} \in \mathcal{H}, A\mathbb{U} \in \mathcal{H}\} = H^1_\Delta(\Omega) \times H^1(\Omega), \\ \left(\mathbb{U}, \widetilde{\mathbb{U}}\right)_{\mathcal{H}_A} &= \left(\mathbb{U}, \widetilde{\mathbb{U}}\right)_{\mathcal{H}} + \left(A\mathbb{U}, A\widetilde{\mathbb{U}}\right)_{\mathcal{H}}. \end{aligned}$$

We set the domain $\mathcal{D}(A)$ of the operator A as

$$\mathcal{D}(A) = \{\mathbb{U} \in \mathcal{H}_A, B\mathbb{U} = 0\}.$$

This domain embeds the interfacial constraints $B\mathbb{U} = 0$ as essential conditions.

(ii) Interface data lifting.
To put the system in a form allowing the invocation of the Hille-Yosida theorem, we need to define a data lifting and obtain a first-order system with homogeneous BC. This operation consists in finding a function pair $\mathbb{U}_L := (\phi_L, \psi_L)$ in $\Omega \times [0,T]$ such that $g = \partial_n \phi_L$. Moreover, it is convenient to have (ϕ_L, ψ_L) also verify the initial-rest conditions. To this end, assume that $g \in C^2_T(H^{-1/2}(\Gamma))$, $g(0) = 0$. Let $\mu \in \mathbb{R}, \mu \neq 0$; the system

$$\begin{aligned} -\Delta\phi_L + \mu\psi_L &= 0 \quad \text{in } \Omega \times [0,T], \\ \psi_L - \mu\phi_L &= 0 \quad \text{in } \Omega \times [0,T], \\ \partial_n \phi_L &= g \text{ on } \Gamma \times [0,T]. \end{aligned} \tag{21}$$

has a unique solution $\mathbb{U}_L(t) := (\phi_L(t), \psi_L(t))$. More precisely:

Lemma C.1. *Let $g \in C^2_T\left(H^{-1/2}(\Gamma)\right)$ such that $g(0) = 0$. Then, the system (21) has a unique solution $\mathbb{U}_L = \{\phi_L, \psi_L\} \in C^2_T(\mathcal{H}) = C^2_T(H^1 \times L^2(\Omega))$, verifying $\|\mathbb{U}_L\|_{C^2_T(\mathcal{H})} \leq C_1 \|g\|_{C^2_T(L^2(\Gamma))}$.*

Proof of Lemma C.1. Eliminating ψ_L in the system (34), the remaining equations are

$$\begin{aligned} -\Delta\phi_L + \mu^2\phi_L &= 0 \quad \text{in } \Omega \times [0,T], \\ \partial_n \phi_L &= g \quad \text{on } \Gamma \times [0,T]. \end{aligned}$$

They define for each $t \in [0,T]$ an elliptic boundary-value problem. Writing this problem in weak form and using the first Green identity in space (2.62), the velocity potential in Ω verifies:

$$\begin{aligned} &\text{Find } \phi(t) \in H^1_\Delta(\Omega), \\ &\quad a\left(\phi, \widetilde{\phi}\right) + \mu^2 b\left(\phi, \widetilde{\phi}\right) = -\left(g(t), \widetilde{\phi}\right)_\Gamma \quad \forall \widetilde{\phi} \in H^1_\Delta(\Omega). \end{aligned}$$

The bilinear forms are defined by (2.6). For any $\phi \in H^1(\Omega)$, we have $a(\phi,\phi) + \mu^2 b(\phi,\phi) \geq C \|\phi\|^2_{H^1(\Omega)}$ for some $C > 0$, meaning that the bilinear form $a + \mu^2 b$ is coercive on $H^1(\Omega)$. Moreover, the linear functional $\widetilde{\phi} \to \left(g(t), \widetilde{\phi}\right)_\Gamma$ is continuous on $H^1(\Omega)$ by assumption on g. Problem (34) is therefore uniquely solvable in $H^1(\Omega)$ by Lax-Milgram's theorem. The claimed solvability follows from obtaining ψ_L with the remaining equation of (21) and noting that $\Delta\phi_L = \mu\psi_L \in L^2(\Omega)$, the regularity in time of the solution matching that of the data since the governing operator is time-independent. □

Remark. For each $t \in [0,T]$, the system (21) is elliptic, hence the solvability result (Lemma C.1) by invoking the standard Lax-Milgram argument. Moreover, the interior and boundary spatial regularity of ϕ_L and ψ_L results from usual elliptic regularity theory.

(iii) Application of the Hille-Yosida theorem.
We then define the new unknown $\mathbb{U}_c(t) := (\phi_c, \psi_c)(t)$ by $\mathbb{U}_c = \mathbb{U} - \mathbb{U}_L$. Since $\mathbb{U}$ and $\mathbb{U}_L$ verify (17) and (21), the new unknown $\mathbb{U}_c$ is found to verify

$$\begin{cases} -\Delta\phi_c + \partial_t\psi_c = (\mu - \partial_t)\,\psi_L & \text{in } \Omega \times [0,T] \\ -\psi_c + \partial_t\phi_c = (\partial_t - \mu)\,\phi_L & \text{in } \Omega \times [0,T] \\ \partial_n\phi_c = 0 & \text{in } \Gamma \times [0,T] \\ \psi_c(0) = \phi_c(0) = 0 & \text{in } \Omega. \end{cases} \tag{22}$$

with an homogeneous Neumann BC. This system takes the generic operator form, $t \in [0,T]$:

$$\frac{d\mathbb{U}_c}{dt} + A\mathbb{U}_c = \mathbb{F}, \quad \mathbb{U}_c(0) = 0, \qquad B\mathbb{U}_c = 0. \tag{23}$$

This reformulation of the initial Robin IBVP as a non-homogeneous first-order system with homogeneous interface conditions allows to apply the Hille-Yosida theorem to prove its solvability. This yields the desired strong solvability result:

Proposition 6 (Strong solvability for the Neumann IBVP)**.** *For any $g \in C^2_T(H^{-1/2}(\Gamma))$ such that $g(0) = 0$, the system (23) has a unique solution $\mathbb{U}_c = (\phi_c, \psi_c)$ such that*

$$\mathbb{U}_c \in C^0_T\left(D(A)\right) \cap C^1_T\left(\mathcal{H}\right).$$

Proof of Proposition 6. To prove the solvability of problem (23), we check that it verifies the conditions of the Hille-Yosida theorem. In the present context, we need to verify that there exists $\lambda \in \mathbb{R}$ such that $A_\lambda = A + \lambda I : \mathcal{D}(A) \to \mathcal{H}$, which is *maximal monotone*. A_λ is said to be maximal monotone if it satisfies

1. $(A_\lambda \mathbb{U}, \mathbb{U})_H \geq 0$ for any $\mathbb{U} \in D(A)$ (A_λ monotone),
2. For any $F \in H, \exists \mathbb{U} \in D(A)$ such that $(A_\lambda + I)\mathbb{U} = F$ ($A_\lambda + I$ surjective).

1. Monotonicity. Recalling the definitions (19) of A and (20) of the scalar product in $\mathcal{H}$, we have

$$(A\mathbb{U}, \mathbb{U})_{\mathcal{H}} + \lambda(\mathbb{U}, \mathbb{U})_{\mathcal{H}} = -a(\psi, \phi) - b(\psi, \phi) - b(\Delta\phi, \psi) + \lambda\left[a(\phi, \phi) + b(\phi, \phi) + a(\psi, \psi)\right].$$

Since by assumption $\phi \in H^1_\Delta(\Omega)$, the first Green identity in space (2.62), holds

$$-b(\Delta\phi, \psi) = a(\psi, \phi) + (\partial_n\phi, \psi)_\Gamma = a(\psi, \phi) \tag{24}$$

(recalling that the normal $\mathbf{n}$ points inwards of Ω), it can be applied in the above equality. We also recall that the Neumann condition implies $\partial_n\phi = 0$ on Γ. Thus,

$$\begin{aligned} (A\mathbb{U}, \mathbb{U})_{Hcal} &= (\partial_n\phi, \psi) - b(\psi, \phi), & \mathbb{U} \in Hcal_A, \\ &= -b(\psi, \phi), & \mathbb{U} \in D(A) \end{aligned}$$

Rearranging terms, it gives, for $\mathbb{U} \in D(A)$:

$$\begin{aligned} (A\mathbb{U}, \mathbb{U})_{\mathcal{H}} + \lambda(\mathbb{U}, \mathbb{U})_{\mathcal{H}} &= \lambda a(\phi, \phi) + \lambda b(\phi, \phi) + \lambda b(\psi, \psi) - b(\psi, \phi) \\ &= \lambda a(\phi, \phi) + \frac{1}{2} b(\phi - \psi, \phi - \psi) + \left(\lambda - \frac{1}{2}\right)\left[b(\phi, \phi) + b(\psi, \psi)\right] \end{aligned}$$

implying that $(A\mathbb{U},\mathbb{U})_{\mathcal{H}} + \lambda(\mathbb{U},\mathbb{U})_{\mathcal{H}} \geq 0$, i.e. monotonicity holds, for any $\lambda \geq \frac{1}{2}$.

2. Surjectivity. Now, for $\mu \in \mathbb{R}$, we consider the solvability in $\mathcal{D}(A)$ of $(A+\mu I)\mathbb{U} = \mathbb{F}$ for a given $\mathbb{F} = (f_1, f_2)^T \in \mathcal{H}$, i.e. that of the system

$$\begin{aligned} &\text{(a)} \quad \mu\phi - \psi = f_1 \quad \text{in } \Omega, \\ &\text{(b)} \quad \mu\psi - \Delta\phi = f_2 \quad \text{in } \Omega, \\ &\text{(c)} \quad \partial_n\phi = 0 \quad \text{on } \Gamma \end{aligned} \tag{25}$$

Using (a) to eliminate ψ, the problem on ϕ defined by the two remaining equations (b) and (c) reads

$$\text{(b) } \mu^2\phi - \Delta\phi = f_2 + \mu f_1 \ \text{ in } \Omega, \quad \text{(c) } \partial_n\phi = 0 \ \text{ on } \Gamma$$

and is set in variational form as

$$\begin{aligned} &\text{Find } \phi \in H^1_\Delta(\Omega), \\ &a\left(\phi,\widetilde{\phi}\right) + \mu^2 b\left(\phi,\widetilde{\phi}\right) = \left(f_2 + \mu f_1, \widetilde{\phi}\right)_\Gamma \quad \text{for all } \widetilde{\phi} \in H^1_\Delta(\Omega). \end{aligned} \tag{26}$$

The bilinear form $a + \mu^2 b$ is already known to be coercive on $H^1(\Omega)$, and the linear functional $\widetilde{\phi} \to \left(f_2 + \mu f_1, \widetilde{\phi}\right)_\Omega$ is clearly continuous on $H^1(\Omega)$ for any $(f_1, f_2) \in \mathcal{H}$. Consequently, Lax-Milgram's theorem applies again and problem (26) is uniquely solvable. On reconstructing ψ from (25a) this implies the unique solvability in $D(A)$ of (25), and hence of the system $(A + \mu I)\mathbb{U} = \mathbb{F}$ for any $\mathbb{F} \in \mathcal{H}$.

3. Conclusion. Choosing $\mu = \lambda + 1$, the monotonicity *(1)* and the surjectivity *(2)* show that $A+\lambda I : \mathcal{D}(A) \to \mathcal{H}$ is maximal monotone for any $\lambda \geq \frac{1}{2}$. The Hille-Yosida theorem [91, Chap. II, Theorem 1.3] hence applies to the generic system (23) and gives Proposition 6. □

At this point, we know according to Lemma C.1, that if $g \in C^2_T(H^{-1/2}(\Gamma))$ with $g(0) = \partial_t g(0) = 0$, we have $\mathbb{U}_L \in C^2_T(\mathcal{H})$ with $\mathbb{U}_L(0) = 0$. We have also shown that the system (23) has a unique strong solution $\mathbb{U}_c$ for any $\mathbb{F} = \mu\mathbb{U}_L - \mathbb{U}'_L$ with sufficient regularity. Moreover, by definition, the strong solution of the Neumann IBVP (17) is given by $\mathbb{U} = \mathbb{U}_L + \mathbb{U}_c$, so that

$$\mathbb{U} \in C^0_T(\mathcal{H}_A) \cap C^1_T(\mathcal{H}).$$

Existence and uniqueness of a weak solution

We now aim at finding a weak solution of the Neumann IBVP. It will be defined and shown to exist on the basis of energy estimates verified by the strong solution $\mathbb{U}$. We set the Neumann IBVP (17) in weak form as:

$$\begin{aligned} &\text{Find } \phi \in H^1(\Omega), \\ &a\left(\phi(t),\widetilde{\phi}\right) + b\left(\partial_t^2\phi(t),\widetilde{\phi}\right) = -\left(g(t),\widetilde{\phi}\right)_\Gamma \quad \text{for all } \widetilde{\phi} \in H^1(\Omega). \end{aligned} \tag{27}$$

(iv) Energy estimates. To define the weak solution for the Neumann IBVP (18), we first derive energy estimates verified by the strong solution $\mathbb{U}$ of problem (17). The estimate is given by the following Lemma:

Lemma C.2 (Energy estimates)**.** *For any $g \in C^2_T(H^{-1/2}(\Gamma))$ with $g(0) = 0$, the strong solution $\mathbb{U}$ of the Neumann IBVP (17) verifies the estimate*

$$\sup_{t\in[0,T]} \|\mathbb{U}(t)\|^2_{\mathcal{H}} \leq C\|g\|^2_{H^1_T(H^{-1/2}(\Gamma))}. \tag{28}$$

The constant $C > 0$ depends on T and Γ but not on the datum g.

Proof of Lemma C.2. The first step consists in testing the Neumann IBVP (18) with $\widetilde{\phi} = \partial_t\phi$ at each time instant $s \in [0, T]$ and applying the Green identity in space (24) to the strong solution. This yields, for $s \in [0, T]$:

$$\begin{aligned} 2\left(A\mathbb{U} + \mathbb{U}', \mathbb{U}\right)_{\mathcal{H}} = 2\left(A\mathbb{U}, \mathbb{U}\right)_{\mathcal{H}} + \frac{d}{dt}\left(\mathbb{U}, \mathbb{U}\right)_{\mathcal{H}} &= 0 \\ \rightarrow \quad 2\left(g, \psi\right)_{\Gamma} - 2b\left(\psi, \phi\right) + \frac{d}{dt}\left(\mathbb{U}, \mathbb{U}\right)_{\mathcal{H}} &= 0. \end{aligned}$$

On integrating the above equality over $s \in [0, t]$, we obtain

$$2\left(\mathbb{U}(t), \mathbb{U}(t)\right)_{\mathcal{H}} = -2\int_0^t \left(g(s), \psi(s)\right)_{\Gamma} ds + 2\int_0^t b\left(\psi(s), \phi(s)\right) ds. \tag{29}$$

We now majorise the right-hand side of this equation. Firstly, since $g \in H^1_T(H^{-1/2}(\Gamma))$ with $g(0) = 0$ by assumption, we can apply the Green identity in time to $\int_0^t \left(g(s), \psi(s)\right)_{\Gamma} ds$ to obtain

$$\int_0^t \left(g(s), \psi(s)\right)_{\Gamma} ds = \left(g(t), \phi(t)\right)_{\Gamma} - \int_0^t \left(\partial_t g(s), \phi(s)\right)_{\Gamma} ds$$

and Young's inequality applied to each term in the right-hand side then gives

$$\begin{aligned} 2\int_0^t \left(\partial_t g(s), \phi(s)\right)_{\Gamma} ds \; - 2\left(g(t), \phi(t)\right)_{\Gamma} \leq \alpha \left\|\phi(t)\right\|^2_{H^{1/2}(\Gamma)} + \frac{1}{\alpha}\left\|g(t)\right\|^2_{H^{-1/2}(\Gamma)} \\ + \int_0^t \left[\beta \left\|\phi(s)\right\|^2_{H^{1/2}(\Gamma)} + \frac{1}{\beta}\left\|\partial_t g(s)\right\|^2_{H^{-1/2}(\Gamma)}\right] ds. \end{aligned}$$

We then use the theorem of continuity of the trace which holds

$$\left\|\phi(t)\right\|^2_{H^{1/2}(\Gamma)} \leq c_T \left\|\phi(t)\right\|^2_{H^1(\Omega)},$$

with c_T the continuity constant of the trace theorem. Recalling the definition of the scalar product (20), we thus have $\left\|\phi(t)\right\|^2_{H^{1/2}(\Gamma)} \leq c_T\left(\mathbb{U}, \mathbb{U}\right)_{\mathcal{H}}$. Secondly, we apply the Young's inequality the second term $b\left(\psi(s), \phi(s)\right)$ in the right-hand side of (29). The equation (29) becomes

$$\begin{aligned} 2\left(\mathbb{U}, \mathbb{U}\right)_{\mathcal{H}} \leq & \alpha c_T \left(\mathbb{U}, \mathbb{U}\right)_{\mathcal{H}} + \frac{1}{\alpha}\left\|g(t)\right\|^2_{H^{-1/2}(\Gamma)} + \int_0^t \left[\beta c_T \left(\mathbb{U}, \mathbb{U}\right)_{\mathcal{H}}(s) + \frac{1}{\beta}\left\|\partial_t g(s)\right\|^2_{H^{-1/2}(\Gamma)}\right] ds \\ & + \int_0^t \left[\gamma \left\|\psi(s)\right\|^2_{L^2(\Gamma)} + \frac{1}{\gamma}\left\|\phi(s)\right\|^2_{L^2(\Gamma)}\right] ds. \end{aligned}$$

We choose $\alpha = \frac{1}{c_T}$ and $\gamma = 1$ such that

$$\begin{aligned}(\mathbb{U},\mathbb{U})_{\mathcal{H}}(t) &\leq C_1 \int_0^t (\mathbb{U},\mathbb{U})_{\mathcal{H}}(s)ds + c_T \|g(t)\|^2_{H^{-1/2}(\Gamma)} + \int_0^t \frac{1}{\beta} \|\partial_t g(s)\|^2_{H^{-1/2}(\Gamma)} ds \\ &\leq C_1 \int_0^t (\mathbb{U},\mathbb{U})_{\mathcal{H}}(s)ds + D_1 \|g\|^2_{H^1_T(H^{-1/2}(\Gamma))}\end{aligned}$$

by virtue of the fact that $H^1_T(H^{-1/2}(\Gamma)) \subset C^0_T\left(H^{-1/2}(\Gamma)\right)$ with continuous injection. Gronwall's lemma 2.7.7 can then be applied to this inequality, with $\Phi(s) = (\mathbb{U},\mathbb{U})_{\mathcal{H}}(s)$ and $C_2 = D_1 \|g\|^2_{H^1_T(H^{-1/2}(\Gamma))}$. It results in

$$\|\mathbb{U}(t)\|^2_{\mathcal{H}} \leq C \|g\|^2_{H^1_T(H^{-1/2}(\Gamma))}, \quad t \in [0,T].$$

We finally have the Lemma C.2. This estimate shows that a weaker norm of the strong solution $\mathbb{U}$ is controlled by a weaker norm of the data. □

(v) Existence and uniqueness of a weak solution. Estimate (28) shows that the strong solution $\mathbb{U}$ with data $g \in C^2_T(H^{-1/2}(\Gamma))$ in fact has its weaker $C^0_T(\mathcal{H})$ norm controlled by the weaker $H^1_T(H^{-1/2}(\Gamma))$ norm of the data. This allows to obtain a well-posedness result for the Neumann IBVP in variational form, under weaker regularity assumptions on the data g.

To this aim, we take any Neumann data $g \in H^1_T(H^{-1/2}(\Gamma))$ with $g(0) = 0$. Let $\widehat{g}(t) = g(t) - \frac{t}{T}g(T)$, we have $\widehat{g} \in H^1_0\left([0,T]; H^{-1/2}(\Gamma)\right)$. As the space $C^2_C([0,T]; H^{-1/2}(\Gamma))$ is dense in $H^1_0([0,T]; H^{-1/2}(\Gamma))$, there exists a sequence $\widehat{g}_n \in C^2_T(H^{-1/2}(\Gamma))$ approximating $\widehat{g}$. An approximating sequence g_n of g therefore exists, such that

$$\|g_n - g\|_{H^1_T(H^{-1/2}(\Gamma))} \to 0.$$

By Proposition 6, the Neumann IBVP (18) has for each data g_n a unique solution $\mathbb{U}_n \in C^1_T(\mathcal{H}) \cap C^0_T(\mathcal{H}_A)$. We apply by linear superposition the estimate (28) to the data $g_n - g_m$ and corresponding solution $\mathbb{U}_n - \mathbb{U}_m$. We readily find that $(\mathbb{U}_n)$ is a Cauchy sequence in $C^0_T(\mathcal{H})$ and therefore converge to a limit $\mathbb{U} \in C^0_T(\mathcal{H})$ since $C^0_T(\mathcal{H})$ is complete. Upon taking the limit $n \to \infty$ in that estimate, the limit $\mathbb{U}$ satisfies

$$\sup_{t\in[0,T]} \|\mathbb{U}(t)\|^2_{\mathcal{H}} \leq C \|g\|^2_{H^1_T(H^{-1/2}(\Gamma))}.$$

The limit $\mathbb{U}$ is the expected weak solution of the Neumann IBVP in variational form (27). We still need to prove that this is indeed the case, and that the limit $\mathbb{U}$ is the only such solution.

1. $\mathbb{U}$ defines a solution of the variational problem (27). Let $\widetilde{\phi} \in H^1(\Omega)$ be a time-independent function and let $\varphi \in C^\infty_0([0,T])$. Each $\mathbb{U}_n$ is a strong solution and $\mathbb{U}_n \in \mathcal{H}_A$, so each $\mathbb{U}_n$ verifies the wave equation in $L^2_T(\Omega)$. Testing against $\widetilde{\phi}\varphi$ the wave equation, we have

$$\int_0^T \left(-\Delta\phi_n + \phi_n'', \widetilde{\phi}\right)_\Omega \varphi(t)dt = 0. \tag{30}$$

We first apply the Green identity (2.62) and express $\partial_n \phi_n$ by means of the Neumann boundary condition (which is verified in the $L^2_T(\Gamma)$ weak sense), to obtain

$$\int_0^T \left[a\left(\phi_n, \widetilde{\phi}\right) + b\left(\phi_n'', \widetilde{\phi}\right) \right] \varphi(t) dt = -\int_0^T \left(g_n(t), \widetilde{\phi}\right)_\Gamma \varphi(t) dt$$

in terms of the bilinear forms a, b defined by (2.6). Then, all time derivatives are transferred to φ via integrations by parts, without any boundary terms, yielding (since $\varphi \in C_0^\infty([0,T])$)

$$\int_0^T \left[a\left(\phi_n, \widetilde{\phi}\right) \varphi(t) + b\left(\phi_n, \widetilde{\phi}\right) \varphi''(t) \right] dt = -\int_0^T \left(g_n(t), \widetilde{\phi}\right)_\Gamma \varphi(t) dt.$$

By assumption, we have $g_n \to g$ in $L^2_T(H^{-1/2}(\Gamma))$, which implies $\mathbb{U}_n \to \mathbb{U}$ in $L^2_T(\mathcal{H})$. Using the continuity of the bilinear forms a, b, we take the limit $n \to \infty$ in the above variational formulation, which gives, for any $\varphi \in C_0^\infty([0,T])$

$$\int_0^T \left[a\left(\phi, \widetilde{\phi}\right) \varphi(t) + b\left(\phi, \widetilde{\phi}\right) \varphi''(t) \right] dt = -\int_0^T \left(g(t), \widetilde{\phi}\right)_\Gamma \varphi(t) dt.$$

The components of $\mathbb{U}$ therefore satisfy the variational formulation (27) in the sense of distributions in the time variable with support in $[0,T]$.

2. Uniqueness. Assume that the variational formulation (27) has two distinct nonzero solutions $\mathbb{U}_1$ and $\mathbb{U}_2$ for the same datum g, both satisfying initial-rest conditions. By linearity, the components of $\mathbb{W} := \mathbb{U}_1 - \mathbb{U}_2 = (\xi, \partial_t \xi)$, must then solve the homogeneous form of the variational problem (27), for all $\widetilde{\phi} \in H^1(\Omega)$,

$$\int_0^s \left[a\left(\xi(t), \widetilde{\phi}\right) + b\left(\partial_t^2 \xi(t), \widetilde{\phi}\right) \right] dt = 0,$$

with $(\xi, \partial_t \xi) \in L^2_T(\mathcal{H})$. The antiderivative $\mathbb{Z}(t) := \int_0^t \mathbb{W}(s) ds$ is also at initial-rest and (by integration over the time interval $[0,t]$) solves the same homogeneous variational problem. Moreover, as a result of the integration in time $\mathbb{Z} \in C^1_T(\mathcal{H}) \cap C^0_T(\mathcal{D}(A))$, i.e., is a strong solution of the homogeneous evolution problem. By Proposition 6, we must hence have $\mathbb{Z} = 0$, implying $\mathbb{W} = 0$. This proves the uniqueness of the weak solution. This concludes the proof of the Theorem 2.3.2.

D Proof of solvability for Robin IBVPs (Theorem 2.4.2)

We prove the well-posedness for the acoustic and elastic Robin IBVPs (2.48) and (2.47) given by Theorem 2.4.2. The approach is similar to the one for the FSIP (2.4) in Section 2.7. We follow the same main steps: we first assume a sufficient regularity in the data with respect to time to allow the existence of classical time derivatives wherever needed. We reformulate the evolution problem as a first-order in time, and prove the existence and uniqueness of the strong solution using the Hille-Yosida theorem. We then use energy identities to extend the solvability results to a problem in weak form, assuming lower data regularity. To illustrate the steps of the proof of solvability we consider an acoustic Robin IBVP of the form

$$\begin{aligned} -\Delta\phi + \partial_t^2\phi &= 0 \quad \text{in } \Omega \times [0,T], \\ -\partial_t\phi + k_c\partial_n\phi &= g \quad \text{in } \Gamma \times [0,T], \\ \phi(0) = \partial_t\phi(0) &= 0 \text{ on } \Omega. \end{aligned} \tag{31}$$

Initial rest is assumed since the FSIP of interest is to be solved under that assumption and we use the same space and norm definitions as introduced in 2.2. We prove the well-posedness of (31) and focus on how the solvability depends on the Robin datum g.

Existence and uniqueness of a strong solution.

(i) First-order form of the Robin IBVP.
In preparation to applying the Hille-Yosida theorem, we begin by recasting the IBVP (31) in first-order form. We set $\psi := \partial_t\phi$ to treat the velocity as separate unknown. The system (31) yields the following first-order system for $\mathbb{U}(t) := (\phi, \psi)(t)$:

$$\mathbb{U}' + A\mathbb{U} = 0, \quad \mathbb{U}(0) = 0, \quad B\mathbb{U} = g \tag{32}$$

where g is the boundary data. The unbounded differential operator A in $\Omega \times \Omega$ and the boundary operator B are defined by

$$A\mathbb{U} = \begin{Bmatrix} -\psi \\ -\Delta\phi \end{Bmatrix} \quad \text{and} \quad B\mathbb{U} = k_c\partial_n\phi - \psi. \tag{33}$$

We use the same Hilbert spaces $\mathcal{H}$, $\mathcal{H}_A$ and scalar products as defined in Appendix C. We set the domain $\mathcal{D}(A)$ of operator A as

$$\mathcal{D}(A) = \{\mathbb{U} \in \mathcal{H}_A, B\mathbb{U} = 0\}.$$

This domain embeds the Robin interfacial constraints $B\mathbb{U} = 0$ as essential conditions.

(ii) Boundary data lifting.
To put the system in a form allowing the invocation of the Hille-Yosida theorem, we need to define a data lifting and obtain a first-order system with homogeneous BC. This operation consists in finding a function pair $\mathbb{U}_L := (\phi_L, \psi_L)$ in $\Omega \times [0,T]$ such

that $g = k_c\partial_n\phi_L - \psi_L$. Moreover, it is convenient to have (ϕ_L, ψ_L) also verify the initial-rest conditions. To this end, assume that $g \in C^2_T(L^2(\Gamma))$, $g(0) = g'(0) = 0$. Let $\mu \in \mathbb{R}, \mu \neq 0$; the system

$$\begin{aligned} -\Delta\phi_L + \mu\psi_L &= 0 \quad \text{in } \Omega \times [0,T], \\ \psi_L - \mu\phi_L &= 0 \quad \text{in } \Omega \times [0,T], \\ k_c\partial_n\phi_L - \psi_L &= g \text{ on } \Gamma \times [0,T]. \end{aligned} \tag{34}$$

has a unique solution $\mathbb{U}_L(t) := (\phi_L(t), \psi_L(t))$. More precisely:

Lemma D.1. *Let $g \in C^2_T(L^2(\Gamma))$ such that $g(0) = 0$. Then, the system (34) has a unique solution $\mathbb{U}_L = \{\phi_L, \psi_L\} \in C^2_T(\mathcal{H}) = C^2_T(H^1(\Omega) \times L^2(\Omega))$, verifying $\|\mathbb{U}_L\|_{C^2_T(\mathcal{H})} \leq C_1\|g\|_{C^2_T(L^2(\Gamma))}$.*

Proof of Lemma D.1. Eliminating ψ_L in the system (34), the remaining equations are

$$\begin{aligned} -\Delta\phi_L + \mu^2\phi_L &= 0 \quad \text{in } \Omega \times [0,T], \\ k_c\partial_n\phi_L - \mu\phi_L &= g \text{ on } \Gamma \times [0,T]. \end{aligned}$$

They define for each $t \in [0,T]$ a boundary-value problem. Writing this problem in weak form and using the first Green identity (2.62), the velocity potential in Ω verifies:

$$\begin{aligned} &\text{Find } \phi(t) \in H^1(\Omega), \\ &\quad a\left(\phi, \widetilde{\phi}\right) + \mu^2 b\left(\phi, \widetilde{\phi}\right) + \frac{\mu}{k_c}\left(\phi, \widetilde{\phi}\right)_\Gamma = -\frac{1}{k_c}\left(g, \widetilde{\phi}\right)_\Gamma \quad \forall \widetilde{\phi} \in H^1(\Omega). \end{aligned}$$

The bilinear forms are defined by (2.6). To apply the Lax-Milgram theorem, the bilinear form $a\left(\phi, \widetilde{\phi}\right) + \mu^2 b\left(\phi, \widetilde{\phi}\right) + \frac{\mu}{k_c}\left(\phi, \widetilde{\phi}\right)_\Gamma$ has to be continuous and coercive, and $\widetilde{\phi} \mapsto \left(g(t), \widetilde{\phi}\right)$ has to be continuous on $H^1(\Omega)$. We obtain the continuity by using the triangle and Cauchy-Schwarz inequalities, and then applying theorem of continuity of the trace:

$$\begin{aligned} \left|a\left(\phi, \widetilde{\phi}\right) + \mu^2 b\left(\phi, \widetilde{\phi}\right) + \frac{\mu}{k_c}\left(\phi, \widetilde{\phi}\right)_\Gamma\right| &\leq \left|a\left(\phi, \widetilde{\phi}\right) + \mu^2 b\left(\phi, \widetilde{\phi}\right)\right| + \frac{\mu}{k_c}\left|\left(\phi, \widetilde{\phi}\right)_\Gamma\right| \\ &\leq \|\phi\|_{H^1(\Omega)} \cdot \left\|\widetilde{\phi}\right\|_{H^1(\Omega)} + \frac{\mu}{k_c}\|\phi\|_{L^2(\Gamma)} \cdot \left\|\widetilde{\phi}\right\|_{L^2(\Gamma)} \\ &\leq \|\phi\|_{H^1(\Omega)} \cdot \left\|\widetilde{\phi}\right\|_{H^1(\Omega)} + \frac{\mu}{k_c}C_T^2\|\phi\|_{H^1(\Omega)} \cdot \left\|\widetilde{\phi}\right\|_{H^1(\Omega)} \\ &\leq \left(1 + \frac{\mu}{k_c}C_T^2\right)\|\phi\|_{H^1(\Omega)} \cdot \left\|\widetilde{\phi}\right\|_{H^1(\Omega)} \end{aligned}$$

where C_T is the constant of continuity of the trace operator on Γ. The continuity of the right handside term is also obtained with the theorem of continuity of the trace:

$$\begin{aligned} \|\phi\|_{L^2(\Gamma)} &\leq \|\phi\|_{H^{1/2}(\Gamma)} \\ &\leq C_T\|\phi\|_{H^1(\Omega)}. \end{aligned}$$

Moreover, as $(\phi,\phi)_\Gamma \geq 0$, for any $\phi \in H^1(\Omega)$ we have

$$a(\phi,\phi) + \mu^2 b(\phi,\phi) + \frac{\mu}{k_c}(\phi,\phi)_\Gamma \geq \|\phi\|^2_{H^1(\Omega)},$$

which gives the coercivity on $H^1(\Omega)$ of the bilinear form. Problem (34) is therefore uniquely solvable in $H^1(\Omega)$ by Lax-Milgram's theorem. The remaining equation (34) then gives $\psi_L = \mu\phi_L \in H^1(\Omega)$ and as $\Delta\phi_L = \mu\psi_L \in L^2(\Omega)$, the governing operator is time independent, so the regularity in time of the solution matches that of the data. Lax-Milgram's theorem finally gives

$$\|\mathbb{U}_L(t)\|_{\mathcal{H}} \leq C\|g(t)\|_{L^2(\Gamma)} \quad \text{for each} \quad t \in [0,T],$$

hence the claimed space-time estimate. □

Remark. For each $t \in [0,T]$, the system (34) is elliptic, hence the solvability result (Lemma D.1) by invoking the standard Lax-Milgram argument. Moreover, the interior and boundary spatial regularity of ϕ_L and ψ_L results from usual elliptic regularity theory.

(iii) Application of the Hille-Yosida theorem.
We then define the new unknown $\mathbb{U}_c(t) := (\phi_c,\psi_c)(t)$ by $\mathbb{U}_c = \mathbb{U} - \mathbb{U}_L$. Since $\mathbb{U}$ and $\mathbb{U}_L$ verify (31) and (34), $\mathbb{U}_c$ is found to verify

$$\begin{cases} -\Delta\phi_c + \partial_t\psi_c = (\mu - \partial_t)\psi_L & \text{in } \Omega\times[0,T] \\ -\psi_c + \partial_t\phi_c = (\partial_t - \mu)\phi_L & \text{in } \Omega\times[0,T] \\ -\psi_c + k_c\partial_n\phi_c = 0 & \text{in } \Gamma\times[0,T] \\ \psi_c(0) = \phi_c(0) = 0 & \text{in } \Omega. \end{cases}$$

This system takes the generic operator form, $t \in [0,T]$:

$$\frac{d\mathbb{U}_c}{dt} + A\mathbb{U}_c = \mathbb{F}, \quad \mathbb{U}_c(0) = 0, \qquad B\mathbb{U}_c = 0. \tag{35}$$

$\mathbb{U}_c$ solves (35) with the particular data $\mathbb{F} = \mu\mathbb{U}_L - \mathbb{U}_L'$. This reformulation of the initial Robin IBVP as a non-homogeneous first-order system with homogeneous interface conditions allows to apply the Hille-Yosida theorem to prove its solvability. This yields the desired strong solvability result:

Proposition 7 (Strong solvability for the Robin IBVP)**.** *Assume that either* $\mathbb{F} \in C^1_T(\mathcal{H})$ *or* $\mathbb{F} \in C^0_T(\mathcal{D}(A))$*. Then, the system* (35) *has a unique solution*

$$\mathbb{U}_c \in C^1_T(\mathcal{H}) \cap C^0_T(\mathcal{D}(A)).$$

Proving the Proposition 7 will be facilitated by the following lemma:

Lemma D.2. *For any* $\mathbb{U} \in \mathcal{H}_A$*, we have*

$$(A\mathbb{U},\mathbb{U})_{\mathcal{H}} = \frac{1}{k_c}\|\psi\|^2_\Gamma + \frac{1}{k_c}(g,\psi)_\Gamma - b(\psi,\phi)$$

Proof of Lemma D.2. We obtain the identity by using the definition (20) of the scalar product $(.,.)_{\mathcal{H}}$ and the first Green identity (2.62):

$$\begin{aligned}(A\mathbb{U},\mathbb{U})_{\mathcal{H}} &= a(-\psi,\phi)+b(-\psi,\phi)+b(-\Delta\phi,\psi)\\ &= b(\Delta\phi,\psi)+(\partial_n\phi,\psi)_\Gamma+b(-\psi,\phi)+b(-\Delta\phi,\psi)\\ &= \frac{1}{k_c}\|\psi\|^2_{L^2(\Gamma)}+\frac{1}{k_c}(g,\psi)_\Gamma-b(\psi,\phi)\end{aligned}$$

□

Proof of Proposition 7. To prove the solvability of problem (35), we check that it verifies the conditions of the Hille-Yosida theorem. In the present context, we need to verify that there exists $\lambda\in\mathbb{R}$ such that $A_\lambda = A+\lambda I : \mathcal{D}(A)\to\mathcal{H}$, which is *maximal monotone*. A_λ is said to be maximal monotone if it satisfies

1. $(A_\lambda\mathbb{U},\mathbb{U})_H\geq 0$ for any $\mathbb{U}\in D(A)$ (A_λ monotone),
2. For any $F\in H, \exists\mathbb{U}\in D(A)$ such that $(A_\lambda+I)\mathbb{U}=F$ ($A_\lambda+I$ surjective).

1. Monotonicity. Using definitions (33) of A and (20) of the scalar product in $\mathcal{H}$ and appling Lemma D.2, we obtain

$$\begin{aligned}(A\mathbb{U},\mathbb{U})_{\mathcal{H}}+\lambda(\mathbb{U},\mathbb{U})_{\mathcal{H}} = \frac{1}{k_c}\|\psi\|^2_{L^2(\Gamma)}+\frac{1}{k_c}(g,\psi)_\Gamma-b(\psi,\phi)+\lambda a(\phi,\phi)\\ +\lambda b(\phi,\phi)+\lambda b(\psi,\psi)\end{aligned}\tag{36}$$

for any $\mathbb{U}\in D(A)$. Rearrangind terms it gives

$$\begin{aligned}(A\mathbb{U},\mathbb{U})_{\mathcal{H}}+\lambda(\mathbb{U},\mathbb{U})_{\mathcal{H}} = \frac{1}{k_c}\|\psi\|^2_{L^2(\Gamma)}+\frac{1}{k_c}(g,\psi)_\Gamma+\lambda a(\phi,\phi)\\ +\frac{1}{2}b(\phi-\psi,\phi-\psi)+\left(\lambda-\frac{1}{2}\right)\left[b(\phi,\phi)+b(\psi,\psi)\right],\end{aligned}$$

implying that $(A\mathbb{U},\mathbb{U})_{\mathcal{H}}+\lambda(\mathbb{U},\mathbb{U})_{\mathcal{H}}\geq 0$, i.e. monotonicity holds, for any $\lambda\geq\frac{1}{2}$.

2. Surjectivity. Now, for $\mu\in\mathbb{R}$, we investigate whether the equation $(A+\mu I)\mathbb{U}=\mathbb{F}$ is solvable for $\mathbb{U}=(\phi,\psi)\in\mathcal{D}(A)$ given $\mathbb{F}=(f_1,f_2)\in\mathcal{H}$, i.e. that of the system

$$\begin{aligned}&\text{(a)} && \mu\phi-\psi=f_1 && \text{in }\Omega,\\ &\text{(b)} && \mu\psi-\Delta\phi=f_2 && \text{in }\Omega,\\ &\text{(c)} && k_c\partial_n\phi-\psi=0 && \text{on }\Gamma\end{aligned}\tag{37}$$

Using (a) to eliminate ψ, the problem on ϕ defined by the two remaining equations (b) and (c) reads

$$\text{(b) } \mu^2\phi-\Delta\phi=f_2+\mu f_1 \text{ in }\Omega,\quad \text{(c) } k_c\partial_n\phi-\mu\phi=-f_1 \text{ on }\Gamma$$

and is set in variational form as

Find $\phi\in H^1(\Omega)$,

$$a\left(\phi,\widetilde{\phi}\right)+\mu^2 b\left(\phi,\widetilde{\phi}\right)+\frac{\mu}{k_c}\left(\phi,\widetilde{\phi}\right)_\Gamma=\left(f_2+\mu f_1,\widetilde{\phi}\right)_\Omega+\frac{1}{k_c}\left(f_1,\widetilde{\phi}\right)_\Gamma\tag{38}$$

for all $\widetilde{\phi} \in H^1(\Omega)$. The bilinear form $a\left(\phi, \widetilde{\phi}\right) + \mu^2 b\left(\phi, \widetilde{\phi}\right) + \frac{\mu}{k_c}\left(\phi, \widetilde{\phi}\right)_\Gamma$ is already known to be coercive on $H^1(\Omega)$, and the linear functional $\widetilde{\phi} \to \left(f_2 + \mu f_1, \widetilde{\phi}\right)_\Omega + \frac{1}{k_c}\left(f_1, \widetilde{\phi}\right)_\Gamma$ is continuous on $H^1(\Omega)$ for any $\mathbb{F} = (f_1, f_2) \in \mathcal{H}$. Consequently, Lax-Milgram's theorem applies again and problem (38) is uniquely solvable. Elliptic regularity then shows that $\phi \in H^1_\Delta(\Omega)$, whereupon reconstructing ψ with the remaining equation yields $\psi \in H^1(\Omega)$. The system $(A+\mu I)\mathbb{U} = \mathbb{F}$ is therefore uniquely solvable in $\mathcal{D}(A)$ for any $\mathbb{F} \in \mathcal{H}$.

3. Conclusion. Choosing $\mu = \lambda + 1$, the monotonicity *(1)* and the surjectivity *(2)* show that $A+\lambda I : \mathcal{D}(A) \to \mathcal{H}$ is maximal monotone for any $\lambda \geq \frac{1}{2}$. The Hille-Yosida theorem [91, Chap. II, Theorem 1.3] hence applies to the generic system (35) and gives Proposition 7. □

At this point, we know according to Lemma D.1, that if $g \in C^2_T(L^2)$ with $g(0) = 0$, we have $\mathbb{U}_L \in C^2_T(\mathcal{H})$ with $\mathbb{U}_L(0) = 0$. We also have shown that the system (35) has a unique strong solution $\mathbb{U}_c$ for any $\mathbb{F} = \mu\mathbb{U}_L - \mathbb{U}'_L$ with sufficient regularity. If $\mathbb{F} \in C^1_T(\mathcal{H})$, then $\mathbb{U}_c \in C^1_T(\mathcal{H})$. Moreover, by definition, the strong solution of the Robin IBVP (31) is given by $\mathbb{U} = \mathbb{U}_L + \mathbb{U}_c$ and

$$\mathbb{U} \in C^1_T(\mathcal{H}) \cap C^0_T(\mathcal{H}_A).$$

Existence and uniqueness of a weak solution

We now aim at finding a weak solution of the Robin IBVP. It will be defined and shown to exist on the basis of energy estimates verified by the strong solution $\mathbb{U}$. We set the Robin IBVP (31) in weak form as:

$$\begin{aligned} &\text{Find } \phi \in H^1(\Omega), \\ &a\left(\phi(t), \widetilde{\phi}\right) + b\left(\partial_t^2\phi(t), \widetilde{\phi}\right) + \frac{1}{k_c}c\left(\partial_t\phi(t), \widetilde{\phi}\right)_\Gamma = -\frac{1}{k_c}\left(g(t), \widetilde{\phi}\right)_\Gamma \\ &\text{for all } \widetilde{\phi} \in H^1(\Omega). \end{aligned} \tag{39}$$

(iv) Energy estimates. To define the weak solution for the Robin IBVP (32), we first derive energy estimates verified by the strong solution $\mathbb{U}$ of problem (31). These estimates are given by the following Lemma:

Lemma D.3 (Energy estimates)**.** *For any $g \in C^2_T(L^2(\Gamma))$ with $g(0) = 0$, the strong solution $\mathbb{U}$ of the Robin IBVP (31) verifies the estimate*

$$\sup_{t\in[0,T]} \|\mathbb{U}(t)\|^2_{\mathcal{H}} \leq C\|g\|^2_{L^2_T(\Gamma)}. \tag{40}$$

Moreover, the velocity trace on Γ verifies the estimate

$$\|\psi\|^2_{L^2_T(\Gamma)} \leq C\|g\|^2_{L^2_T(\Gamma)}. \tag{41}$$

The constants $C > 0$ in each estimate depend on T and Γ but not on the datum g.

Proof of Lemma D.3. The first step consists in testing the Robin IBVP (32). On expressing $(A\mathbb{U},\mathbb{U})_{\mathcal{H}}$ by means of Lemma D.2 at each time instant $s\in[0,T]$, this yields:

$$\begin{aligned} 2\left(A\mathbb{U}+\mathbb{U}',\mathbb{U}\right)_{\mathcal{H}}&=0\\ 2\left(A\mathbb{U},\mathbb{U}\right)_{\mathcal{H}}+\frac{d}{dt}\left(\mathbb{U},\mathbb{U}\right)_{\mathcal{H}}&=0\\ \frac{2}{k_c}\left\|\psi\right\|^2_{L^2(\Gamma)}+\frac{2}{k_c}\left(g,\psi\right)_{\Gamma}-2b\left(\psi,\phi\right)+\frac{d}{dt}\left(\mathbb{U},\mathbb{U}\right)_{\mathcal{H}}&=0 \end{aligned}$$

On integrating the above equality over $s\in[0,t]$, we obtain

$$\frac{2}{k_c}\int_0^t\left\|\psi(s)\right\|^2_{L^2(\Gamma)}ds+\left(\mathbb{U},\mathbb{U}\right)_{\mathcal{H}}=-\frac{2}{k_c}\int_0^t\left(g(s),\psi(s)\right)_{\Gamma}ds+2\int_0^t b\left(\psi(s),\phi(s)\right)ds.$$

We now majorise the right-hand side of this equality. Applying Young's inequality to each term in the right-hand side with $\alpha=\beta=1$, gives

$$\begin{aligned}\frac{2}{k_c}\int_0^t\left\|\psi(s)\right\|^2_{L^2(\Gamma)}ds+\left(\mathbb{U},\mathbb{U}\right)_{\mathcal{H}}(t)\leq&\int_0^t\left[\left\|\phi(s)\right\|^2_{L^2(\Omega)}+\left\|\psi(s)\right\|^2_{L^2(\Omega)}\right]ds\\&+\int_0^t\left[\left\|g(s)\right\|^2_{L^2(\Gamma)}+\left\|\psi(s)\right\|^2_{L^2(\Gamma)}\right]ds.\end{aligned}\tag{42}$$

Adding a term $\int_0^t a(\phi(s),\phi(s))ds$ to the right-hand side of the above inequality, we have

$$\frac{1}{k_c}\int_0^t\left\|\psi(s)\right\|^2_{L^2(\Gamma)}ds+\left(\mathbb{U},\mathbb{U}\right)_{\mathcal{H}}(t)\leq\int_0^t\left[\left\|\phi(s)\right\|^2_{L^2(\Omega)}+\left\|\psi(s)\right\|^2_{L^2(\Omega)}\right]ds+\frac{1}{k_c}\int_0^t\left\|g(s)\right\|^2_{L^2(\Gamma)}ds$$

which implies

$$\left(\mathbb{U},\mathbb{U}\right)_{\mathcal{H}}(t)\leq\int_0^t\left(\mathbb{U},\mathbb{U}\right)_{\mathcal{H}}(s)ds+\frac{1}{k_c}\int_0^t\left\|g(s)\right\|^2_{L^2(\Gamma)}ds.$$

Grönwall's lemma plays as usual, a key role in the derivation of energy estimates. We use the version (2.7.7), with $\Phi(s)=\left(\mathbb{U},\mathbb{U}\right)_{\mathcal{H}}(s)$ and $C_2=\frac{2}{k_c}\int_0^t\left\|g(s)\right\|^2_{L^2(\Gamma)}ds$. Consequently there exists $C>0$ such that

$$\left\|\mathbb{U}(t)\right\|^2_{\mathcal{H}}\leq C\left\|g\right\|^2_{L^2_T(\Gamma)}\qquad t\in[0,T].\tag{43}$$

i.e. the sought estimate (40) holds. This estimate shows that a weaker $L^2_T(\mathcal{H})$ norm of the strong solution $\mathbb{U}$ is controlled by a weaker norm $L^2_T(\Gamma)$ of the data g. Moreover, we can then use (42) to obtain an estimate on the boundary velocity.

$$\frac{1}{k_c}\int_0^t\left\|\psi(s)\right\|^2_{L^2(\Gamma)}ds\leq\int_0^t\left(\mathbb{U},\mathbb{U}\right)_{\mathcal{H}}(s)ds+\frac{1}{k_c}\left\|g\right\|^2_{L^2_T(\Gamma)}.$$

As $\int_0^t\left(\mathbb{U},\mathbb{U}\right)_{\mathcal{H}}(s)ds\leq\left(\mathbb{U},\mathbb{U}\right)_{L^2_T(\mathcal{H})}\leq CT\left\|g\right\|^2_{L^2_T(\Gamma)}$ and using the energy estimate (43), we then obtain

$$\frac{1}{k_c}\int_0^t\left\|\psi(s)\right\|^2_{L^2(\Gamma)}ds\leq t\left(\mathbb{U},\mathbb{U}\right)_{\mathcal{H}}(t)+\frac{1}{k_c}\left\|g\right\|^2_{L^2_T(\Gamma)}\leq\left(tC+\frac{1}{k_c}\right)\left\|g\right\|^2_{L^2_T(\Gamma)}.$$

which gives the final energy estimate for the velocity trace of the strong solution. We finally have the Lemma D.3 and the sought energy estimates. □

(v) Existence and uniqueness of a weak solution. Estimate (40) shows that the strong solution $\mathbb{U}$ with data $g \in C^2_T(L^2(\Gamma))$ in fact has its weaker $C^0_T(\mathcal{H})$ norm controlled by the weaker $L^2_T(\Gamma)$ norm of g. This allows to obtain a well-posedness result for the Robin IBVP in variational form, under weaker regularity assumptions on the data g.

To this aim, let $g \in L^2_T(\Gamma)$ be some transmission data. By a density argument, as the space $\{f \in C^2_T(L^2(\Gamma)),\ f(0) = 0\}$ is dense in $L^2_T(\Gamma)$, there exists a sequence $g_n \in C^2_T(L^2(\Gamma))$ with $g_n(0) = 0$ such that

$$\|g_n - g\|_{L^2_T(\Gamma)} \to 0.$$

By Proposition 7, the Robin IBVP (32) has for each data g_n a unique solution $\mathbb{U}_n \in C^1_T(\mathcal{H}) \cap C^0_T(\mathcal{H}_A)$. We apply by linear superposition the estimate (40) to the data $g_n - g_m$ and corresponding solution $\mathbb{U}_n - \mathbb{U}_m$. We readily find that $(\mathbb{U}_n)$ is a Cauchy sequence in $C^0_T(\mathcal{H})$, which therefore converges to some limit $\mathbb{U} \in C^0_T(\mathcal{H})$ since the space $C^0_T(\mathcal{H})$ is complete. Upon taking the limit $n \to \infty$ in the estimate (41), the limit $\mathbb{U}$ satisfies

$$\sup_{t\in[0,T]} \|\mathbb{U}(t)\|^2_{\mathcal{H}} \leq C \|g\|^2_{L^2_T(\Gamma)}.$$

The limit $\mathbb{U}$ is the expected weak solution of the Robin IBVP in variational form (39). We still need to prove that this is indeed the case, and that the limit $\mathbb{U}$ is the only such solution.

1. $\mathbb{U}$ defines a solution of the variational problem (39). Let $\widetilde{\phi} \in H^1(\Omega)$ be a time-independent function and let $\varphi \in C^\infty_0([0,T])$. Each $\mathbb{U}_n$ is a strong solution and $\mathbb{U}_n(t) \in \mathcal{H}_A$, so each ϕ_n verifies the wave equation in $L^2_T(\Omega)$. Testing against $\widetilde{\phi}\varphi$ the wave equation, we have

$$\int_0^T \left(-\Delta\phi_n + \phi_n'', \widetilde{\phi}\right)_\Omega \varphi(t)dt = 0. \tag{44}$$

We first apply the Green identity (2.62) and express $\partial_n\phi_n$ by means of the Robin boundary condition (which is verified in the $L^2_T(\Gamma)$ weak sense), to obtain

$$\int_0^T \left[a\left(\phi_n, \widetilde{\phi}\right) + b\left(\phi_n'', \widetilde{\phi}\right) + \frac{1}{k_c}\left(\phi_n', \widetilde{\phi}\right)_\Gamma\right] \varphi(t)dt = \frac{-1}{k_c}\int_0^T \left(g_n(t), \widetilde{\phi}\right)_\Gamma \varphi(t)dt$$

in terms of the bilinear forms a, b defined by (2.6). Then, all time derivatives are transferred to φ via integrations by parts in time, without any boundary terms, yielding (since $\varphi \in C^\infty_0([0,T])$

$$\int_0^T \left[a\left(\phi_n, \widetilde{\phi}\right)\varphi(t) + b\left(\phi_n, \widetilde{\phi}\right)\varphi''(t) + \frac{1}{k_c}\left(\phi_n, \widetilde{\phi}\right)_\Gamma \varphi'(t)\right] dt = \frac{-1}{k_c}\int_0^T \left(g_n(t), \widetilde{\phi}\right)_\Gamma \varphi(t)dt.$$

We have $\mathbb{U}_n \to \mathbb{U}$ in $L^2_T(\mathcal{H})$ and, by assumption, we have $g_n \to g$ in $L^2_T(\Gamma)$. Using the continuity of the bilinear forms a, b, we take the limit $n \to \infty$ in the above variational formulation, which gives, for any $\varphi \in C^\infty_0([0,T])$

$$\int_0^T \left[a\left(\phi, \widetilde{\phi}\right)\varphi(t) + b\left(\phi, \widetilde{\phi}\right)\varphi''(t) + \frac{1}{k_c}\left(\phi, \widetilde{\phi}\right)_\Gamma \varphi'(t)\right] dt = \frac{-1}{k_c}\int_0^T \left(g(t), \widetilde{\phi}\right)_\Gamma \varphi(t)dt.$$

The components of $\mathbb{U}$ therefore satisfy the variational formulation (39) in the sense of distributions in the time variable with support in $[0, T]$.

2. Uniqueness. Assume that the variational formulation (39) has two distinct solutions $\mathbb{U}_1$ and $\mathbb{U}_2$ for the same datum g, both satisfying initial-rest conditions. By linearity, the components of $\mathbb{W} := \mathbb{U}_1 - \mathbb{U}_2 = (\xi, \partial_t \xi)$, must then solve the homogeneous form of the variational problem (39): for all $\widetilde{\phi} \in H^1(\Omega)$,

$$\int_0^s \left[a\left(\xi(t), \widetilde{\phi}\right) + c\left(\partial_t \xi(t), \widetilde{\phi}\right) + b\left(\partial_t^2 \xi(t), \widetilde{\phi}\right) \right] dt = 0,$$

with $(\xi, \partial_t \xi) \in L^2_T(\mathcal{H})$. The antiderivative $\mathbb{Z}(t) := \int_0^t \mathbb{W}(s) ds$ is also at initial rest and (by integration over the time interval $[0, t]$) solves the same homogeneous variational problem. Moreover, as a result of the integration in time, $\mathbb{Z} \in C^1_T(\mathcal{H}) \cap C^0_T(\mathcal{D}(A))$, i.e., is a strong solution of the homogeneous evolution problem. By Proposition 7, we must hence have $\mathbb{Z} = 0$, implying $\mathbb{W} = 0$. This proves the uniqueness of the weak solution. This concludes the proof of the Theorem 2.4.2.

E In-house Z-BEM solvers

This appendix presents a complementary validations regarding the in-house 2D Matlab Z-BEM solver used in Chapters 2 and 4. These validations and studies of convergence are done by comparison to analytical solutions on simple 2D problems. We developed our frequency BEM solver, which solves frequency acoustic Robin problems, and our Z-BEM solver, which solves time-domain acoustic Robin problems on Matlab. Both are validated by solving respectively a frequency-domain and a time-domain problem, for which an analytical solution is known. We then introduce a high frequency approximation (HFA) adapted to the acoustic problem with Robin boundary condition. This approximation completes the high frequency approximations proposed by [146] for Neumann acoustic problems.

E.1 Acoustic Robin problems in frequency-domain

As detailed in Chapter 1, we aim to solve the boundary integral equation (BIE) associated with a transient wave propagation problem. The scalar velocity potential ϕ verifies the wave equation and the boundary value problem (3.1) in the acoustic domain Ω. The BIE defined on Γ_f is (3.7). At an iteration n, the boundary integral equation we aim to solve is:

$$\frac{1}{2}\phi^n(\mathbf{x},t) - \mathcal{H}\left\{\phi^n\right\}(\mathbf{x},t) = -\mathcal{G}\left\{\partial_n \phi^{\text{n-1}}\right\}(\mathbf{x},t) \qquad \forall t \in [0,T], \text{ with } \mathbf{x} \in \Gamma \tag{45}$$

where $\partial_{\mathbf{t}}\mathbf{u}^{\text{i-1}}.\mathbf{n}$ and ϕ^n are the normal elastic velocity at the previous iteration $n-1$ and the fluid velocity potential at iteration n, defined on the interface Γ. Introducing a Robin boundary condition, with a coupling parameter k_a:

$$-\rho\partial_t\phi^n + k_a\partial_n\phi^n = f^{n-1}$$

the boundary integral equation (45) is written with the velocity potential ϕ^n and its temporal derivative:

$$\left(\frac{1}{2}Id - \mathcal{H}\right)\left\{\phi^n\right\}(\mathbf{x},t) = -\frac{1}{k_a}\mathcal{G}\left\{\rho\partial_t\phi^n + f^{n-1}\right\}(\mathbf{x},t) \qquad \forall t \in [0,T], \text{ with } \mathbf{x} \in \Gamma \tag{46}$$

As we aim to define an equivalent problem in the frequency-domain to use the CQM procedure, we use the Laplace transform of ϕ^n, with a Laplace variable s. With the Laplace transform, a convolution product becomes:

$$\begin{aligned} q(t) = \left(\dot{G} \star \phi^n\right)(t) &= \int_0^t \dot{G}(t-\tau)\phi^n(\tau)d\tau \\ &= \int_0^t \left(\frac{1}{2\pi i}\int_{\gamma-i\infty}^{\gamma+i\infty} \mathcal{L}\left\{\dot{G}(t)\right\} e^{s(t-\tau)}\right)\phi^n(\tau)d\tau \\ &= \frac{1}{2\pi i}\int_{-\infty}^{+\infty} \mathcal{L}\left\{\dot{G}(t)\right\} h(t;s)ds \end{aligned}$$

where h is the term $h(t;s) = \int_0^t e^{s(t-\tau)}\phi^n(\tau)d\tau$. Moreover, the Laplace transform of G is

$$\mathcal{L}\left\{\dot{G}(t)\right\} = s * \mathcal{L}\left\{G(t)\right\} - G(0) = s * \overline{G}(s) - G(0)$$

with $G(0) = 0$ because G is the fundamental function defined by $G(r,t|f) = \frac{1}{2\pi}\int_r^{ct} \frac{f(t-\eta/c)}{\sqrt{\eta^2-r^2}}d\eta$ and it is zero everywhere except in r=0 at t=0. The Laplace transform of the convolution product is finally

$$Q(\xi) = s * \overline{G}(\frac{p(\xi)}{\Delta t})F(\xi)$$

where $s = \frac{p(\xi)}{\Delta t}$ is the problem's complex frequency. $\overline{G}$ is the Green function Laplace transform and F is the Z-transform of f. They are defined in Section 3.2.1. The Robin frequency problems are then for all $\mathbf{x} \in \Gamma$:

$$\left(\frac{1}{2}Id - \mathcal{H}\right)\{\Phi^n\}(\mathbf{x},s) + \frac{\rho_f s}{k_a}\mathcal{G}\{\Phi^n\}(\mathbf{x},s) = -\frac{1}{k_a}\mathcal{G}\left\{h - \mathbf{t^{n-1}}.\mathbf{n} + k_a(\partial_t \mathbf{u^{n-1}}.\mathbf{n}) + k_a\nu\right\} \tag{47}$$

Numerical validation of the 2D frequency BEM solver. We choose to validate our in-house frequency BEM solver on a simple configuration: an acoustic plane wave $\Phi^{\text{inc}} = e^{i\mathbf{k}.\mathbf{x}}$ is defined by an angle of incidence θ and a wave number $\mathbf{k} := k[\cos(\theta);\sin(\theta)]$, with $k = \frac{is}{c_f}$. It propagates in an unbounded acoustic medium Ω_f at speed c_f before interacting with a circular obstacle Ω_s of radius a, whose surface is Γ. The reflected field Φ verifies the problem:

$$\text{Find } \Phi \text{ such that } \begin{cases} (\Delta + k^2)\Phi = 0 & \text{in } \Omega_f \\ (-\rho s - k_a\partial_n)\Phi|_\Gamma = \Phi^{\text{inc}}_{|\Gamma} & \text{on } \Gamma \\ \lim\limits_{x\to\infty} \|\mathbf{x}\|^{1/2}(\nabla\Phi.\frac{\mathbf{x}}{\|\mathbf{x}\|} - ik\Phi) = 0 \end{cases}$$

The acoustic incident wave is decomposed with the Jacobi identity in the form:

$$\Phi^{inc}(r,\theta) = \sum_{m\in\mathbb{Z}}(-i)^m J_m(kr)e^{im\theta} \tag{48}$$

where J_m is the first order Bessel function and the reflected solution is expressed as a Fourier series in r and θ:

$$\Phi(r,\theta) = \sum_{m\in\mathbb{Z}}\psi_m(r)e^{im\theta}$$

where the ψ_m coefficients are linear solutions of the Helmholtz equation in polar coordinates such as

$$(\Delta + k^2)\psi_m = (r^2\partial_r^2 + r\partial_r + (k^2 - m^2))\psi_m = 0$$

which implies that $\psi_m(r) = J_m(kr)$. Introducing the modified Bessel functions $\forall m \in \mathbb{Z}$:

$$\begin{cases} H_m^{(1)}(x) := J_m(x) + iY_m(x) \\ H_m^{(2)}(x) := J_m(x) - iY_m(x) \end{cases}$$

the reflected field ϕ holds as

$$\Phi(r,\theta) = \sum_{m\in\mathbb{Z}} A_m^+ H_m^{(1)}(kr)e^{im\theta} + A_m^- H_m^{(2)}(kr)e^{im\theta}$$

As Φ must satisfy the Sommerfeld radiation condition, it implies that $A_m^- = 0$ for all $m \in \mathbb{Z}$. Finally, the Robin boundary condition on Γ (r=a) provides the relation:

$$k_a A_m^+ H_m^{(1)'}(ka) e^{im\theta} + s\rho_f A_m^+ H_m^{(1)}(k\ a) = -(-i)^m J_m(k\ a)$$

And we deduce the analytical form of the reflected field

$$\Phi^*(r,\theta) = \sum_{m\in\mathbb{Z}} \frac{-(-i)^m J_m(k\ a)}{(k_a H_m^{(1)'}(k\ a) + \rho_f s H_m^{(1)}(k\ a))} H_m^{(1)}(k\ r) e^{im\theta} \quad \text{for any } r > a \tag{49}$$

We replace in (47) the excitation term $h - \mathbf{t}.\mathbf{n} - k_a(\partial_t \mathbf{u}.\mathbf{n})$ by a plane wave Φ^{inc} as defined by (48), and we compare the analytical field (49) to the numerical solution trace Φ on the boundary Γ. We choose a complex frequency $s = -i\pi$, the circular boundary has a radius a=1 and E=800 boundary elements, the wave's angle of incidence is θ=0 and the coupling parameter is $k_a = c_f \rho_f = 1$. Figure 17 shows the boundary trace $\Phi(\theta)$ on Γ computed using the frequency BEM solver. It agrees very well with the analytical solution Φ^*. For this example, the relative error between the computed solution and the analytical solution is

$$e_\Phi^{res} := \frac{\|\Phi^n - \Phi^*\|_{L^2([0,T],\Gamma)}}{\|\Phi^*\|_{L^2([0,T],\Gamma)}} = 3,6.10^{-3}.$$

This is corroborated by Figure 18 which shows the analytical field Φ^* and the integral representation in the exterior domain computed from the frequency BEM solution.

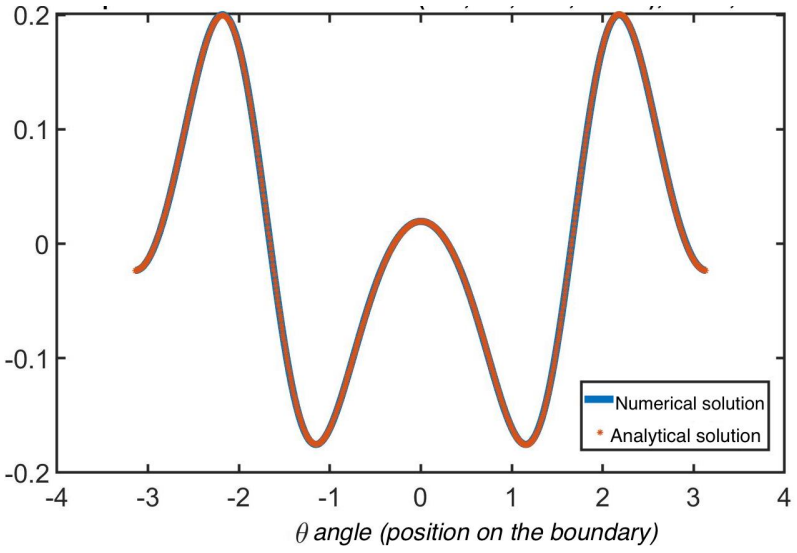

Figure 17: *Numerical boundary trace Φ computed with the BEM solver for a Robin BC and analytical solution Φ^* on Γ as a functions of θ ($a = 1, k = \pi$). $e_\Phi^{res} = 3.6\ 10^{-3}$.*

E.2 2D Z-BEM acoustic solver

Our Z-BEM solver is validated on a transient Robin acoustic problem. The Z-BEM solver developed on Matlab uses the frequency BEM solver validated in Section E.1.

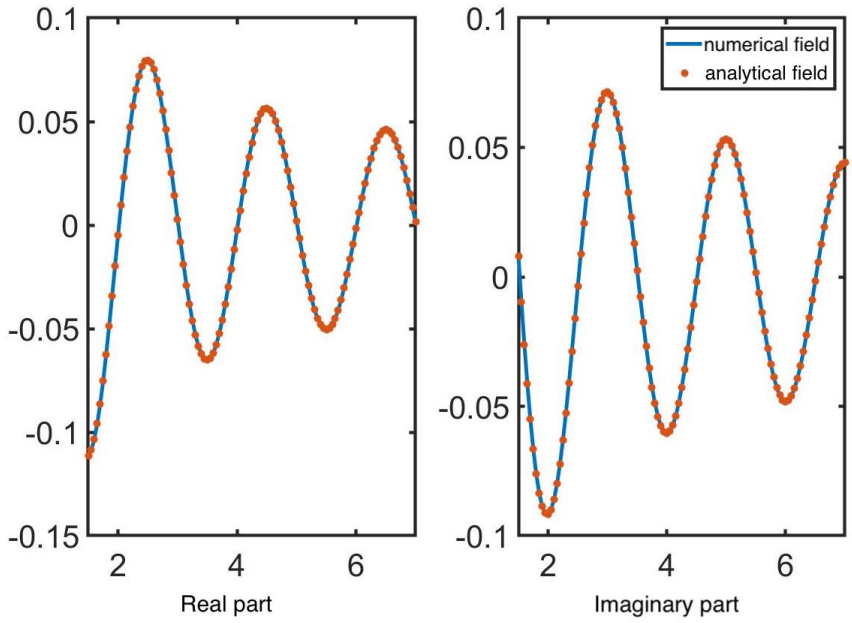

Figure 18: *Integral representation of* Φ *in* Ω_f *and analytical solution* Φ^* *as functions of* $r (a = 1, \theta = r, k = \pi)$. $e_\Phi^{res} = 3.5\ 10^{-5}$.

We consider a fixed point source $\mathbf{x}$ placed at the origin in an acoustic interior domain Ω_f^{int}. The point source produces an acoustic field ϕ^{inc} equal to the 2D fundamental acoustic solution G in time-domain, with a time-modulated intensity $f(t)$ and quiescent past [26]:

$$\phi^{\text{inc}}(x, z, t|f) := G(x, z, t|f) = \frac{1}{2\pi} \int_r^{ct} \frac{f(t - \eta/c)}{\sqrt{\eta^2 - r^2}} d\eta$$

$$\text{with} \qquad f(t|a) = \begin{cases} at^4 (T_{\text{pulse}} - t)^4 & \text{if } t \in [0, T_{\text{pulse}}] \\ 0 \text{ else} \end{cases}$$

where a is the pulse's amplitude and T_{pulse} is its width. The source function $f(t)$ is assumed to be twice continuously differentiable and identically vanishing for $t < 0$. The fundamental solution G depends on t through all the retarded times $t - \eta/v$ for $r/t \leq v \leq c$.

Remark. This contrasts with the 3D free-space fundamental solution (see Section E.3). For the 3D solution, only the retarded time $t - r/c$ appears, due to causality, the fact that information travels at finite speed c through the medium. In 2D, this lagging effect reflects the fact that the 2D solution results from an integration of its 3D counterpart over $]-\infty, +\infty[$, i.e. is actually the wave function generated in the 3D free space by an infinite line of point sources.

As G is the 2D acoustic fundamental solution for a point source it verifies the BIE for the exterior problem in Ω_f^{ext}. The solution ϕ verifies

$$\frac{1}{2}\phi(x, t) = \mathcal{H}\{\phi\}(x, t) - \mathcal{G}\left\{\frac{\partial \phi}{\partial n}\right\}(x, t) \qquad x, y \in \Gamma \tag{50}$$

Solving the Dirichlet exterior problem consists in determining the unknown trace $q = \frac{\partial \phi}{\partial n}$ on the boundary using the CQM algorithm and checking that the numerical computation of q is equal to the analytical derivative of the known fundamental solution G. The circular boundary Γ has a radius a=1 and is discretised with $E =$ 1700 boundary elements. The celerity is c=2000 and the angle of incidence is $\theta = 0$. The time interval [0, 3.4 10^{-3}] sec is discretised by N_t =550 time steps, which corresponds to L=1100 complex frequencies. The Z-BEM algorithm is accelerated with an H-matrix method and we use the numerical parameters $N_{leaf} = 50$, $\eta = 3$ and a tolerance $\epsilon = 10^{-4}$. The numerically computed reflected trace $\partial_n \phi(x,t)$ and the analytical normal derivative $\partial_n G$ evaluated on a boundary element are depicted on Figure 19. With this discretisation the relative space-time L2 error on the trace $q = \frac{\partial \psi}{\partial n}$ evaluated on the interface is $\delta(\Gamma) = 0.035$, which validates the Z-BEM algorithm with CQM and H-matrix methods. The error's convergence with the mesh

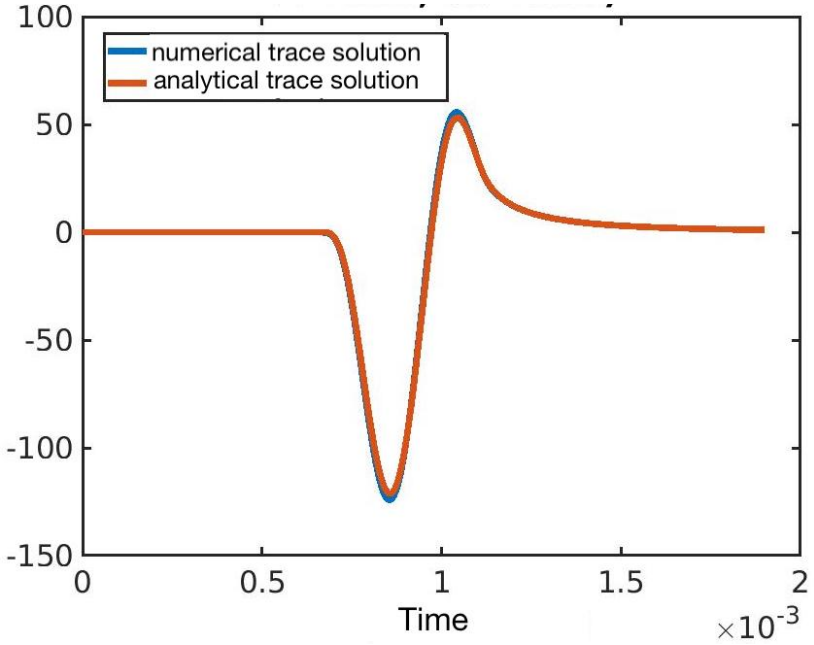

Figure 19: *Numerical boundary trace $\partial_n \phi$ and analytical solution $\partial_n G$ on an boundary element of Γ ($\Delta t = 1.7\ 10^{-6}, N_t = 1118, El = 2336$).*

size is ensured as, at a fixed mesh density, the more boundary elements are used, the smaller the relative space-time L2 error on boundary is. The numerical parameters of some computations of the trace solution $\frac{d\phi}{dn}$ and the corresponding relative errors are provided in Table 7 (with a fixed size of boundary element 3.7 10^{-3}).

E.3 3D Z-BEM acoustic solver

In this Section we validate the in-house Z-BEM solver on 3D transient acoustic problem. We consider reference problems for which the analytical solution is known.

Frequency BEM resolution. The Matlab 3D frequency BEM solver is verified by solving the boundary integral equation (50) with Dirichlet boundary condition.

Number of boundary elements	1400	1700	1800	2500	5000
Circle radius	0.824	1	1.0594	1.472	2.94
Relative CQM error	4.41%	4.36%	4.33%	4.21%	3.79 %

Table 7: *Relative space-time L2 error on the trace of $\partial_n\phi = \partial_n G$ with the number of mesh elements, at fixed mesh density*

To verify the BEM solver, we choose the data as the normal derivative of the fundamental solution G of the Helmholtz equation for a 3D sphere with a radius $r = 1$ (in this case the solution does not depend on the angles θ and ψ):

$$\partial_n\phi = \partial_n G = \frac{e^{-ikr}}{r^2}(1 + ikr).$$

The solution is the trace

$$\phi = G = \frac{e^{-ikr}}{r}$$

on the 3D sphere. Table 8 and 9 (for 7 and 12 points per wavelength) show that the relative L2 error on the trace on the boundary is smaller than 5.10^{-3} for 7 points per wavelength and smaller than 3.5 10^{-3} for 12 points per wavelength, which verifies the 3D BEM solver. For high-frequency problems, it is necessary to substantially refine the mesh to preserve a sufficient number of points per wavelength (10 points per wavelength is the usual condition).

|k|	Mesh elements	BEM error	Hmat BEM error	Calculation (Hmat)
2.03	2562	4.273 10^{-3}	4.248 10^{-3}	15.2 s
3.65	10242	1.477 10^{-3}	1.473 10^{-3}	64.6 s
8.15	40962	6.133 10^{-4}	6.099 10^{-4}	398.0 s
9.95	61033	1.011 10^{-3}	1.019 10^{-3}	725.0 s

Table 8: *Relative error depending on the frequency, with and without H-mat acceleration (7 points per wavelength, $\eta = 3$, $n_{leaf} = 20$).*

|k|	Mesh elements	BEM error	Hmat BEM error	Calculation (Hmat)
1.19	2562	3.63 10^{-3}	3.50 10^{-3}	15 s
2.38	10242	/	1.30 10^{-3}	227 s
4.76	40962	/	4.66 10^{-4}	281 s
5.81	61033	/	9.38 10^{-4}	2260 s

Table 9: *Relative error depending on the frequency, with and without H-mat acceleration (12 points per wavelength, $\eta = 3$, $n_{leaf} = 20$).*

Transient Z-BEM resolution. To validate the transient Z-BEM solver, we consider a sphere Ω_s and an infinite exterior domain $\Omega := \mathbb{R}^3 \setminus \overline{\Omega_s}$. The spherical

boundary is $\Gamma = \partial\Omega_f = \partial\Omega_s$. An arbitrary fixed point $\mathbf{z}$ is in the interior acoustic domain Ω_s and has a time-modulated intensity $f(t)$ and quiescent past. We define the incident potential

$$\phi^{\text{ref}} := G(\mathbf{x}, \mathbf{z}, t|f) = (G(\mathbf{x}, \mathbf{z}, .) \star f)(t) \quad \mathbf{x} \in \Omega, \mathbf{z} \in \Omega_s$$

The source function $f(t)$ is assumed to be twice continuously differentiable and identically vanishing for $t < 0$. The function ϕ^{ref} is thus causal and as it is equal to the fundamental solution G, it solves

$$\left(\Delta - \frac{1}{c^2}\partial_t^2\right)\phi^{\text{ref}}(\mathbf{x}, t) = 0 \quad \text{in } \Omega$$

The 3D fundamental solution for the infinite space is

$$G[\mathbf{x}, \mathbf{y}, t|f] = \frac{f(t - r/c)}{4\pi r}$$

and depends on t through the retarded time t $-\frac{r}{c}$, due to causality. To verify the CQM algorithm we define the Dirichlet trace on Γ:

$$\phi^{\text{ref}}(\mathbf{x}, t) = G(\mathbf{x}, \mathbf{z}, t) \star f(t)$$

and compute the Z transform of the series $\left(\phi^{\text{ref}}(\mathbf{x}, t_n)\right)_{n\in\mathbb{N}}$ as

$$\overline{\Phi}^{\text{ref}}(\mathbf{x}, \xi) = \overline{G}\left(\mathbf{x}, \mathbf{z}, \frac{p(\xi)}{\Delta t}\right) \times F(\xi)$$

where we denote $s(\xi) = \frac{p(\xi)}{\Delta t}$, the CQM complex frequencies (p is the backward differentiation formula of order 2 scheme BDF2). $\overline{G}$ is the Laplace transform of the fundamental solution defined by

$$\overline{G}(\mathbf{x}, \mathbf{z}, s) = \frac{e^{\frac{-sr}{c}}}{4\pi r}$$

and $F(\xi)$ is the Z transform of the series $(f(t_n))_{n\in\mathbb{N}}$. We then solve a boundary integral problem for each complex frequency $s(\xi) = \frac{p(\xi)}{\Delta t}$.

$$\frac{1}{2}\overline{\Phi}^{\text{ref}}(\mathbf{x}, \xi) - \mathcal{H}\left\{\overline{\Phi}^{\text{ref}}\right\}(\mathbf{x}, \xi) = -\mathcal{G}\{Q\}(\mathbf{x}, \xi) \qquad \forall t \in [0, T], \text{ with } \mathbf{x} \in \Gamma.$$

The inverse Z transform of $Q(\mathbf{x}, \xi)$ gives the transient solution $q(\mathbf{x}, t)$ and we verify the relative L^2 error between the numerical q and the analytical $\partial_n\phi^{\text{ref}}(\mathbf{x}, t) = \partial_n G(\mathbf{x}, \mathbf{z}, t \mid f) = \nabla G.\mathbf{n}$, using G first derivative given by [23]:

$$G_{,j}(\mathbf{x}, \mathbf{z}, t \mid f) = \frac{-r_{,j}}{4\pi r^2}\left[f(t - r/c) + \frac{r}{c}\dot{f}(t - r/c)\right].$$

Some frequency problems do not need to be solved: the definition of a HFA allows only the lowest-frequency problems to be solved. For higher frequencies we use the HFA described in [147], which involves the pressure p and velocity u:

$$-\rho\partial_t\phi(t) = \rho c\partial_n\phi(t), \quad t \in [0, T].$$

In the frequency domain, the HFA is written

$$\partial_n \overline{\Phi}(s) = -\frac{s}{c}\overline{\Phi}^{\text{ref}}(s), \tag{51}$$

where $\overline{\Phi}$ is the the Laplace transform of ϕ, with a Laplace variable s.

Numerical validation. We consider a sphere with a radius $r = 1$. The wave celerity is $c = 1$ and there is an interior point source that has a time-modulated amplitude f(t):

$$f(t) = \begin{cases} t^4(T-t)^4 \text{ if } t \in]0, T[\\ 0 \qquad\qquad \text{otherwise} \end{cases}$$

with a pulse width T=4.5. The time step is chosen according to the pulse width: $\Delta t = \frac{T}{55} = 8.10^{-2}$. The 36 first frequency BEM problems are solved with the frequency BEM solver. Taking the higher frequencies into account does not improve the relative error on the solution $\partial_n G$ (less than 3% of improvement), so we use the high frequency approximation from the 36th computation. The relative error computed on the whole time interval, on a node of the boundary Γ is:

$$e_r = \frac{\left\| q(\mathbf{x},t) - \partial_n u^{\text{ref}}(\mathbf{x},t) \right\|_{L^2([0,T])}}{\left\| \partial_n u^{\text{ref}}(\mathbf{x},t) \right\|_{L^2([0,T])}}, \quad \mathbf{x} \in \Gamma$$

The normal derivative $\partial_n G$ computed with a Z-BEM solver is illustrated on Figure 20 on a node of the boundary Γ, and compared to the analytical solution.

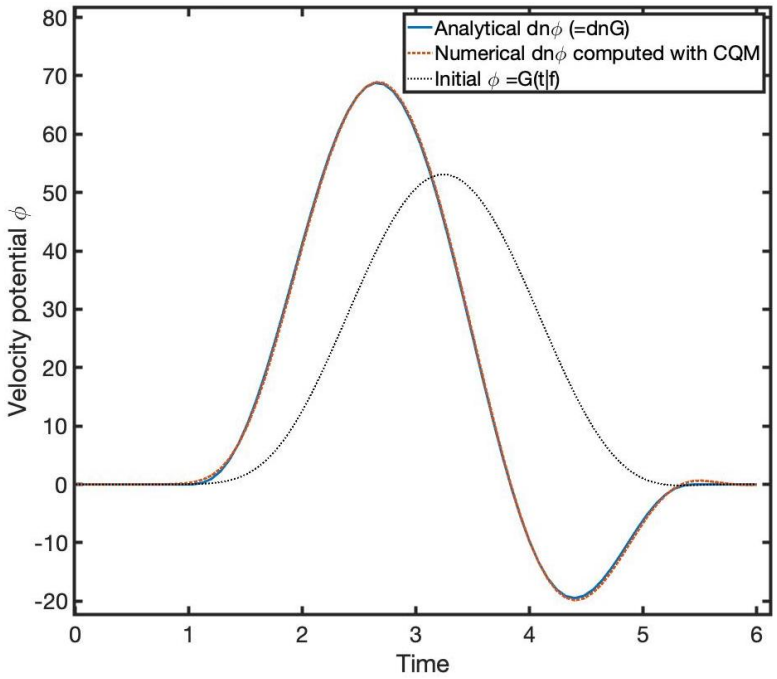

Figure 20: *Relative L^2 error on $\partial_n\phi$: $e_r = 1.2\ 10^{-2}$ ($\Delta t = 8\ 10^{-2}, N_t = 76$, T=4.5, HFA= 36).*

ECOLE
DOCTORALE

Titre : Méthode de décomposition de domaine pour les problèmes couplés acoustique-élastiques, dans le domaine temporel. Application aux explosions sous-marines

Mots clés : Couplage acoustique-élastique; Décomposition de domaine; Méthode itérative

Résumé : Ce travail étudie les approches globales en temps de décomposition de domaine pour résoudre des problèmes transitoires d'interaction fluide-structure. Afin de déterminer un algorithme optimal, nous étudions dans un premier temps la solvabilité des problèmes élastodynamiques et acoustiques transitoires avec des conditions aux frontières de type Robin et de Neumann. Nous énonçons des résultats de solvabilité, en soulignant les différentes régularités espace-temps des solutions. Nous étudions également la solvabilité du problème couplé élastodynamique-acoustique transitoire. Puis en nous basant sur ces résultats mathématiques, nous proposons ensuite un algorithme itératif global en temps basé sur les conditions aux limites de type Robin pour le problème couplé et prouvons sa convergence.
Ces résultats sont ensuite mis en œuvre pour coupler deux méthodes numériques efficaces. La réponse du fluide en temps discret est obtenue à l'aide d'une approche Z-BEM qui combine (i) une méthode d'éléments de frontière (BEM) accélérée par la méthode des matrices hiérarchiques dans le domaine de Laplace et (ii) une quadrature de convolution. La réponse de la structure est modélisée à l'aide de la méthode des éléments finis. Nous développons de cette manière une méthode numérique de couplage itérative globale en temps à convergence garantie, permettant en outre d'utiliser deux méthodes numériques distinctes de manière non intrusive.
Plusieurs améliorations sont ensuite proposées : une méthode d'accélération de convergence est mise en œuvre et une approximation à haute fréquence est proposée pour améliorer l'efficacité de la Z-BEM. On propose ensuite un deuxième couplage itératif global-en-temps basé sur une interface acoustique-acoustique, dont la convergence est également démontrée. Ce couplage permet ensuite d'introduire des effets non linéaires dus au phénomène de cavitation pour préciser le modèle fluide. La Z-BEM est enfin adaptée en utilisant la méthode des images pour permettre la prise en compte d'une surface libre.
Cette méthode est appliquée à des problèmes à dynamique rapide de dispersion d'ondes de choc acoustiques par des structures élastiques immergées et permet de simuler des configurations réalistes rencontrées dans l'industrie navale.

Title : Domain decomposition method for coupled acoustic-elastic problems in the time domain. Application to underwater explosions.

Keywords : Acoustic-elastic coupling; Domain decomposition method; Iterative method

Abstract : This work addresses global-in-time domain decomposition approaches for the numerical solution of transient fluid-structure interaction problems. To determine an optimal algorithm, we first study the solvability for the transient acoustic and elastodynamic problems with Robin and Neumann boundary conditions. We state solvability results along with the different space-time regularities of the solutions. We also study the solvability for the transient coupled elastodynamic-acoustic problem. Using on these mathematical results we then propose a global-in-time iterative algorithm based on Robin boundary conditions for the coupled elastodynamicacoustic problem and we prove its convergence.
These results are leveraged to design a computational methodology by coupling two efficient numerical methods. The fluid response is formulated in the discrete-time domain, using a Z-BEM approach that combines (i) a boundary element method (BEM) accelerated with hierarchical matrix implemented in the Laplace domain and (ii) a convolution quadrature method. The structure response is modelled using the finite elements method. We thus propose a global-in-time iterative coupling with guaranteed convergence, which enables the use of two distinct numerical methods in a non-intrusive manner.
Several improvements are then explored : an acceleration method is implemented and a high-frequency approximation is proposed to improved the Z-BEM efficiency. A second iterative global-in-time coupling based on an acoustic-acoustic interface is then proposed and its convergence is also proved. This coupling enables the addition of non linear effects due to the cavitation phenomenon to derive a more realistic fluid model. The Z-BEM is lastly adapted using the method of images to take a free surface into account.
This method is applied on fast-time problems of acoustic shock wave scattering by submerged elastic structures and enables to simulate realistic configurations from naval industry.

Institut Polytechnique de Paris
91120 Palaiseau, France